UNIVERSITÀ DEGLI STUDI DI SALERNO

Dipartimento di Medicina, Chirurgia ed Odontoiatria

Dottorato di Ricerca in

Medicina Traslazionale dello Sviluppo e dell'Invecchiamento Attivo

XXXVII ciclo

Curriculum: Medicina Traslazionale e Clinica

Tesi di Dottorato

Extracellular vesicles, an intelligent stem cell delivery strategy for tendon therapeutic application

Coordinatore:

Ch.mo Prof. Palmiero Monteleone

Candidato:

Marta Clerici

Matricola: 8803100026

Tutor:

Prof. Giovanna Della Porta

Prof. Nicholas R. Forsyth

Dr. Tina P. Dale

In cotutela con la Keele University (UK)

Anno Accademico 2024/2025

Extracellular vesicles, an intelligent stem cell delivery strategy for tendon therapeutic application

Marta Clerici

Thesis submitted for the degree of

Doctor of Philosophy

December 2025

Keele University

In cotutelle with the University of Salerno, as part of a double doctoral degree

ABSTRACT

Tendons are specialised connective tissues that transmit forces from muscle to bone, enabling movement and maintaining postural stability. Their limited intrinsic healing capacity contributes to frequent tendinopathies and re-injury. Conventional treatments often fail to restore full function, creating a need for alternative regenerative approaches. Tendon stem/progenitor cells (TSPCs) have been proposed as candidates for tendon repair due to their self-renewal capacity and tenogenic potential. Extracellular vesicles (EVs) secreted by TSPCs may also play a therapeutic role by modulating inflammation, supporting cell proliferation, and influencing extracellular matrix (ECM) remodelling. However, the contribution of TSPC-derived conditioned medium (CM) and crude EVs (cEVs) remains incompletely defined.

This thesis investigated the properties of porcine and human TSPC-derived CM and cEVs, and their potential relevance for tendon repair. Type II TSPCs (TSPCs II), isolated from the deep digital flexor tendon, were characterised under different culture conditions. Hypoxia appeared to increase EV secretion and to influence the expression of selected tenogenic markers. Dynamic culture and GDF-5 supplementation were associated with changes in cell behaviour and matrix deposition. Comparative analysis highlighted species-specific responses: in 2D cultures, porcine secretomes induced tenogenic marker expression without the need for exogenous GDF-5, whereas in 3D culture systems, human secretomes showed more pronounced effects on tenogenic differentiation and ECM organisation.

The study followed a stepwise approach, beginning with cell and EV characterisation and progressing through the evaluation of oxygen tension, mechanical stimulation, and biomaterial integration. Collectively, the findings suggest that microenvironmental cues influence the bioactivity of TSPC-derived secretomes. While further studies are required to clarify underlying mechanisms and confirm therapeutic efficacy, these results provide insights into the potential

of cell-free, EV-based approaches for tendon repair and contribute to ongoing work in musculoskeletal regenerative medicine.

Keywords: Tendon stem/progenitor cells (TSPCs); extracellular vesicles (EVs); conditioned medium (CM); tenogenic differentiation; hypoxia; mechanical stimulation; GDF-5; dynamic culture; 3D scaffolds; tendon regeneration; cell-free therapy; regenerative medicine.

TABLE OF CONTENTS

Abstract I

Table of Contents III

Figures XII

Tables XVI

Schemes XVI

Acknowledgements XVII

Abbreviations XIX

1. Introduction 2

1.1 Tendon structure 2

1.1.1 Tendon cells 4

1.2 Tendon mechanical properties 8

1.2.1 Cellular responses to mechanical loading 10

1.3 Tendon injury and healing 12

1.3.1 Tendon healing mechanisms 15

1.4 Current strategies for enhancement of tendon healing 17

1.5 Extracellular vesicles 20

1.5.1 Biogenesis of EVs 21

1.5.2 Composition of EVs 24

1.5.3 Role of EVs in intercellular communication 27

1.6 Extracellular vesicle isolation 30

1.6.1 Density-based isolation 31

1.6.2 Size-based isolation 32
1.6.3 Immunoaffinity-based isolation 33
1.6.4 Polymer precipitation 34
1.6.5 Microfluidic technologies 34
1.7 Extracellular vesicles characterisation 36
1.7.1 Size and morphology characterisation 36
1.7.2 Concentration and size distribution 37
1.7.3 Surface marker, protein and lipid profiling 38
1.7.4 RNA profiling 39
1.7.5 Emerging techniques 39
1.8 New approaches for tendon healing 40
1.8.1 Stem cell therapies 40
1.8.2 Bioactive mediators 42
1.8.2.1 Growth-differentiation factor 5 44
1.8.3 Scaffolds 45
1.8.4 Synergistic approaches: tendon tissue engineering 47
1.9 The role of EVs in tendon healing 49
1.10 Hypoxic culture 54
1.11 Dynamic culture systems 56
1.12 Thesis objectives 58
2. Materials and methods 60
2.1 Materials 60
2.2 General cell culture techniques 65

2.2.1 Enzymatic sub-culture with trypsin 65
2.2.2 Haemocytometer cell counting 66
2.2.3 Cryopreservation of cells 66
2.2.4 Cell thawing 66
2.3 Isolation and culture of cells 67
2.3.1 Isolation and culture of porcine tendon stem progenitor cells 67
2.3.2 Isolation and culture of porcine tenocytes 68
2.3.3 Isolation and culture of human tendon stem progenitor cells 68
2.3.4 Isolation and culture of human bone marrow mesenchymal stromal/stem cells from bone marrow aspirate (BMA) 69
2.3.5 Culture of BALB/3T3 clone A31 murine fibroblast cells 70
2.4 Growth rate 70
2.5 Cell aspect ratio 71
2.6 Trilineage differentiation 71
2.6.1 Adipogenic differentiation 71
2.6.2 Chondrogenic differentiation 71
2.6.3 Osteogenic differentiation 72
2.7 Histological staining of differentiated monolayers 72
2.7.1 Oil Red O monolayer staining 72
2.7.2 Alcian blue monolayer staining 72
2.7.3 Alizarin red monolayer staining 72
2.8 Induction of tenogenic differentiation using GDF-5 supplemented medium 73
2.9 Flow cytometry 73

2.9.1 Flow cytometry for porcine TSPCs and Tncs....73
2.9.2 Flow cytometry for human TSPCs....74
2.10 Cell lysis....75
2.11 RNA Extraction....75
2.12 Quantitative reverse transcription-polymerase chain reaction (RT-qPCR)....75
2.12.1 RT-PCR primer sequences....76
2.13 PicoGreen double-stranded DNA assay....78
2.14 Immunofluorescence analysis....79
2.14.1 Nuclei aspect ratio....80
2.15 Giemsa stain....80
2.16 Picro-Sirius Red staining....80
2.16.1 Quantification of Picro-Sirius Red staining....81
2.17 Live/Dead viability/cytotoxicity assay....81
2.18 Dynamic culture of human TSPCs....81
2.18.1 Perfusion bioreactor....81
2.18.1.1 FEM Analysis....83
2.18.2 Lab-rocker system....83
2.19 Conditioning of medium....84
2.20 Alamar Blue assay....85
2.21 Conditioned media ultracentrifugation....85
2.22 Morphological analysis of crude pellet....86
2.22.1 Scanning electron microscopy....86
2.22.2 Transmission electron microscopy....87

2.22.3 Nanoparticle tracking analysis 87
2.23 Protein analysis of crude pellet 87
2.23.1 Bradford assay 87
2.23.2 Multiplex surface marker analysis 88
2.23.3 Western blotting 89
2.24 Cytokines analysis 89
2.25 Hydrogels 90
3. Optimising porcine TSPCs for EV production and tenogenic potential 93
3.1 Introduction 93
3.2 Aim 94
3.3 Methods 95
3.3.1 Statistical analysis 96
3.4 Results 98
3.4.1 Cell yield after isolation 98
3.4.2 Cell proliferative capacity 99
3.4.3 Cell aspect ratio 100
3.4.4 Trilineage differentiation capacity 104
3.4.5 Flow cytometry analysis 107
3.4.5.1 Cell size and complexity 107
3.4.5.2 Cell immunophenotype 109
3.4.6 Gene expression 113
3.4.7 Immunofluorescence analysis 118
3.4.8 Porcine crude EVs characterisation 119

3.4.8.1 SEM and TEM analysis 120
3.4.8.2 Total protein concentration 121
3.4.8.3 Cytokine profiling 123
3.4.8.4 MACSPlex analysis 124
3.5 Discussion 126
3.6 Conclusion 131
4. Enhancing EV production from human TSPCs through dynamic culture and GDF-5 supplementation 134
4.1 Introduction 134
4.2 Aim 135
4.3 Methods 136
4.3.1 Statistical analysis 137
4.4 Results 138
4.4.1 Human tendon-derived cell characterisation 138
4.4.1.1 Cell proliferative capacity and aspect ratio 138
4.4.1.2 Flow cytometry and trilineage differentiation 139
4.4.1.3 Gene expression 142
4.4.2 GDF-5 effect on hTSPCs 143
4.4.2.1 Picro-Sirius Red staining and quantification 143
4.4.2.2 Gene expression 144
4.4.2.3 Immunofluorescence analysis 145
4.4.3 Perfusion bioreactor-derived human cEVs characterisation 146
4.4.3.1 Morphological and size analysis 148

4.4.3.2 Protein analysis 151
4.4.4 Lab-rocker system-derived human cEVs characterisation 153
4.4.4.1 Total protein concentration 154
4.4.4.2 MACSPlex analysis 156
4.4.4.3 Cytokine profiling 160
4.5 Discussion 161
4.6 Conclusion 170
5. Evaluating the tenogenic potential of porcine TSPC-derived CM and cEVs 173
5.1 Introduction 173
5.2 Aim 174
5.3 Methods 175
5.3.1 Statistical analysis 177
5.4 Results 177
5.4.1 Short-term evaluation of CM effect on TSPCs II (5 days) 177
5.4.1.1 Cell viability 178
5.4.1.2 Giemsa staining 179
5.4.2 Cytotoxicity assessment of CM 181
5.4.3 Long-term evaluation of CM effect on TSPCs II (14 days) 184
5.4.3.1 Giemsa staining 184
5.4.3.2 Immunofluorescence analysis 185
5.4.3.3 Gene expression 187
5.4.4 Long-term evaluation of CM and cEVs on hBM-MSCs (14 days) 191
5.4.4.1 Immunofluorescence analysis 191

5.4.4.2 Histological analysis 196
5.4.4.3 Gene expression analysis 197
5.4.4.4 DNA quantification 201
5.5 Discussion 202
5.6 Conclusion 209
6. Investigating the tenogenic potential of human TSPC-derived CM and cEVs in 2D and 3D cultures 212
6.1 Introduction 212
6.2 Aim 213
6.3 Methods 213
6.3.1 Statistical analysis 214
6.4 Results 215
6.4.1 2D culture: hBM-MSCs in hTSPCs-CM 215
6.4.1.1 Immunofluorescence analysis 216
6.4.1.2 Nuclei aspect ratio 220
6.4.1.3 Histological analysis 222
6.4.1.4 Gene expression 224
6.4.2 3D culture: hBM-MSCs embedded with cEVs and cultured in hTSPCs-CM 227
6.4.2.1 Live/Dead assay 227
6.4.2.2 Collagen gel contraction 231
6.4.2.3 Immunofluorescence analysis of TNMD 233
6.4.2.4 Nuclei aspect ratio 235
6.4.2.5 Gene expression 237

6.5 Discussion 240
6.6 Conclusion 247
7. Summative discussion, conclusions and future perspectives....250
7.1 Summative discussion 250
7.2 Conclusions 252
7.3 Future perspectives 252
8. References....255
9. Appendices 292
9.1 Appendix A – Publications and presentations 292
9.2 Appendix B – Ethical approval documents, University of Salerno....296

FIGURES

Figure 1-1. Tendon multi-hierarchical structure. 2
Figure 1-2. Tendon cellular niches. 5
Figure 1-3. Stress-strain curve of tendon mechanical properties. 9
Figure 1-4. Histological differences between healthy and pathological tendons. 14
Figure 1-5. Tendon healing process. 17
Figure 1-6. Biogenesis of extracellular vesicles. 24
Figure 1-7. Composition of extracellular vesicles. 27
Figure 1-8. Overview of EV isolation methods. 31
Figure 1-9. Schematic representation of tendon tissue engineering, highlighting the interplay between cells, bioactive signals, and scaffolds. 47
Figure 1-10. Schematic representation of EVs' the regenerative effects in tendon healing. ..50
Figure 2-1. Porcine tendon extraction. 67
Figure 2-2. Human tendon tissue preparation. 69
Figure 2-3. Perfusion bioreactor. 82
Figure 2-4. Lab rocker system. 84
Figure 2-5. Crude pellet obtained after the ultracentrifugation of conditioned media. 86
Figure 2-6. Collagen hydrogel moulding procedure. 91
Figure 3-1. Tendon-derived cell populations isolation. 97
Figure 3-2. Isolation of tendon-derived cell populations. 98
Figure 3-3. Cell growth curves. 100
Figure 3-4. Aspect ratios of tendon cell populations at passage 1 (P1). 101
Figure 3-5. TSPCs I aspect ratio. 102
Figure 3-6. TSPCs II aspect ratio. 103
Figure 3-7. Tncs aspect ratio. 103
Figure 3-8. Trilineage differentiation of TSPCs I. 105
Figure 3-9. Trilineage differentiation of TSPCs II. 106

Figure 3-10. Trilineage differentiation of Tncs. 107
Figure 3-11. Tendon cell size and complexity. 108
Figure 3-12. Immunophenotype of TSPCs I. 110
Figure 3-13. Immunophenotype of TSPCs II. 111
Figure 3-14. Immunophenotype of Tncs. 112
Figure 3-15. Quantification of positive immunophenotype markers. 113
Figure 3-16. Gene expression of stem cell markers in tendon-derived cell populations. 115
Figure 3-17. Gene expression of tenogenic markers in tendon-derived cell populations. 117
Figure 3-18. Immunofluorescence analysis of TNMD expression in TSPCs II over 14 days. 119
Figure 3-19. SEM analysis of porcine cEVs. 120
Figure 3-20. TEM analysis of porcine cEVs. 121
Figure 3-21. Total protein concentration in conditioned media and crude pellet. 122
Figure 3-22. Cytokine profiling in CM from TSPCs II and Tncs. 124
Figure 3-23. Surface marker expression on cEVs derived from TSPCs II. 126
Figure 4-1. Proliferative capacity and cell aspect ratio of human TSPCs. 139
Figure 4-2. Immunophenotype of hTSPCs. 140
Figure 4-3. Trilineage differentiation of hTSPCs. 141
Figure 4-4. Gene expression of tenogenic markers in hTSPCs. 142
Figure 4-5. Collagen deposition in GDF-5-treated human TSPCs, assessed by Picro-Sirius Red staining. 144
Figure 4-6. Gene expression of tenogenic markers in GDF-5-treated TSPCs. 145
Figure 4-7. Immunofluorescence analysis and cell aspect ratio of GDF-5-treated TSPCs. 146
Figure 4-8. Finite Element Method analysis of medium flow in a custom-made perfusion bioreactor. 147
Figure 4-9. Morphological analysis of human TSPC-derived cEVs using SEM and TEM. 149
Figure 4-10. Size and concentration analysis of human TSPC-derived cEVs using NTA. 150

Figure 4-11. Total protein content and western blot analysis of EVs isolated from human TSPCs.....151
Figure 4-12. Surface marker expression on crude EVs derived from hTSPCs.....153
Figure 4-13. Total protein concentration of CM from human TSPCs under static and dynamic conditions at 21% and 2% oxygen.....155
Figure 4-14. Total protein concentration of CP from human TSPCs under static and dynamic conditions at 21% and 2% oxygen.....156
Figure 4-15. Surface marker expression on cEVs derived from hTSPCs cultured under static and dynamic conditions at 21% and 2% O_2.....159
Figure 4-16. Cytokine profiling of cEVs from hTSPCs under static and dynamic conditions at 21% and 2% O_2.....160
Figure 5-1. Cell viability of TSPCs II cultured in different conditioned media for 5 days. 179
Figure 5-2. Giemsa staining of TSPCs II cultured in TSPCs II-derived CM under different oxygen conditions.....180
Figure 5-3. Giemsa staining of TSPCs II cultured in Tncs-derived CM under different oxygen conditions.....181
Figure 5-4. Cytotoxicity assessment of TSPCs II-CM using Alamar blue assay.....183
Figure 5-5. Giemsa staining of TSPCs II cultured for 14 days in different media conditions. 185
Figure 5-6. Immunofluorescence analysis of TNMD expression in TSPCs II cultured for 14 days under different media conditions. 187
Figure 5-7. Gene expression of tenogenic markers in TSPCs II cultured for 14 days under different media conditions.....190
Figure 5-8. Immunofluorescence analysis of TNMD expression in hBM-MSCs cultured for 14 days under different media conditions. 193
Figure 5-9. Immunofluorescence analysis of COL1 expression in hBM-MSCs cultured for 14 days under different media conditions. 195

Figure 5-10. Picro-Sirius Red staining of collagen deposition in hBM-MSCs cultured for 14 days under different media conditions. 197
Figure 5-11. Gene expression of tenogenic marker expression in hBM-MSCs cultured for 14 days under different media conditions. 200
Figure 5-12. Total DNA quantification in hBM-MSCs cultured for 14 days under different media conditions. 202
Figure 6-1. Immunofluorescence analysis of TNMD expression in hBM-MSCs cultured in 2D under different oxygen concentrations and media conditions. 217
Figure 6-2. Immunofluorescence analysis of COL1 expression in hBM-MSCs cultured in 2D under different oxygen concentrations and media conditions. 219
Figure 6-3. Nuclei aspect ratio analysis of hBM-MSCs cultured in 2D under different oxygen concentrations and media conditions. 222
Figure 6-4. Picro-Sirius Red staining of collagen deposition in hBM-MSCs cultured in 2D under different oxygen concentrations and media conditions. 223
Figure 6-5. Gene expression of tenogenic markers in hBM-MSCs cultured in 2D for 14 days under different oxygen concentrations and media conditions. 226
Figure 6-6. L/D assay at day 1 for hBM-MSCs embedded in collagen scaffolds with cEVs under different oxygen concentrations and media conditions. 228
Figure 6-7. L/D assay at day 14 for hBM-MSCs embedded in collagen scaffolds with cEVs under different oxygen concentrations and media conditions. 230
Figure 6-8. Collagen gel contraction over time under different oxygen concentrations and media conditions. 232
Figure 6-9. Immunofluorescence analysis of TNMD expression in hBM-MSCs cultured in 3D under different oxygen concentrations and media conditions. 234
Figure 6-10. Nuclei aspect ratio analysis of hBM-MSCs cultured in 3D under different oxygen concentrations and media conditions. 236
Figure 6-11. Gene expression of tenogenic markers in hBM-MSCs cultured in 3D for 14 days under different oxygen concentrations and media conditions. 239

TABLES

Table 1. Comparison of commonly used isolation methods for extracellular vesicles. 35

Table 2. List of materials, catalogue number and suppliers 60

Table 3. Primer sequences and conditions for RT-PCR in porcine cells 77

Table 4. Primer sequences and conditions for RT-PCR in human cells 78

SCHEMES

Scheme 1. Summary of the methodology adopted in Chapter 3. 97

Scheme 2. Summary of the methodology adopted in Chapter 4. 137

Scheme 3. Summary of the methodology adopted in Chapter 5. 177

Scheme 4. Summary of the methodology adopted in Chapter 6. 215

ACKNOWLEDGEMENTS

I am deeply grateful to my supervisors, Prof. Nick Forsyth and Dr Tina Dale, for their continuous support, patience, and guidance throughout these years. Their mentorship has been a major part of my growth as a researcher, challenging me to think critically, helping me through tough moments, and celebrating the wins along the way.

I would also like to thank my co-supervisor, Prof. Giovanna Della Porta, for her valuable input throughout the project and for the opportunity to collaborate with her group during my secondment in Italy. A special thank you as well to Prof. Nicola Maffulli for providing the tendon biopsies and for his scientific feedback and advice during the project.

This work was supported by the Marie Skłodowska-Curie Actions and the European Union's Horizon 2020 research and innovation programme under the P4FIT project (grant agreement No. 955685). I am thankful for the training, resources, and opportunities this programme has provided. A special thank you goes to the network coordinator, Prof. Hélder Santos, for his excellent coordination, problem-solving skills, and for keeping the network well connected throughout the project. Many thanks to the project manager, Pauliina Hallikas, for her great organisation and constant availability, which helped keep everything running smoothly.

I am also incredibly grateful for all the experiences that P4FIT allowed me to have, and for all the people I had the chance to meet through it. A special thank you to all the ESRs—especially to Veronica—for the endless calls and shared laughter, which often cheered me up and brightened even the most challenging days.

I'm grateful to everyone in the labs at Guy Hilton and the University of Salerno for creating a work environment that was not only productive and engaging, but also friendly and supportive. A special thank you to Vera for your friendship, support, and the many moments—inside and outside the lab—that helped lighten this journey. Special thanks also to Arjan, Alfred, and Amy, and to everyone at Guy Hilton, for making it a nicer place to work and for all the laughter we

shared. To Giacomo and Rubén—for all the support in and out of the lab, the endless chats, the laughs, and the good times that made this journey more fun and a bit less stressful. I'm really glad we shared this experience together. To Gennaro, Domenico, Biagio, and Luigi—for making me feel welcome in Salerno from day one. Thank you for showing me around and for all the great moments we shared, which made my time there truly unforgettable. Thanks also to Marika, Erwin, Pasqualina, and Valentina for their help and support during my time conducting research in Salerno.

I would also like to acknowledge the collaborators at the University of Bologna, Prof. Emanuele Giordano and Dr Joseph Lovecchio, for their contribution to the development of the bioreactor and FEM analysis, and Dr Valentina Giudice at the University of Salerno for her support with flow cytometry experiments and data analysis.

Special thanks also go to Dr Davis Galesso, Dr Alba Di Lucia, and Dr Anna Marchetti, as well as the team at Fidia Farmaceutici, for hosting me during the secondment, assisting with cytotoxicity assays, and providing materials and training essential to this project.

To my family: thank you for believing in me and supporting me from day one. Your encouragement has been the foundation of this journey. And to Herman—thank you for always being there, cheering me on, and making even the tough days a bit brighter with your optimism.

Finally, to my friends, colleagues, and everyone I had the pleasure of meeting over the past four years—thank you for the laughs, the pep talks, the coffee breaks, and all the shared moments that made this PhD experience such a rollercoaster, full of unexpected turns, challenges, and unforgettable highs.

ABBREVIATIONS

α-MEM	Minimum Essential Medium Alpha
AA	Ascorbic Acid
ACTβ	Actin beta
AEC(s)	Amniotic epithelial stem cells
AFM	Atomic Force Microscopy
APC	Allophycocyanin
AF4	Asymmetrical Flow Field-Flow Fractionation
BMA	Bone Marrow Aspirate
BMP(s)	Bone Morphogenetic Protein(s)
BSA	Bovine Serum Albumin
CD	Cluster of differentiation
cEVs	crude Extracellular vesicles
CircRNA(s)	Circular RNAs
CM	Conditioned Media
COL1	Collagen type I
COL1A1	Collagen type I alpha 1 chain
COL1A2	Collagen type I alpha 2 chain
COL3A1	Collagen type III alpha 1 chain
COX-2	Cyclooxygenase-2
CP	Crude pellet
CTGF	Connective tissue growth factor
CTRL	Control
DAPI	4',6-diamidino-2-phenylindole
DCN	Decorin
DEX	Dexamethasone
dH_2O	Distilled water
DLS	Dynamic Light Scattering
DMEM	Dulbecco′s Modified Eagle′s Medium - high glucose
DMSO	Dimethyl sulphoxide
DPBS	Dulbecco's Phosphate-Buffered Saline
ECM	Extracellular Matrix
EGF	Epidermal Growth Factor
ELISA	Enzyme-Linked Immunosorbent Assay

ESC(s)	Embryonic stem cells
ERK	Extracellular-signal regulated kinase
ESCRT	Endosomal sorting complex required for transport
ESWT	Extracorporeal Shockwave Therapy
EVs	Extracellular Vesicles
FasL	Fas Ligand
FBS	Foetal Bovine Serum
FEM	Finite element modeling
FFF	Field-Flow Fractionation
FGF2	Fibroblast Growth Factor 2
FITC	Fluorescein isothiocyanate
FSC	Forward Scatter
GAG(s)	Glycosaminoglycan(s)
GAPDH	Glyceraldehyde-3-phosphate dehydrogenase
GDF-5	Growth Differentiation factor 5
HBSS	Hanks' Balanced Salt Solution
HIF(s)	Hypoxia-inducible factor(s)
HPL	Human Platelet Lysate
HRE(s)	Hypoxia-Response Element(s)
HTSPC(s)	Human Tendon Stem/Progenitor cell(s)
IBMX	3-Isobutyl-1-methylxanthine
IF	Immunofluorescence
IFN-γ	Interferon-gamma
IGF-1	Insulin-like growth factor 1
IL(s)	Interleukin(s)
ILV(s)	Intraluminal vesicle(s)
IPSCs	Induced Pluripotent Stem Cells
ISCT	International Society for Cell and Gene Therapy
ISEV	International Society for Extracellular Vesicles
ITS	Insulin–Transferrin–Selenium
L/D assay	Live/Dead viability/cytotoxicity assay
L-DMEM	Dulbecco’s Modified Eagle’s Medium - low glucose
L-glut	L-glutamine
LLLT	Low-Level Laser Therapy
Long noncoding RNA(s)	lncRNA(s)

LTB4	Leukotriene B4
MAPK	Mitogen-activated protein kinase
MCSP	Melanoma-associated Chondroitin Sulfate Proteoglycan
MFI	Mean Fluorescence Intensity
MiRNA(s)	MicroRNAs
MKX	Mohawk homeobox
MLCK	Myosin light chain kinase
MMP(s)	Matrix Metalloproteinase(s)
MRA	Mycoplasma Removal Agent
MRI	Magnetic resonance imaging
MRNA(s)	Messenger RNA
MSC(s)	Mesenchymal Stromal/Stem Cells
MV(s)	Microvesicle(s)
MVB(s)	Multivesicular body(ies)
NaCl	Sodium Chloride
NANOG	Nanog Homeobox
NaOH	Sodium hydroxide
NEAA	Non-Essential Amino Acids
NTA	Nanoparticle Tracking Analysis
OCT-4	Octamer-binding transcription factor 4
OD	Optical density
PBS	Phosphate-Buffered Saline
PCL	Polycaprolactone
PD(s)	Population Doubling(s)
PDGF	Platelet-Derived Growth Factor
PE	Phycoerythrin
PEG	Polyethylene glycol
PGE2	Prostaglandin E2
PHD	Prolyl Hydroxylase Domain
piRNAs	piwi-interacting RNA(s)
PLGA	polylactic-co-glycolic acid
PolyQ	Polyglutamine
PRP	Platelet-Rich Plasma
PS	Phosphatidylserine
PSA	Penicillin-Streptomycin-Amphotericin B Mixture

PSC(s)	Pluripotent stem cells
ROI(s)	Region(s) of Interest
RT-qPCR	quantitative Reverse Transcription-Polymerase Chain Reaction
RT	Room Temperature
SCF	Stem Cell Factor
SCX	Scleraxis
SDS	Sodium Dodecyl Sulfate
SEC	Size-exclusion chromatography
SEM	Scanning Electron Microscopy
SPR	Surface Plasmon Resonance
SSC	Side Scatter
TIMP(s)	Tissue Inhibitors of Metalloproteinases
TEM	Transmission Electron Microscopy
TGF-β	Transforming growth factor- β
TGF-β3	Transforming growth factor-β3
Tnc(s)	Tenocyte(s)
TNC	Tenascin C
TNF-α	Tumor necrosis factor-α
TNMD	Tenomodulin
TRAIL	TNF-related apoptosis-inducing ligand
Tris-HCl	Tris hydrochloride
TRPS	Tunable Resistive Pulse Sensing
TSPC(s)	Tendon Stem/Progenitor Cell(s)
VEGF	Vascular Endothelial Growth Factor
YWHAZ	Tyrosine 3-monooxygenase/tryptophan 5-monooxygenase activation protein zeta



Chapter 1

Introduction

1. INTRODUCTION

1.1 Tendon structure

Tendons are specialised connective tissues within the musculoskeletal system that play a critical role in maintaining joint stability during movement and transmitting mechanical forces from muscles to bones or other structures[1]. Tendons consist of two distinct compartments: the extrinsic compartment and the intrinsic compartment, which may not always be physically distinct but serve different structural and functional roles[2,3] (Figure 1-1).

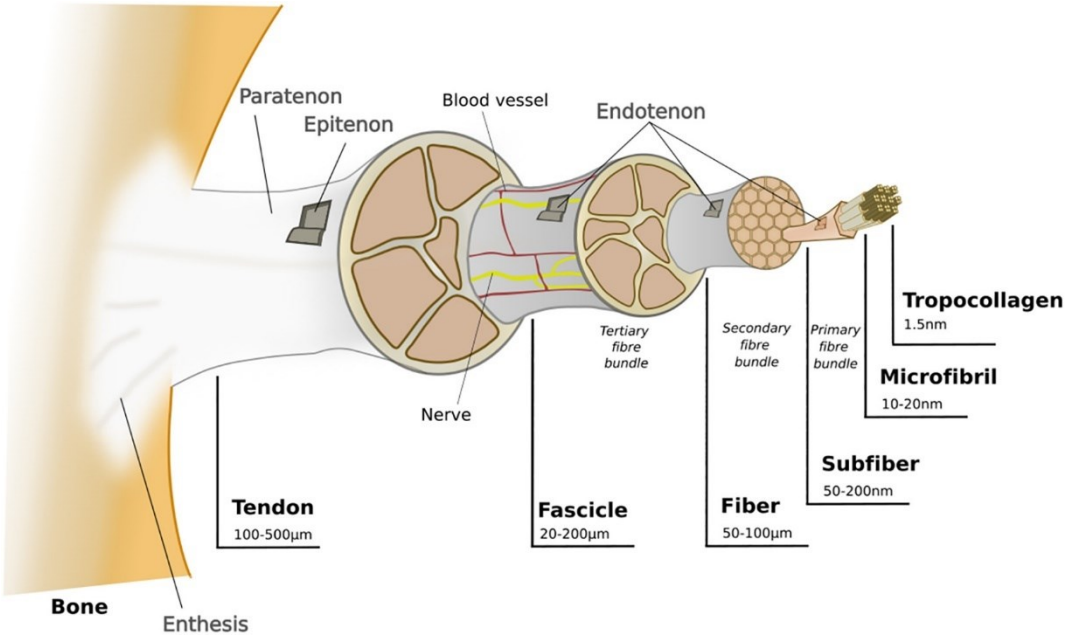


Figure 1-1. Tendon multi-hierarchical structure. Schematic representation of tendon structure, showing the hierarchical organisation from the outer paratenon, epitenon, and endotenon to the collagen fibre bundles (fascicles, fibres, microfibrils, and tropocollagen). This diagram highlights the structural units of the tendon, including blood vessels and nerves, and their roles in force transmission and tendon function. Image reprinted from Ruiz-Alonso et al., 2021[4], under CC BY-NC-ND 4.0 License.

The extrinsic compartment comprises synovium-like tissues, which are structurally similar to the synovial membrane found in joints. These tissues maintain tendon homeostasis through their function of lubrication, reduction of friction, and provision of nutrient exchange. The tissues create an interface between tendons and their surrounding structures, establishing

connections to the immune, vascular, and nervous system[5,6]. This compartment includes the paratenon, epitenon and endotenon, which contains differentiated and progenitor cells[7–9], such as tenocytes, tenoblasts and tendon stem progenitor cells. The paratenon is a loose connective tissue surrounding the tendon, primarily composed of type I and III collagen fibres and elastin. It acts as a protective gliding tissue, allowing the tendon to move smoothly over adjacent tissues during movement[7,10]. Beneath the paratenon lies the epitenon, a thin connective tissue layer that binds the tendon fascicles together, contributing to the overall structural integrity[11]. The endotenon is a fine network of connective tissue within the tendon, characterised by a crisscross arrangement of collagen fibrils that bind the tendon fibres[12]. It facilitates fascicle sliding and supports the transport of blood vessels, lymphatics, and nerves to deeper tendon regions[10,11]. The epitenon and endotenon further assist the tendon by maintaining the alignment of the collagen fibres and facilitating the transmission of mechanical loads from the tendon fibres to the surrounding tissues[12]. These structures are essential for tendon load-bearing capacity and efficient movement while also contributing to tendon healing, as they house progenitor cells supporting regeneration[8].

These tissues form enveloping layers around the intrinsic tendon, also known as the tendon core. The tendon core, or intrinsic compartment, is primarily made of type I collagen, which comprises approximately 65–80% of the tendon by weight[3]. This collagen forms a multi-hierarchical fibrillar structure, starting with collagen fibrils that aggregate into fibres and bundles aligned along the direction of mechanical force transmission[13]. This structural organisation confers tensile strength and resistance to excessive strain, which is critical for tendon function. At higher organisational levels, the collagen subunits are interspersed with ground substance, a hydrated matrix that provides additional support to the collagen fibres and contributes to the tendon's viscoelastic properties[14]. The tendon fibres containing interspersed tenocytes are organised into fascicles, the fundamental functional units within the intrinsic tendon and surrounded by the endotenon[9,12]. Type III collagen, which makes up about 10% of tendon collagen content, plays a crucial role in tendon healing and scar formation after tendon

injury[15]. Additionally, type IV and type V collagen participate in the self-assembly of type I collagen and improve the mechanical properties of tendons[14,16]. The tendon's extracellular matrix (ECM) is not only composed of collagen but also contains elastin, which provides the elastic component of the tendon ECM after repetitive loading. When tendon fibres are loaded, they elongate and pull along elastin fibres with them. After the load is released, elastin helps restore the tendon's original shape, compensating for the lack of intrinsic recoil in collagen fibres[17]. Proteoglycans are also a significant part of the tendon ECM, comprising 1–5% of the dry weight. These molecules consist of a core protein to which one or more glycosaminoglycan (GAG) side chains are attached[15]. The negatively charged GAGs attract water, helping the tendon resist compressive forces and facilitating the diffusion of nutrients and metabolites. Decorin is a major proteoglycan in tendons, and it is involved in tendon development and collagen fibrillogenesis by interacting with small-diameter fibril intermediates during the early stages of collagen assembly. Other proteoglycans, including fibromodulin and lumican, contribute to tendon development during later stages by regulating collagen fibril width, which improves tendon structural organisation[18,19].

1.1.1 Tendon cells

Tendons are specialised connective tissues characterised by low cellular density, with approximately 90%–95% of the cellular content composed of tendon-specific cell types, namely tenocytes and tenoblasts[8] (Figure 1-2).

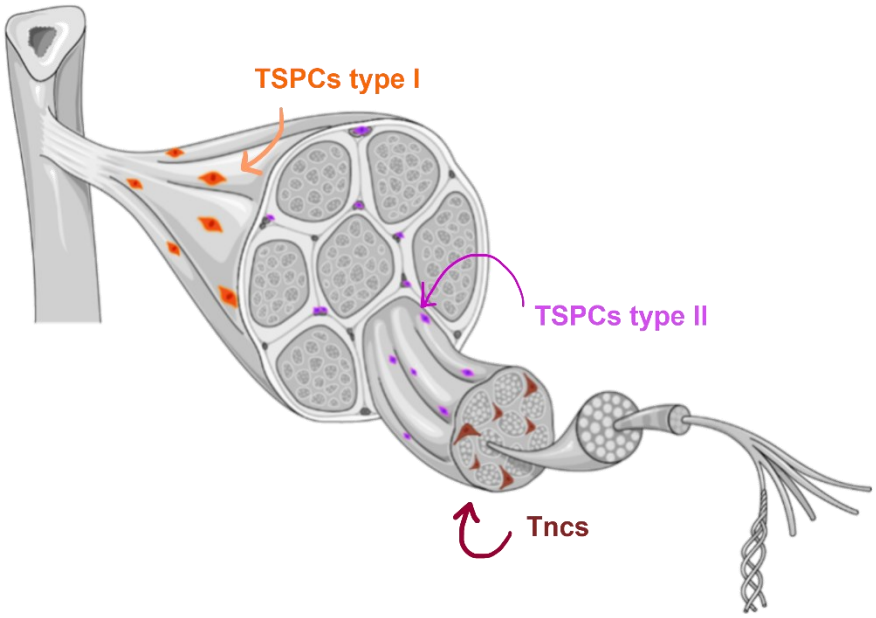


Figure 1-2. Tendon cellular niches. Schematic of tendon organisation showing TSPCs type I (orange) in the paratenon/sheath, TSPCs type II (purple) in fibre-associated niches, and Tncs (brown) between collagen fibres. Perivascular TSPCs may also be present in the endotenon and peritenon. Image adapted from Citro, Clerici et al., 2023[2], under CC BY 4.0 License.

These cells play crucial roles in the maintenance, repair, and remodelling of tendon tissues, with each cell type contributing uniquely to tendon function[2]. Tenocytes are terminally differentiated fibroblasts that exhibit a spindle-shaped morphology, with elongated nuclei and thin cytoplasmic extensions that anchor them to the collagen fibres within the tendon. These cells are primarily located between collagen fibrils and are responsible for the production and maintenance of the ECM and for regulating tendon remodelling. Tenocytes produce collagen, proteoglycans, and other ECM components necessary to maintain tendon integrity. Due to their role in preserving tendon structure, tenocytes actively respond to mechanical load and stress, ensuring proper tissue function. The tenogenic differentiation of these cells is often identified through markers such as scleraxis (SCX) and tenomodulin (TNMD). Unlike stem cells, tenocytes lack the expression of stem cell-specific markers like OCT-4 and SSEA-1/4, signalling their differentiated status[20,21]. Tenoblasts, in contrast, are relatively round, immature tendon cells with large, ovoid nuclei. These cells are more prevalent in younger tendons and gradually differentiate into tenocytes as the tendon matures with age. Tenoblasts are

considered a transient population that facilitates tendon growth and repair. Interestingly, there is some flexibility in the relationship between tenoblasts and tenocytes. Under certain conditions, such as exercise, trauma, or tendon injury, interconversion between these cell types can occur[22]. However, this interconversion is mainly based on changes in cell morphology, and there is no clear molecular marker that can definitively distinguish between tenoblasts and tenocytes in situ[23]. It is also suggested that tenoblasts may represent an activated form of tenocytes during tendon healing, which helps regenerate the tissue after injury[22].

In addition to tenocytes and tenoblasts, tendons also contain other specialised cells that contribute to tendon function and repair. These include chondrocytes, which are found at the pressure and insertion sites of tendons, synovial cells within the tendon sheath, capillary endothelial cells and smooth muscle cells that make up the vasculature of the tendon[23]. These diverse cell populations are essential for supporting the tendon's overall function, particularly in regions where tendons interface with other tissues such as bone or muscle.

Tendons also contain a population of tendon stem/progenitor cells (TSPCs), which comprise a smaller fraction (approximately 5%) of the total tendon cell population. TSPCs were first identified by Bi et al. in 2007[24] in human hamstring tendons, where they were shown to exhibit typical mesenchymal stem/stromal cell (MSC) characteristics, including self-renewal, clonogenicity and the potential for tri-lineage differentiation (adipogenic, osteogenic, and chondrogenic) under specific conditions. TSPCs also express tendon-specific genes, such as *SCX* and *TNMD*, which allow them to differentiate into tenocytes and contribute to tendon homeostasis[8]. TSPCs are situated in a unique niche that is primarily ECM-based, distinct from other known stem cell niches[9,25]. Unlike the bulge niche for skin stem cells[26] or the osteoblast niche for haematopoietic stem cells[27], the TSPC niche is characterised by a rich ECM environment containing type I and type III collagens, large proteoglycans such as aggrecan and versican, and small leucine-rich proteoglycans like decorin, biglycan, and fibromodulin, which play a crucial role in organising collagen fibrils and providing structural support[10,18].

Additionally, the perivascular niche may serve as another source of stem/progenitor cells within tendons, where cells in the perivascular space express both tendon-specific and pericyte-associated markers. Therefore, recent research has highlighted a regional distribution of TSPCs within tendons, with distinct subpopulations identified in different regions of the tendon[28]. TSPCs type I, located in the paratenon, the outer tendon sheath, exhibit characteristics like vascular stem cells. In contrast, TSPCs type II, found within the tendon core, are more proliferative, with higher expression of SCX and TNMD, key markers of tenogenic differentiation[8]. The TSPCs niche plays a critical role in maintaining these subpopulations of TSPCs, providing a microenvironment that regulates their behaviour and differentiation. This niche, particularly the perivascular niche in the paratenon and the ECM-rich environment of the tendon proper, supports TSPC self-renewal and differentiation under physiological and injury conditions. TSPCs also express several surface markers commonly associated with MSCs, such as Sca-1, CD44, CD90, CD105, CD146, STRO-1, and OCT-4, but they are negative for markers like CD31, CD34, and CD45[10]. Despite these advancements in identifying TSPCs, distinguishing these cells from tenoblasts and tenocytes remains difficult due to the lack of specific molecular markers for each differentiation stage. Some studies[20,24,29] have classified CD44+ tendon-derived cells as TSPCs based on their expression of markers like CD146 and STRO1. However, the precise role of TSPCs in tendon maintenance, healing, and regeneration remains unclear, and further *in vitro* and *in vivo* studies are necessary to elucidate their functions and locations within the tendon.

Tendon cells exhibit peak metabolic activity during growth, a process that gradually declines with ageing[8]. In mature tendons, cells mainly rely on anaerobic energy production, which is thought to minimise the risk of ischemia and necrosis during prolonged tensile stress. This low metabolic rate allows tendons to function effectively under sustained mechanical load but presents a limitation when tendon healing is required. The limited metabolic activity of mature tendon cells can delay recovery from injuries, making tendon repair challenging[30].

1.2 Tendon mechanical properties

Tendons form vital elements of the musculoskeletal system by transferring muscle-force energy to bones, allowing joint movement and stability. Tendon mechanical properties will enable them to receive and transfer tensile forces, which protect bones and muscle tissues from excessive strain. Tendons are viscoelastic tissues, meaning they exhibit both elastic and viscous behaviours depending on the rate of mechanical loading[31]. This viscoelasticity enables tendons to absorb energy and adjust their mechanical properties in response to varying strain rates[32].

Tendons are highly sensitive to mechanical loading, enabling them to function effectively during activities such as exercise[25]. This capacity to support mechanical loads is due to the hierarchical organisation of their structure, which enables tendons to respond to various mechanical signals. Mechanical loading is, therefore, an important determinant that can either enhance functional tissue remodelling or contribute to chronic tendon diseases, depending on the magnitude and type of forces exerted[33].

The structural organisation of tendons contributes significantly to their mechanical properties. Tendons are primarily composed of bundles of collagen fibres that are organised in a highly structured, uniaxial pattern. This fibrillar extracellular matrix provides a scaffold for the attachment of cells and macromolecules[2]. The primary purpose of collagen fibres in the tendon structure is to absorb tensile forces without compromising its structural framework under mechanical loading conditions[34]. The proteoglycans in the ECM help the tendon show viscoelastic properties, which allow it to stretch and return to its original shape under applied loads. The endotenon, a connective tissue layer, not only binds collagen fibres but also enables them to glide over one another, reducing friction and facilitating smooth tendon movement during muscle contraction[2].

The stress-strain curve of tendons reveals their mechanical behaviour under different loading conditions, which can be divided into several phases[13]. The first phase is the toe region, where

strain is below 2%. In this region, collagen fibrils within the tendon straighten, transitioning from their crimped state, initially allowing tendons to absorb low-level forces without damage. The toe region is a critical phase for tendons, as the "crimping" in the collagen fibres contributes to the tendon's flexibility, allowing it to stretch and store energy without significant tissue damage. Depending on the tendon type and location, this crimping results in different initial mechanical properties influenced by the angle and length of the fibril pattern[32]. The second phase of the stress-strain curve is the linear region, where strain increases up to 4%. In this region, collagen fibrils align along the direction of the applied force, and the tendon demonstrates elastic behaviour. The stress-strain relationship is linear, and Young's modulus, which measures tendon stiffness, defines this phase. As strain increases and the fibres straighten, the tendon's stiffness increases. When the strain exceeds 4%, the tendon enters the failure region, where microscopic damage occurs. Further strain (above 8-10%) leads to macroscopic rupture due to the breakdown of collagen fibers[35] (Figure 1-3).

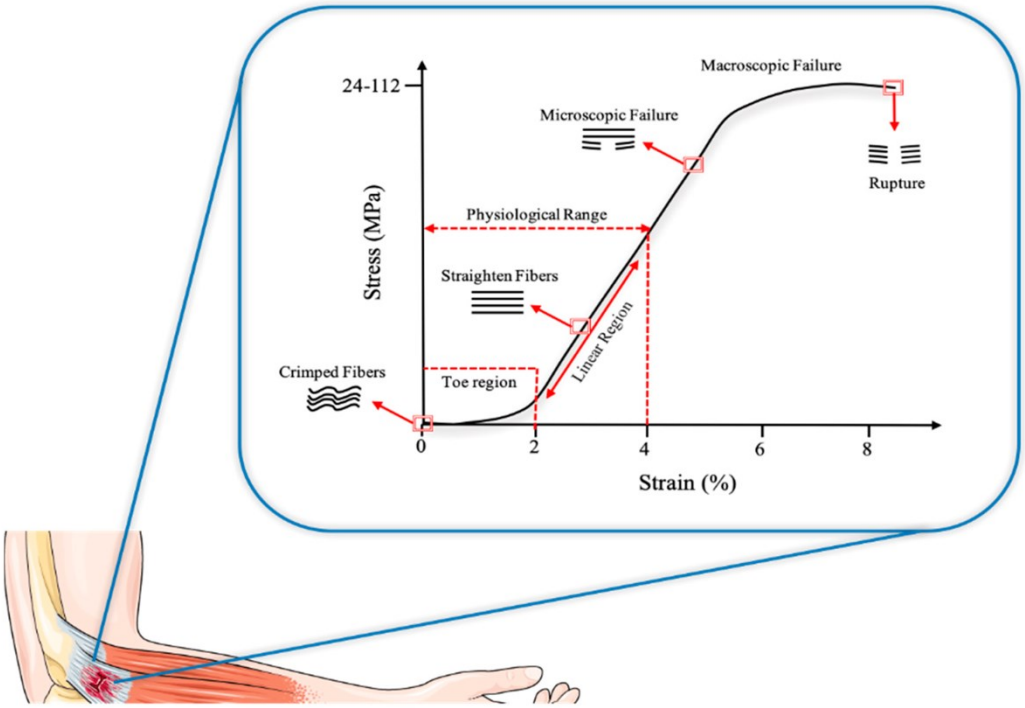


Figure 1-3. Stress-strain curve of tendon mechanical properties. The image illustrates a tendon under mechanical load, showing the four main regions of tendon behaviour under mechanical loading. The toe region (0-2% strain) represents the "stretching out" of crimped collagen fibres, leading to increased tendon compliance. The linear region (up to 4% strain) corresponds to the alignment of

collagen fibres and the elastic behaviour of the tendon. Beyond 4% strain, the tendon enters the failure region, with microscopic failure occurring between 4-8% strain and macroscopic rupture at strains greater than 8-10%. Image reprinted from Citeroni et al., 2020[7], under CC BY 4.0 License.

Tendons' tensile strength is strongly related to their collagen content and thickness. The stiffness (Young's modulus) of tendons varies depending on their location, with values typically ranging from 100 MPa to 2 GPa, demonstrating their ability to withstand high mechanical loads while maintaining flexibility[36]. The ultimate tensile strength can also vary, with the Achilles tendon exhibiting approximately 50–100 MPa strengths, while the flexor tendon can reach up to 150 MPa[37,38]. For instance, a tendon with an area of 1 cm² can support forces between 500-1,000 kg[39]. During high-impact activities such as running, the human Achilles tendon can withstand forces up to 9 kN, approximately 12.5 times body weight[40]. Tendons are especially vulnerable to rupture under conditions of rapid loading or eccentric muscle contractions, where forces are applied quickly or obliquely[31,41]. The specialised collagen arrangement in tendons allows them to transmit and absorb cyclical tensile forces effectively. The hierarchical structure of collagen fibres, ranging from individual collagen molecules to fibrils, fibres, and fascicles, allows for mechanical resilience and adaptability. This uniaxial force-transmitting structure is essential for tendon function, as it enables efficient force transmission along a single axis, which is critical for joint stability and movement. The viscoelastic behaviour of tendons allows them to adjust to different loading rates. Tendons use low strain rates below 1% per second to absorb mechanical energy while dissipating stress, thus preventing injuries. High strain rates above 10% per second increase tendon stiffness, yet they simultaneously raise the possibility of tendon rupture during extreme loading conditions[13]. Tendons need their ability to adapt strain rate levels for performing their functions during dynamic movements when tendon loading conditions undergo quick changes[32].

1.2.1 Cellular responses to mechanical loading

The mechanoreponses of tendons, both anabolic and catabolic, are significantly influenced by the responses of tendon cells, particularly tenocytes. Tenocytes play a crucial role in adapting

tendon tissue to mechanical loading by altering ECM gene and protein expression[13,42]. The mechanoresponses of tenocytes depend on the magnitude and type of mechanical loading[32]. *In vitro* studies have demonstrated that applying cyclic stretching (typically at magnitudes of 4–8% strain, frequencies of 0.5–1 Hz, and durations ranging from 6 to 24 hours[43–46]) results in increased proliferation of tenocytes, as well as increased tenogenic gene and protein expression (Col I, Col III, TNMD, TNC), in a stretching magnitude-dependent manner[47–49]. Additionally, cyclic stretching also increases the expression of cyclooxygenase-2 (COX-2), an important enzyme involved in the inflammatory process, and inflammatory mediators such as prostaglandin E2 (PGE2) and leukotriene B4 (LTB4), with high levels of PGE2 being associated with decreased proliferation and collagen production, which can contribute to the development of tendinopathy[44].

Mechanical loading not only affects tenocytes but also influences TSPCs. These cells are critical for tendon homeostasis and repair, and their responses to mechanical loading are essential for maintaining tendon structure and function. Cyclic loading has been shown to enhance the proliferation of TSPCs and stimulate collagen production[33]. However, *in vitro* studies showed that the differentiation of TSPCs is magnitude-dependent: low-intensity mechanical stretching promotes the differentiation of TSPCs into tenocytes, while higher stretching magnitudes (such as 8%) induce TSPCs to differentiate into non-tenocyte cell types, including adipocytes, chondrocytes, and osteocytes[32,43,48]. This non-tenocyte differentiation may contribute to the development of tendinopathy, as seen with lipid deposition, calcification, and increased proteoglycan accumulation in response to excessive mechanical loading[2,43,50].

Furthermore, mechanical loading also affects the expression of various genes associated with tendon remodelling, such as *SCX* and *TNMD*, both of which are crucial for tenocyte proliferation, collagen organisation, and ECM maintenance[51]. Excessive loading may disrupt this balance, leading to pathological changes in tendon structure[52]. The interplay between mechanical loading, cytokines, and integrins is another crucial aspect of tendon mechano-transduction. Cytokines such as interleukins (ILs), tumour necrosis factor-α (TNF-α), and

interferon-gamma (IFN-γ) are released in response to mechanical stress or tissue injury and can alter the cellular phenotype and matrix production and can contribute to tendon disorders[45,53,54].

Therefore, the homeostasis of tendons depends strongly on mechanical stimuli since these factors control tenocyte survival rates, tendon healing processes, and cytokine profile development, and these interactions influence tendon function. The beneficial effects of moderate loading on tendon health emerge, while abnormal or excessive loading produces degenerative changes that lead to tendinopathy development. Developing suitable treatments for tendon injuries requires a full comprehension of cellular responses to mechanical forces and their effects on tendon remodelling processes.

1.3 Tendon injury and healing

Tendon injuries, or tendinopathies, are common musculoskeletal disorders and a principal cause of functional disability, affecting athletes, active workers, and the elderly population worldwide[55]. They can be acute or chronic and are caused by intrinsic or extrinsic factors, either independently or in combination[31]. The most common clinical types of tendon injuries include rotator cuff tears, Achilles tendon ruptures, and tendinopathies such as patellar tendinitis and tennis elbow[56]. Rotator cuff tears, often associated with repetitive overhead movements, can cause significant shoulder pain and restricted motion. Achilles tendon ruptures, common in athletes, are marked by sudden calf pain and weakness. Tendinopathies, including chronic conditions like tendinosis, emerge from repetitive strain and can develop in both patellar tendons and elbow tendons, producing pain and functional impairment. The mechanisms underlying tendinopathy remain somewhat unclear, but several factors have been implicated, including hypoxia, ischemic damage, oxidative stress, and matrix metalloproteinase imbalance, among others[57–59].

Acute tendon injuries are often caused by extrinsic factors such as sudden trauma or excessive loading. At the same time, chronic tendinopathies are more frequently the result of a

combination of intrinsic and extrinsic factors[4]. In chronic tendon disorders, intrinsic factors such as genetics, sex, age, nutrition or general health are commonly cited as contributing to tendon degeneration. For instance, hyperpronation of the foot has been linked to an increased incidence of Achilles tendinopathy, particularly in athletes[60]. Chronic tendinopathies often develop due to repetitive overload of tendons during physical activities or sports, which surpasses the physiological threshold of the tendon's capacity to repair itself[61]. In the presence of intrinsic risk factors, this excessive loading may carry an even greater risk of inducing tendinopathy[31].Tendons respond to repetitive overload beyond their physiological capacity by either sheath inflammation, structural degeneration, or a combination of both[62]. Different stresses lead to various cellular responses in tendons. Resident tenocytes must actively repair fatigue damage to prevent weakening and potential tendon rupture. However, damage can also occur from microtrauma even within physiological limits, as frequent cumulative stress may not allow the tendon enough time to repair itself. Microtrauma is also induced by non-uniform stress distributions within tendons, producing abnormal load concentrations and frictional forces between fibrils, leading to localised fibre damage[63].

Histologically, tendinopathy is characterised by a disorganised healing process with minimal inflammatory cell presence, poor tissue repair, and degeneration of collagen[57]. The tendon fibres may become misaligned, thinner, and more cellular, with irregular blood vessel development. Additionally, glycosaminoglycans, by accumulating in the interfibrillar matrix, contribute to the injury's pathophysiology[64] (Figure 1-4). Macroscopically, tendons affected by tendinopathy lose their normal smooth, white appearance and become grey-brown and amorphous, often accompanied by tissue thickening, which can be diffuse, fusiform, or nodular[65].

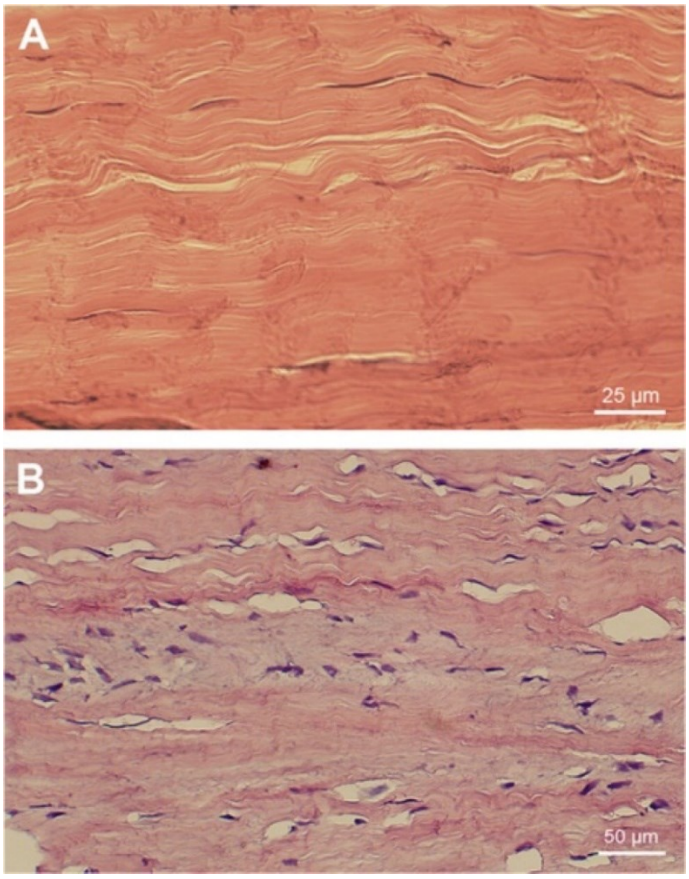


Figure 1-4. Histological differences between healthy and pathological tendons. (A) The normal tendon shows organised collagen fibres and a sparse amount of tendon cells tightly packed between the collagen bundles. (B) In tendinopathic tissue, the tendon structure becomes disorganised, and tenocytes change morphology and proliferate. Haematoxylin and eosin staining was used for both panels. Scale bars = 25 µm (A) and 50 µm (B). Image reprinted from Christensen et al., 2015[66] under CC BY 4.0 License.

Tendon rupture, typically considered an acute injury, is often caused by extrinsic factors such as sudden, forceful movements or trauma. However, intrinsic factors also play a significant role in predisposing tendons to rupture. While tendon ruptures can be spontaneous or induced by excessive loading, most tears are preceded by histological and degenerative changes, including collagen breakdown and disorganised fibril structures, consistent with chronic tendinopathy[67]. The tendinopathic changes often remain clinically silent and do not manifest until the rupture occurs[2]. In fact, studies show that a large percentage of tendon ruptures, like Achilles tendon tears, involve degenerative changes, and these tendons exhibit greater degrees of degeneration compared to tendons that have only experienced chronic overuse[67,68].

1.3.1 Tendon healing mechanisms

The healing of tendon injuries generally proceeds through two main mechanisms: intrinsic and extrinsic healing[69]. Intrinsic healing occurs when tenocytes and fibrocytes at the injury site promote repair, often involving the proliferation of cells from the epitenon and endotenon[2]. This process is limited due to the low number of resident cells and poor vascularisation. On the other hand, extrinsic healing occurs through the migration of fibroblasts and inflammatory cells from surrounding tissues, such as the tendon sheath and periosteum, to the injury site. The rate of extrinsic healing depends on the blood supply reaching the injury site, and external cells enable the formation of new collagen tissue to restore damaged areas. However, the overuse of external cells for healing can create scar tissue and adhesions, which stand as unfavourable results from the healing process[8,70,71].

The tendon healing process is generally divided into three overlapping phases: inflammation, proliferation, and remodelling. During these phases, molecular and cellular processes transition in response to the injury and the healing environment, with each phase playing a critical role in restoring tendon function.

Inflammation is the first phase, occurring immediately after injury and typically lasting a few days. During this phase, inflammatory cells, such as macrophages, neutrophils, platelets, and circulation-derived MSCs, infiltrate the wound site. These cells release growth factors and cytokines that stimulate the recruitment of fibroblasts and tenocytes to the injury site[72], initiating tissue repair. Macrophages play a critical role in resolving inflammation and promoting tissue repair through the secretion of growth factors such as insulin-like growth factor 1 (IGF-1), platelet-derived growth factor (PDGF) and vascular endothelial growth factor (VEGF). These factors promote tissue repair by initiating the breakdown of damaged tissue, clearing necrotic debris, and setting the stage for new tissue formation. This phase also triggers the formation of a fibrin clot, which temporarily stabilises the injured tendon and provides biomechanical support as the healing process begins[2].

The second phase, known as the proliferative phase, lasts from days 2 to 4 weeks and sees an increase in cell proliferation and collagen synthesis. Macrophages shift from their phagocytic function to a reparative role, continuing to release growth factors, including fibroblast growth factor 2 (FGF2), bone morphogenetic proteins (BMPs), and transforming growth factor-beta (TGF-β)[2,67,70]. They also direct cell recruitment, resulting in a marked increase in the number of fibroblasts and tenocytes, which synthesise type III collagen to form a provisional matrix. Although this collagen is weak and disorganised, it serves as a bridge to connect the injured tendon ends. This phase also marks the activation of TSPCs, which contribute to tendon healing, as they have been shown to generate tenocytes and self-renew after tendon injury[73,74].

The final phase, remodelling, begins around 6-8 weeks after injury and can last several months. During this phase, type III collagen is replaced by type I collagen, and the collagen fibres begin to align in the direction of tensile forces. As the remodelling process progresses, there is a decrease in cellularity, and the ECM is reorganised[8]. Tendon strength gradually improves, and the tendon is considered "healed" after approximately 12 weeks[70] (Figure 1-5). However, despite extensive remodelling, the repaired tendon rarely regains the full mechanical properties of the original tissue. It often remains hypercellular, with smaller and less aligned collagen fibrils, which makes it more susceptible to re-injury[75].

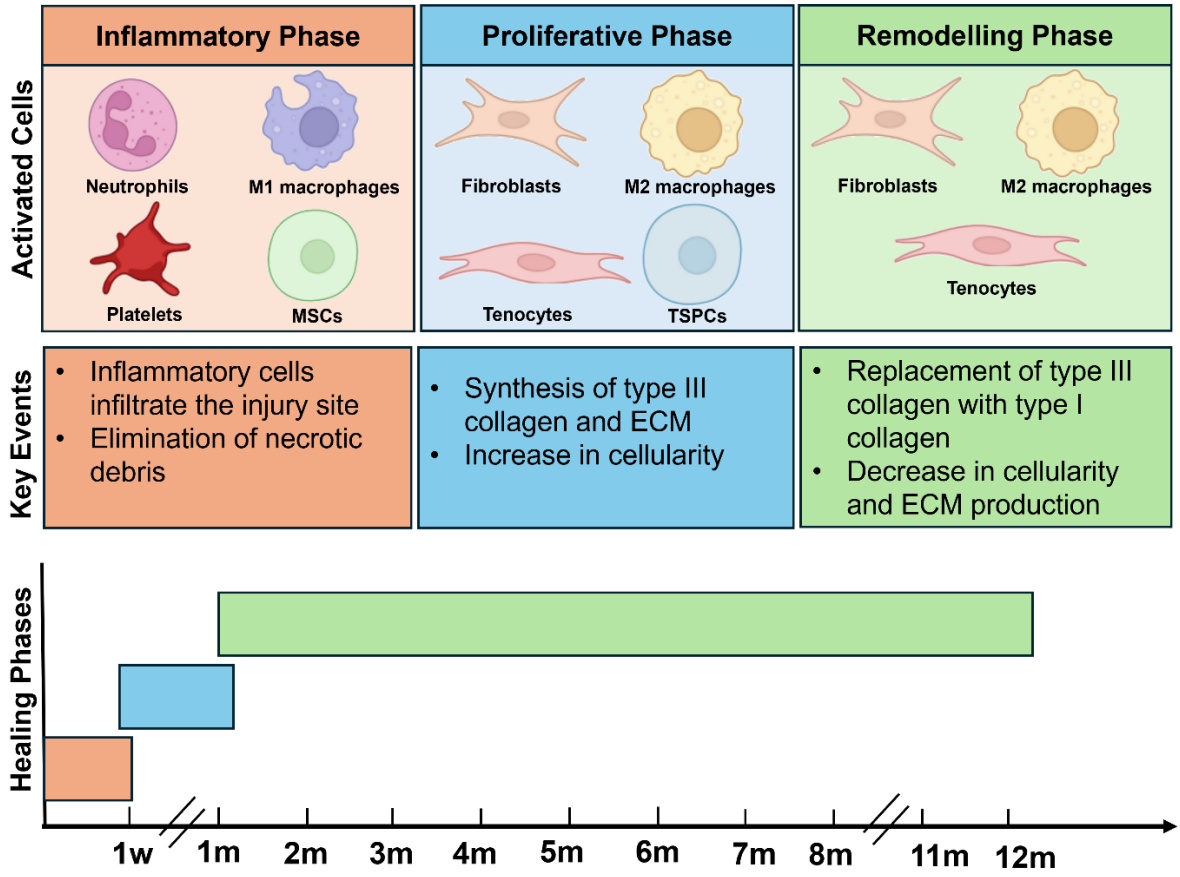


Figure 1-5. Tendon healing process. The diagram illustrates the three overlapping phases of tendon healing: inflammation, proliferation, and remodelling. The inflammation phase is characterised by cell infiltration and the release of growth factors to initiate tissue repair. During the proliferation phase, collagen synthesis and cell recruitment occur, followed by the remodelling phase, where collagen fibres realign and tendon strength improves. The figure highlights the key cellular and molecular events in each phase. Image partially created with https://www.biorender.com/, adapted from Hu et al., 2023[73] and Brebels et al., 2022[70].

Additionally, tendons with a history of tendinopathy or rupture may exhibit an abnormal increase in type III collagen and a reduction in type I collagen, further compromising tensile strength and increasing the risk of re-rupture[76,77]. The need for better tendon healing strategies becomes evident due to challenges that require optimising cellular responses and ECM composition and vascularisation at injury sites.

1.4 Current strategies for enhancement of tendon healing

Depending on the type of tendon injury, different therapeutic approaches are employed. The main priority for treating chronic tendon injuries is decreasing pain symptoms and restoring

functional abilities. The treatment regimen includes physical therapy with exercises, together with pharmaceutical interventions[78,79]. On the other hand, acute tendon injuries, such as tendon ruptures, usually require surgical treatment followed by post-operative rehabilitation because tendon ruptures need invasive medical procedures[80].

The treatment of tendon injuries, whether acute or chronic, begins with a thorough clinical evaluation. This includes assessing the type and severity of the injury, often assisted by imaging techniques like ultrasound or magnetic resonance imaging (MRI)[81]. This helps determine whether conservative management or surgical intervention is necessary. In the case of surgical treatment, the outcomes vary based on factors such as the tendon involved, the location of the injury, and the surgical technique employed. One common surgical approach is tendon repair, where the damaged tendon is sutured or reconstructed. In cases of significant tendon loss, tendon autografts (using the patient's tendon tissue) may be utilised to repair the defect. Autografts offer the benefit of reduced immunological complications and promote better tissue integration; however, they also come with specific challenges, such as limited donor tendon availability, longer operation times, and the sacrifice of healthy tendon function. Despite these challenges, autografts have been shown to be effective in tendon reconstruction[82,83], though the newly formed tendon does not always replicate the mechanical properties of a healthy tendon and may take considerable time to remodel fully.

Conservative approaches to tendon healing focus on reducing inflammation, promoting tissue repair, and restoring tendon function. Rehabilitation is a key treatment component for acute and chronic tendon injuries. For tendinopathy, eccentric exercise therapy, where the muscle and the tendon lengthen under load, has been shown to be particularly effective. Research has demonstrated that eccentric strengthening exercises provide substantial improvements in both pain and function, with some studies reporting a 60% to 90% improvement in patient's symptoms[84,85]. Through exercise, the tendon tissue undergoes remodelling because exercises trigger collagen production and enhance the correct alignment of collagen fibres.

In addition to exercise, controlled mechanical loading has become crucial to post-operative rehabilitation protocols for tendon injuries. Mobilisation techniques that incorporate controlled mechanical loading encourage the realignment of collagen fibres, stimulate fibroblast activity, and improve the overall strength of the tendon[43,86]. This mechanical stimulation leads to increased tensile strength, greater tendon diameter, and fewer adhesions compared to immobilised tendons during the healing process. Conversely, immobilisation can have a negative impact on tendon healing, as it reduces the water and proteoglycan content in tendons, resulting in lower tensile strength and poor collagen cross-linking[87,88]. Therefore, a carefully balanced rehabilitation program that involves a combination of rest, targeted exercises, and mechanical loading is essential for optimising tendon healing.

Steroid therapy is another commonly used approach for treating tendinopathy. Corticosteroid injections are often employed to manage pain and inflammation in tendon injuries. While they can provide effective short-term relief, their long-term effects on tendon healing remain uncertain. Some studies suggest that steroid injections may lead to tendon degeneration, with reduced collagen organisation and increased collagen necrosis, making the tendon more susceptible to re-rupture[89]. However, other studies have shown that corticosteroids can improve short-term biomechanical properties by alleviating pain and promoting greater mobility, which can be beneficial for recovery, especially when other conservative treatments have failed to provide sufficient relief[90]. Despite these potential risks, corticosteroids are still widely used in clinical practice, especially when other conservative treatments have failed to provide sufficient relief. Their use should, however, be carefully considered and closely monitored due to the potential impact on tendon repair.

Autologous therapies, such as platelet-rich plasma (PRP) injections, have also been explored as potential treatments for tendon injuries. PRP is derived from the patient's blood and is rich in growth factors that have the potential to accelerate tissue healing. Although PRP therapy is considered to be relatively safe due to its autologous nature, its efficacy in tendon healing is still debated, with some studies showing positive outcomes while others report minimal or no

benefit[91,92]. Despite these mixed results, PRP remains an attractive option for treating tendon injuries, as it can enhance the body's natural healing processes.

Additional therapeutic options for tendon injuries include extracorporeal shockwave therapy (ESWT) and low-level laser therapy (LLLT)[93]. ESWT has been used effectively for treating conditions like Achilles tendonitis and calcific tendinopathy of the rotator cuff, with some studies showing it promotes neovascularisation, collagen metabolism, and enhanced tenocyte proliferation[94,95]. LLLT has also been shown to reduce inflammation, increase collagen synthesis, and promote tissue regeneration in tendons[96,97], though the exact mechanisms remain unclear, and the optimal treatment parameters are still under investigation.

Despite these advancements in tendon healing therapies, the process remains challenging. Tendons often heal with structural deficiencies, particularly those with repeated injuries or long-term tendinopathy. The healed tissue tends to be hypercellular, with smaller and misaligned collagen fibrils, which makes it more prone to re-injury. Chronic degeneration or rupture can also lead to an imbalance in collagen types, with an overproduction of type III collagen and a reduction in type I collagen. This imbalance compromises tendon strength and increases the risk of re-rupture. While current treatments, such as surgical repair, rehabilitation, and biologic therapies like PRP and shockwave therapy, offer benefits, tendon healing rarely restores the original mechanical properties, and the risk of re-injury remains high. As such, there is a pressing need for ongoing research to develop more effective therapeutic strategies to optimise tendon repair and improve healing outcomes.

1.5 Extracellular vesicles

EVs are particles naturally released from cells, delimited by a lipid bilayer, and incapable of replication. Once considered "waste products"[98], EVs are now recognised as critical mediators of intercellular communication and valuable biomarkers for disease. They have been detected in multiple body fluids, including plasma, serum, urine, saliva, cerebrospinal fluid, and cell culture supernatant[99]. EVs carry bioactive molecules such as proteins, lipids, mRNA, miRNA,

and DNA, facilitating long-distance cell communication and impacting numerous biological processes.

As a result of their diverse contents, EVs can play crucial roles in maintaining cellular homeostasis, immune modulation, tissue repair, and disease progression. They are implicated in a range of diseases, including cancer, neurodegenerative disorders, and cardiovascular conditions, highlighting their potential not only as biomarkers but also as therapeutic targets. Ranging in size from 30 nm to approximately 5 μm, EVs lack a functional nucleus, meaning they cannot replicate independently[100]. Their ability to carry bioactive cargo makes them ideal candidates for diagnostic and therapeutic applications. In addition to their diagnostic potential, EVs contribute to various physiological processes such as coagulation, immune response, and tissue regeneration, underlining their importance in both health and disease[101].

1.5.1 Biogenesis of EVs

The definition of EVs follows the minimal information for studies of EVs (MISEV 2018[102]) guidelines set by the International Society for Extracellular Vesicles (ISEV). According to these guidelines, EVs are defined as lipid-bilayer-enclosed particles released from cells that cannot replicate on their own. Based on their biogenesis pathways, size, and molecular composition, EVs are broadly categorised into three subtypes: exosomes, microvesicles (MVs), and apoptotic bodies[100] (Figure 1-6).

1. Exosomes: Exosomes are the smallest subtype of EVs, typically ranging from 30–150 nm in diameter[101]. They are generated through the inward budding of the plasma membrane, which forms early endosomes that mature into multivesicular bodies (MVBs)[103]. Inside the MVBs, small intraluminal vesicles (ILVs) are created, carrying cargo such as proteins (e.g., tetraspanins like CD9, CD63, and CD81), lipids, and nucleic acids (mRNA and miRNA). The formation of ILVs within MVBs is primarily regulated by the endosomal sorting complex required for transport (ESCRT), which is crucial for sorting cargo and driving membrane deformation. However, an ESCRT-independent mechanism for ILV formation has also been identified, where proteins like

CD63 and lipid metabolism enzymes participate in the process[104]. This alternative pathway provides flexibility in ILV biogenesis, mainly when ESCRT proteins are not fully functional. The MVBs can then either fuse with the lysosome, where their contents are degraded or with the plasma membrane, releasing the exosomes into the extracellular space[105]. Exosomes are critical for cell-cell communication as they transfer bioactive molecules to recipient cells, altering their function. For example, exosomes derived from dendritic cells present antigenic peptides to T cells, activating and modulating immune responses[106].

2. Microvesicles: Microvesicles, also called ectosomes or microparticles, range from 100 nm to 1 μm in diameter and are formed by outward budding of the plasma membrane[107]. This process is regulated by the activation of ADP-ribosylation factor 6 (ARF6), which stimulates phospholipase D, leading to the remodelling of the membrane. This membrane remodelling is followed by the recruitment of extracellular-signal regulated kinase (ERK) and myosin light chain kinase (MLCK), which ultimately induce the fission of the membrane and the release of MVs. MVs are enriched with various proteins, including ARF6, VAMP3, β1-integrin, and matrix metalloproteinases (MMPs), such as MT1-MMP and MMP9[108]. These proteins are involved in cell migration, tissue remodelling, and ECM degradation. MVs play a role in various physiological processes, including wound healing and immune responses, by transferring cargo that modulates cellular functions[105].
3. Apoptotic Bodies: Apoptotic bodies are released during apoptosis, a form of programmed cell death. This process involves complex signalling pathways that lead to cellular shrinkage, membrane blebbing, and the formation of apoptotic bodies. These vesicles, which range in size from 500 nm to 5 μm, contain cellular components, including organelles, DNA, and proteins[109]. The formation of apoptotic bodies is marked by the translocation of phosphatidylserine to the outer leaflet of the plasma membrane, which serves as a signal for phagocytic cells to clear the dying cells. Apoptotic bodies

play a vital role in removing apoptotic cells from tissues, thus maintaining homeostasis[107].

In addition to these well-established categories, other types of EVs have also been described, including large oncosomes, which are cancer cell–derived vesicles greater than 1 μm in diameter that play roles in tumour progression, and migrasomes, which are vesicular structures formed during cell migration and involved in intercellular signalling and organ development[110,111]. These non-canonical EVs highlight the structural and functional diversity within the EV landscape and continue to be a focus of active research.

Although the subtypes of EVs are distinguished by their biogenesis pathways, the terminology is flexible. Many studies use terms based on size or the cellular process with which they are associated rather than strict classification by biogenesis pathway. The term "exosome" is specifically used for vesicles released from the MVB pathway, while "microvesicles" refer to vesicles produced by the direct budding of the plasma membrane. However, there is no consensus on universal molecular markers to differentiate these subtypes clearly, and most studies categorise EVs broadly[102].

The ISEV recommends the use of the term "extracellular vesicle" as a generic descriptor, with operational extensions like "small EV" and "large EV" used as needed. However, terms like "small" and "large" should be used cautiously, as there is no universally agreed-upon size classification, and different separation techniques can yield EV populations with overlapping size distributions[112].

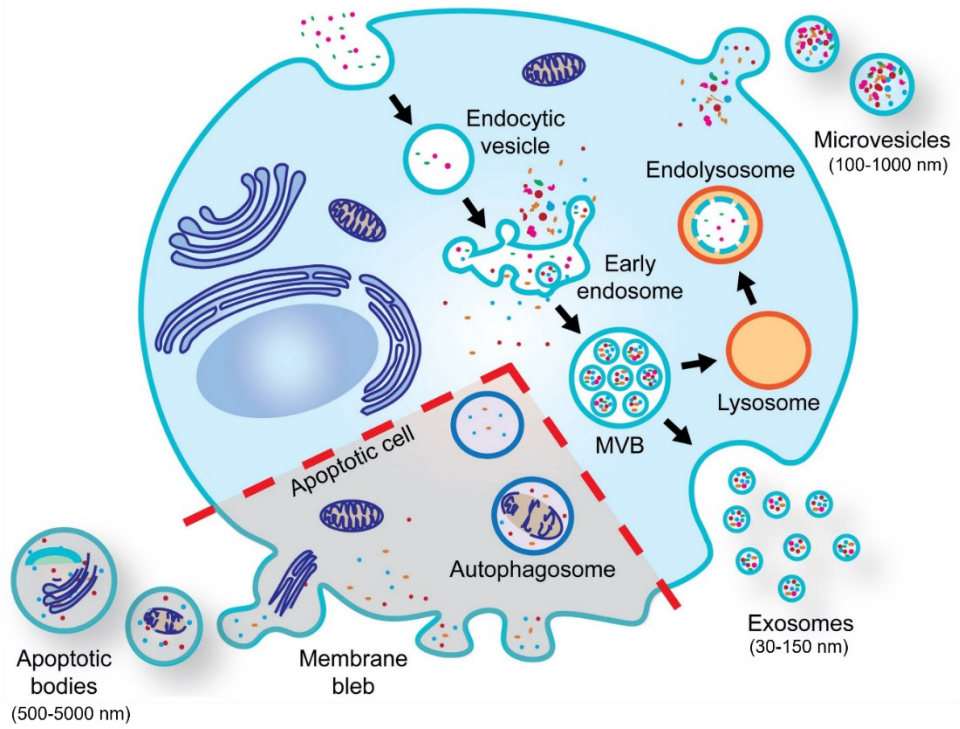


Figure 1-6. Biogenesis of extracellular vesicles. The biogenesis pathways of the three major subtypes of EVs are illustrated. Exosomes are formed through the endosomal pathway, originating from early endosomes that mature into MVBs. Microvesicles are produced by direct budding from the plasma membrane. Apoptotic bodies, released during apoptosis, originate from membrane blebbing. Image reprinted and adapted from Shahi et al., 2024[113], under CC BY 4.0 License.

1.5.2 Composition of EVs

The composition of EVs is complex and varies based on the cell type from which they are derived. However, several key components are commonly found in all kinds of EVs, including proteins, nucleic acids and lipids[107] (Figure 1-7).

- Proteins: The protein content of EVs can be broadly classified into structural proteins, which contribute to EV formation and stability, and cargo or 'payload' proteins, which mediate biological functions by being actively loaded into EVs and are specific to the cell type of origin[101]. Structural proteins are essential for the biogenesis, stability, and release of EVs. These include tetraspanins (CD9, CD63, CD81, and CD82), which serve as markers of exosomes, and MVB-associated proteins such as TSG101, ALIX

and Rab proteins, which regulate the formation and trafficking of EVs. Additionally, cytoskeletal proteins like actins, cofilin-1, moesin, myosin, tubulin, and vimentin support EV structure and assist in their release from parent cells. They also include cell adhesion molecules (e.g., integrins), which mediate EV targeting and uptake, stress-related proteins (e.g., heat shock proteins like HSP70 and HSP90) and signalling proteins (e.g., kinases), which assist in EV formation, protein folding, and cargo sorting[114]. These structural proteins ensure that EVs maintain their integrity, size, and appropriate surface markers, influencing their uptake by recipient cells. However, once EVs are released into the extracellular space or introduced into a biological system, they rapidly acquire a "protein corona", a layer of adsorbed proteins, lipids, and biomolecules from their surrounding environment[115]. This corona affects EV stability, biodistribution, cellular uptake, and immunogenicity, ultimately shaping their biological function[116]. The composition of this corona depends on the biological milieu and can significantly alter EV targeting efficiency or immune clearance[115,117]. Understanding and controlling the EV corona is an emerging area of research, particularly in the context of EV-based therapeutics, where modifications to the corona could improve target specificity or enhance therapeutic efficacy.

In contrast, payload proteins define EVs' functional roles and vary depending on the cell of origin. These include growth factors and cytokines (e.g., TNF-α, VEGF, epidermal growth factor (EGF), and TGF-β), which regulate inflammation, tissue repair, and cell signalling[118]. Enzymes such as fatty acid synthase, phosphoglycerate kinase, ATPase, and aldehyde reductase are involved in metabolic functions, while histones, ribosomal proteins, and ubiquitin contribute to gene expression regulation and protein turnover[119]. EVs also contain matrix metalloproteinases like MT1-MMP and MMP13, which play key roles in ECM remodelling and cell migration[120,121]. Furthermore, antigen presentation-related proteins such as MHC class I and II/peptide complexes facilitate immune responses, and apoptotic regulators like Fas ligand (FasL) and TNF-related

apoptosis-inducing ligand (TRAIL) contribute to cell death signalling pathways[105,107]. Iron transport proteins such as the transferrin receptor and other immune-related molecules further expand the diverse functional roles of EVs[118].The diverse protein composition of EVs highlights their multifunctional roles in intercellular communication, immune modulation, tissue repair, and disease progression.

- Nucleic acids: EVs carry various nucleic acids, including microRNAs (miRNAs), mRNA, long noncoding RNAs (lncRNAs), piwi-interacting RNAs (piRNAs), and circular RNAs (circRNAs), which play vital roles in gene regulation and protein production in recipient cells[122]. MiRNAs are the most abundant RNA type in EVs, particularly in human plasma[123], and have been linked to processes such as immune modulation and cancer progression. EVs also contain lncRNAs and circRNAs, which influence biological processes like tumour progression and may serve as biomarkers or therapeutic targets[122]. Additionally, DNA has been reported in small EVs, particularly in MVB-dependent exosomes. Recent studies suggest that nuclear DNA may be transported either through the exosome biogenesis pathway[124], or via an amphisome-dependent mechanism[125], suggesting that EVs can also carry genetic material beyond RNA, enhancing their potential role in intercellular communication and genetic transfer.

- Lipids: EVs require their lipid composition for essential structural integrity, vesicle fusion, and membrane stability. Derived from the plasma membrane, EVs carry lipids such as cholesterol, sphingomyelin, ceramide, and phosphatidylserine, which are essential for maintaining their function[126]. Exosomes and MVs show an enrichment of sphingomyelin, phosphatidylserine, and cholesterol when compared to total cell membranes. EVs may also contain functional lipolytic enzymes that generate bioactive lipids capable of influencing surrounding cells[127]. Ceramide is particularly abundant in EVs and plays a key role in vesicle formation. In some EV populations, lipids like gangliosides and lactosylceramide have been identified as enriched[122]. EVs' lipid composition often reflects lipid rafts in the plasma membrane, with associated proteins

such as GPI-anchored proteins and flotillins. Recent studies suggest that the presence of phosphatidylserine on the outer leaflet of EV membranes may be a distinctive feature for EV characterisation, aiding in detection and isolation, with applications such as cancer detection biomarkers[128].

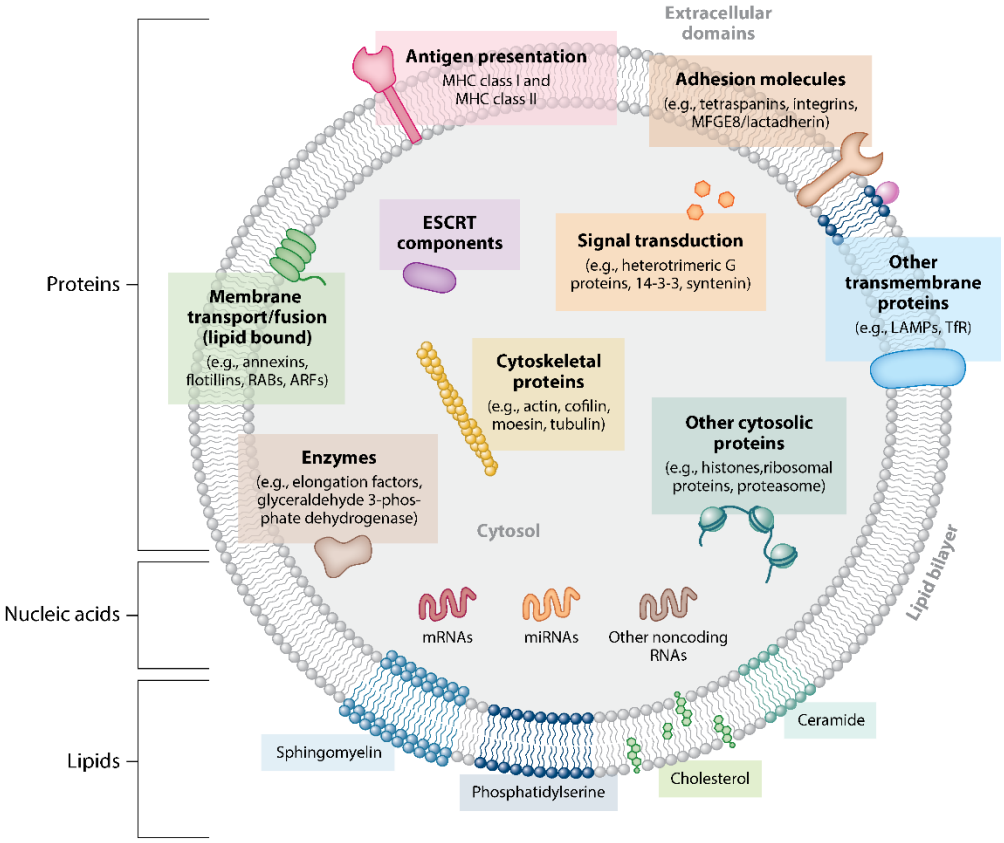


Figure 1-7. Composition of extracellular vesicles. This figure highlights the key components of EVs, including proteins involved in antigen presentation, adhesion, membrane transport, signalling, and cytoskeletal functions. The lipid bilayer contains sphingomyelin, phosphatidylserine, cholesterol, and ceramide. EVs also carry nucleic acids such as mRNA, miRNA, and other noncoding RNAs, which contribute to their role in intercellular communication. Image reprinted from Colombo et al., 2014[101] with permission from Annual Reviews, Inc.

1.5.3 Role of EVs in intercellular communication

EVs are essential mediators of intercellular communication and play a significant role in various biological processes. The bioactive molecules carried by EVs, including proteins, lipids, and nucleic acids, can alter recipient cells' gene expression and function, driving cellular activities

such as immune modulation, cell differentiation, tissue repair, and tumour progression[105]. Some of the key roles of EVs are as follows:

- Immune regulation: EVs are involved in immune regulation by carrying pro-inflammatory mediators that influence immune responses during infections, autoimmune diseases, and cancer. They can deliver antigens to antigen-presenting cells, initiating immune responses. For instance, EVs derived from dendritic cells and macrophages play a crucial role in antigen presentation[129]. Additionally, T-cell-derived EVs can modulate immune cell activation, apoptosis, and immune tolerance, depending on the context of the immune response[130]. EVs can also influence the balance between immune activation and suppression, which is essential in maintaining immune homeostasis.
- Tissue repair: EVs are integral to tissue regeneration and repair by delivering pro-angiogenic factors, growth factors, and matrix remodelling enzymes to the injury site. In regenerative medicine, EVs derived from stem cells, such as MSCs, mimic the regenerative effects of the parent stem cells themselves[131]. These EVs promote tissue healing by enhancing cellular migration, collagen synthesis, and matrix remodelling. Their role in tissue regeneration also extends to promoting wound healing, organ repair, and preventing fibrosis, further establishing their therapeutic potential[105,132].
- Tumour progression: In cancer, EVs are often protumorigenic, meaning they facilitate tumour cell migration, angiogenesis, and metastasis. Tumour-derived EVs carry tumour-specific antigens and can modulate immune responses, influencing tumour immunity. EVs can either promote or suppress immune responses to tumours, depending on their cargo and the type of immune cells they interact with[105]. By transferring oncogenic proteins, RNAs, and lipids, EVs contribute to the formation of a pro-tumorigenic microenvironment that facilitates cancer progression[113].
- Cellular waste management: EVs help cells remove waste by secreting cytosolic materials, such as DNA fragments and proteins, from stressed or damaged cells. This

process helps prevent the accumulation of potentially harmful substances, maintaining cellular homeostasis. For instance, EVs can excrete DNA fragments in response to DNA damage, preventing activation of the DNA-sensing machinery that could lead to apoptosis[133]. EVs can carry viral DNA to trigger immune responses during viral infections, reducing infection spread[113].

- Intercellular communication and signalling: EVs are essential for intercellular communication, transporting biomolecules to distant cells, including those in hard-to-reach organs such as the brain, via crossing the blood-brain barrier[134]. Through receptor-ligand interactions or cargo transfer, EVs influence gene expression and signalling pathways in recipient cells. EVs regulate the modulation of Wnt, Hedgehog, and Notch signalling pathways, crucial for development and cellular differentiation[113,135].
- Neuroprotection and nervous system function: EVs are involved in neuroprotection, particularly in neurodegenerative diseases. In the brain, microglial and neuronal cells secrete EVs that influence neuronal communication and synaptic activity[105,136]. For instance, EVs from brain cells aid in the clearance of aggregated proteins, such as polyglutamine (polyQ) aggregates in Huntington's disease, promoting excretion and reducing intracellular accumulation[137].
- Coagulation and haemostasis: EVs play a role in coagulation and haemostasis, and they are involved in both procoagulant and anticoagulant activities depending on their content and the physiological context. EVs contribute to blood clotting and the formation of new blood vessels during tissue repair. EVs derived from platelets and immune cells promote clot formation and wound healing, assisting in vascular remodelling[113].

EVs also hold potential applications in gene therapy, drug delivery, and diagnostic markers. They act as powerful tools for therapeutic applications because they function in physiological and pathological processes, creating beneficial opportunities for future use.

1.6 Extracellular vesicle isolation

The expanding interest in EVs as biomarkers has led to rapid research growth that has developed several isolation techniques. However, many of these methods are poorly standardised, resulting in inconsistent experimental outcomes. EVs are heterogeneous in size, origin, and molecular constituents, with significant overlap in size and phenotype across different populations[138]. Experiment reproducibility and cross-study comparison face challenges because of the non-standardised approach to EV isolation. To address these challenges, strategies for isolating EVs can be categorised into density-based, size-based, immunoaffinity-based methods, precipitation reagents, and emerging microfluidic technologies (Figure 1-8). These methods must be combined to obtain highly pure EVs with high yield and quality while minimising contamination from viral particles and protein aggregates, lipoproteins and other aggregates[139].

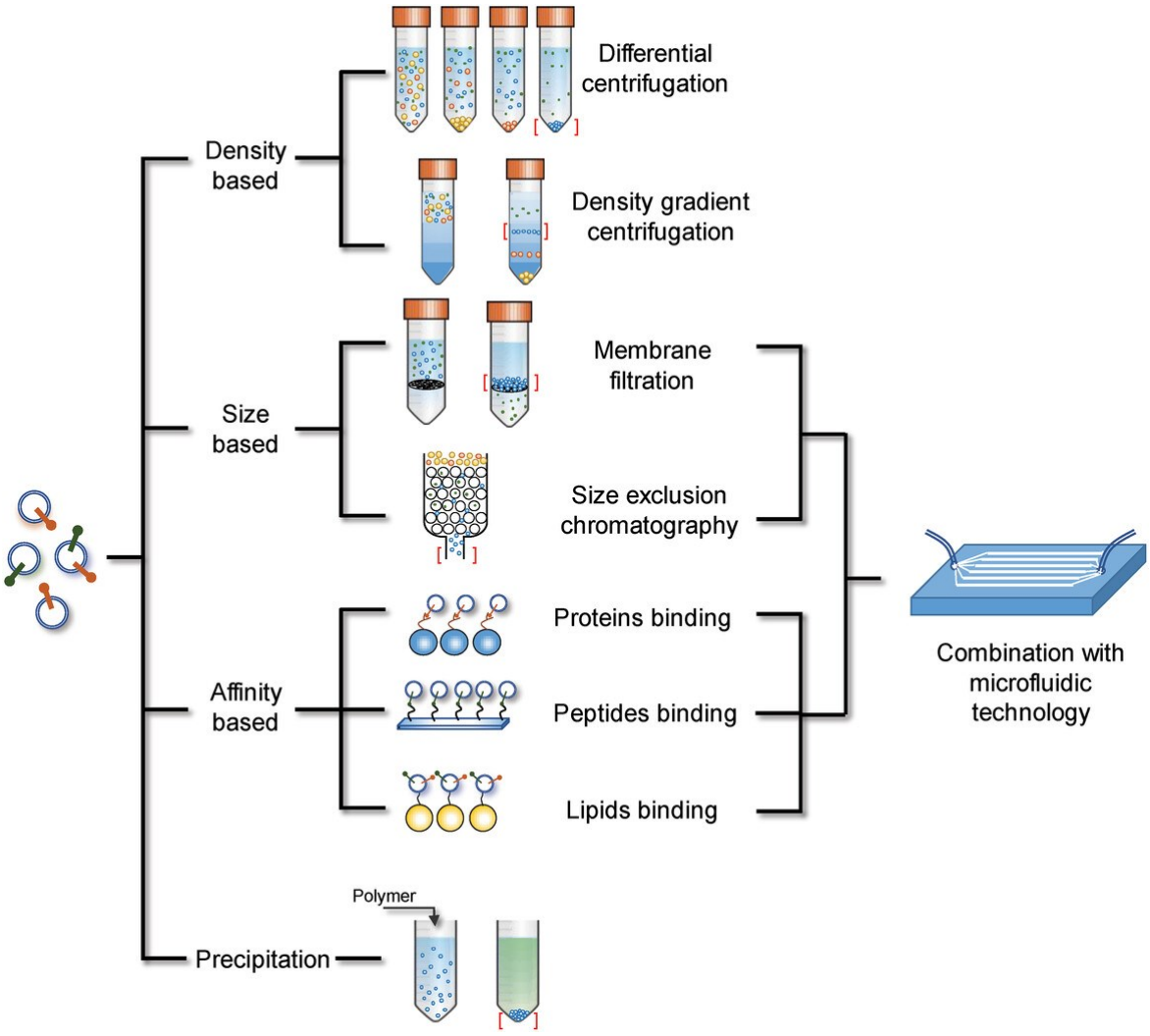


Figure 1-8. Overview of EV isolation methods. This diagram categorises isolation techniques into density-based, size-based, affinity-based methods, and polymer precipitation, each including specific methods like centrifugation, filtration, and immunoaffinity capture. The flowchart also highlights the integration of microfluidic technology. Image reprinted from Wang et al., 2019[140] with permission from Wiley.

1.6.1 Density-based isolation

Density-based methods rely on the differential density of EVs to isolate them from other cellular components. These techniques include ultracentrifugation and density gradient ultracentrifugation.

Ultracentrifugation is the most commonly used technique and is widely regarded as the "gold standard" for EV isolation due to its historical precedence, broad accessibility in research laboratories, and ability to isolate relatively pure vesicle populations without requiring

specialised reagents. The technique involves a series of differential centrifugation steps to separate EVs based on their size and density, starting with low centrifugal force to remove cellular debris, followed by a higher force (e.g.,100,000 ×g) to concentrate the EVs. Though widely used, ultracentrifugation is time-consuming, requires expensive equipment, and has limitations such as low recovery rates and the requirement for a large sample volume[141]. Moreover, contamination by proteins and lipoproteins can occur due to the lack of specificity in the separation[142].

Density gradient ultracentrifugation overcomes some of these limitations by using a density gradient (e.g., sucrose or iodixanol) to isolate EVs at specific density layers, typically between 1.13 and 1.19 g/mL[143]. This method enhances the purity of isolated EVs, separating them from contaminating proteins and aggregates. However, it still requires ultracentrifuge equipment and has a similar drawback of lengthy processing times and the potential for sample degradation[140].

1.6.2 Size-based isolation

The current research literature offers numerous protocols for EV isolation utilising the separation of micro/nanoparticles according to their size, including ultrafiltration, size-exclusion chromatography (SEC), and field-flow fractionation (FFF).

Ultrafiltration is one of the most popular size-based methods, in which EVs are separated from larger particles and proteins through membranes with specific pore sizes, typically between 0.2 and 0.45 μm[144]. This technique is cost-effective, relatively simple to perform, and has a high throughput, making it useful for large sample volumes. However, several limitations exist. EVs and their protein components might attach to membrane surfaces, thus decreasing recovery efficiency. Furthermore, the filter may become clogged with larger aggregates, resulting in sample loss. Additionally, proteins that are smaller than the membrane pores may pass through, causing potential contamination of the isolated EVs[139].

Size-exclusion chromatography separates particles based on their size using a column filled with porous beads[145]. Smaller particles, such as exosomes, enter the pores, causing them to have a longer retention time in the column, while larger particles are eluted faster. SEC has the advantage of preserving the biological activity of EVs due to its gentle, gravity-driven flow. It also has high reproducibility and sensitivity for EV isolation. However, SEC can be time-consuming and may require additional techniques, such as ultracentrifugation, to further concentrate EVs. It may also require specialised equipment, such as dedicated columns and buffers[141].

Field-flow fractionation, including asymmetrical flow field-flow fractionation (AF4), is a less commonly used but promising size-based technique. FFF applies a perpendicular force to the sample flow, causing particles to move toward a boundary at different rates based on size. This technique allows for broad size range separation, providing high purity with minimal sample disruption. However, FFF is complex, requires specialised equipment, and is often less accessible than other methods[141].

1.6.3 Immunoaffinity-based isolation

Immunoaffinity-based isolation methods capture EVs by utilising surface-specific proteins, such as tetraspanins (e.g., CD9, CD63, CD81), and other biomarkers (e.g., EpCAM, EGFR)[140]. These surface proteins are often targeted by antibodies that bind to them, allowing EVs to be isolated through specific interactions[146]. In magnetic bead-based immunoaffinity capture, antibodies specific to surface markers are conjugated to magnetic beads. The beads bind to the EVs, and the complexes are then isolated using a magnet. This method allows for high specificity in capturing targeted EV subsets and is highly effective when isolating exosomes from complex mixtures. One advantage is that this method can provide a high yield of pure EVs and is more efficient than ultracentrifugation. However, it can be more expensive and requires careful optimisation to avoid non-specific binding, which could lead to contamination[142].

1.6.4 Polymer precipitation

Polymer precipitation uses polymeric reagents like polyethene glycol (PEG) to reduce the solubility of EVs, causing them to precipitate out of the solution. Commercial kits, such as ExoQuick and Exo-Spin, are widely used for this purpose[140]. This method is less labour-intensive than ultracentrifugation and often yields a higher quantity of EVs in less time. Precipitation-based methods provide cost-effective scalability, which makes them well-suited to large-scale production needs. However, the main disadvantage of these methods is the lower purity. The reduced solubility of proteins, lipoproteins, and other contaminants leads to their co-precipitation with EVs and impairs subsequent analysis procedures. Additionally, some polymer precipitation kits can be expensive and may not provide the same level of purity or specificity as other isolation methods.

1.6.5 Microfluidic technologies

Microfluidic technologies are an emerging field for EV isolation, offering precise, rapid, and cost-effective solutions. These devices, often referred to as "labs on a chip," work by using small-scale fluid channels with integrated features to manipulate the flow of fluids and isolate particles such as EVs[142]. Microfluidic isolation typically uses immunoaffinity capture or size-based separation techniques, where antibody-coated surfaces or specialised membranes isolate EVs directly from biological samples. Microfluidic platforms have been shown to be faster, require smaller sample volumes, and use fewer reagents than traditional methods. For example, the ExoChip microfluidic device uses antibodies to capture exosomes from serum in a single step. The potential for rapid, on-site diagnostics is a significant advantage of microfluidic technology, especially for point-of-care applications[140]. However, these devices are still in the early stages of development and often require specialised equipment, making them less accessible for routine use in some labs. The technology is also evolving, with ongoing research focused on optimising microfluidic devices' sensitivity, scalability, and versatility.

Therefore, the selection of EV isolation techniques depends on research requirements, sample volume, purity yield, and specific experimental needs. Multiple research methods exist for EV isolation, each with its benefits and drawbacks, which necessitate the combination of techniques to achieve optimal results. The following table presents both the advantages and disadvantages of each isolation procedure (Table 1).

Table 1. Comparison of commonly used isolation methods for extracellular vesicles.

Method	Purity	Advantages	Limitations
Ultracentrifugation	Medium	Gold standard High throughput Cost-effective	Time-consuming Expensive equipment
Density gradient ultracentrifugation	High	High purity Effective for small sample volumes	Time-consuming Complex protocol
Ultrafiltration	Medium	Simple and fast Scalable Lower cost	Risk of contamination Membrane clogging
Size-exclusion chromatography	High	High purity High yield	Time-consuming Lower throughput
Field flow fractionation	High	Versatile Minimal sample loss	Expensive equipment Time-consuming
Immunoaffinity capture	High	Highly specific High purity Easy to perform	Expensive Limited to known markers
Polymer co-precipitation	Low	Simple and fast Scalable	Low purity Lack of specificity

		Cost-effective	
Microfluidic isolation	Strategy-dependent	Fast and efficient High precision	Expensive Expertise needed Limited scalability

1.7 Extracellular vesicles characterisation

Accurate identification and functional characterisation of EVs, free from co-isolated contaminants, is critical for understanding their biological roles, diagnostic potential, and therapeutic applications and essential for their practical use. EVs are complex and heterogeneous in size, origin, and molecular composition, requiring a combination of analytical techniques for their complete characterisation[147].

The ISEV, in its MISEV guidelines, emphasises the need for standardised approaches to EV studies. These guidelines recommend that each EV preparation should be quantified based on the source (e.g., number of secreting cells, volume of biofluid, or tissue mass) and characterised for abundance (total particle number and protein or lipid content). EVs should also be tested for the presence of components associated with specific EV subtypes and the potential co-isolation of non-vesicular components[102,112,148].

1.7.1 Size and morphology characterisation

The size and morphology of EVs are commonly determined using high-resolution imaging techniques. Transmission Electron Microscopy (TEM) provides detailed images of the size, shape, and structure of EVs and can also be used with immunogold labelling to detect specific surface markers. TEM is one of the most widely used techniques for EV morphology but requires extensive sample preparation, which may cause some distortions. Similarly, Scanning Electron Microscopy (SEM) enables researchers to examine EV surface features through high-resolution imaging, although extensive sample preparation is needed. Atomic Force

Microscopy (AFM) is another technique that measures the surface properties of EVs and can assess the mechanical stiffness of individual vesicles, making it valuable for understanding EV biophysics. However, AFM, like TEM and SEM, does not provide direct concentration measurements[139].

Cryo-TEM allows for the imaging of EVs in their near-native state by freezing samples without the need for dehydration or fixation. This technique eliminates the distortions typically caused by traditional TEM sample preparation, providing more accurate structural details of EVs, including their membrane integrity and internal structure. Cryo-TEM is especially useful for visualising intact EVs without the artefacts that can occur with conventional electron microscopy techniques[149].

1.7.2 Concentration and size distribution

Nanoparticle Tracking Analysis (NTA) is widely used to measure EVs' concentration and size distribution. NTA tracks the Brownian motion of individual particles to give complete information about particle size, concentration and distribution, measuring sizes up to 30 nm. The technique offers a quick and straightforward analysis, making it particularly useful for high-throughput measurements. NTA captures video of the particles moving in suspension and then analyses their movement to calculate their size based on the Stokes-Einstein equation[150]. It also enables real-time measurements of size distribution, concentration data, and particle phenotypes when combined with fluorescent labelling. However, careful sample preparation remains essential to avoid contamination and minimise errors in size distribution since the presence of other particles may interfere with accurate measurements.

Another technique used for EV characterisation is Dynamic Light Scattering (DLS), which measures EVs' size and zeta potential by analysing light scattering fluctuations caused by particle movement in a liquid. While DLS is effective for mono-disperse particles, it can struggle to resolve heterogeneous EV populations and may not provide accurate measurements when the sample contains a wide range of particle sizes[151].

An emerging technique, tunable resistive pulse sensing (TRPS), is gaining attention for measuring the size distribution and concentration of EVs. Using a nanopore, TRPS detects transient changes in ionic current as particles pass through, allowing for high-resolution particle characterisation. TRPS is particularly useful for analysing larger EVs, such as microvesicles, but may detect fewer small EVs compared to NTA[141].

1.7.3 Surface marker, protein and lipid profiling

Characterising the molecular content of extracellular vesicles is crucial for understanding their function, origin, and potential applications. Surface marker analysis, protein profiling, and lipidomic analysis are key components of EV characterisation, and various techniques are employed to evaluate these molecular components. A standard method for analysing surface proteins and biomarkers on EVs is Western Blotting. Western blot is used to detect and quantify specific proteins, such as tetraspanins (CD9, CD63, CD81), cytoskeletal proteins, or other proteins that are known to be present in EVs. This technique is widely used for its specificity and ability to identify multiple proteins within a single sample. However, high-quality antibody reagents and optimisation are required to ensure accurate detection. Enzyme-linked immunosorbent assay (ELISA) is another method frequently employed for protein quantification, especially for surface markers. ELISA is a sensitive, quantitative method used to measure the presence of proteins on EVs by using antigen-antibody interactions. Both techniques are crucial for understanding the protein content of EVs and their role in cellular communication, particularly in disease processes like cancer and neurodegenerative diseases[139,149].

In addition to proteins, the lipid content of EVs plays an essential role in their structural integrity and function. Lipidomics is the study of the lipid composition of EVs and involves techniques such as mass spectrometry and thin-layer chromatography. These methods allow for the identification and quantification of lipid species such as phospholipids, sphingolipids, and cholesterol, which are integral to the bilayer structure of EVs. Lipidomics can provide valuable insights into the biological processes that govern EV formation, cargo packaging, and

membrane interactions, which are critical for their potential use in drug delivery and as biomarkers. The lipid composition present in EVs can uncover findings about their cell origins together with their release-based pathways[141,152].

1.7.4 RNA profiling

Molecular profiling of the RNA content in extracellular vesicles, including microRNAs (miRNA) and messenger RNA (mRNA) fragments, is essential for understanding the functional roles of EVs in cellular communication and disease progression. Techniques such as quantitative reverse transcription PCR (qRT-PCR), next-generation sequencing, and microarray analysis are commonly used to evaluate the RNA cargo of EVs. These methods are essential for identifying the cellular origin of EVs and assessing their potential as diagnostic biomarkers for various diseases, including cancer, cardiovascular diseases, and neurodegenerative disorders[139].

1.7.5 Emerging techniques

In addition to the conventional techniques, emerging technologies such as surface plasmon resonance (SPR)[153], Raman spectroscopy[154], and microfluidic devices[149] are being explored for their potential in EV characterisation. SPR enables real-time detection of protein interactions on the surface of EVs, while Raman spectroscopy offers molecular-level insights into the composition of EVs, including lipids and proteins. Microfluidic devices provide a high-throughput, label-free approach for isolating and analysing EVs with minimal sample volumes, offering great potential for clinical applications[139].

In summary, a precise characterisation of EVs is essential for their application in diagnostics and therapeutics. Combining techniques, including imaging, particle tracking, and molecular profiling, provides crucial insights into EV size, morphology, and molecular content. Multiple complementary methods combined with regular research-based innovation in EV characterisation will produce vital results needed for clinical EV adoption.

1.8 New approaches for tendon healing

Tendon injuries are often difficult to treat due to the tendons' limited regenerative properties and complicated structural characteristics. While traditional treatment methods, including surgery, physical therapy, and medications, have been used to manage tendon injuries, they often fail to restore full function and prevent re-injury. However, with the rapid progress in regenerative medicine and tissue engineering, new approaches are emerging to promote tendon healing by enhancing tissue repair and accelerating recovery.

1.8.1 Stem cell therapies

Stem cell-based therapies have become a cornerstone of regenerative medicine due to their ability to regenerate damaged tissues.

MSCs are widely used in tendon repair due to their high proliferative capacity and ability to differentiate into tenocytes, the specialised cells responsible for tendon tissue formation[155,156]. MSCs can be derived from a variety of sources, including bone marrow, adipose tissue, umbilical cord, foetal membranes and synovial fluid, and recent studies have also identified MSCs-like populations from tendon tissue itself (tendon stem/progenitor cells, TSPCs) in different species[24,157–161]. Among these, bone marrow-derived MSCs (BM-MSCs) and adipose-derived MSCs (AD-MSCs) are the most extensively studied due to their well-documented regenerative potential[162,163]. BM-MSCs are typically isolated through bone marrow aspiration from the iliac crest. At the same time, AD-MSCs are obtained via liposuction procedures and are valued for their high yield and less invasive extraction methods. MSCs are characterised by their ability to adhere to plastic, their expression of surface markers (CD73, CD90, and CD105), and their lack of haematopoietic markers (CD34, CD45, CD14, and HLA-DR)[164], as defined by the International Society for Cell and Gene Therapy (ISCT) guidelines[164,165]. Furthermore, they exhibit self-renewal ability, immunomodulatory properties, and differentiation potential into multiple cell lineages, including adipogenic, osteogenic, and chondrogenic lineages[163]. Their immunomodulatory functions arise from their secretion of anti-inflammatory cytokines and their ability to interact with immune cells such as T-cells, B-cells,

and macrophages, making them valuable candidates for allogeneic therapy[166]. Moreover, the allogeneic MSC therapy model provides off-the-shelf donor cell solutions for regenerative medicine because it does not need patient-specific cell harvesting or expansion like autologous MSC transplantation. However, additional research is required to identify solutions for the issues involving immune compatibility, donor variability, and rejection potential[167,168]. In tendon repair, MSCs not only contribute to tissue regeneration by differentiating into tendon cells but also secrete bioactive components like growth factors, cytokines, and EVs that modulate the local healing environment[162,163]. MSC-based therapies stimulate tendon healing by enhancing cell proliferation, migration, and differentiation at the injury site[2]. They also secrete key signalling molecules such as TGF-β1 and VEGF, which promote collagen production, angiogenesis, and tissue remodelling[169].

In addition to MSCs, pluripotent stem cells (PSCs), such as embryonic stem cells (ESCs) and induced pluripotent stem cells (iPSCs), also show promise for tendon repair. ESCs have the potential to differentiate into any cell type, offering significant regenerative capacity. Research has demonstrated that human ESCs, when differentiated into MSCs, can integrate into tendon scaffolds and enhance tendon regeneration[170]. Similarly, iPSCs, which are reprogrammed from adult somatic cells, offer the advantage of low immunogenicity and may be a viable source of cells for tendon repair therapies. For example, iPSC-derived neural crest stem cells have been shown to accelerate tendon repair in animal models without the risk of ectopic tissue formation[171]. However, challenges remain in optimising the differentiation potential of these cells and ensuring their long-term efficacy for tendon regeneration.

Amniotic epithelial stem cells (AECs), derived from the amniotic membrane, represent another promising source for tendon regeneration. These cells exhibit multipotent properties and can differentiate into tendon-like cells, promoting collagen synthesis, angiogenesis, and ECM remodelling. AECs also possess immunomodulatory properties, making them an attractive candidate for tendon repair without the ethical concerns associated with other stem cell types[172,173].

Moreover, culturing stem cells under optimal conditions, such as hypoxic environments, has been shown to increase their regeneration capacity. Research indicates that hypoxic conditions prevent stem cells from losing their stem potential and enhance their differentiation into tendon cells[9,174,175].

While stem cell therapies offer great potential for tendon healing, challenges remain regarding selecting the most suitable stem cell types and the safe and efficient delivery of stem cells to the injury site. These challenges include immune rejection, especially when using stem cells from non-autologous sources, and ethical concerns in the case of embryonic stem cells, which raise moral and legal issues related to their use. Moreover, the clinical implementations of stem cell therapies face regulatory barriers because of non-standardised protocols and concerns about stem cell therapy's long-term safety, duration and patient-to-patient result consistency[167].

Several preclinical studies have shown that stem cells, particularly MSCs, improve tendon healing with increased collagen production, enhanced tissue integration, and improved mechanical properties[162,176]. Although early clinical trials have demonstrated promising outcomes, including improved pain relief and functional recovery, stem cell-based therapies' long-term efficacy and safety for tendon injuries require further investigation[174,177]. More rigorous studies are needed to optimise these approaches for clinical application.

1.8.2 Bioactive mediators

Bioactive mediators, including growth factors and EVs, play a critical role in tendon healing by influencing cellular behaviour and promoting tissue regeneration. Growth factors such as TGF-β, IGF-1, VEGF, and FGF are essential for regulating various biological processes during tendon repair, including cell proliferation, migration, ECM synthesis, and angiogenesis[1]. These growth factors, together with BMPs (BMP-12, 13, 14), connective tissue growth factor (CTGF) and PDGF, are also involved in tenogenesis and the regulation of progenitor cell biology[7]. They are synthesised and secreted by various cells, such as inflammatory cells, platelets, fibroblasts, and tendon progenitor cells. These factors bind to receptors on cell membranes,

triggering intracellular pathways that influence DNA synthesis, cell differentiation, matrix synthesis, and cell migration.

After injury, the release of growth factors is triggered by platelets and activated immune and resident tendon cells, leading to the recruitment of inflammatory cells (e.g., neutrophils and macrophages) and fibroblast-like cells, as well as the activation of tendon progenitor cells near the injury site. Mechanical loading on the injured tendon can also modulate growth factor production and release, highlighting the importance of a dynamic healing environment[8,57].

Using a "growth-factor cocktail" approach, where multiple growth factors are administered together in a temporal and spatial distribution that mimics the body's natural healing process, has been shown to be more effective than using a single growth factor[178]. For example, TGF-β and VEGF stimulate collagen synthesis and angiogenesis, while factors like PDGF enhance cell recruitment to the injury site[179]. This combined strategy helps to optimise tendon healing by supporting multiple stages of the regenerative process[4]. A physiological tendon-inductive microenvironment requires various growth factors, released in a specific temporal pattern and optimised ratio, to promote successful healing[93]. These growth factors can be delivered directly to the injury site through various delivery methods, such as local injections, coated sutures, or scaffold-based systems[7]. Scaffold-based delivery offers the advantage of sustained release, providing a controlled environment for optimal growth factor action.

While growth factors act as key signals for tendon repair, EVs, secreted by MSCs and other cell types, offer an additional layer of regenerative potential[168,180,181]. These nanoscale vesicles carry proteins, lipids, and nucleic acids, including miRNAs, which regulate key processes such as inflammation, ECM remodelling, and cellular differentiation. MSC-derived EVs have been shown to enhance tendon healing by modulating inflammation, promoting ECM synthesis, and improving the cellular response to injury[131,182,183]. EVs also help to reduce fibrosis and scarring, which are common complications in tendon healing[184]. The synergy between growth factors and EVs in tendon regeneration is increasingly recognised. Growth factors can act through direct receptor-ligand interactions, stimulating cell proliferation, differentiation, and ECM

production. Meanwhile, EVs can deliver bioactive molecules like growth factors, cytokines, and miRNAs to recipient cells, amplifying the regenerative signals and enhancing the effects of growth factors. For example, EVs derived from MSCs can deliver TGF-β1 and VEGF to tendon cells, promoting collagen synthesis and angiogenesis while simultaneously reducing inflammation and modulating the immune response[184–186]. This collaborative action between growth factors and EVs creates a more comprehensive and coordinated regenerative environment that accelerates tissue repair.

Gene therapy is also an emerging approach with significant potential for tendon healing. By allowing for targeted, localised production of growth factors and other bioactive molecules at the site of injury, gene therapy provides a way to modulate the healing process at a molecular level[8]. The delivery of genes encoding growth factors like TGF-β1 or VEGF using viral or non-viral vectors can directly influence cell behaviour, promoting tissue regeneration and improving tendon repair[93]. Gene therapies also have the potential to provide sustained production of bioactive molecules, thus enhancing the healing process over a more extended period. Although still in its early stages, gene therapy is an exciting addition to bioactive mediator-based therapies and may complement the use of growth factors and EVs in tendon healing.

1.8.2.1 Growth-differentiation factor 5

Growth differentiation factor 5 (GDF-5), also known as BMP-14, is a member of the TGF-β superfamily and has been extensively studied for its role in skeletal development. Beyond its well-established functions in bone and cartilage formation[187,188], GDF-5 has gained attention due to its potential therapeutic applications in tendon healing and regeneration. It plays a pivotal role in modulating the cellular environment within tendons, influencing cell proliferation, migration, and differentiation[189].

GDF-5 exerts its effects primarily through the activation of Smad-dependent signalling pathways. Upon binding to its receptors, GDF-5 induces the phosphorylation of Smad1, Smad5, and Smad8, which subsequently form a complex with Smad4 and translocate into the nucleus[189]. This complex regulates the expression of genes associated with ECM remodelling

and tenogenic differentiation, including key markers such as SCX, TNMD and COL1A1. In addition to the canonical Smad pathway, GDF-5 can also activate non-Smad signalling cascades, such as the p38 mitogen-activated protein kinase (MAPK) and ERK pathways, which further contribute to tendon cell survival, proliferation, and matrix production[190].

Preclinical studies have demonstrated that GDF-5 promotes tendon healing by enhancing fibroblast proliferation, increasing collagen synthesis, and improving the structural organisation of newly formed tendon tissue[191–193]. These studies also report improved biomechanical properties of healing tendons, such as increased tensile strength and enhanced collagen alignment. *In vitro* experiments using MSCs cultured with GDF-5 further support these findings, as they exhibit upregulation of tenogenic markers such as SCX and TNMD, indicating its potential to drive tenocyte differentiation[194–197].

Despite promising findings, optimising the delivery of GDF-5 remains a focus of ongoing research to ensure sustained and localised effects at the tendon injury site. Scaffold-based systems have been explored to enhance their stability and bioavailability[198–200], while investigations into optimal dosage and potential synergies with other growth factors such as TGF-β and VEGF continue[189]. Due to its capacity to promote tenogenic differentiation, stimulate ECM remodelling, and improve tendon mechanical properties, GDF-5 holds significant therapeutic promise. Future investigations will enhance its clinical implementation as a therapeutic agent in regenerative medicine and tissue engineering.

1.8.3 Scaffolds

Scaffolds are an essential component of tissue engineering, providing mechanical stability and a 3D structure for the growth of regenerative tissue and the attachment of biologically active molecules, such as growth factors[201]. To develop a viable tissue substitute for tendon repair, the engineered scaffold should mimic the dynamic ECM microenvironment of native tissue[202]. The biological response of cells is influenced by structural and physicochemical properties, which differ between various materials. Bionic scaffolds regulate cell behaviour and tissue

regeneration through their biological features, which include flexibility along with stiffness surface topography, and chemical composition[203].

Scaffolds are typically made from natural polymers like collagen, fibrin, and hyaluronic acid or synthetic polymers like PLGA (polylactic-co-glycolic acid) and PCL (polycaprolactone). These materials can be tailored to mimic the mechanical properties of native tendon tissue, including elasticity, strength, and biodegradability, to match the mechanical loads experienced by tendons[204,205]. This allows for effective integration and support during tendon healing. The ideal scaffold must also support biological functionality by promoting cell adhesion, growth, proliferation, and differentiation, facilitating ECM secretion and the development of tendon tissue[206].

Collagen-based scaffolds have gained significant attention among natural polymers due to collagen's predominant role in tendon ECM structure and function[207]. Collagen provides biocompatibility, bioactivity, and mechanical reinforcement, supporting cell adhesion and ECM deposition, making it an excellent candidate for tendon repair applications[7]. Studies have shown that collagen scaffolds can serve as biodegradable matrices, facilitating tenocyte attachment and proliferation while supporting tissue remodelling and vascularisation[7,207–209]. Moreover, collagen scaffolds can be chemically crosslinked or combined with other biomaterials, such as glycosaminoglycans or synthetic polymers, to enhance mechanical strength and longevity[210]. Collagen-based scaffolds are also widely used as carriers for growth factor delivery, ensuring sustained release of tenogenic cues like GDF-5 and TGF-β, further improving tendon regeneration outcomes[211].

Moreover, scaffolds should exhibit strong biodegradability and resorption rates that align with the cell growth rate of the repaired tissue, ensuring the scaffold degrades as new tissue forms[212]. The scaffold must have low immunogenicity and be biocompatible, causing minimal immune response before and after degradation. Additionally, scaffolds must be processable, allowing fabrication into intricate structures using techniques like electrospinning, 3D printing,

and wet-spinning. These methods enable the production of scaffolds with specific properties, such as pore size, mechanical strength, and shape, that are crucial for tendon regeneration[201].

1.8.4 Synergistic approaches: tendon tissue engineering

Tendon tissue engineering represents a synergistic approach to tendon healing, combining stem cells, bioactive signals, and scaffolds to promote more effective tendon repair (Figure 1-9). Each component leverages its regenerative potential to enhance the healing process. Stem cells provide the cellular foundation for tissue regeneration, while bioactive mediators, such as growth factors and EVs, regulate cellular behaviour and promote healing. On the other hand, scaffolds provide structural support for guiding tissue formation while serving as delivery vehicles for bioactive molecules, ensuring a controlled signal release similar to the body's healing process[4].

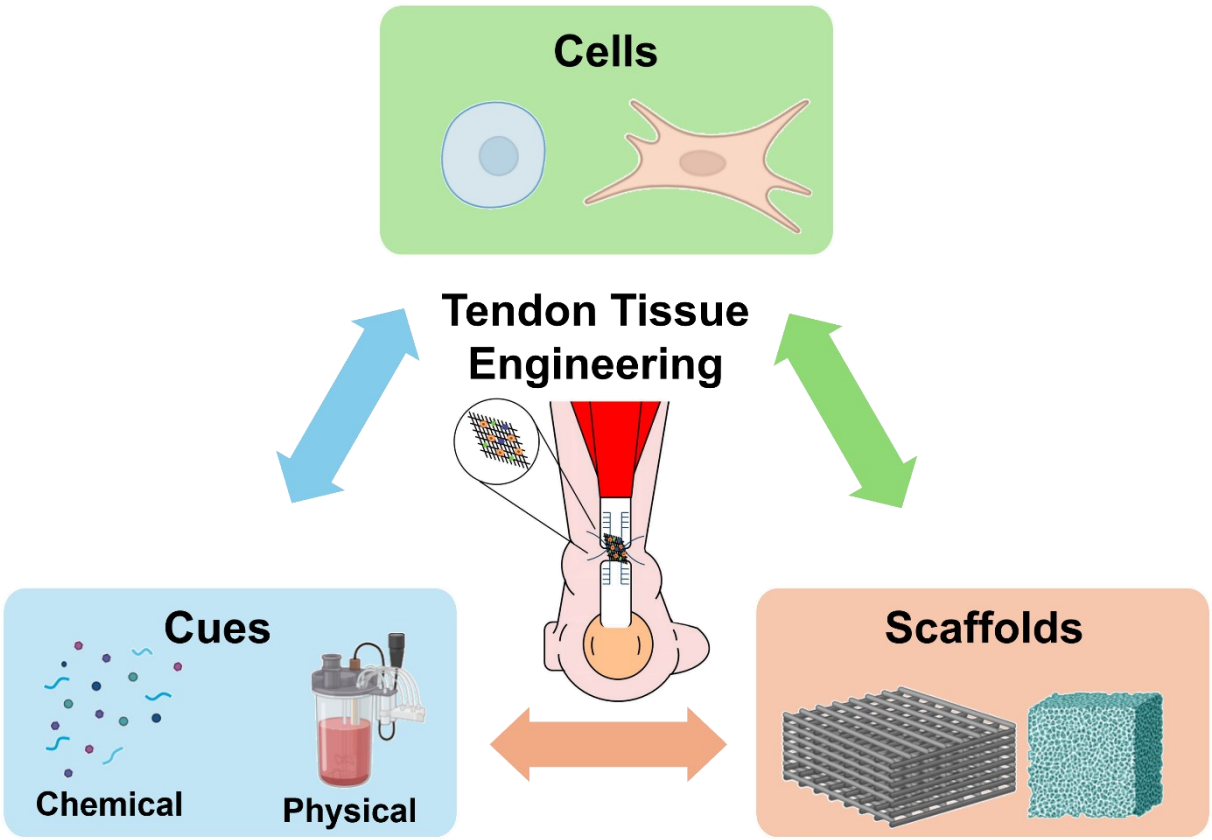


Figure 1-9. Schematic representation of tendon tissue engineering, highlighting the interplay between cells, bioactive signals, and scaffolds. Cells, such as tendon stem cells and tenocytes, respond to chemical and physical signals, which regulate cellular behaviour and support tendon regeneration. Scaffolds provide the necessary structural support while serving as vehicles for delivering

bioactive components to guide tissue formation. This integrated approach promotes effective tendon repair and regeneration. Image adapted from Vasiliadis et al., 2020[213] under CC BY 4.0 License, partially created with https://www.biorender.com/.

Combining these components creates a more dynamic and coordinated healing environment. Stem cells can be seeded onto scaffolds embedded with growth factors, such as TGF-β and VEGF, which promote stem cell differentiation and collagen production[206]. Simultaneously, EVs derived from MSCs can be delivered through the scaffold to modulate inflammation, promote ECM remodelling, and enhance the regenerative potential of the cells[183]. This combined strategy enables tendon healing to occur across multiple levels, supporting cell regeneration, ECM synthesis, and overall tissue repair.

Biomimetic strategies for tendon repair aim to replicate the tendon microenvironment, including the biological signals, ECM components, and cell-matrix interactions, ultimately accelerating tendon regeneration. For instance, coculturing stem cells that can secrete collagen proteins and other key elements, along with biological scaffolds, has been shown to enhance tendon regeneration[201]. Additionally, introducing bioactive molecules, such as growth factors and matrix proteins, helps simulate the biological signals within the tendon microenvironment[4]. Recent advancements have focused on fabricating scaffolds with ECM-like properties using different biomaterials, which help mediate cellular attachment and promote the desired differentiation spectrum. These biomimetic scaffolds not only support cell function but also help induce the correct differentiation needed for tendon regeneration. As a result, these scaffolds show promising potential for clinical application in tendon repair, offering a platform for developing functional tendon tissue[201].

An important enhancement to these synergistic strategies is the use of mechanically active bioreactors, which apply physiologically relevant mechanical loading to promote tendon differentiation[214]. Mechanical stimulation has been shown to enhance ECM organisation, collagen synthesis, and overall tissue maturation[7]. These systems play a key role in replicating

the tendon's natural mechanical environment and will be discussed further in the following section 1.11.

Additionally, oxygen availability is a critical factor in tendon regeneration. Tendons are naturally poorly vascularised, which limits oxygen supply and influences cellular behaviour[215,216]. In tissue engineering, oxygen tension must be carefully regulated to mimic physiological conditions and enhance the regenerative potential of engineered tendon constructs.

Therefore, integrating stem cells, bioactive components, scaffolds, bioreactors, and environmental controls in tendon healing represents a promising new direction in regenerative medicine and tissue engineering. Combining stem cells' regenerative power, the therapeutic effects of bioactive components (such as growth factors and EVs), and the structural support of scaffolds offer a comprehensive approach to tendon repair. Adding bioreactors and controlled oxygen environments further enhances the regenerative capacity of tendon tissue engineering. While challenges remain in optimising these therapies for clinical use, continued advancements in tissue engineering, regenerative medicine, and bioreactor technology hold the potential to improve tendon healing outcomes significantly. These approaches offer a powerful alternative to traditional tendon repair methods and may soon become standard treatments, enhancing recovery and reducing the risk of re-injury.

1.9 The role of EVs in tendon healing

EVs have emerged as promising agents in regenerative medicine, particularly for tendon healing. In tendon healing, they contribute to regenerative processes by promoting cell proliferation, migration, and differentiation, modulating inflammation, and enhancing the tendon-bone interface[217] (Figure 1-10). By carrying bioactive cargoes, EVs help to orchestrate the complex processes of tissue repair and regeneration, making them an essential component in tendon healing[2].

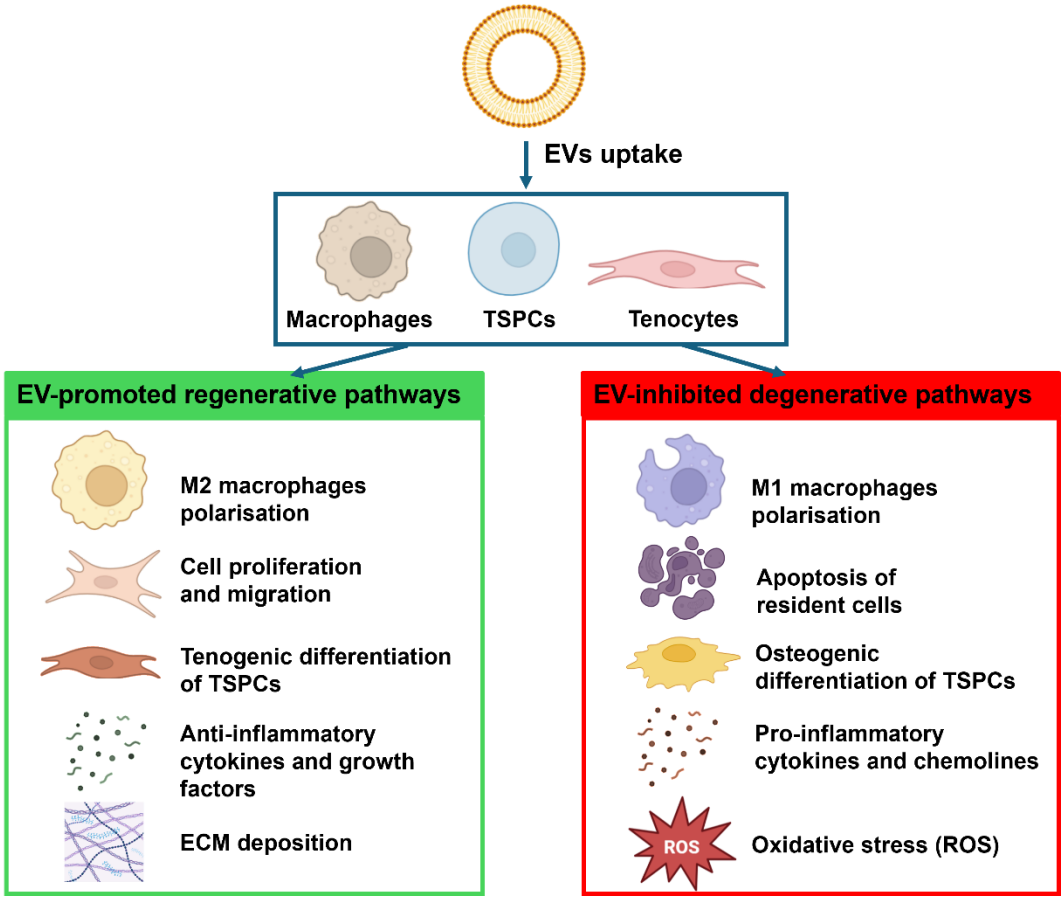


Figure 1-10. Schematic representation of EVs' the regenerative effects in tendon healing. EVs are taken up by macrophages, TSPCs, and tenocytes, where they modulate inflammation and promote tissue regeneration. EVs stimulate M2 macrophage polarisation, supporting cell proliferation, migration, tenogenic differentiation, and ECM deposition, while suppressing M1 macrophages, thereby reducing oxidative stress and inhibiting osteogenic differentiation of TSPCs. This coordinated balance of stimulatory and inhibitory effects contributes to effective tendon repair. Image adapted from Liu et al., 2024[218], with permission from Elsevier, and created with https://www.biorender.com/.

One of the primary regenerative roles of EVs is their ability to promote the proliferation and migration of tendon-derived cells, such as TSPCs and tenocytes, which are critical for synthesising the ECM and regenerating injured tendon tissue. EVs derived from BM-MSCs have been shown to significantly enhance tenocyte proliferation while increasing the expression of growth factors such as TGF-β1, further promoting tendon repair[184]. Similarly, the application of BM-MSC-derived EVs was also reported to stimulate the proliferation, migration and tenogenic differentiation of TSPCs to the injury site, both *in vitro* and *in vivo*, facilitating the regeneration of tendon tissue and enhancing the expression of key tenogenic markers

such as TNMD and COL I[182]. This ability to drive cellular responses at the injury site makes EVs crucial for restoring tendon tissue.

Beyond promoting cell proliferation, EVs help regulate the function of TSPCs and tenocytes by maintaining microenvironment homeostasis. Tenocyte apoptosis, a significant factor in tendon degeneration, is countered by EVs, which contain bioactive molecules like TGF-β1, promoting tenocyte survival and ECM secretion[184]. Additionally, TSPCs-derived EVs have been shown to activate key signalling pathways such as PI3K/AKT and MAPK/ERK1/2, essential for cell survival, migration, and ECM deposition[219]. In tendinopathy, oxidative stress and inflammation impair the function of TSPCs, hindering tendon repair. TSPC-EVs protect TSPCs from oxidative stress-induced apoptosis, promote their differentiation into tenocytes, and inhibit their osteogenic and adipogenic differentiation[220]. MSC-derived EVs can activate the Nrf2/HO-1 pathway in TSPCs, reducing oxidative stress and enhancing the survival of these stem cells at the injury site[221]. Moreover, miRNAs such as miR-29a, carried by EVs, regulate the expression of genes that promote TSPC migration and differentiation, ensuring effective tissue repair and regeneration[185,218].

In addition to their regenerative effects on tendon cells, EVs also play an essential role in modulating inflammation[222], which is a critical aspect of tendon healing. Prolonged inflammation can lead to fibrosis and impair the healing process, making regulating the inflammatory response vital. iPSC-derived MSC EVs have been shown to promote a shift in macrophage polarisation from a pro-inflammatory M1 phenotype to a pro-regenerative M2 phenotype[223,224] in a rat tendinopathy model[225]. This shift reduces the expression of harmful inflammatory cytokines like IL-1β, IL-6, and TNF-α while enhancing the production of anti-inflammatory cytokines such as IL-10 and TGF-β1[226]. By modulating the inflammatory environment, EVs create a more favourable healing environment, reducing scar formation and promoting a more efficient healing process.

EVs can be administered in two primary forms: as part of secretome/conditioned media (CM) or as isolated EVs. Conditioned media contains not only EVs but also soluble proteins,

cytokines, and other secreted factors, all of which may contribute to tendon healing[227,228]. Studies suggest that CM can have similar or even greater regenerative effects compared to isolated EVs due to the presence of additional bioactive molecules[172,229–231]. However, isolated EVs offer a more defined and concentrated therapeutic formulation, reducing the variability associated with the heterogeneous composition of CM. It should also be noted that, as EVs are harvested from CM, they inherently reflect the biological variability of the original secretome, influenced by the donor cell type and isolation method. The choice between CM and purified EVs depends on the therapeutic goal, as CM may support broader biological effects, whereas isolated EVs allow for more controlled dosing and targeted delivery[229,232].

A key challenge in tendon repair is regenerating the tendon-bone interface, known as the enthesis, where tendons and ligaments attach to bone. Injuries to this area often result in poor healing outcomes and a high risk of re-tear due to difficulties regenerating this complex structure[233]. EVs have shown promise in improving tendon-bone healing by promoting better integration of the tendon into the bone. Studies have demonstrated that EVs derived from BM-MSCs, delivered with hydrogels, significantly improve tendon-bone healing by reducing inflammation and promoting tissue regeneration at the tendon-bone interface[223]. Similarly, adipose-derived stem cells EVs also reduce fatty infiltration in models of rotator cuff tears, contributing to better histological and mechanical properties at the repair site[234].

EVs also contribute to ECM remodelling, which is an essential part of tendon healing. By promoting collagen synthesis and ECM component production, EVs enhance the structural support of the healing tendon. Specifically, EVs derived from TSPCs have been shown to stimulate the production of type I and type III collagen, which are essential for tissue strength and elasticity[235,236]. This collagen synthesis supports tendon strength and helps maintain the tendon’s functionality and integrity during the healing process.

Furthermore, excess scar tissue formation is another challenge in tendon healing[237]. EVs have demonstrated anti-fibrotic effects by regulating the expression of MMPs, enzymes involved in ECM degradation and fibrosis. Studies have shown that MSC-derived EVs can reduce the

expression of fibrotic markers and promote ECM degradation, resulting in a more organised and functional tissue structure[236,238]. This anti-fibrotic effect can significantly improve tendon healing by preventing the formation of excessive scar tissue and enhancing the long-term functionality of the tendon.

Finally, EVs also play a vital role in enhancing angiogenesis, the new blood vessel formation process critical for tendon healing. Tendon injuries often suffer from poor vascularisation, limiting the supply of oxygen and nutrients to the tissue. EVs have been shown to increase the expression of pro-angiogenic factors like VEGF, which promotes the formation of new blood vessels around the injury site[239]. This enhanced angiogenesis helps to improve the nutrient and oxygen supply to the healing tendon, speeding up the repair process and improving the overall quality of the healed tissue in the short term. However, while these effects are well-documented in early tendon healing, the long-term impact of EV-induced angiogenesis on tendon regeneration remains an area of ongoing research.

Beyond their natural role in tendon healing, EVs hold significant promise for enhancing tendon tissue engineering. In tendon regeneration, EVs can be integrated into engineered systems, such as scaffolds or bioreactors, to provide a sustained, controlled release of bioactive molecules directly to the injury site. The therapeutic potential of EVs is not limited to their capacity to modulate inflammation and support ECM remodelling; they can also facilitate the development of functional tendon-like tissue within engineered constructs[240]. When combined with scaffolds, EVs can support cellular differentiation, matrix production, and the alignment of collagen fibres, all of which are critical for tendon regeneration. Furthermore, EVs can work synergistically with stem cells or growth factors embedded in scaffolds, enhancing their regenerative effects and improving tissue integration[217]. This dual approach, using EVs in combination with other tissue engineering strategies, holds the potential to revolutionise tendon repair, offering a more efficient and effective means of addressing tendon injuries, especially those that are challenging to heal with traditional methods.

However, a key challenge in EV-based therapy is maintaining the stability and bioactivity of EVs during storage and delivery. Freeze-thaw cycles, lyophilisation, and cryopreservation techniques are commonly used to preserve EVs, but these methods may alter EV integrity and function[241,242]. Recent advancements in hydrogel-based and scaffold-mediated EV delivery provide controlled release systems that prolong EV bioavailability at the injury site[243,244]. Further optimisation of EV storage and delivery technologies will be crucial for translating EV-based therapies into clinical applications.

In summary, EVs play a pivotal role in tendon healing by promoting the proliferation and migration of tendon-derived cells, modulating inflammation, improving tendon-bone interface healing, supporting ECM remodelling, and stimulating angiogenesis. These regenerative effects make EVs a promising therapeutic tool for tendon injuries. However, further research is needed to optimise EV-based therapies and better understand their long-term safety and efficacy in clinical settings. With continued advancements, EVs could offer a powerful alternative or complement to traditional tendon repair strategies.

1.10 Hypoxic culture

Hypoxia, defined as oxygen levels below atmospheric 21% O_2, plays a crucial role in stem cell behaviour and tendon healing[245]. Physiological oxygen levels vary across tissues[246], with bone marrow[247] maintaining oxygen tensions between 1 and 4% O_2, skeletal muscle[248] at approximately 4-6% O_2, and kidneys ranging from 9-11% O_2. Being relatively hypovascular, tendons are naturally adapted to low oxygen availability (1-5%), making hypoxia a key factor in their development and repair[216,249].

Oxygen serves as both a metabolic substrate and a signalling molecule, influencing cellular processes by activating hypoxia-inducible factors (HIFs)[216,250]. Under normoxic conditions, HIF-1α undergoes hydroxylation by prolyl hydroxylase domain (PHD) enzymes, marking it for degradation via the ubiquitin-proteasome pathway[251]. However, in low oxygen environments, PHD activity is inhibited, leading to HIF-1α stabilisation and nuclear translocation[252]. Once in

the nucleus, HIF-1α dimerises with HIF-1β, binding to hypoxia-response elements (HREs) in the promoters of target genes, initiating the transcription of factors involved in cell survival, ECM remodelling, angiogenesis, and differentiation[245,252].

In stem cell culture, hypoxia significantly impacts self-renewal, proliferation, and differentiation[245,253,254]. MSCs and TSPCs cultured under low oxygen conditions (2-5% O_2) exhibit enhanced proliferation, reduced senescence, and increased maintenance of their stem-like properties[255–259]. HIF-1α activation in these cells upregulates tenogenic markers such as SCX and TNMD, facilitating their differentiation into tenocytes[249]. Furthermore, hypoxia has been shown to enhance EV secretion, which plays a key role in intercellular communication and tendon repair[260,261].

Beyond its effects on stem cells, hypoxia is integral to tendon healing. Given their inherently poor vascularisation, tendons rely on hypoxia-adaptive mechanisms during repair[249]. HIF-1α activation promotes collagen type I and III synthesis, regulates MMPs and tissue inhibitors of metalloproteinases (TIMPs) to maintain ECM homeostasis, and induces VEGF expression, stimulating angiogenesis at the injury site[249,262]. These effects contribute to an enhanced reparative response, improved structural integrity, and more effective tendon remodelling.

In tendon tissue engineering, precise control of oxygen levels is critical to optimising regenerative strategies. Studies indicate that hypoxic conditions improve the biomechanical properties of engineered tendon grafts, enhance stem cell survival, and minimise fibrotic scarring[175,215,249,263]. By modulating HIF pathways, researchers aim to enhance tendon integration, optimise cellular responses, and refine tissue engineering techniques for more effective clinical applications.

Despite these promising effects, variability in hypoxia responses across different experimental models underscores the need for further refinement. Standardising oxygen exposure levels, duration, and culture conditions will be essential for translating hypoxia-based regenerative strategies into reliable clinical therapies. Future research should focus on optimising hypoxia

protocols to maximise stem cell efficacy and tendon healing outcomes, ensuring reproducible and practical applications in regenerative medicine.

1.11 Dynamic culture systems

Dynamic cell culture systems are critical for mimicking the *in vivo* mechanical conditions that tendons experience, providing a more physiologically relevant environment for tendon research and regeneration[264]. Traditional static cell culture systems are often insufficient for replicating the complex mechanical forces that tendons undergo in the body, such as tensile strain, compression, and shear forces. These mechanical forces are known to play a crucial role in tendon homeostasis, tissue repair, and the differentiation of stem cells into tendon-like cells. As such, dynamic culture systems are increasingly used to replicate these forces in the laboratory setting, enhancing the relevance and effectiveness of tissue engineering strategies aimed at tendon regeneration.

Various dynamic culture systems have been developed to apply mechanical stimuli to cells, including bioreactors, stretchers, and fluid shear devices[205,264–267]. These systems enable the application of cyclic mechanical loading, which has been shown to promote cell proliferation, enhance matrix production, and improve the alignment of collagen fibres, which are critical factors for tendon healing. Applying dynamic loading to MSCs and TSPCs can also stimulate their differentiation into tenocytes, facilitating tendon regeneration[268–270].

Perfusion bioreactors have gained attention as a promising dynamic culture system due to their ability to enhance mass transport and nutrient distribution, which is critical for optimal cell growth and EV production. The perfusion bioreactor concept was first introduced by Carrel and Lindbergh in the early 20th century when they developed an apparatus to culture whole organs[271]. This apparatus was designed to nourish tissue explants through continuous nutrient flow, overcoming the limitations of diffusion-limited nutrient transport that hindered cell viability and tissue growth in static cultures. Carrel's work laid the foundation for developing modern

perfusion bioreactors, which are widely used today to improve cell culture environments and promote the efficient production of bioactive components like EVs[272].

Perfusion bioreactors operate by circulating culture medium through a chamber where scaffolds or cell cultures are placed. The flow of the medium can be either direct or indirect: in direct perfusion systems, the culture medium is forced through the construct, ensuring even distribution of nutrients and oxygen. The medium flows around the construct in indirect perfusion systems, providing mass transport without direct contact. These systems help mitigate challenges such as nutrient deprivation, cell clumping, and sedimentation, commonly encountered in static cultures, making them ideal for applications where high cell viability and productivity are required[273].

The dynamic conditions in perfusion bioreactors have been shown to result in higher EV yields compared to static culture systems, likely due to the improved distribution of nutrients, oxygen, and other essential factors throughout the culture[274]. The constant flow of culture medium in perfusion bioreactors also facilitates better cell viability and reduces the buildup of metabolic waste products, which can hinder cell function in static systems[269,275]. Furthermore, the shear stress applied by the perfusion system can promote cellular differentiation and alignment, which is essential for tissue regeneration[276,277], and support the production of functional tendon-like tissue. By mimicking the physiological conditions that cells experience *in vivo*, perfusion bioreactors provide an optimal environment for tendon regeneration and the large-scale production of EVs, offering new possibilities for tendon tissue engineering.

Together with scaffolds and bioactive mediators like growth factors and EVs, perfusion bioreactors enable the development of functional, bioengineered tendon tissue that more closely resembles native tendons. This approach not only enhances the regenerative potential of tendon constructs but also improves their integration when transplanted into the body, offering promising prospects for tendon repair in clinical applications.

1.12 Thesis objectives

The thesis aims to:

1. Establish and characterise tendon-derived cell populations (TSPCs and Tncs) from porcine and human tendons by assessing morphology, proliferative capacity, and EV secretion under static vs. dynamic conditions and hypoxia (Chapters 3 and 4).
2. Investigate the tenogenic potential of porcine and human TSPC-derived CM and cEVs by evaluating their effects on hBM-MSC differentiation, ECM organisation, and cell viability using gene expression analysis, immunofluorescence, and histological assays (Chapters 5 and 6).
3. Compare the effectiveness of CM vs. isolated cEVs in promoting tenogenesis, assessing whether CM provides additional regenerative benefits beyond purified EVs and determining the role of GDF-5 supplementation in enhancing tenogenic differentiation (Chapters 5 and 6).
4. Examine the impact of hypoxia and dynamic culture conditions on EV secretion, bioactivity, and molecular cargo, determining how these culture conditions influence their tenogenic potential and regenerative capacity (Chapters 3, 4, 5, and 6).

The findings of this thesis are expected to provide valuable insights into the role of EVs in tendon regeneration. These results could contribute to developing novel therapeutic strategies to improve tendon repair outcomes, addressing challenges such as incomplete healing and the high risk of re-injury.



Chapter 2

Materials and Methods

2. MATERIALS AND METHODS

2.1 Materials

This chapter details the fundamental methods used throughout the thesis. The materials which were used are listed in Table 2.

Table 2. List of materials, catalogue number and suppliers

Material	Catalogue number	Supplier
3-Isobutyl-1-methylxanthine (IBMX)	I5879	Sigma Aldrich
4′,6-Diamidino-2-phenylindole dihydrochloride (DAPI)	D8417	Sigma Aldrich
AlamarBlue™ Cell Viability Reagent	DAL1025	Invitrogen™
Alcian blue 8GX	A3157-10G	Sigma Aldrich
Alexa Fluor™ 488 goat-anti-rabbit IgG	ab150081	Abcam
Alexa Fluor™ 594 goat-anti-mouse IgG	A-11005	Thermo Fisher Scientific
Alizarin red S sodium salt	42040	Alfa Aesar
Allophycocyanin (APC) conjugated antibodies: CD73	130-095-183	Miltenyi Biotech
Ascorbic Acid (AA)	A4544-25G	Sigma Aldrich
BCA assay	23225	Thermo Scientific™
Bovine serum albumin (BSA)	A9418	Sigma Aldrich
Ciprofloxacin	17850	Sigma Aldrich
Collagen I solution, High Concentration, Rat Tail, 100 mg	354249	Corning®
Collagenase	17101015	Gibco™
Dexamethasone (DEX)	D2915	Sigma Aldrich

Dimethyl sulphoxide (DMSO)	D2650	Sigma Aldrich
Direct Red 80	365548	Sigma Aldrich
DMEM, powder, high glucose	12100061	Gibco™
Dulbecco's Phosphate-Buffered Saline (DPBS)	20-030-CV	Corning®
Dulbecco′s Modified Eagle′s Medium– High glucose (DMEM)	15-013-CV	Corning®
Dulbecco′s Modified Eagle′s Medium - Low glucose (L-DMEM)	10-014-CV	Corning®
Epidermal Growth Factor	SRP3027	Sigma Aldrich
Foetal Bovine Serum (FBS)	FB-1001/500	Biosera
Fibroblast growth factor 2 (FGF2)	SRP4037-50UG	Sigma Aldrich
Fibronectin from human plasma	F0895	Sigma Aldrich
Fluorescein isothiocyanate (FITC) - conjugated antibodies: CD90 HLA-DR	 IM1839U IM0463U	Beckman Coulter
Fresh human bone marrow aspirate (BMA)29/30/31	1M-105	Lonza®
Growth Differentiation factor 5 (GDF-5) human recombinant protein	120-01	Peprotech
Gentamicin	17-518L	Lonza®
Giemsa Stain	32884	Sigma Aldrich
Glutagro	25-015-CI	Corning®
Hanks' Balanced Salt Solution (HBSS)	BE10-543F	Lonza®
Heparin sodium salt	A16198	Alfa Aesar

HRP-conjugate Goat Anti-Rabbit IgG (H + L)	1706515	Biorad
Human Platelet Lysate (HPL)	06961	STEMCELL Technologies
Immunofluorescence primary antibodies: Collagen I Monoclonal Antibody (COL1) Anti-Collagen Type I Antibody (COL1) Anti-tenomodulin antibody (TNMD)	 MA1-26771 MAB3391 ab203676	 Thermo Fisher Scientific Sigma Aldrich Abcam
Indomethacin	I7378	Sigma Aldrich
Insulin	I9278	Sigma Aldrich
Insulin–Transferrin–Selenium (ITS)	41400045	Gibco™
L-glutamine (L-glut)	BE17-605E	Lonza®
L-proline	81709	Sigma Aldrich
LIVE/DEAD Viability/Cytotoxicity Kit (L/D)	L3224	Thermo Fisher Scientific
Minimum Essential Medium Alpha (α-MEM)	15-012-CV	Corning®
Mycoplasma Removal Agent (MRA)	BUF035	Biorad
Non-Essential Amino Acids (NEAA)	13-114E	Lonza®
Non-fat dry milk	Sc-2325	Santacruz
Oil red O	O0625-100G	Sigma Aldrich
Penicillin-Streptomycin-Amphotericin B Mixture (PSA)	17-745E	Lonza®
Phycoerythrin (PE) conjugated antibodies: CD14 CD19	 130-113-709 130-113-646	Miltenyi Biotech

CD34 CD44 CD45 CD73 CD90 CD105 HLA-DR IgG1 IgG2	130-113-741 130-102-66 130-110-770 130-120-152 130-114-902 130-112-321 130-113-402 130-119-859 130-123-273	
Phycoerythrin (PE) conjugated antibodies: CD34 CD105	 A07776 A07414	Beckman Coulter
Phycoerythrin Cyanin 7 (PC7) conjugated antibodies: CD14 CD45	 A22331 IM3548	Beckman Coulter
Phosphate-buffered saline (PBS)	21-040-CM	Corning®
Picric acid solution	P6744-1GA	Sigma Aldrich
Pierce™ Bradford Plus Protein Assay Reagent	23238	Thermo Scientific™
Pierce™ ECL Western blotting substrate	32106	Thermo Scientific™
PrimePCR™ SYBR Green assay primer pairs (desalted): GAPDH COL1A1 COL3A1	10025636 qHsaCED0038674 qHsaCED0043248 qHsaCED0046560	Biorad

SCX DCN TNC	qHsaCED0041755 qHsaCED0041978 qHsaCED0057376	
Protease and Phosphatase inhibitor cocktail solution	PPC1010	Sigma Aldrich
Quant-iT™ PicoGreen™ dsDNA Assay Kit	P7589	Invitrogen™
QuantiNova SYBR Green RT-PCR Kit	208156	Qiagen
Ripa buffer	R0278	Sigma Aldrich
RLT buffer	79216	Qiagen
RNase ZAP	R2020	Sigma Aldrich
RNeasy Mini Kit	74104	Qiagen
Sodium bicarbonate	S6014	Sigma Aldrich
Sodium chloride (NaCl)	S9888	Sigma Aldrich
Sodium Dodecyl Sulfate (SDS)	L4509	Sigma Aldrich
Sodium hydroxide (NaOH)	221465	Sigma Aldrich
Sodium pyruvate	11360070	Gibco™
Stem Cell Factor (SCF)	300-07	Peprotech
Transforming growth factor-β3 (TGF-β3)	100-36E	Peprotech
Triton® X-100	9036-19-5	Sigma Aldrich
Tris hydrochloride (Tris-HCl)	PHG0002	Sigma Aldrich
Trypan blue	T8154	Sigma Aldrich
Trypsin/EDTA	15400-54	Gibco™
Western blot primary antibodies: anti-Calnexin anti-CD9 anti-CD63	 ab133615 ab263019 ab134045	 Abcam

anti-CD81 anti-Hsp70 anti-TSG101 anti-α-tubulin	ab109201 ab181606 ab125011 T5168	 Sigma Aldrich
TWEEN® 20	P1379	Sigma Aldrich
β-glycerophosphate	G9422	Sigma Aldrich
β-mercaptoethanol	444203	Sigma Aldrich

2.2 General cell culture techniques

All cell culture procedures were carried out in a class 2 microbiological safety cabinet using disposable sterile consumables to maintain sterility. All cells were expanded in humidified incubators at 37°C in 5% CO_2 and either 21% or 2% O_2 and N_2.

2.2.1 Enzymatic sub-culture with trypsin

Cells were cultured in the relevant cell culture media to a necessary confluency between 70-90% using the appropriate cell culture flask. Flasks were washed with PBS to remove all traces of serum, then a solution of 0.05% trypsin-EDTA (diluted 1 in 10 in phosphate-buffered saline (PBS)) was added (5 mL for T175, 3 mL for T75 and 1.5 mL for T25) and cells were incubated at 37°C until cells began to detach from the flask. Flasks were gently tapped against the hand palm to ensure all cells were dislodged. Approximately 3 volumes of the relevant cell culture medium were added to the flask to neutralise the trypsin, and a small volume was taken for cell counting with a haemocytometer. The counting method is described in section 2.2.2. Cell suspensions were transferred to an appropriately sized centrifuge tube and pelleted at 300 RCF for 3 min. The supernatant was aspirated, and cells were re-suspended in media in preparation for seeding. The appropriate cell concentrations were then seeded, with the media changed every 2-3 days.

2.2.2 Haemocytometer cell counting

All cell counts were performed by trypsinising (as described in 2.2.1) to obtain a uniform cell suspension. Using capillary action, 10 µL of the cell suspension was pipetted under the coverslip of a Neubauer haemocytometer and cells were counted under a brightfield microscope. If trypan blue exclusion assay was being used, 10 µL of the suspension was diluted and mixed 1 in 2 with trypan blue. A mean count was determined from the 4, 1 mm^2 corner regions to give the number of cells per 0.1 µL. To determine the number of cells/mL and the total cells, the mean number of cells/0.1 µL was multiplied by 10^4 and the total number of mL of cell suspension, respectively. The calculation would also consider the dilution factor if trypan blue was used.

2.2.3 Cryopreservation of cells

For long-term storage, all cells were trypsinised as described in 2.2.1, resuspended in a freezing medium, composed of foetal bovine serum (FBS) supplemented with 10% (v/v) dimethyl sulphoxide (DMSO) and immediately transferred to cryovials and placed in an isopropanol-filled Mr Frosty freezing container for controlled cooling to -80 °C before being moved to liquid nitrogen storage dewars.

2.2.4 Cell thawing

To recover cryopreserved cells, the cryovials were briefly thawed in a water bath for a few seconds until only a small ice core remained. The thawed cell suspension was then transferred into a 10 mL centrifuge tube. The cryovial was rinsed with fresh cell culture media to maximise cell recovery, which was subsequently added to the same tube. Fresh media was added dropwise to the cell suspension gently (e.g., equal parts of cell suspension and media, such as 2 mL of cells and 2 mL of media) to minimise osmotic shock. The mixture was gently mixed to ensure uniform distribution. The cell suspension was centrifuged at 200 RCF for 3 minutes to pellet the cells. The supernatant was carefully discarded, and the cell pellet was resuspended in an appropriate volume of fresh culture media. The resuspended cells were divided evenly into the designated flasks for subsequent culture.

2.3 Isolation and culture of cells

2.3.1 Isolation and culture of porcine tendon stem progenitor cells

The isolation of porcine tendon stem progenitor cells (TSPCs), both from the paratenon (type I) and from endotenon (type II), was performed by adding some variations to a published protocol[278], as we previously described[9]. Briefly, tendon tissues were dissected from the deep digital flexor tendon of 6 months old pigs, sourced from a local abattoir, and washed 3 times in sterile PBS with 10% Penicillin-Streptomycin-Amphotericin B Mixture (PSA), 1% Ciprofloxacin and 1% Gentamicin, and then washed in Hanks' Balanced Salt Solution (HBSS) with 2% PSA, 0.2% Ciprofloxacin and 0.2% Gentamicin (Figure 2-1).

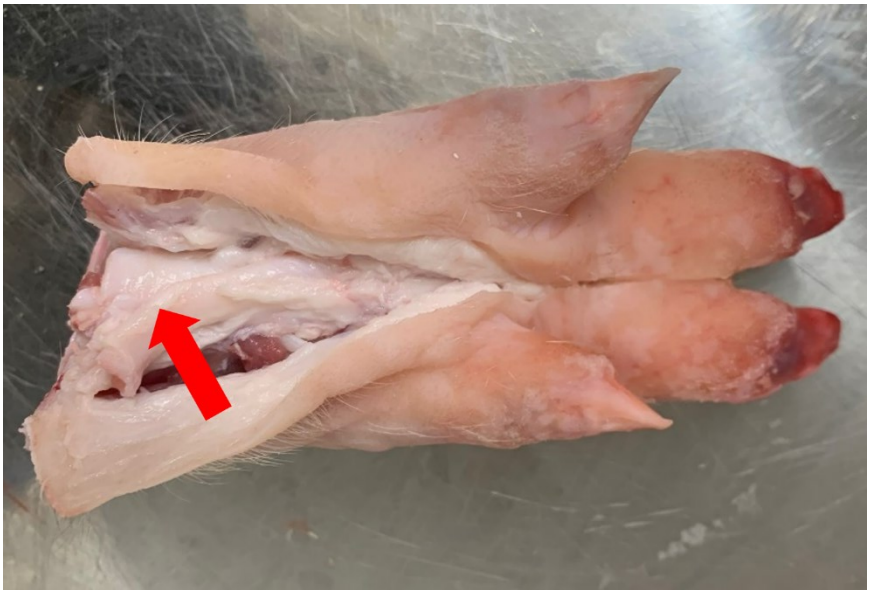


Figure 2-1. Porcine tendon extraction. The deep digital flexor tendon was pointed at by a red arrow, from which tendon cells were isolated after any visible fat or muscle was removed. Image reprinted from Clerici et al., 20239 under CC BY 4.0 License.

After washing, the tissue was minced and enzymatic digestion with type II collagenase (3mg/mL) was performed overnight at 37˚C. The enzymatic activity was neutralised with FBS, and the remaining tissue pieces passed through a 70-µm cell strainer (Falcon®, 352350) to yield single-cell suspension and then centrifuged at 350 RCF for 8 minutes at room

temperature (RT). The obtained cells were resuspended in Dulbecco′s Modified Eagle′s Medium - low glucose (L-DMEM) with L-glutamine & sodium pyruvate,15% FBS, 1% PSA, 0.4 ng/mL epidermal growth factor (EGF), 2.5 ng/mL fibroblast growth factor 2 (FGF2) and 2.5 ng/mL stem cell factor (SCF). To minimise the risk of contamination, 0.1 µg/mL of Mycoplasma Removal Agent (MRA) was added. Cells were initially plated at a density of 50,000 cells/well and incubated at 37˚C under two distinct oxygen levels: atmospheric (21%) and physiological (2%). After 48h of initial seeding, the cells were washed twice to eliminate any non-adherent bodies. After one week, once the cells reached confluence, they were split and reseeded at a density of 5,000 cells/cm² into T-75 flasks with 15 mL of fresh media and T-175 flasks with 30 mL of fresh media, maintaining the same density for CM collection.

2.3.2 Isolation and culture of porcine tenocytes

Tenocytes (Tncs) were isolated using an explant method which consisted of plating some tiny pieces of minced endotenon directly into 6-well plates, letting them adhere for 2 to 3 hours, and cautiously covering them with standard culture media; DMEM High Glucose,10% FBS, 1% PSA, 1% L-glutamine 2mM (L-glut), and 1% Non-Essential Amino Acids (NEAA). 6-well plates were pre-scratched with a surgical blade to promote tissue adhesion. They were incubated at 37˚C under two distinct oxygen levels: atmospheric (21%) and physiological (2%). MRA was added at 0.1 µg/mL for the first 2 weeks as a preventive measure. Weekly changes in culture media were made until Tncs emerged and reached 50% confluence, at which point tissue fragments were discarded, and new fresh media were added. Tncs were marked as passage 0 (P0) when they reached 80-90% confluence, split enzymatically, and then seeded at a 5,000 cells/cm^2 density.

2.3.3 Isolation and culture of human tendon stem progenitor cells

Following protocols approved by the Institutional Review Board of “San Giovanni di Dio e Ruggi D’Aragona Hospital” (Salerno, Italy) (Review Board prot./SCCE n. 151 achieved on 29 October 2020), TSPCs were extracted from biopsies of healthy human semitendinosus tendons as previously described by Ciardulli et al[53,279]. In detail, tendon samples were taken from tissue

sections that were unsuitable for autologous semitendinosus transplants to reconstruct the anterior cruciate ligament. Tendon samples (n = 3) were washed 3 times in PBS, containing 1% PSA (Figure 2-2). The tissue was cleaned and then minced, and any visible fat or muscle was removed before being put in a pre-scratched Petri dish. Each dish was filled with 3 mL of 0.05% trypsin-EDTA and incubated for 30 minutes at 37°C in 21% O_2. 12 mL of Minimum Essential Medium Alpha (α-MEM) supplemented with 1% Glutagro, 1% PSA, and 10% FBS was used to neutralise the enzymatic activity. Weekly changes in culture media were made until TSPCs reached 50% confluence, at which point tissue fragments were discarded, and new fresh media were added. TSPCs were enzymatically detached as previously described in 2.2.1; once they reached confluence, they were centrifuged for 10 minutes at 1400 rpm and re-seeded.

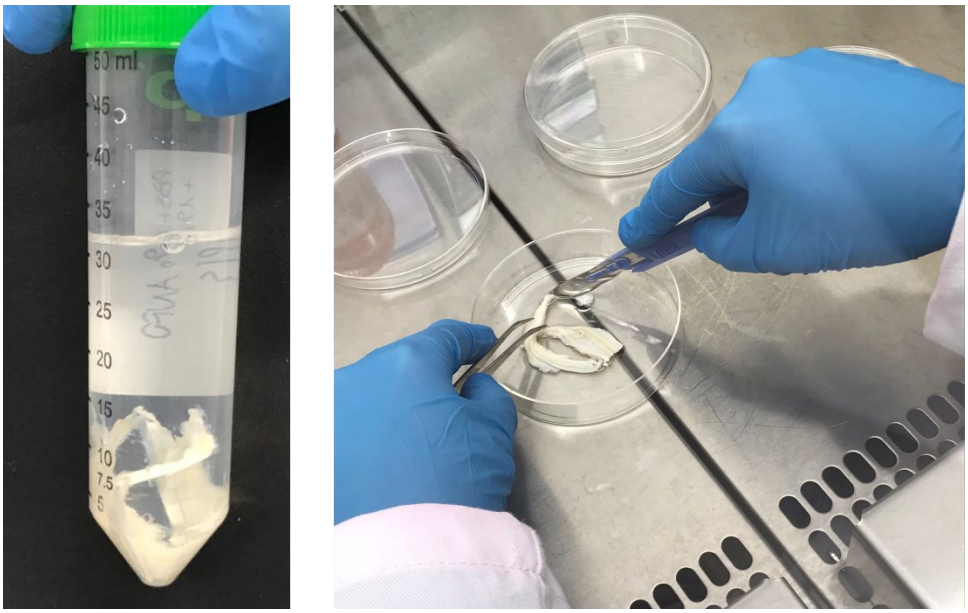


Figure 2-2. Human tendon tissue preparation. The image shows human tendon tissues that were washed in an antibiotic solution, carefully cleaned to remove visible fat or muscle, and subsequently minced and plated for further processing.

2.3.4 Isolation and culture of human bone marrow mesenchymal stromal/stem cells from bone marrow aspirate (BMA)

Whole BMA commercially obtained from healthy consenting donors (Lonza, 1M-105), harvested from the bilateral iliac crests, and supplemented with approximately 100 U/mL of

heparin, was seeded within 48 hours of collection at a density of $1x10^5$ mononuclear cells (MNCs)/cm² in T-75 cm² culture flasks, according to the MNC count provided by the supplier. The culture flasks were pre-coated with 10 ng/mL of fibronectin diluted in PBS and stored for at least 30 minutes at 37°C, after which the fibronectin solution was removed and the BMA was seeded into the coated flasks using DMEM supplemented with 5% human platelet lysate (HPL), 2 u/mL heparin, 1% L-glut, 1% NEAA, and 1% PSA and cultured for one week. After a week of incubation and a 50% media change, the cells were subjected to a 100% media change, eliminating most of the remaining non-adherent leukocytes and erythrocytes. Following isolation, the media were changed twice a week. BMA was obtained from three different patients, and the isolated adherent cells were designated BMA29, BMA30, and BMA31.

2.3.5 Culture of BALB/3T3 clone A31 murine fibroblast cells

The BALB/3T3 clone A31 cell line, purchased from ATCC (CCL-163™), was originally developed by S.A. Aaronson and G.T. Todaro in 1968 from disaggregated 14- to 17-day-old BALB/c mouse embryos[280]. Cells were thawed following the protocol outlined in section 2.2.4, with a modification in the centrifugation step. After thawing, the cells were centrifuged at 1200 rpm for 5 minutes and then resuspended in high-glucose DMEM supplemented with 10% FBS. Cells were split at a 1:6 ratio once a week, with media changes performed twice a week.

2.4 Growth rate

Cells were cultured for 120 days to determine the growth rate. The formula for calculating population doublings (PDs) was $PD = \log_{10} (N/N_0)/\log_{10}(2)$, where N denotes the number of harvested cells at the passage and N_0 denotes the initial cell count. The resulting values were then used to plot a growth curve (X-axis for time point; Y-axis for CPD) and calculate the cumulative population doublings (CPDs) as a function of time using the formula $CPDn = PD_0 + PD_n + PD_{n-2}$, where "n" is the time point that is equivalent to the days in culture.

2.5 Cell aspect ratio

Images of all cell types were taken using an inverted optical microscope (Olympus CKX4). The images were then analysed for shape, cell area, and aspect ratio. The manual tool in the ImageJ analysis software[281] (v 1.53c) was used to draw the perimeter of the cells, and the aspect ratio was calculated by dividing the major axis length (length) of the cell area over the minor axis length (width). Thirty distinct cells were randomly chosen within each of the three image fields.

2.6 Trilineage differentiation

Cells at passage 3 (P3, early passage) were seeded at a density of 5,000 cells/cm² to determine the differentiation potential and cultured in differentiation induction media for 21 days. For initial attachment, cells were seeded overnight in standard culture medium, which consisted of high-glucose DMEM supplemented with 10% FBS, 1% NEAA, 1% L-glut, and 1% PSA. The standard medium was replaced with the appropriate differentiation medium the following day. Media changes were performed twice a week.

2.6.1 Adipogenic differentiation

Adipogenesis was induced in cell monolayers with DMEM supplemented with 0.1µM dexamethasone (DEX), 0.5 mM 3-Isobutyl-1-methylxanthine (IBMX), 10 mg/mL insulin, 100µM indomethacin, 10% FBS, 1% NEAA, 1% L-glut, and 1% PSA. Cells were fixed with 10% formalin, washed with PBS, and stored at 4°C until they were stained with Oil Red O.

2.6.2 Chondrogenic differentiation

Chondrogenesis was induced in monolayers with DMEM supplemented with 1% Insulin–Transferrin–Selenium (ITS), 0.1 µM DEX, 50 µM ascorbic acid (AA), 40 µg/mL L-proline, 1% sodium pyruvate, 10 ng/mL Transforming growth factor-β3 (TGF-β3), 1% FBS, 1% NEAA, 1% L-glut, and 1% PSA. Cells were fixed with 10% formalin, washed with PBS and stored at 4°C until staining with Alcian blue.

2.6.3 Osteogenic differentiation

Osteogenesis was induced in monolayers with DMEM supplemented with 50μM AA, 10 μM β-glycerophosphate, 0.1 μM DEX, 10% FBS, 1% NEAA, 1% L-glut, and 1% PSA. Cells were fixed with 10% formalin, washed with PBS and stored at 4°C with PBS until staining with Alizarin red.

2.7 Histological staining of differentiated monolayers

2.7.1 Oil Red O monolayer staining

Oil Red O was used to stain fixed monolayers to detect intracellular lipid droplets. Before being used, an Oil Red O stock solution was made by combining 300 mg of Oil Red O with 100 mL of 99% (v/v) isopropanol and left overnight to allow maximum saturation. Before staining, the working solution was freshly made by some stock solution to 60% (v/v) in distilled water (dH_2O), filtering the resulting mixture through a 0.22 μm syringe filter. After removing the PBS covering the wells, the cell monolayer was quickly washed with 60% isopropanol and covered for five minutes with the filtered Oil Red O working solution. The stain was removed, the wells were washed rapidly once with 60% isopropanol, and imaging was done immediately.

2.7.2 Alcian blue monolayer staining

Alcian blue was used to stain fixed monolayers to detect sulphated glycosaminoglycans. After making 1% (w/v) Alcian blue 8GX in 0.1 M aqueous HCl, it was paper-filtered. This produced a stain with a pH of 1.0, which has good specificity for GAGs. Cells were washed with PBS, and then the Alcian blue stain was applied overnight. After removing the stain, the wells were carefully washed until clear under running tap water. Following that, stained monolayers were imaged as soon as possible.

2.7.3 Alizarin red monolayer staining

Alizarin red S was used to stain fixed monolayers to detect mineralised calcium nodules. An aqueous solution of 2% (w/v) Alizarin red S sodium salt was prepared in dH_2O and was paper-filtered. After removing the PBS and washing the cells, alizarin red S solution was applied for

10 minutes. After removing the stain, monolayers were carefully washed until clear under running tap water. Wells were then left to dry before image acquisition.

2.8 Induction of tenogenic differentiation using GDF-5 supplemented medium

The effect of GDF-5-supplemented medium on tenogenic differentiation was evaluated using hTSPCs at early and late passages[279]. Cells were seeded at a 5,000 cells/cm² density and cultured for 21 days in a tenogenic differentiation medium. The medium consisted of high-glucose DMEM with L-glutamine, supplemented with 50 µM AA, 100 ng/mL recombinant human GDF-5, 10% FBS, 1% NEAA, and 1% PSA.

Control media, previously optimised for trilineage differentiation, were used for comparison. On day -1, cells were seeded in a control medium. After 24 hours (day 0), the control medium was replaced with the differentiation medium, which was maintained for the duration of the experiment. Media were changed twice weekly, and cells were harvested on days 7, 14, and 21. At each time point, cells were fixed with 4% paraformaldehyde and stored at 4°C in PBS. After 21 days, histological staining was performed using 0.1% Sirius Red in picric acid to assess collagen deposition.

2.9 Flow cytometry

2.9.1 Flow cytometry for porcine TSPCs and Tncs

Cells at P3 were trypsinised, and 150,000 cells for each marker were taken for labelling, which was performed following the manufacturer's instructions (Miltenyi Biotech). Briefly, cells were spun down at 300 RCF for 3 minutes. Then, the following directly Phycoerythrin (PE) conjugated anti-human antibodies were added and incubated for 10 minutes at 4°C: IgG1, CD14, CD19, CD34, CD45, CD73, CD90, HLA-DR, CD105; and the anti-mouse antibodies CD44 and IgG2. As controls, unstained cells, IgG1, and IgG2 were used. Following the antibody incubation, the samples were washed twice with PBS and resuspended in PBS for acquisition. The CytExpert 2.2 software was used to analyse the samples after they were

measured using CytoFlex (Beckman Coulter, High Wycombe, UK). A minimum of 20,000 events were recorded. Flow cytometry events were first gated by plotting forward scatter (FSC) vs side scatter (SSC) and then excluding doublets (FSC-A vs. FSC-H) before determining CD surface marker expression.

Porcine tendon-derived cell populations were evaluated for their immunophenotypic profile according to the ISCT guidelines[164,165]. Marker expression analysis confirmed positive detection of CD44 and CD90, while CD14, CD19, CD34, CD45, CD73, CD105, and HLA-DR were not expressed.

2.9.2 Flow cytometry for human TSPCs

Cells at passages P3 were detached, and 50,000 cells were taken for staining. Following consecutive washings in PBS, cells were incubated for 20 minutes at RT with the following mouse–anti-human directly conjugated antibodies: CD73-APC, CD34-PE, CD90-FITC, CD105-PE, CD45-PC7, Anti-HLA-DR-FITC, and CD14-PC7. Following the antibody incubation, samples were washed twice in PBS and resuspended in the same buffer for acquisition. A Becton Dickinson BD FACSVerse™ flow cytometer with two lasers (red: 628 nm and blue: 488 nm) was used for the acquisition process. A minimum of 30000 events were recorded. Kaluza software (v.2.1, Beckman Coulter) was used for post-acquisition analysis and compensation. Before determining CD surface marker expression, flow cytometry events were first gated by plotting FSC vs SSC, then doublets exclusion (FSC-A vs. FSC-H). We acknowledge Dr. Valentina Giudice for her assistance in sample preparation and expertise in performing data analysis.

The immunophenotypic profile of human TSPCs was evaluated following the ISCT guidelines[164]. Flow cytometry analysis confirmed positive CD73, CD90, and CD105 expression, while CD14, CD34, CD45, and HLA-DR were not expressed.

2.10 Cell lysis

All cell types were lysed according to the manufacturer's instructions (Qiagen) using the RLT lysis buffer that came with the RNeasy mini kit. Cell monolayers were washed with PBS, and then 350 µL of RLT buffer supplemented with 10 µL/mL β-mercaptoethanol was added. A cell scraper or vigorous pipetting was used to ensure cells were detached from the culture flask, and the resulting lysate was either processed for RNA extraction immediately, used for DNA quantitation or stored at -80°C until required.

2.11 RNA Extraction

All pipettes and surfaces were treated with RNase ZAP before RNA extraction. Frozen lysates were put on ice after being defrosted. RNA extraction was performed using the RNeasy Mini Kit, according to the manufacturer's instructions. 350 µL of 70% ethanol was added to the lysate, mixed by pipetting, and the solution was added to the RNeasy spin column and centrifuged for 15 seconds at 10,000 RCF. The flow-through was discarded, and the column membrane was washed using the appropriate buffers according to the manufacturer's protocol and centrifuged at 10,000 RCF (700 µL of buffer RW1, 15 seconds centrifugation, 500 µL of buffer RPE, 15 seconds centrifugation, 500 µL of buffer RPE, 2 minutes centrifugation). All flow-through was discarded after each centrifugation. After the final buffer was discarded, the collection tube was replaced with a clean 1mL centrifuge tube. 10-30 µL of RNase-free water was added to the spin column to elute the RNA. The spin column was centrifuged for 1 minute at 10,000 g. The eluted water was then re-added onto the spin column membrane, and the tube was centrifuged again at 10,000 RCF for 1 minute. Extracted RNA concentration was quantified using a NanoDrop2000 spectrophotometer (ThermoFisher, Horsham, UK) and stored at -80°C until required.

2.12 Quantitative reverse transcription-polymerase chain reaction (RT-qPCR)

Relative gene expression was assessed using quantitative reverse transcription-polymerase chain reaction (RT-qPCR) using QuantiNova SYBR Green RT-PCR Kit, according to the

manufacturer's instructions (Qiagen). Cells used for gene expression analyses were harvested at early passages (P2–P4) or late passages (P10–P11). Using RT-qPCR, the product specified by the primer pair can be amplified, and its abundance can be measured during the process. Due to the presence of SYBR green, a DNA-binding cyanine dye, a fluorescent signal is produced during the amplified product, which is measured after each PCR cycle. At the end of the PCR run, the relative abundance of product in each sample can be quantified by comparing the number of cycles at which each sample has acquired enough fluorescence to surpass a predetermined threshold. The thermal cycler sets this threshold, which is within the exponential phase of product amplification for all samples and is set above background levels. All samples were normalised to the housekeeping gene, and relative gene expression was determined using the $2^{-\Delta\Delta CT}$ method.

The RNA extracts were diluted in RNase/DNase-free water to a concentration of 10 ng/µL. Samples were prepared by aliquoting 2 µL of each diluted RNA sample to 0.2 mL PCR tubes, and a master mix of 5 µL 2x QuantiNova SYBR Green RT-PCR master mix, 0.5 µL of each relevant primer (10 µM), 0.1 µL of QN SYBR Green RT-Mix and 1.9 µL RNAse/DNAse free water per sample was prepared. 8µL of the master mix was added to each sample, and the tubes were sealed. If required, the tube strip was briefly centrifuged before being transferred to an AriaMx Real-Time PCR (Agilent Technologies, Santa Clara, CA, USA). The thermal cycler was programmed as follows: reverse transcription at 50°C for 10 min and hot start at 95°C for 2 min, followed by 40 repeated cycles of amplification at 95°C for 5 s for denaturation and combined annealing/extension at 60°C for 10 s. The final melt cycle was for 30 s at 95°C, followed by 30 s at 65°C and 30 s at 95°C.

2.12.1 RT-PCR primer sequences

All porcine primers were designed using NCBI Primer-BLAST and synthesised by Sigma-Aldrich, while human primers were either synthesised or bought as commercially validated primer pairs from Biorad for *SCX*, *TNC*, *COL1A1*, *COL3A*, *DCN* and *GAPDH*. RT-qPCR was run with all the established primers to check for product amplification, which was visualised

with ethidium bromide on 2% agarose gel electrophoresis. The housekeeping genes (*ACTβ*, *GAPDH*, *YWHAZ*) were included. Primers were dissolved in RNase/DNase-free water according to the manufacturer's instructions to achieve 100μM. 10μM stock solutions were stored at -20°C. Porcine primer sequences are listed in Table 3, and human primer sequences in Table 4.

Table 3. Primer sequences and conditions for RT-PCR in porcine cells

Gene name	Sequence	Tm (°C)
ACTβ (Actin beta)	F 5′-GCTAAGGGGGCGCTCTGTC-3′	60.4
	R 5′-GTGTTGGCGTAGAGGTCCTTC-3′	60.9
NANOG (Nanog Homeobox)	F 5'-CAGTGATTTGGAGGCCGTCT-3'	66.4
	R 5'-TCCATGATTTGCTGCTGGGT-3'	67.8
NESTIN	F 5′-GTCTTAGTCTCAGCTCCGTGG-3′	62.9
	R 5′-GTCAGGCTGAATGGTTGGGG-3′	68.9
OCT-4 (Octamer-binding transcription factor 4)	F 5'-ACCCCTCCCAGAGCTTATGAT-3'	64.8
	R 5'-CTGCTTGATCGTTTGCCCTT-3'	66.3
SCX (Scleraxis)	F 5'-CAGCAGCACCTGTAACCCAAG-3'	57.4
	R 5'-AGACTCGTGGGGACGAAGA-3'	58.6
TNMD (Tenomodulin)	F 5'-AGAAGACCCGTCATGCCAGA-3'	60.8
	R 5'-AAGGAGCAGTGAGTTTTGCGA-3'	60.0
THBS4 (Thrombospondin 4)	F 5′-ACCAGGGTACATCGGGATCA-3′	60.8
	R 5′-GCAAGGGTTCAGCTCTGGAT-3′	60.4
TNC (Tenascin C)	F 5′-AGATCTCGATTCTCCAAGAG-3′	60.4
	R 5′-CCGTCAACAGATTCATACAC-3′	58.6

Table 4. Primer sequences and conditions for RT-PCR in human cells

Gene name	Sequence	Tm (°C)
YWHAZ (Tyrosine 3-monooxygenase/tryptophan 5-monooxygenase activation protein zeta)	F 5′-AACTTGACATTGTGGACATC-3′	57.3
	R 5′-AAAACTATTTGTGGGACAGC-3′	58.2
COL1A2 (Collagen type I alpha 2 chain)	F 5′-GACTTTGTTGCTGCTTGC-3′	56.2
	R 5′-CAAGTCCAACTCCTTTTCC-3′	56.4
COL3A1 (Collagen type III alpha 1 chain)	F 5′-AAGGACACAGAGGCTTCG-3′	57.1
	R 5′-CTGGTTGACCATCACTGC-3′	57.3
MKX (Mohawk homeobox)	F 5′-GTTCTGAAGATGGAGAAAATCC-3′	60.5
	R 5′-TTAATCACAGGATGGTGAAC-3′	57.4
SCX	F 5’-CAAACAGATCTGCACCTTC-3’	58.4
	R 5’-CGAATCGCTGTCTTTCTG-3’	59.7
TNMD	F 5’-ACATGGAAATTGATCCTGTG-3’	59.8
	R 5’-TCTCATCTATTTCCTCTTCTGG-3’	59.0

2.13 PicoGreen double-stranded DNA assay

The Quant-iT PicoGreen double-stranded DNA assay was performed on lysates. Double-stranded DNA standards were prepared from the kit's Lambda DNA standard, with 20, 10, 5, 2.5, and 1.25 µg/mL concentrations in RLT buffer supplemented with 10 µl/mL β-mercaptoethanol. Duplicate aliquots of samples and standards (5 µL each) were diluted 1:10 in 1X TE buffer and loaded into a 96-well microplate. The Quant-iT™ PicoGreen™ dsDNA working solution was freshly prepared by diluting the reagent 1:200 in TE buffer, and 50 µL of

this solution was added to each sample or standard. The samples were incubated for five minutes at RT, protected from light, before being read on a Synergy 2 plate reader (excitation at 480 nm, emission at 520 nm). DNA concentrations were determined using a calibration curve based on linear regression.

2.14 Immunofluorescence analysis

All cell types underwent fixation with 10% formalin for 30 minutes at RT, followed by permeabilisation using 0.15% Triton X-100 in PBS for 10 minutes. Subsequently, cells were treated with a blocking buffer consisting of 1% bovine serum albumin (BSA) and 0.1% Tween 20 for 1 hour. For primary antibody staining, cells were incubated overnight at 4°C with mouse monoclonal anti-COL1 primary antibody (1:200) or rabbit polyclonal anti-TNMD primary antibody (1:200), which had been previously diluted in blocking buffer, as indicated by the manufacturer. After primary antibody incubation, cells were washed three times for 5 minutes with PBS and incubated for 1 hour at RT with secondary antibodies: Alexa Fluor™ 594 goat-anti-mouse IgG (1:500) or Alexa Fluor™ 488 goat-anti-rabbit IgG (1:500) antibodies. Cell nuclei were stained with 4′,6-Diamidino-2-phenylindole dihydrochloride (DAPI) solution for 10 minutes. A final wash with PBS was done, and then the samples were ready for imaging. Fluorescence images were acquired using either a Nikon Eclipse Ti-S microscope (micro-Manager software) or an Olympus Fluoview FV3000 confocal microscope (FV31S-SW software). For each condition, 2–3 random, non-overlapping fields of view were captured at the same magnification to ensure comparability across samples.

Semi-quantitative analysis was performed in ImageJ. Individual cells were outlined manually as regions of interest (ROIs), and the mean fluorescence intensity (MFI) was measured for each cell, with local background subtraction applied. Per condition, approximately 30–35 individual cells were quantified across three independent biological replicates (n = 3). Each data point therefore corresponds to the average intensity of a single cell, and results are reported as the mean ± standard deviation of all analysed cells per condition.

2.14.1 Nuclei aspect ratio

The nuclei aspect ratio was measured to evaluate morphological changes in cells under different culture conditions. Images of DAPI-stained nuclei were acquired using a fluorescence microscope. Image analysis was performed using ImageJ (v 1.53c, NIH, USA), where the manual tracing tool was used to outline the nuclear perimeter. The aspect ratio was calculated as the ratio of the minor axis to the major axis of each nucleus. A value closer to 1.0 corresponds to rounded nuclei, whereas lower values indicate elongated nuclei. At least 20 randomly selected nuclei per image field were analysed for each condition to ensure representative quantification.

2.15 Giemsa stain

Giemsa stain is a widely used histological stain that gives a dark blue colour to the nuclei and shades the cytoplasm from blue to pink, depending on its acidity. The staining solution was prepared by diluting the Giemsa reagent 1:20 in distilled water. Cells, which had been previously fixed in 10% formalin, were stored at 4°C in PBS. Following the removal of the PBS, Giemsa solution was added to each well, and the samples were incubated for 2 hours at RT. After incubation, the samples were washed with tap water. The stained plates were imaged using the EVOS™ XL Core Configure microscope.

2.16 Picro-Sirius Red staining

Picro-Sirius Red staining is a widely used method for detecting and visualising collagen fibres in histological samples. The dye specifically binds to collagen, staining it red and creating contrast against other tissue components. To perform the staining, samples were incubated with 0.1% Picro-Sirius Red solution in saturated aqueous picric acid for 1 hour at RT. Following staining, samples were washed twice in acidified water to remove any unbound dye. Imaging was conducted using bright-field microscopy, where collagen fibres appeared red against a pale-yellow background.

2.16.1 Quantification of Picro-Sirius Red staining

Quantification of collagen content was performed by extracting the bound Picro-Sirius Red dye. To achieve this, 0.1 M NaOH solution was added to each well to elute the dye bound to cell-associated collagens. Samples were incubated for 30 minutes at RT on a continuous shaker set to 115 rpm. After elution, the resulting solutions were transferred to a transparent, flat-bottom 96-well plate, and the optical density (OD) was measured at 550 nm using an Infinite F200 PRO microplate reader. NaOH alone was used as a blank control, and all sample values were normalised to the day 0 sample.

2.17 Live/Dead viability/cytotoxicity assay

The Live/Dead (L/D) viability/cytotoxicity kit is a two-colour assay used to assess cell viability based on plasma membrane integrity and esterase activity. Cells were cultured in an appropriate medium and vessel for microscopy for the assay. The kit components were thawed, and a staining solution was prepared by adding 5 µL of calcein AM and 20 µL of ethidium homodimer-1 to 10 mL of Dulbecco's Phosphate-Buffered Saline (DPBS). The medium was then removed from the cells, and 100–200 µL of the staining solution was added directly to the cells. The cells were incubated at RT for 30 minutes. After incubation, the cells were imaged using a confocal microscope.

2.18 Dynamic culture of human TSPCs

In addition to static culture, dynamic culture conditions were used for the culture of human TSPCs to evaluate their effects on cell behaviour, particularly in terms of proliferation and EV production. The dynamic culture aimed to replicate the mechanical environment that tendons are exposed to *in vivo*, which can influence cellular activity, including differentiation and EV secretion.

2.18.1 Perfusion bioreactor

A customised perfusion bioreactor was used for dynamic stimulation, operating within a standard cell culture incubator (21% O_2). The bioreactor consisted of two T-175 cm² culture

flasks, each featuring holes designed to insert two 20G needles (BD Microlance™, 301300) (Figure 2-3).

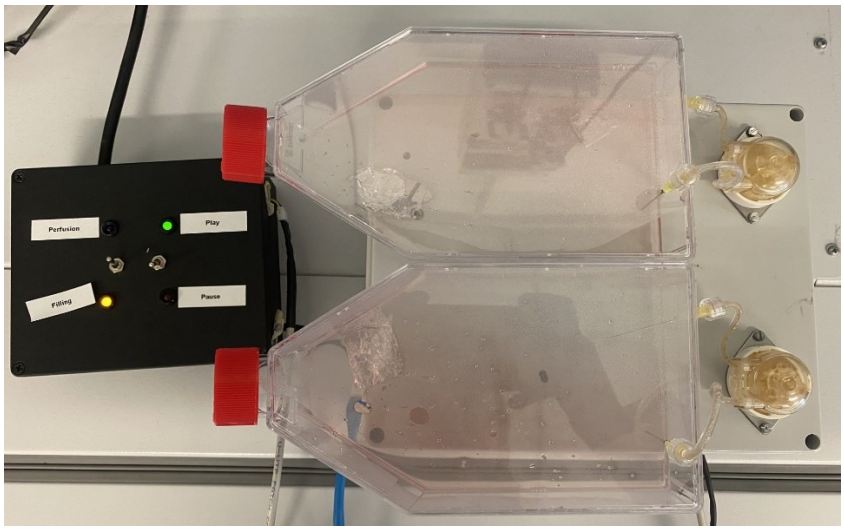


Figure 2-3. Perfusion bioreactor. The image represents the perfusion bioreactor setup with two peristaltic pumps (flow rate: 1 mL/min) and two T-175 cm² culture flasks for dynamic cell culture.

These needles were connected to Tygon® silicon tubing that allowed perfusion through peristaltic pumps, maintaining a constant flow rate of 1 mL/min. The dynamic culture system ensured the transfer of metabolites and oxygen to the cells while minimising shear stress, which is important for maintaining cell viability and function. As a comparison, static culture conditions were employed, where TSPCs were seeded into two T-175 cm² flasks, each containing 30 mL of medium. In both culture setups, TSPCs were seeded at a 5,000 cells/cm² density in GDF-5 supplemented media. The medium was continuously recirculated within the flasks under dynamic culture and replaced twice a week. In both culture conditions, the duration of the culture was the same (usually one week) until they reached 80% confluence. Both setups were maintained under identical environmental conditions (e.g., temperature, medium replacement schedule, same culture duration), ensuring a fair comparison between static and dynamic conditions.

2.18.1.1 FEM Analysis

Finite Element Modeling (FEM) was conducted using COMSOL Multiphysics to evaluate the medium velocity distribution in a dynamic culture plate. The analysis was performed in collaboration with the University of Bologna, with Dr. Joseph Lovecchio and prof. Emanuele Giordano providing expertise in computational modelling. Their contribution was instrumental in assessing the effects of flow on cell culture and EV production compared to static culture conditions. Laminar flow was modelled under steady-state conditions, with the culture plate represented as a rectangular geometry (length = 137 mm, width = 116 mm, height = 11 mm) and the inlet and outlet as cylindrical geometries (diameter = 0.6 mm, height = 40 mm). The flow rate was set at 1 mL/min, corresponding to an inner velocity of 0.06 m/s.

Boundary conditions included a uniform inlet velocity, zero pressure at the outlet, and no-slip conditions on the walls. A mesh sensitivity study was performed, comparing coarse, medium, and fine mesh configurations to identify the most computationally efficient and accurate solution. The simulation provided detailed insights into velocity distribution within the plate, highlighting the impact of dynamic culture conditions on medium flow patterns.

2.18.2 Lab-rocker system

The Lab-rocker system consists of a Cole-Parmer see-saw rocking shaker, typically set at a minimum speed of 5 rpm, which gently rocks the T-175 cm² culture flasks back and forth (Figure 2-4). This continuous motion mimics the mechanical forces that cells encounter *in vivo*, such as those experienced by tendon tissues subjected to movement and mechanical loading. In this setup, human TSPCs were cultured in flasks containing standard cell culture media at a density of 5,000 cells/cm² and exposed to dynamic conditions for the culture period (typically one week). Once the cells reached confluence, the culture medium was switched to a serum-free medium for 24 hours to allow for the collection of conditioned media. The samples were then harvested and stored for further analysis. The experiment was performed in both a 21% O_2 incubator and a 2% O_2 incubator to assess the effect of oxygen tension on cell behaviour.

For comparison, parallel cultures were maintained under static conditions in the same incubators for the same duration.



Figure 2-4. Lab rocker system. The image represents the dynamic culture setup for human TSPCs consisting of a Cole-Parmer rocker system with 4 T-175 cm^2 culture flasks placed in an incubator.

2.19 Conditioning of medium

CM was collected from both porcine and human tendon-derived cells to isolate and characterise EVs. The collection process began when cells in T175 flasks reached 70–90% confluence. Cells were first washed with 30 mL PBS, followed by addition of 30 mL SF medium (high-glucose DMEM supplemented with 1% PSA, 1% L-glut, and 1% NEAA). The cells were then incubated for 24 h. CM was collected and filtered using 0.22 µm syringe filters and stored at –20 °C until further use. CM was obtained from *n* = 3 independent porcine TSPC preparations and *n* = 3 independent human TSPC preparations. As the exact cell number at 70–90% confluency may vary between preparations, CM/cEV yields were normalised to the number of viable cells determined after collection or to total protein content.

2.20 Alamar Blue assay

The Alamar Blue assay was used to evaluate the cytotoxicity of CM by assessing cell viability through metabolic activity measurements. Different dilution ratios of CM samples were tested: undiluted, 1:2, 1:4, and 1:8, with each dilution prepared in standard cell culture medium (high-glucose DMEM supplemented with 10% FBS). Control samples included SF medium prepared in the same dilution ratios to compare cytotoxic effects. Standard cell culture medium (CTRL) was used as a negative control, while 0.5 mM sodium dodecyl sulfate (SDS) served as a positive control for cytotoxicity.

The assay was conducted on BALB/3T3 clone A31 murine fibroblast cells, with 10,000 cells seeded per well in 96-well plates. Following initial seeding in a standard culture medium for 24 hours to allow cell adhesion, the medium was replaced with the test and control conditions. Cells were incubated in these conditions for three days, and Alamar Blue assays were performed at 3 time points: 24 hours, 48 hours, and 72 hours.

Cell media were removed for the assay, and wells were washed with PBS. A working solution containing 10% Alamar Blue reagent diluted in high-glucose DMEM with 10% FBS was added to each well, and plates were incubated for 4 hours at 37°C. Fluorescence was measured using an excitation wavelength of 560 nm and an emission wavelength of 590 nm.

We acknowledge Fidia Farmaceutici S.p.A. for providing the necessary materials and equipment and sincerely thank Dr. Alba Di Lucia and Dr. Anna Marchetti for their technical support.

2.21 Conditioned media ultracentrifugation

The CM was thawed, and centrifugal tubes (Beckman Coulter 13.2 mL, Open-Top Thinwall ultra-Clear Tube, 344059) were filled to the top. Before use, tubes and centrifugal inserts were soaked in 70% IMS and allowed to dry overnight in the fume hood. To maintain sterility, all subsequent steps were done in the fume hood. Tubes were filled with CM, weighed for balance and then inserted in the swinging bucket rotor SW41 Ti (Beckman Coulter, 331362).

Centrifugation conditions were set as 100,000 g for 90 minutes using the Optima™ XPN-80 ultracentrifuge (Beckman Coulter, A95765). After centrifugation, the inserts were opened in the fume hood, the supernatant was discarded, and the resulting pellet was resuspended in either PBS or DMEM, collected in Eppendorf tubes and stored at -20°C. The result of the first centrifugation step was called crude pellet (CP) (Figure 2-5). Only after the appropriate characterisation crude pellets were called crude EVs (cEVs).

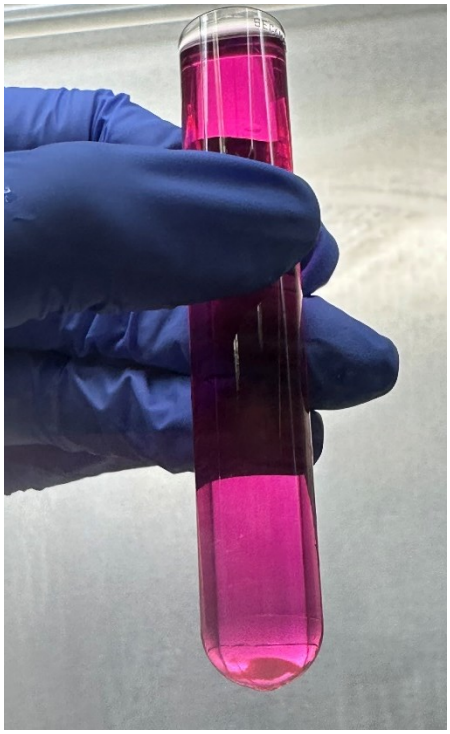


Figure 2-5. Crude pellet obtained after the ultracentrifugation of conditioned media. The image shows the distinct separation of the protein pellet from the supernatant.

2.22 Morphological analysis of crude pellet

Various methods were employed to assess the presence and morphology of EVs in the crude pellet.

2.22.1 Scanning electron microscopy

For sample preparation, several droplets of the crude pellet were placed onto an aluminium stub using double-sided adhesive carbon tape and then dried using a critical point drier (model K850, Quorum Technologies Ltd, East Sussex, United Kingdom). A thin layer of gold (250 Å

thick) was sputter-coated onto the samples using a sputter coater (model 108 A, Agar Scientific, Stansted, UK). Once ready, samples were examined and imaged using a Field Emission Scanning Electron Microscope (FE-SEM, LEO 1525 model, Carl Zeiss SMT AG, Oberkochen, Germany).

2.22.2 Transmission electron microscopy

For TEM imaging, 10 µL of sample was applied to a formvar/carbon 200 mesh copper grid (Ted Pella, USA, Cat. No. 01800-F) and allowed to air dry for several hours. The micrographs were acquired using a transmission electron microscope in bright-field mode, specifically the FEI TECNAI G2 200 kV S-TWIN microscope, equipped with a 4K camera (electron source with LaB6 emitter; FEI Company, Hillsboro, OR, USA). Bright-field TEM images were captured at 120 kV with a spot size of 3 and an integration time of 1 second.

2.22.3 Nanoparticle tracking analysis

The size and concentration of nanoparticles in the pellets were determined using the Nanosight NS300 nanoparticle characterisation system (Nanosight Ltd), which is equipped with fast video capture and particle-tracking software. Samples were not diluted and were introduced into the laser chamber at a constant flow rate controlled by a syringe pump. Three separate recordings were made for each sample. The Nanoparticle Tracking Analysis (NTA) software was used to analyse the size distribution (expressed as mean ± SD) and concentration of nanoparticles. The batch processing feature of the software was employed to integrate the three technical replicates for each sample.

2.23 Protein analysis of crude pellet

Several techniques were employed to measure the samples' total protein concentration and detect specific EV markers to verify the presence of EVs in the CP.

2.23.1 Bradford assay

Total protein concentration was measured in both CM and CP samples. For protein quantification, Pierce™ Bradford Plus Protein Assay Reagent was used according to the

manufacturer's instructions. Standards were prepared with BSA and diluted in SF medium or PBS. FBS diluted to fit the detectable range was used as a positive control. Samples were measured with Biotek Synergy 2 Plate Reader Multi-Mode and analysed with BioTek Gen5 Data Analysis Software and Excel.

2.23.2 Multiplex surface marker analysis

Flow cytometry analysis was conducted using the MACSPlex Exosome Kit for human samples (Miltenyi Biotec, 130-122-209), which detects 37 exosomal surface epitopes, along with two isotype controls. The markers are the following: CD3, CD4, CD19, CD8, HLA-DRDPDQ, CD56, CD105, CD2, CD1c, CD25, CD49e, ROR1, CD209, CD9, SSEA-4, HLA-ABC, CD63, CD40, CD62P, CD11c, CD81, MCSP, CD146, CD41b, CD42a, CD24, CD86, CD44, CD326, CD133/1, CD29, CD69, CD142, CD45, CD31, CD20, CD14, REA control, mIgG1 control. The procedure was performed according to the manufacturer's instructions. Briefly, EV-containing samples were mixed with MACSPlex buffer to a final volume of 120 µL. The mixtures were transferred into 1.5 mL tubes and combined with 15 µL of MACSPlex Exosome Capture Beads. The tubes were incubated overnight at RT on an orbital shaker (450 rpm), protected from light. Following incubation, 500 µL of MACSPlex buffer was added to each tube, and the samples were centrifuged at RT at 3000 RCF for 5 minutes. The supernatant was carefully discarded, and 5 µL of MACSPlex Exosome Detection Reagents (CD9, CD63, and CD81) were added to each tube. Samples were incubated for 1 hour at RT on the orbital shaker (450 rpm). After incubation, a washing step was performed by adding 500 µL of MACSPlex buffer to each tube, followed by a 15-minute incubation at RT in the orbital shaker (450 rpm). The EV-containing samples were then centrifuged again, and the supernatant was removed, leaving approximately 200 µL in each tube. Flow cytometric analysis was performed using either a BD FACSVerse™ flow cytometer (Becton Dickinson) or CytoFlex flow cytometer, acquiring 5,000 events per sample. Data analysis was conducted using either Kaluza software (v.2.1, Beckman Coulter) or CytExpert 2.2 software. We acknowledge Dr. Valentina Giudice for her expertise in sample reading and data analysis.

2.23.3 Western blotting

Human TSPCs were thawed in fresh media, spun down for 15 minutes at 1400 rpm, and then resuspended in 1 mL of PBS. The cells were lysed in 1:4 dilution of RIPA buffer supplemented with protease and phosphatase inhibitor cocktail for 45 minutes on ice, with shaking of the samples every 10 minutes. Cell lysates were centrifuged for 20 minutes at 15,000 g, and the supernatants were transferred to a new 1.5 mL tube. Protein content was determined by BCA, and 25µg of total protein was loaded per lane. EV pellet proteins were determined using Pierce™ Bradford Plus Protein Assay Reagent. The total amount was resuspended in 100 µL of distilled water and then equally split between all lanes (1 µg/lane). Then, protein extracts were separated by SDS-PAGE gels and transferred onto nitrocellulose membranes. Nitrocellulose blots were blocked with 10% non-fat dry milk in TBS-T buffer (20 mM Tris-HCl, pH 7.4, 500 mM NaCl and 0.1% Tween-20) and incubated in TBS-T buffer containing 5% BSA overnight at 4°C with the following primary antibodies (all diluted 1:1000): anti-Calnexin, anti-CD9, anti-CD63, anti-CD81, anti-Hsp70, anti-TSG101 and anti-α-tubulin. Immunoreactivity was detected by sequential incubation with appropriate HRP-conjugated secondary antibodies for 1h at RT and Pierce™ ECL Western blotting substrate on a radiography film. Densitometry of bands was performed with ImageJ software (version 1.53c). The area under each curve, relative to a band, was determined, and the local background was subtracted from the calculated values.

2.24 Cytokines analysis

Cytokine quantification was performed using the Porcine Cytokine/Chemokine 13-Plex Discovery Assay® Array (PD13) for porcine CM samples and the Human Cytokine Proinflammatory Focused 15-Plex Discovery Assay® Array (HDF15) for human cEVs, both designed for the Luminex® 200™ platform and conducted by Eve Technologies. Sample preparation was carried out according to the manufacturer's instructions. Briefly, 75 µL of CM or cEVs were aliquoted without dilution and sent for analysis. The analysis was conducted using commercially available kits, primarily sourced from Millipore, following the provided

protocol. The following biomarkers were measured: GM-CSF, IFNγ, IL-1α, IL-1RA, IL-1β, IL-2, IL-4, IL-6, IL-8, IL-10, IL-12, IL-18, and TNFα for porcine samples, and GM-CSF, IFNγ, IL-1β, IL-1RA, IL-2, IL-4, IL-5, IL-6, IL-8, IL-10, IL-12p40, IL-12p70, IL-13, MCP-1, and TNFα for human samples.

2.25 Hydrogels

Collagen hydrogels were prepared according to the manufacturer's protocol (Corning®), with a modification to replace 10X PBS with 10X DMEM to provide nutrients for the cells. To prepare 10X DMEM, 1.34 g of DMEM powder and 0.37 g of sodium bicarbonate were dissolved in 10 mL of sterile dH_2O. 1N sodium hydroxide (NaOH) was prepared by dissolving 1.6 g in 40 mL sterile dH_2O. All solutions were filtered in a flow hood using a 0.22 µm syringe filter. The collagen, 10X DMEM, sterile dH_2O and 1N NaOH were kept on ice until use. The required volumes of each component were calculated using the following formulas:

- $Volume\ of\ 10X\ DMEM = \frac{Final\ solution\ volume}{10}$
- $Volume\ of\ collagen\ solution = \frac{Final\ solution\ volume \times Final\ collagen\ concentration}{Initial\ collagen\ stock\ concentration}$
- $Volume\ of\ 1N\ NaOH = volume\ of\ collagen\ solution\ \times 0.023$
- $Volume\ of\ dH_2O = \text{final solution volume} - (\text{10X DMEM volume} + \text{collagen solution volume} + \text{1N NaOH volume})$

The components were added in the following order to a sterile bijou tube held on ice: dH_2O, 1 N NaOH, 10X DMEM, and collagen solution. The mixture was thoroughly but gently mixed to avoid introducing bubbles.

For hydrogels containing cells, the appropriate number of cells was trypsinised (as described in section 2.2.1), pelleted by centrifugation, and resuspended in approximately 1/3 of the required dH_2O volume using SF medium. Hydrogels containing cells and cEVs were pelleted by centrifugation and then resuspended in the same volume of SF medium. In these cases, 2/3 of the dH_2O volume was added initially to neutralise the collagen solution, and the

remaining 1/3, substituted with SF-containing cells and/or cEVs, was added as a final step. The solution was mixed gently and swiftly by pipetting to prevent premature gelation. The hydrogels were then injected into the casting apparatus, which consisted of a 1 mL sterile plastic syringe with a modified end (trimmed to maintain a uniform inner diameter of 0.47 cm). Crosslinking was performed at 37°C for 1 hour. After cross-linking, the plunger was gently depressed to eject the collagen tube from the untreated 6-well plates, and the appropriate culture medium was added (Figure 2-6). Media changes were performed twice a week over a 14-day culture period. Hydrogels were prepared to a final collagen concentration of 3 mg/mL with a seeding density of 10^5 cells/mL, as previously described by Lomas et al[282]. The length of the hydrogels was measured noninvasively at different time points using a ruler positioned beneath or adjacent to the culture plate.

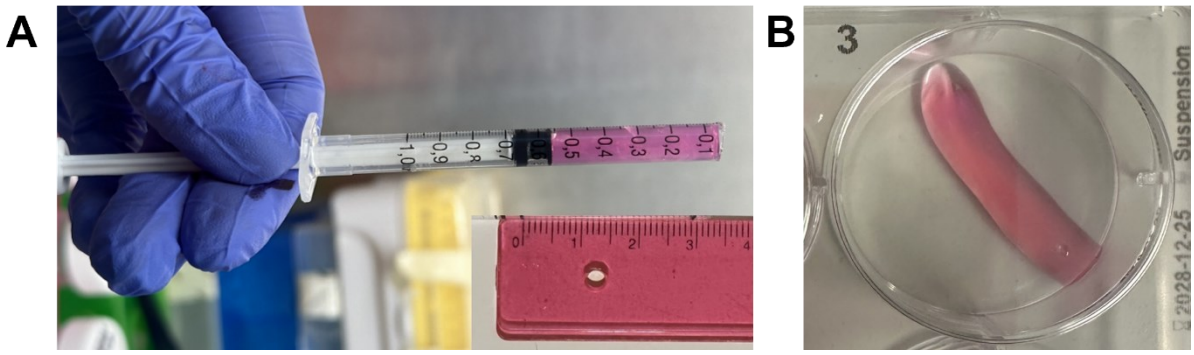


Figure 2-6. Collagen hydrogel moulding procedure. The image shows a collagen gel solution loaded into a 1 mL sterile syringe with a modified end to ensure uniform diameter during extrusion (A) and fully crosslinked collagen hydrogel placed in a culture plate, ready for experimental use (B).

Chapter 3

Optimising porcine TSPCs for EV production and tenogenic potential

3. OPTIMISING PORCINE TSPCS FOR EV PRODUCTION AND TENOGENIC POTENTIAL

3.1 Introduction

Tendon-derived cell populations, including TSPCs I, TSPCs II, and Tncs, occupy distinct anatomical niches within the tendon structure[8,24]. TSPCs I are found in the paratenon, TSPCs II are located in the ECM-rich endotenon, and Tncs are distributed among collagen fibrils in the interfascicular matrix[23]. While these populations play critical roles in tendon biology and healing, their individual characteristics and regenerative potential remain incompletely understood.

Although tendon cell populations in different species have been examined in previous studies[283–286], the simultaneous isolation and characterisation of three distinct populations under atmospheric and physiological oxygen conditions has not been previously reported. The porcine model provides a unique platform for studying tendon-derived cells because of its anatomical and physiological similarities to human tissues[287]. Furthermore, oxygen tension, a key element of the tendon microenvironment, is recognised for its influence on cellular proliferation, differentiation, and marker expression[175]. Understanding how tendon-derived cells react to varying oxygen levels is crucial for optimising their therapeutic potential.

In addition to cellular approaches, EVs have emerged as a promising cell-free therapeutic strategy in regenerative medicine[288]. Their potential to modulate inflammation, promote regeneration, and deliver therapeutic cargo highlights their relevance for tendon repair. Although EV production by tendon-derived cells has been explored in a limited capacity[289–292], the influence of oxygen tension on EV characteristics and function remains understudied[255,260]. Investigating the EV production potential of tendon cell populations may provide novel insights into their therapeutic applications.

This chapter aims to address these gaps by isolating and characterising TSPCs I, TSPCs II, and Tncs from porcine deep digital flexor tendons. Proliferation, morphology, differentiation capacity, and marker expression were analysed under two oxygen conditions. Furthermore, EV production by TSPCs II and Tncs was investigated, including morphology, protein content, cytokine secretion, and surface marker expression, to provide insight into their potential roles in tendon biology and repair.

3.2 Aim

The primary objective of this chapter was to comprehensively characterise and compare tendon-derived cell populations, including TSPCs I, TSPCs II and Tncs, to evaluate their potential for tendon repair and tissue engineering. Additionally, this study sought to investigate these populations' EV production to advance the understanding of their role in intercellular communication and therapeutic applications. Specifically, this study aimed to:

1. Isolate and culture tendon-derived cell populations using optimised protocols, including enzymatic digestion and explant methods, and evaluate their growth and morphological characteristics.

2. Assess the effects of oxygen tension (physiological 2% O_2 and atmospheric 21% O_2) on cell proliferation, morphology, and differentiation potential across these populations.

3. Characterise the trilineage differentiation potential of tendon-derived cell populations to determine their capacity for adipogenic, osteogenic, and chondrogenic differentiation.

4. Analyse immunophenotypic and molecular markers, including tenogenic (e.g., *TNMD*, *SCX*, *THBS4*) and stem cell (e.g., *NANOG*, *NESTIN*, *OCT-4*) markers, to identify distinct functional profiles and adaptations to varying oxygen conditions.

5. Characterise the EVs derived from TSPCs II and Tncs, including their morphology, protein content, cytokine profiles, and surface marker expression, under physiological and atmospheric oxygen conditions.
6. Identify the most promising cell population for tendon regeneration based on proliferative potential, phenotypic stability, and tenogenic characteristics.

Among the cell populations investigated, particular emphasis was placed on TSPCs II, as they demonstrated a functional profile that warranted further characterisation. This chapter thoroughly examined their EV production to establish a solid understanding of their molecular composition and potential tenogenic influence. This focus provides a basis for the following chapters, which will explore the possible influence of TSPCs II-derived EVs in the context of tendon regeneration.

3.3 Methods

The study design is summarised in Scheme 1, with detailed materials and methods provided in Chapter 2.

Porcine tendon-derived cells, including TSPCs I, TSPCs II, and Tncs, were isolated from deep digital flexor tendons using enzymatic digestion and explant methods as described in sections 2.3.1 and 2.3.2 (Figure 3-1). Cells were expanded under atmospheric or physiological oxygen conditions, and their growth, morphology, differentiation capacity, and marker expression were assessed as described in Chapter 2.

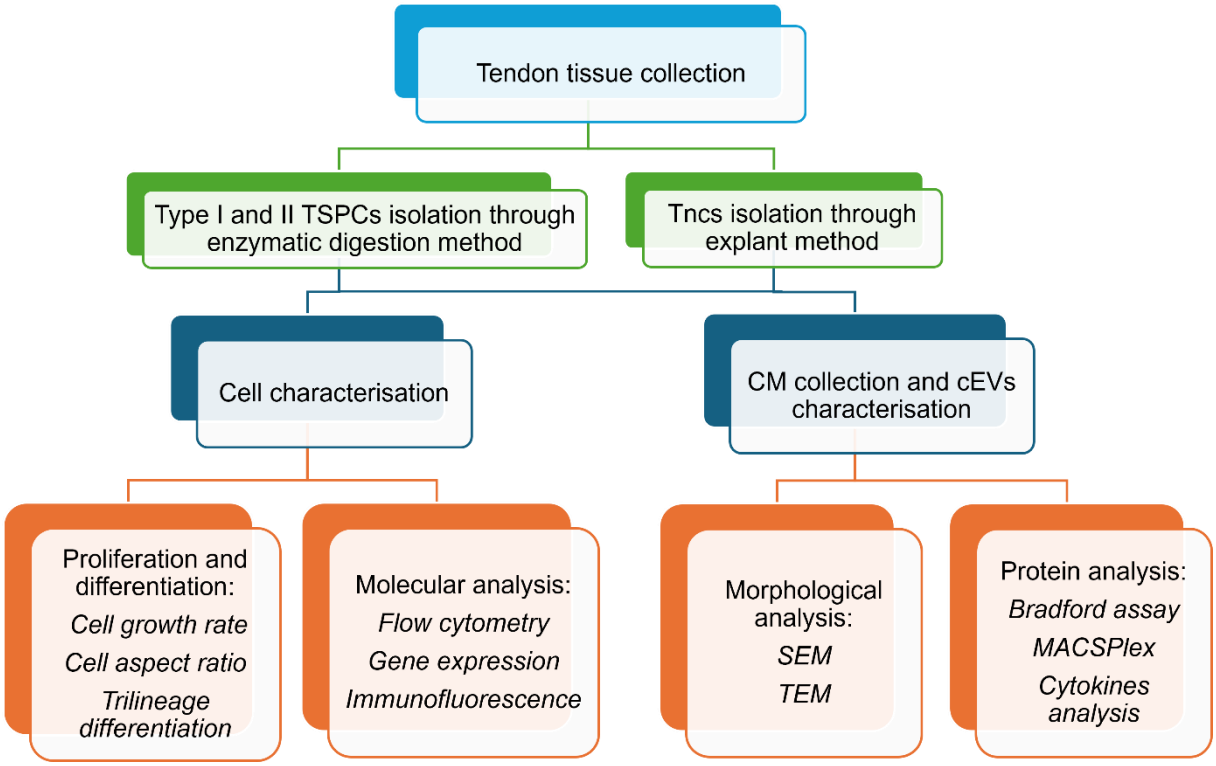
Trilineage differentiation was induced using standard adipogenic, osteogenic, and chondrogenic media, and evaluated by histological staining (see Section 2.6). Immunophenotyping was performed by flow cytometry against MSC-associated markers (see Section 2.9.1), while gene expression was analysed by RT-qPCR to assess tenogenic (*TNMD*, *SCX*, *THBS4*, *TNC*) and stem cell (*NANOG*, *NESTIN*, *OCT-4*) markers (see Section 2.12). TNMD protein expression was analysed by immunofluorescence in TSPCs II cultured under different oxygen conditions (see Section 2.14).

Cells were cultured to explore the EV production potential of TSPCs II and Tncs, as described above. Once confluent, cells were switched to SF media for 24 hours to stimulate EV secretion. CM was collected as outlined in section 2.19 and stored at -80°C until use. Crude EVs were isolated from CM by ultracentrifugation at 100,000 g for 90 minutes, as detailed in section 2.21. The resulting crude pellet was resuspended in PBS for characterisation. Morphological analysis of EVs was performed using TEM and SEM to evaluate size, shape, and structural integrity, as described in section 2.22.

Protein concentration in the CM and crude EVs was measured using the Bradford assay, as outlined in section 2.23.1. Flow cytometry-based MACSPlex analysis was used to evaluate the expression of 37 exosomal surface markers, including immune cell, stem cell, tumour-associated, and extracellular vesicle-associated markers, as detailed in section 2.23.2. Cytokine profiling was conducted on CM derived from TSPCs II and Tncs cultured under both oxygen conditions to assess pro- and anti-inflammatory factors, as described in section 2.24.

3.3.1 Statistical analysis

Data are presented as the mean ± SD from three biological replicates (n = 3). Statistical comparisons were conducted using Student's *t*-test, one-way ANOVA, or two-way ANOVA, as appropriate. When ANOVA indicated significant effects, post-hoc multiple-comparison tests were applied: Tukey's HSD for all-pairwise comparisons and Šídák's test for selected planned comparisons. All analyses were performed using GraphPad Prism software (version 10.2.2), with significance thresholds set as '*' for $p < 0.05$, '**' for $p < 0.01$, '***' for $p < 0.001$, and '****' for $p < 0.0001$.



Scheme 1. Summary of the methodology adopted in Chapter 3.

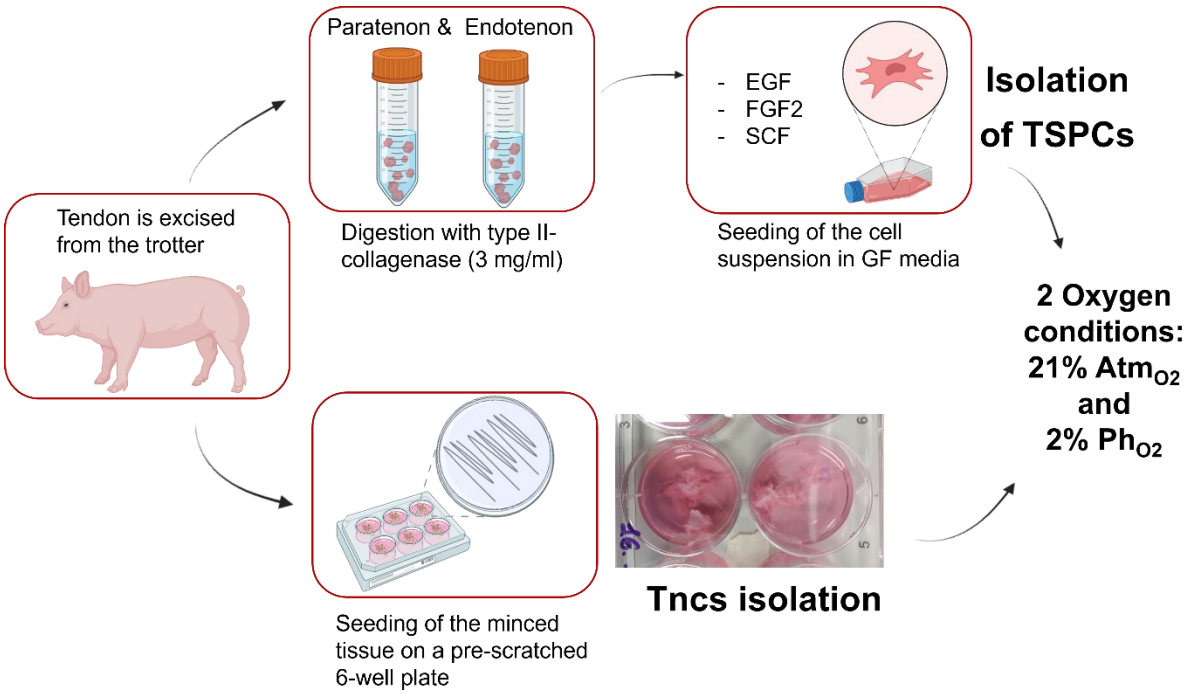


Figure 3-1. Tendon-derived cell populations isolation. Schematic representation of the isolation process for tendon cells derived from porcine tissue, using either enzymatic digestion or explant culture methods. Image partially created with https://www.biorender.com/.

3.4 Results

3.4.1 Cell yield after isolation

Three distinct tendon-derived cell populations were successfully isolated from porcine samples: TSPCs I, TSPCs II, and Tncs. These cell populations were isolated using overnight type II collagenase digestion for TSPCs I and TSPCs II and an explant method for Tncs, as described in sections 2.3.1 and 2.3.2 and summarised in Figure 3-1. The average cell yield obtained from each pig trotter (with an average tendon size of 14x4x2 cm^3) after one day of enzymatic digestion was 1.62 $x10^6$ TSPCs I and 1.54 $x10^6$ TSPCs II. In contrast, the explant method, which relies on the natural migration of cells from the tissue to the culture plate, required several weeks before the cells reached confluence and could be counted. Cell growth rate varied according to oxygen conditions; Tncs cultured under physiological oxygen reached confluence in approximately 19 days, while those cultured in atmospheric oxygen grew more slowly, taking approximately 23 days. The average cell yield per pig trotter, across both oxygen conditions, was 2.12 × 10^6 Tncs (Figure 3-2).

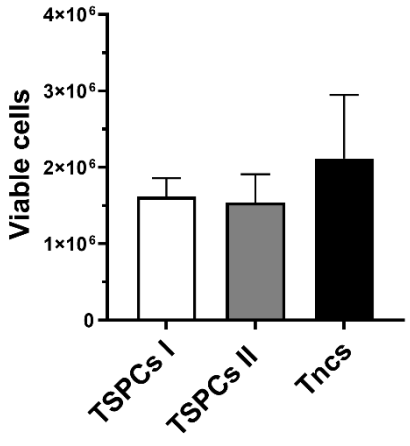


Figure 3-2. Isolation of tendon-derived cell populations. Total number of viable cells obtained per tendon: TSPCs I (paratenon digestion), TSPCs II (endotenon digestion), and Tncs (explant). Values are expressed as mean ± SD, n = 3. Image adapted from Clerici et al., 20239 under CC BY 4.0 License.

3.4.2 Cell proliferative capacity

All cell types (TSPCs I, TSPCs II and Tncs) were cultured over a 120-day culture period in 2% and 21% O_2 to monitor their proliferation rates, expressed through the cumulative population doubling (CPD) (Figure 3-3). TSPCs I cultured in 21% O_2 showed a plateau in growth after 40 days, reaching 15 CPDs, after which cell proliferation slowed significantly. However, in 2% O_2 TSPCs I continued proliferating for 80 days before reaching a reduced growth plateau at 35 CPDs, demonstrating a 57% increase in proliferative capacity compared to those cultured in 21% O_2.

TSPCs II cultured in 21% O_2 reached a plateau after 60 days of growth at 30 CPDs, whereas those cultured in 2% O_2 slowed their growth after 70 days, reaching 40 CPDs, marking a 25% increase compared to their counterparts in 21% O_2. In the case of Tncs, those cultured in 21% O_2 showed limited growth, plateauing at 90 days with a growth rate of 11 CPDs. On the other hand, Tncs in 2% O_2 maintained consistent proliferation throughout the culture period, achieving 19 CPDs, a 42% increase over their counterparts in atmospheric oxygen.

Overall, these results indicate that TSPCs I showed a significant reduction in proliferation in 21% O_2 compared to 2% O_2, while TSPCs II exhibited only a slight decrease in growth under the higher oxygen condition. Tncs, on the other hand, showed a premature proliferative arrest but also demonstrated reduced proliferative capacity in air oxygen compared to 2% O_2. Among the populations, TSPCs II demonstrated the highest overall proliferative potential in both oxygen environments, whereas Tncs were comparatively more restricted in their growth. Enhanced proliferation was observed in all cell types under 2% O_2.

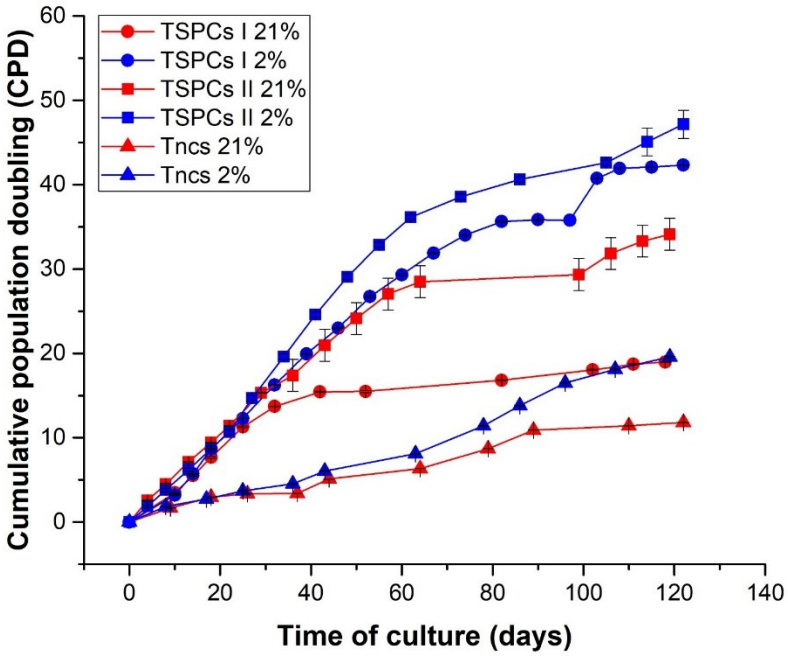


Figure 3-3. Cell growth curves. TSPCs I, TSPCs II, and Tncs were isolated and cultured in 2% and 21% O_2 conditions. Cumulative population doubling (CPD) was calculated over 120 days of culture, with cells serially passaged until proliferation ceased or decreased; n=3. Image adapted from Clerici et al., 2023[9] under CC BY 4.0 License.

3.4.3 Cell aspect ratio

Upon initial adherence to the culture plate, morphological similarities were noted between TSPCs I and Tncs, displaying a more elongated morphology than TSPCs II, which appeared smaller and more compact. To quantify these differences, the cell aspect ratio was calculated, comparing all cell types at passage 1 (P1) under both oxygen conditions and then across early and late passages to assess how ageing influenced their morphological characteristics.

At P1 in atmospheric oxygen, TSPCs I exhibited a significantly more elongated morphology compared to TSPCs II ($p < 0.0001$) and Tncs ($p = 0.0007$). However, in physiological oxygen, TSPCs II demonstrated the highest aspect ratio, significantly differing from TSPCs I and Tncs ($p < 0.0001$ for both comparisons). Additionally, significant differences were observed between the aspect ratios of TSPCs I and Tncs at P1 ($p = 0.0279$) (Figure 3-4).

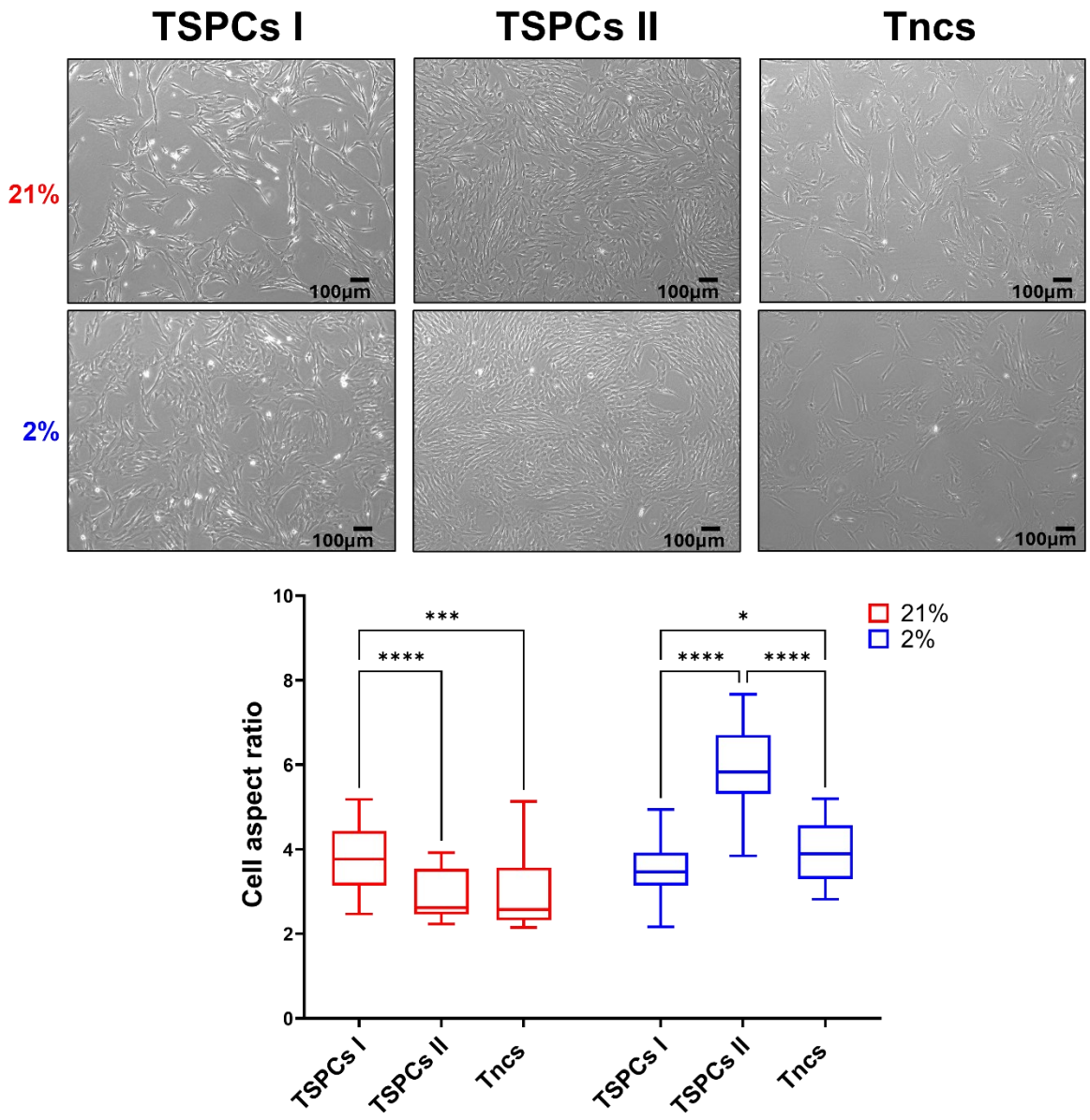


Figure 3-4. Aspect ratios of tendon cell populations at passage 1 (P1). Morphological differences between tendon cell populations cultured in 21% and 2% O_2 at P1 were observed using optical microscopy and quantified by measuring cell aspect ratios. Scale bar = 100 µm. Statistical analysis: two-way ANOVA, followed by Tukey's HSD multiple-comparison post-hoc test; '*' for $p < 0.05$, '***' for $p < 0.001$, and '****' for $p < 0.0001$, n=3.

Furthermore, examining the changes in cell morphology over different passages, the aspect ratio of TSPCs I in 21% O_2 decreased between P1 and P13, shifting from spindle-shaped to more rounded cells ($p = 0.0007$). In contrast, no significant change in morphology was observed for TSPCs I cultured in 2% O_2, even at later passages (Figure 3-5). For TSPCs II, the aspect ratio decreased across both oxygen conditions from P1 to the final passage, with

significant reductions observed at P19 in 21% O_2 ($p = 0.0077$) and P20 in 2% O_2 ($p < 0.0001$). Notably, differences in aspect ratio were observed between early and late passages of TSPCs II when cultured under different oxygen conditions (Figure 3-6). Similarly, Tncs exhibited a reduction in aspect ratio over time, with significant decreases between P1 and P10 in 21% O_2 ($p = 0.0008$) and between P1 and P11 in 2% O_2 ($p < 0.0001$) (Figure 3-7). Overall, passage number and oxygen concentration influenced the morphology of TSPCs II and Tncs. However, compared with TSPCs I, the changes in TSPCs II were less pronounced across conditions, suggesting a relatively greater morphological consistency. This relative stability may support their utility in extended culture, although further studies would be required to confirm their suitability for regenerative applications.

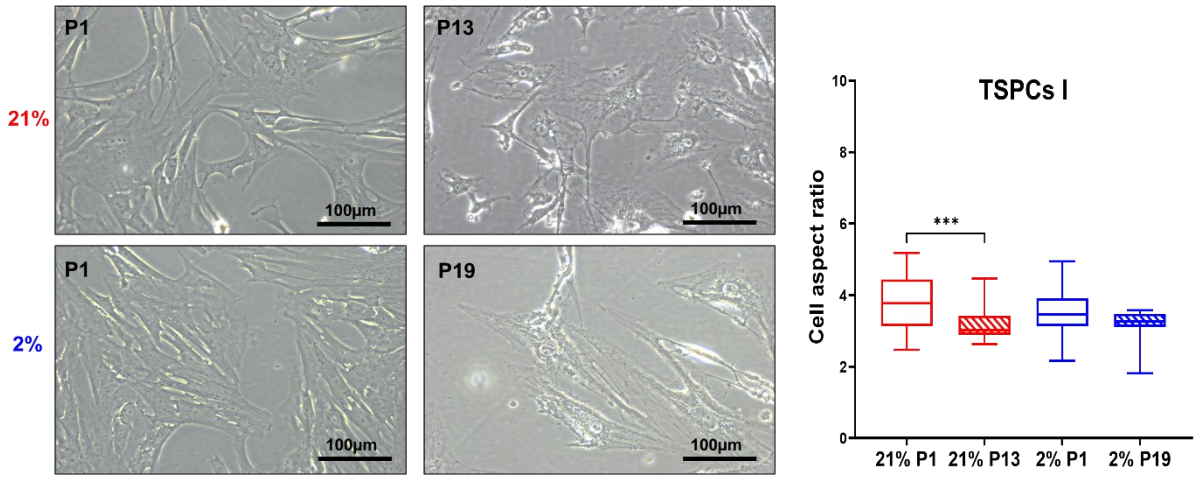


Figure 3-5. TSPCs I aspect ratio. The aspect ratio of TSPCs I is influenced by oxygen conditions, with morphological changes observed between early and late passages in both 21% and 2% O_2, as seen through optical microscopy (scale bar = 100 μm). The aspect ratios of TSPCs I were measured and compared within the same oxygen condition across different passages and between identical passages cultured under different oxygen concentrations. Statistical analysis: one-way ANOVA across four groups (21%-P1, 21%-late, 2%-P1, 2%-late), followed by Šídák's multiple-comparison post-hoc test; '***' = $p < 0.001$, n=3. Image adapted from Clerici et al., 2023[9] under CC BY 4.0 License.

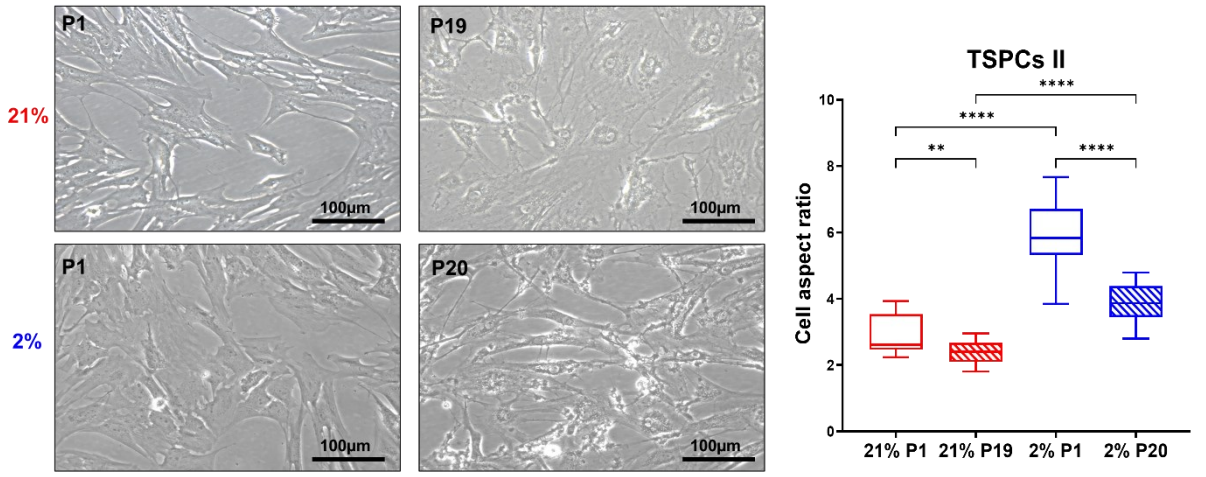


Figure 3-6. TSPCs II aspect ratio. The aspect ratio of TSPCs II is influenced by oxygen conditions and passage number, with morphological changes observed between early and late passages in 21% and 2% O_2, as seen through optical microscopy (scale bar = 100 µm). The aspect ratios of TSPCs II were measured and compared within the same oxygen condition across different passages and between identical passages cultured under different oxygen concentrations. Statistical analysis: one-way ANOVA across four groups (21%-P1, 21%-P19, 2%-P1, 2%-P20), followed by Šídák's multiple-comparison post-hoc test; '**' = $p < 0.01$ and '****' = $p < 0.0001$, n=3. Image adapted from Clerici et al., 2023[9] under CC BY 4.0 License.

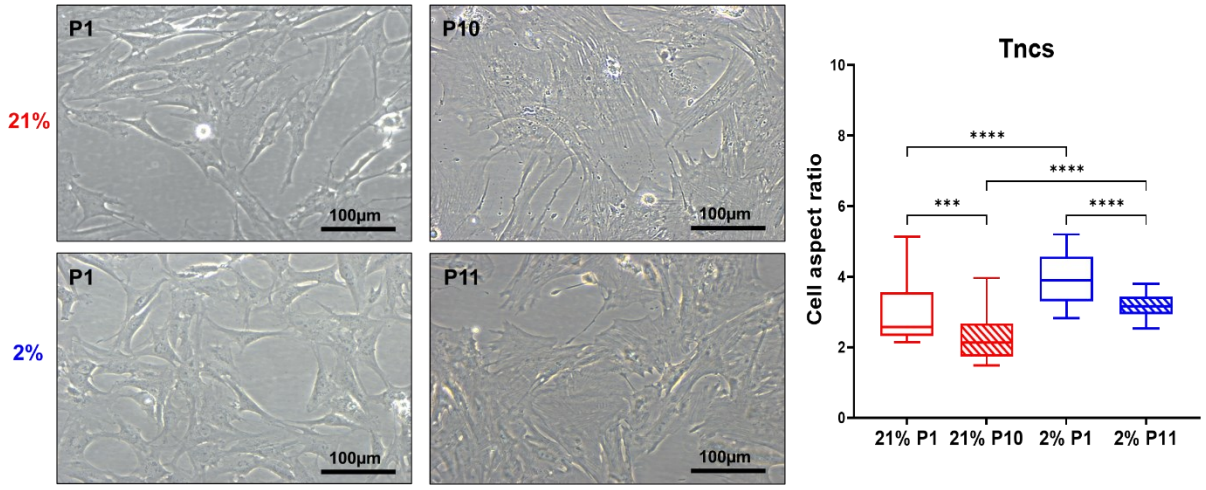


Figure 3-7. Tncs aspect ratio. The aspect ratio of Tncs depends on oxygen conditions and passage number, with morphological changes observed between early and late passages in 21% and 2% O_2, as seen through optical microscopy (scale bar = 100 µm). The aspect ratios of Tncs were measured and compared within the same oxygen condition across different passages and between identical passages cultured under different oxygen concentrations. Statistical analysis: one-way ANOVA across four groups (21%-P1, 21%-P10, 2%-P1, 2%-P11), followed by Šídák's multiple-comparison post-hoc test; '***' = $p < 0.001$ and '****'= $p < 0.0001$, n=3. Image adapted from Clerici et al., 2023[9] under CC BY 4.0 License.

3.4.4 Trilineage differentiation capacity

Trilineage differentiation was induced by exposing cells to adipogenic, osteogenic, and chondrogenic media to assess the differentiation potential of tendon-derived cell populations. Control wells cultured in standard culture medium for 21 days did not show positive staining with Alizarin Red or Oil Red O, although some Alcian Blue staining was observed. Early passage TSPCs I exhibited multipotency, as indicated by positive staining for Oil Red O, Alizarin Red, and Alcian Blue after 21 days of culture (Figure 3-8) under both oxygen conditions. Given their sustained proliferative capacity, TSPCs II were tested for multipotency in both early (P3) and late passage (P13) populations (Figure 3-9). In both passages, TSPCs II exhibited positive histological staining, confirming their ability to differentiate into all three lineages, regardless of the oxygen concentration. The osteogenic differentiation yielded the most efficient results at both passages. Tncs showed partial differentiation potential in early passage cells, with evidence of adipogenic and osteogenic differentiation (Figure 3-10). However, chondrogenesis was less efficient in both oxygen conditions than TSPCs I and early-passage TSPCs II. In summary, TSPCs I and II exhibited full multipotent differentiation potential, with TSPCs II retaining this ability even in later passages. In contrast, Tncs displayed only partial differentiation potential, primarily limited to adipogenic and osteogenic lineages. Furthermore, cultures in low-oxygen conditions (2% O_2) began to detach from the wells after 14 days.

While TSPCs II retained trilineage differentiation potential at both early and late passages, a reduced efficiency in chondrogenic differentiation was observed at later passages. This may indicate that subpopulations within the TSPCs II pool are progressively selected during culture expansion, influencing their differentiation profile.

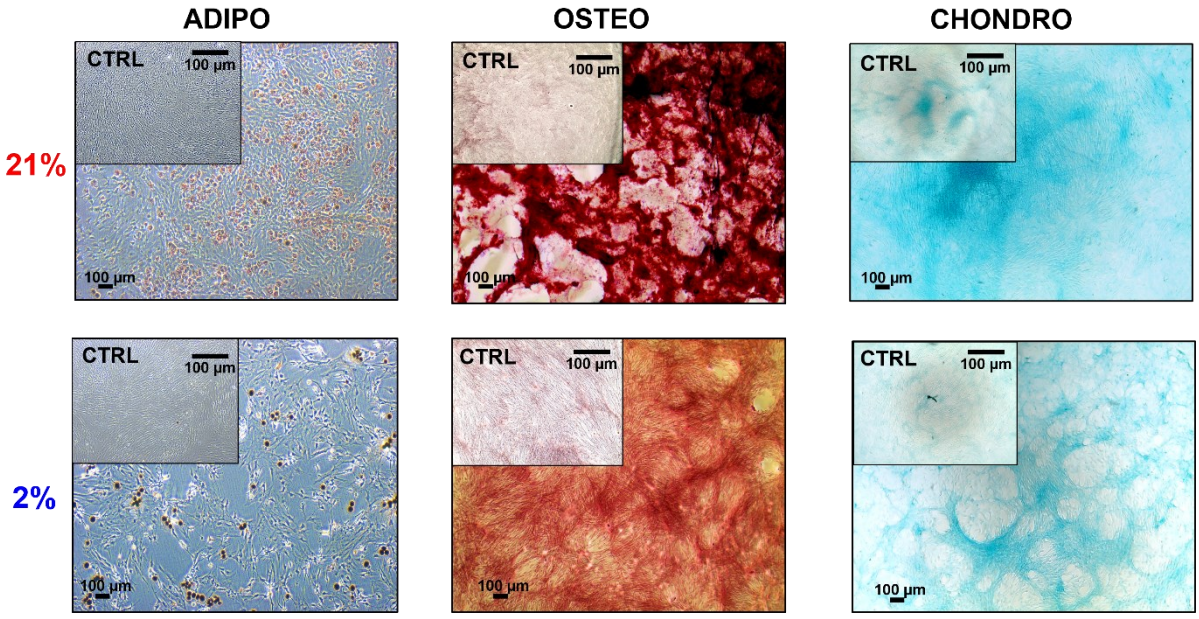


Figure 3-8. Trilineage differentiation of TSPCs I. Images of early passage (P3) TSPCs I cultured in monolayers for 21 days in both 21% and 2% O_2 conditions, with pro-differentiation media supplements, followed by fixation and histological staining. Scale bar = 100 µm. Image adapted from Clerici et al., 2023[9] under CC BY 4.0 License.

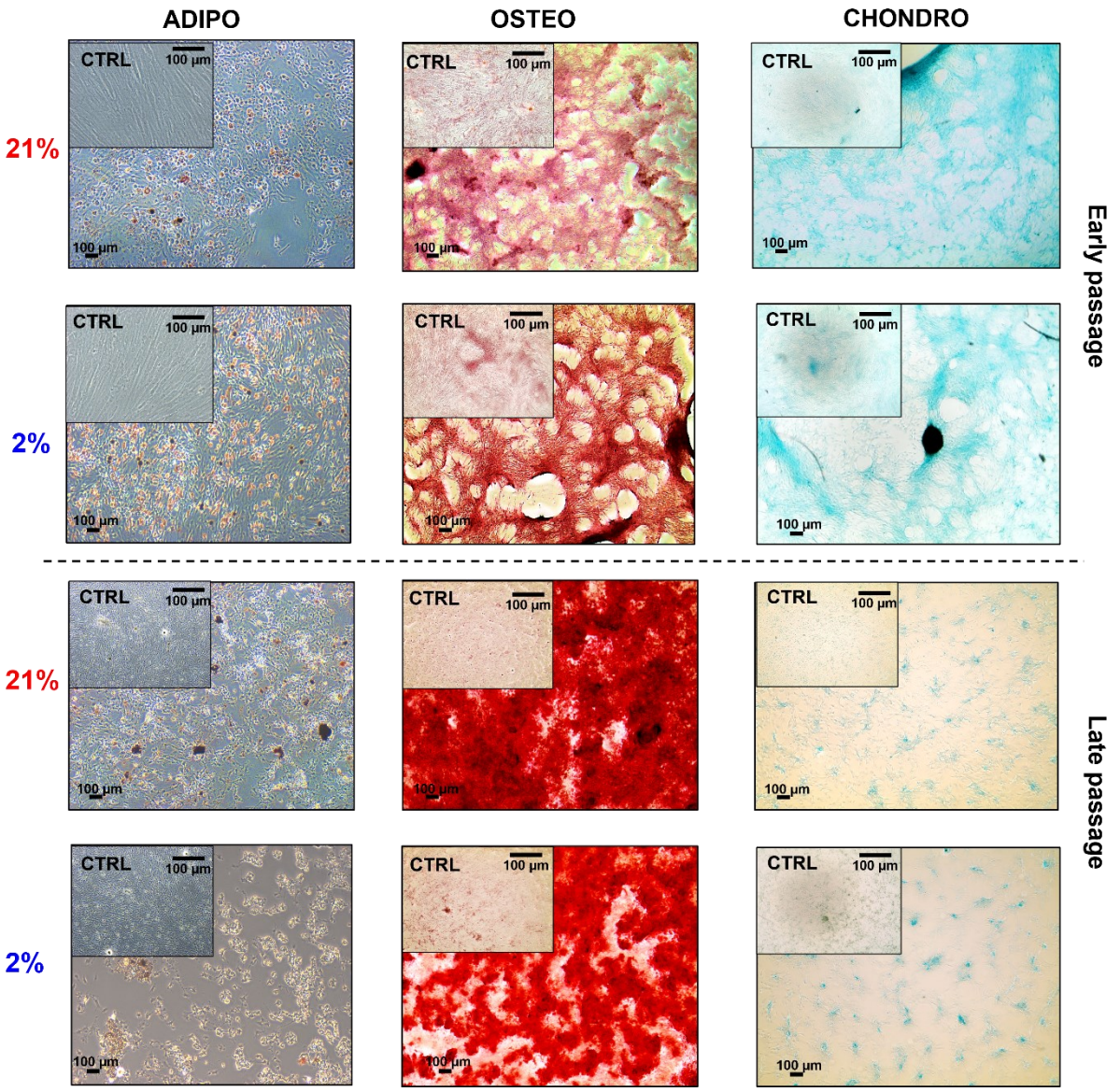


Figure 3-9. Trilineage differentiation of TSPCs II. Images of early (P3) and late (P13) passage TSPCs II cultured in monolayers for 21 days in both 21% and 2% O_2 conditions, with pro-differentiation media supplements, followed by fixation and histological staining. Scale bar = 100 µm. Image adapted from Clerici et al., 2023[9] under CC BY 4.0 License.

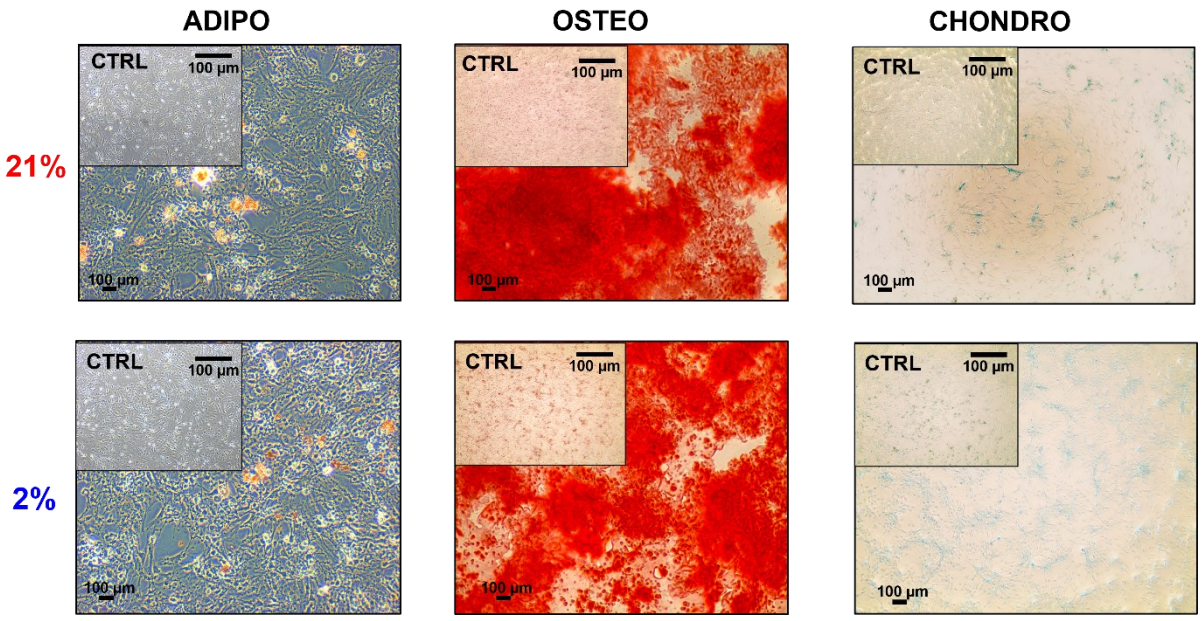


Figure 3-10. Trilineage differentiation of Tncs. Images of early passage (P3) Tncs cultured in monolayers for 21 days in both 21% and 2% O_2 conditions, with pro-differentiation media supplements, followed by fixation and histological staining. Scale bar = 100 µm. Image adapted from Clerici et al., 2023[9] under CC BY 4.0 License.

3.4.5 Flow cytometry analysis

Flow cytometry was used to analyse cell size via the forward scatter parameter, cell complexity or granularity using the side scatter parameter, and to compare the immunophenotype of each cell population against the MSC marker panel recommended by the ISCT[164].

3.4.5.1 Cell size and complexity

Analyses were performed on early-passage cells (P3), following the gating strategy described in Chapter 2 (section 2.9.1), which included debris exclusion (FSC vs SSC) and singlet discrimination (FSC-A vs FSC-H). Forward scatter (FSC-A) and side scatter (SSC-A) area plots were then used to evaluate the size and complexity of all cell populations, as shown in Figure 3-11. In 2% O_2, TSPCs I exhibited a 9% increase in FSC-A compared to 21% O_2 ($p = 0.0215$). For TSPCs II, a 3.2% increase in FSC-A was observed in 2% O_2, but this change was not statistically significant. Tncs, on the other hand, showed a significant 24.4% increase in FSC-A when cultured in 21% O_2 compared to 2% O_2 ($p < 0.0001$). The aspect ratio of Tncs

also showed a significant difference between the two oxygen conditions, with values of 2.98 ± 0.87 for 21% O_2 and 3.95 ± 0.75 for 2% O_2 ($p < 0.0001$) (Figure 3-7). When comparing FSC-A across all three cell populations in the same oxygen condition, Tncs significantly differed from TSPCs I and II. In atmospheric oxygen, the FSC-A mean for Tncs was considerably higher than for TSPCs I ($p = 0.0002$) and TSPCs II ($p = 0.0008$), while in 2% O_2, the FSC-A for Tncs was significantly lower than for both TSPCs I and II ($p < 0.0001$ and $p = 0.0012$, respectively).

Regarding side scatter, TSPCs I exhibited a significant 19.5% increase in 2% O_2, whereas TSPCs II showed a non-significant increase in scatter. Tncs showed a 24.3% reduction in side scatter in 2% O_2. When comparing side scatter among the three cell types under the same oxygen condition, a significant difference ($p = 0.0100$) was only found between TSPCs I and Tncs in 21% O_2.

Overall, Tncs displayed the most significant changes in both forward and side scatter areas in response to oxygen culture conditions, with higher values observed in 21% O_2 and lower values in 2% O_2 compared to the other tendon-derived cell populations.

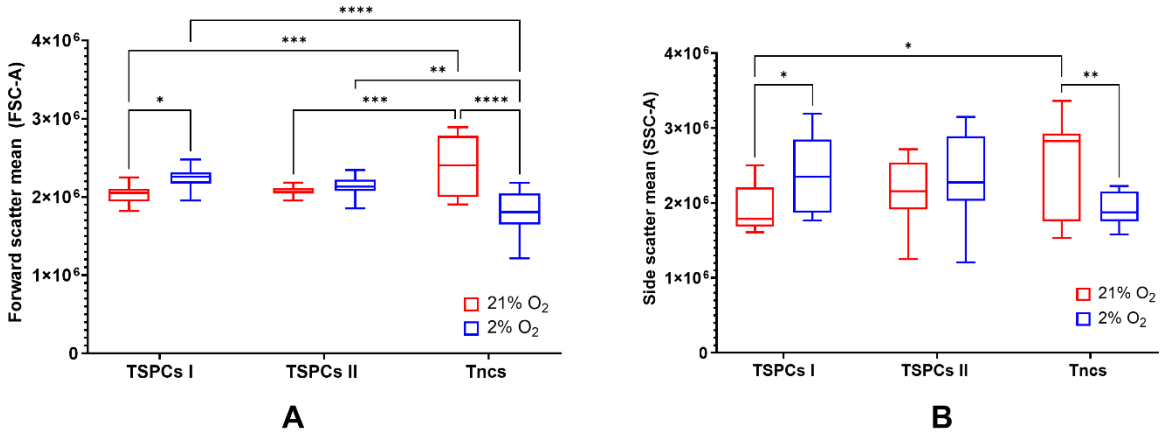


Figure 3-11. Tendon cell size and complexity. Forward scatter area (FSC-A) and side scatter area (SSC-A) plots were used to assess the size (A) and complexity (B) of TSPCs I, TSPCs II, and Tncs. Analyses were carried out at P3, following the gating strategy described in section 2.9.1. Statistical analysis: two-way ANOVA, followed by Tukey's HSD multiple-comparison post-hoc test; '*' for $p < 0.05$, '**' for $p < 0.01$, '***' for $p < 0.001$, and '****' for $p < 0.0001$, n=3. Image adapted from Clerici et al., 2023[9] under CC BY 4.0 License.

3.4.5.2 Cell immunophenotype

Surface marker expression was assessed at P3, using the same gating strategy detailed in Chapter 2 (section 2.9.1). All cell populations were incubated with antibodies targeting CD14, CD19, CD34, CD45, HLA-DR, CD73, CD90, and CD105, which is considered to be a marker panel for hMSCs, and with CD44. Depending on the antibody, staining was compared with the appropriate non-specific isotype controls, either IgG1 or IgG2. Histograms of fluorescence intensity for each marker in both oxygen conditions are presented for TSPCs I in Figure 3-12A, TSPCs II in Figure 3-13A, and Tncs in Figure 3-14A. The percentage of positively stained cells was determined by gating the stained population to exclude 99% of all isotype control events, plotting results below the respective histograms.

Markers typically negative in MSCs, such as CD14, CD19, CD34, CD45, and HLA-DR, showed ≤ 0.5% positivity in all cell populations, confirming their non-haematopoietic lineage in both oxygen conditions (Figure 3-12B, 3-13B, 3-14B).

The expression of MSC-positive markers, including CD73, CD90, CD105, and CD44, was also assessed. In contrast to MSCs, all tendon-derived cell populations showed less than 0.5% positivity for CD73 and CD105. For CD90, TSPCs I exhibited 73.71% positivity in 21% O_2 and 87.85% in 2% O_2 (Figure 3-12B). TSPCs II demonstrated consistent CD90 positivity across both oxygen conditions, with 88.97% in 21% O_2 and 92.90% in 2% O_2 (Figure 3-13B). Tncs exhibited 94.67% CD90-positive cells in 21% O_2, with a slightly lower percentage (87.55%) in 2% O_2 (Figure 3-14B). These results showed that TSPCs II in 2% O_2 and Tncs in 21% O_2 exhibited the highest percentage of CD90-positive cells (Figure 3-15A).

For CD44, TSPCs I showed 59.96% positivity in 21% O_2 and 77.21% in 2% O_2 (Figure 3-12b). TSPCs II demonstrated more than 85% CD44-positive cells in both oxygen conditions, with 89.03% in 21% O_2 and 88.68% in 2% O_2 (Figure 3-13B). Tncs, similar to TSPCs I, exhibited a higher proportion of CD44-positive cells in 2% O_2 (78.21%) compared to 65.04% in 21% O_2 (Figure 3-14B). These findings suggest that TSPCs II tended to show a higher percentage of

CD44-positive cells in both oxygen conditions, although no statistically significant differences were detected among the three populations (Figure 3-15B).

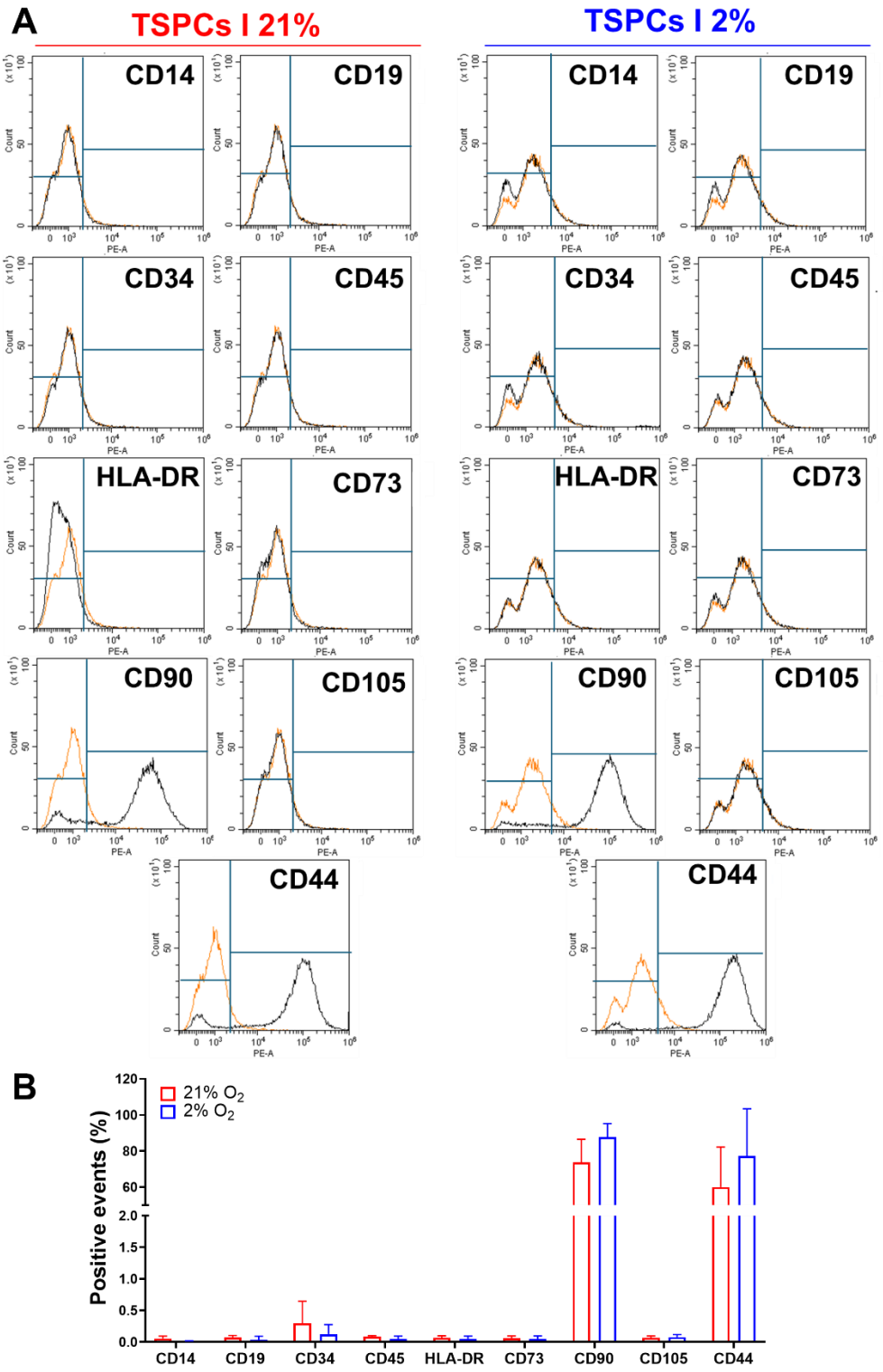


Figure 3-12. Immunophenotype of TSPCs I. TSPCs I cultured in 2% and 21% O_2 were analysed by flow cytometry using a panel of MSC markers. (A) Overlay histograms showing each antibody marker, with the orange line representing the isotype control (IgG1 or IgG2) and the black line representing the

antibody marker. (B) Percentage of positively stained cells compared to the corresponding isotype control.

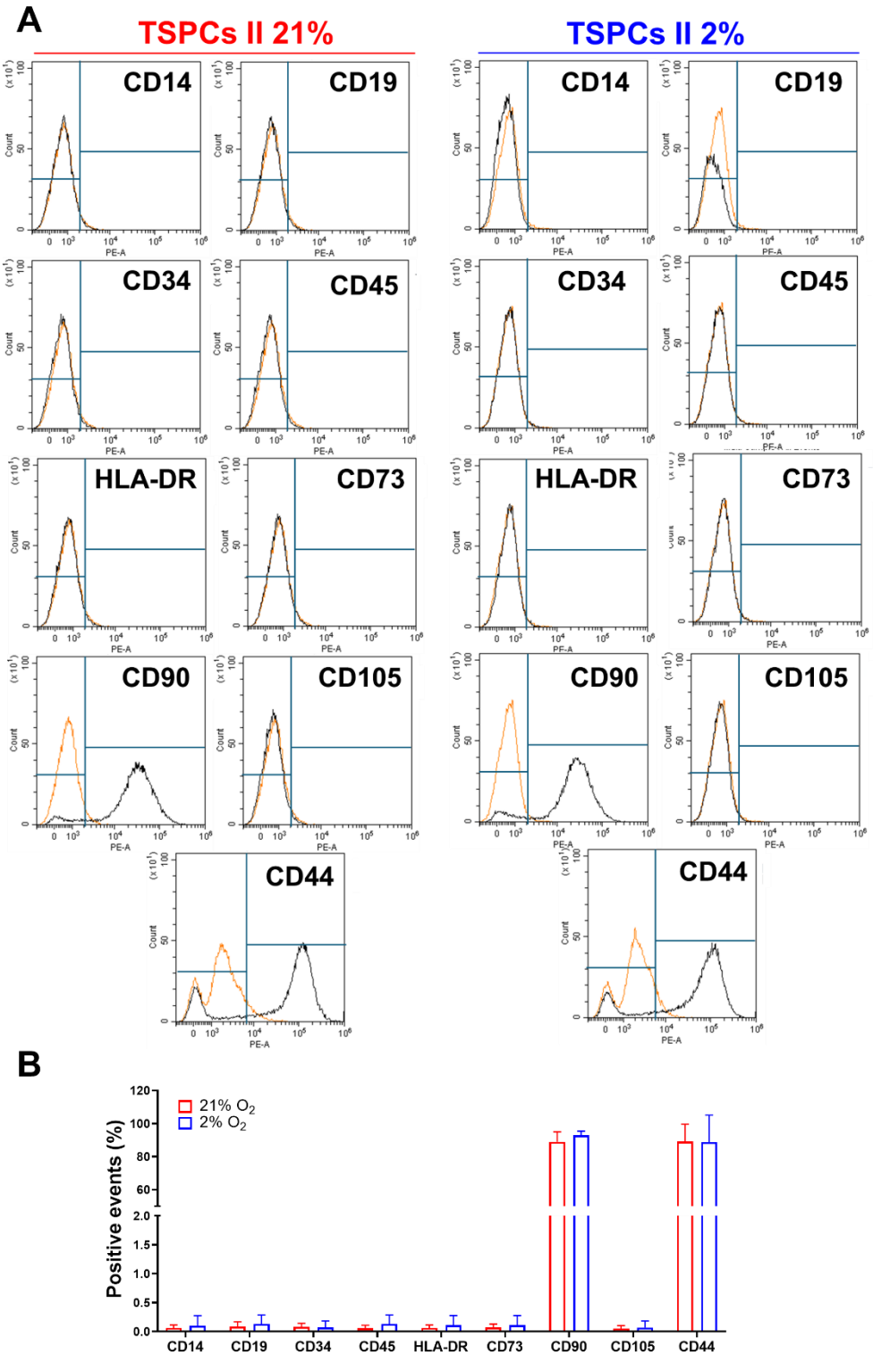


Figure 3-13. Immunophenotype of TSPCs II. TSPCs II cultured in 2% and 21% O_2 were analysed by flow cytometry using a panel of MSC markers. (A) Overlay histograms showing each antibody marker, with the orange line representing the isotype control (IgG1 or IgG2) and the black line representing the

antibody marker. (B) Percentage of positively stained cells compared to the corresponding isotype control.

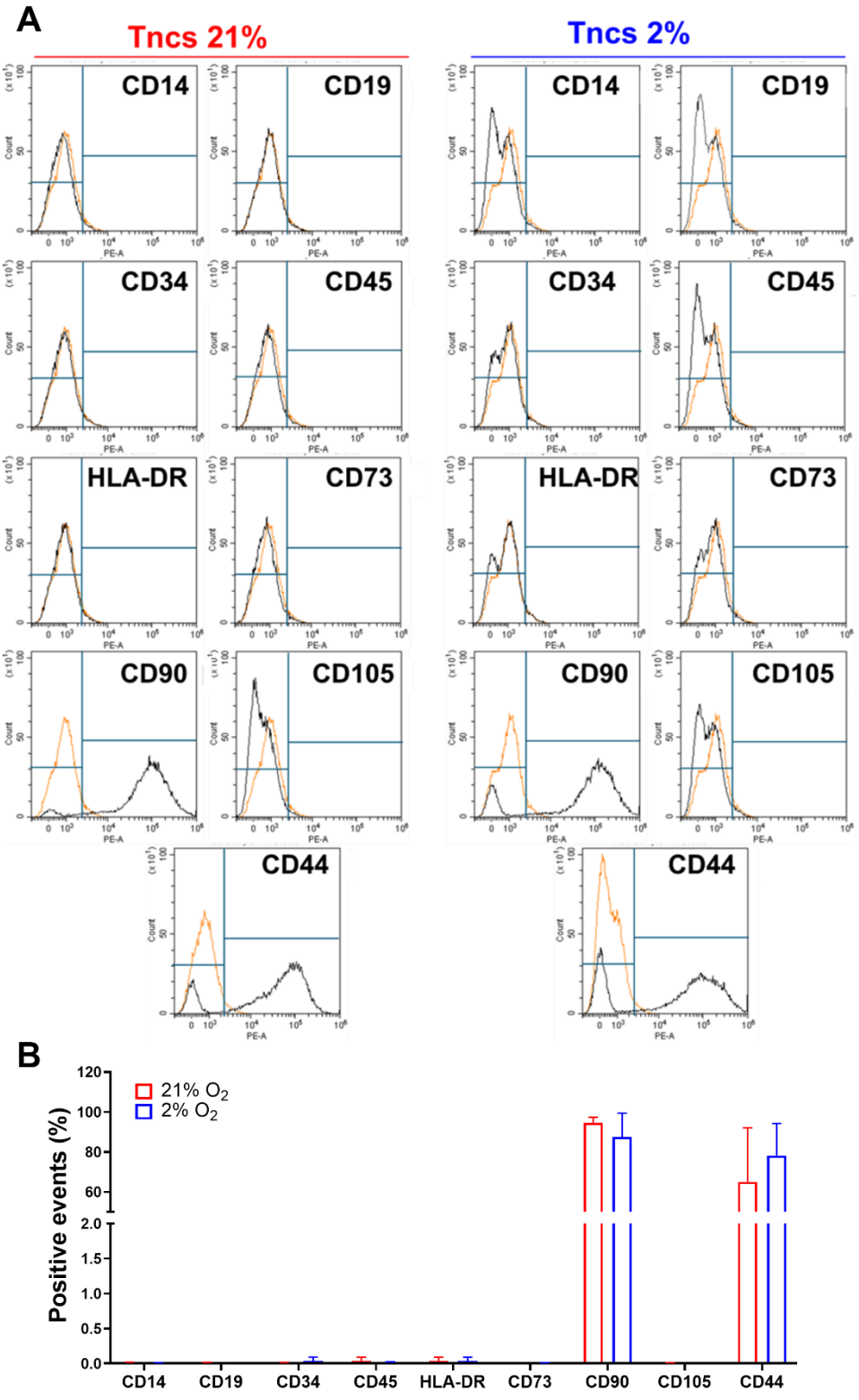


Figure 3-14. Immunophenotype of Tncs. Tncs cultured in 2% and 21% O_2 were analysed by flow cytometry using a panel of MSC markers. (A) Overlay histograms showing each antibody marker, with the orange line representing the isotype control (IgG1 or IgG2) and the black line representing the

antibody marker. (B) Percentage of positively stained cells compared to the corresponding isotype control.

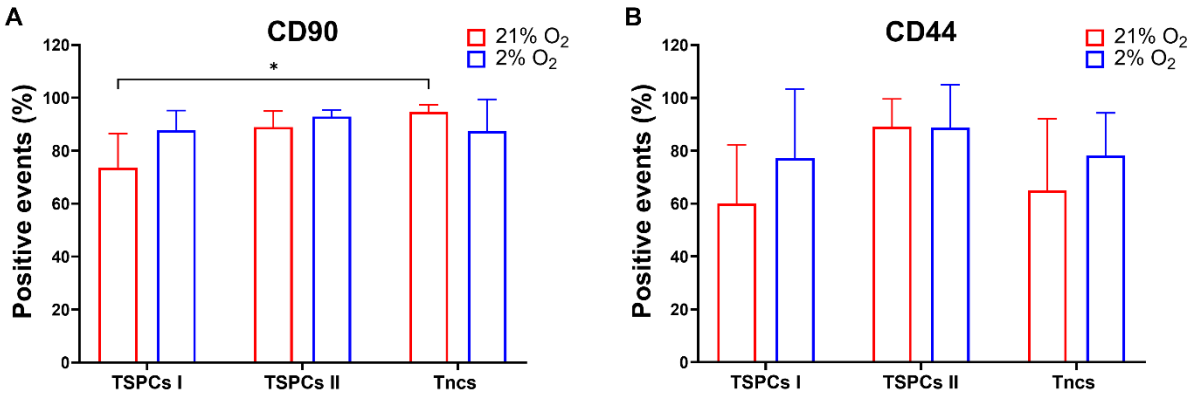


Figure 3-15. Quantification of positive immunophenotype markers. Percentage of CD90-positive (A) and CD44-positive (B) cells (TSPCs I, TSPCs II, and Tncs) under both 2% and 21% oxygen conditions, compared to the corresponding isotype control. Statistical analysis: two-way ANOVA, followed by Tukey's HSD multiple-comparison test; '*' for $p < 0.05$, n=3.

3.4.6 Gene expression

To determine if tendon-derived cell populations retained tendon-specific gene expression and canonical stem cell marker expression over extended culturing, we analysed the expression of both stem cell markers and tendon-related genes in both early (P3) and late passage (P13) cells.

Regarding stem cell markers, *NANOG*, *NESTIN*, and *OCT-4* were assessed across all cell populations. TSPCs I displayed a significant 8.5-fold increase in *NANOG* expression in 21% O_2 ($p < 0.0001$), while expression remained stable in 2% O_2 (Figure 3-16A). Early-passage TSPCs I in 2% O_2 showed 2.2-fold higher *NANOG* expression compared to those cultured in 21% O_2 ($p < 0.0001$), and late-passage cells in 21% O_2 had 3-fold higher *NANOG* expression compared to 2% O_2 ($p = 0.0116$). *NESTIN* expression in TSPCs I showed a 1.4-fold increase in 21% O_2 ($p = 0.0115$) but remained stable in 2% O_2. Early-passage TSPCs I in 2% O_2 showed a 2-fold higher *NESTIN* expression compared to those in 21% O_2 ($p < 0.0001$) (Figure 3-16B). *OCT-4* expression in TSPCs I showed a 7-fold increase in 21% O_2 between different passages

($p < 0.0001$) and remained stable in 2% O_2. Early-passage TSPCs I in 2% O_2 exhibited 2-fold higher *OCT-4* expression compared to 21% O_2 ($p < 0.0001$), while late-passage cells showed 3-fold higher *OCT-4* expression in 21% O_2 compared to 2% O_2 ($p = 0.0003$) (Figure 3-16C).

In contrast, TSPCs II maintained stable *NANOG*, *NESTIN*, and *OCT-4* expression across all passages and oxygen conditions, with no significant changes observed (Figures 3-16A, 3-16B, 3-16C).

For Tncs, *NANOG* expression increased significantly over time, with a 6.6-fold increase in 21% O_2 ($p < 0.0001$) and a 2.5-fold increase in 2% O_2 ($p = 0.0001$) (Figure 3-16A). Similarly, *NESTIN* expression in Tncs increased by 1.4-fold in both 21% O_2 ($p = 0.0006$) and 2% O_2 ($p = 0.0139$), with early-passage Tncs in 21% O_2 showing 1.5-fold higher expression compared to cells in 2% O_2 ($p = 0.0026$) (Figure 3-16B). *OCT-4* expression in Tncs increased by 4.7-fold in 21% O_2 ($p < 0.0001$) and by 3.6-fold in 2% O_2 ($p < 0.0001$) between early and late-passage cells. Early-passage Tncs in 21% O_2 exhibited 2.4-fold higher *OCT-4* expression compared to cells in 2% O_2 ($p < 0.0001$), with late-passage Tncs in 21% O_2 showing 3-fold higher *OCT-4* expression compared to cells in 2% O_2 ($p = 0.0089$) (Figure 3-16C).

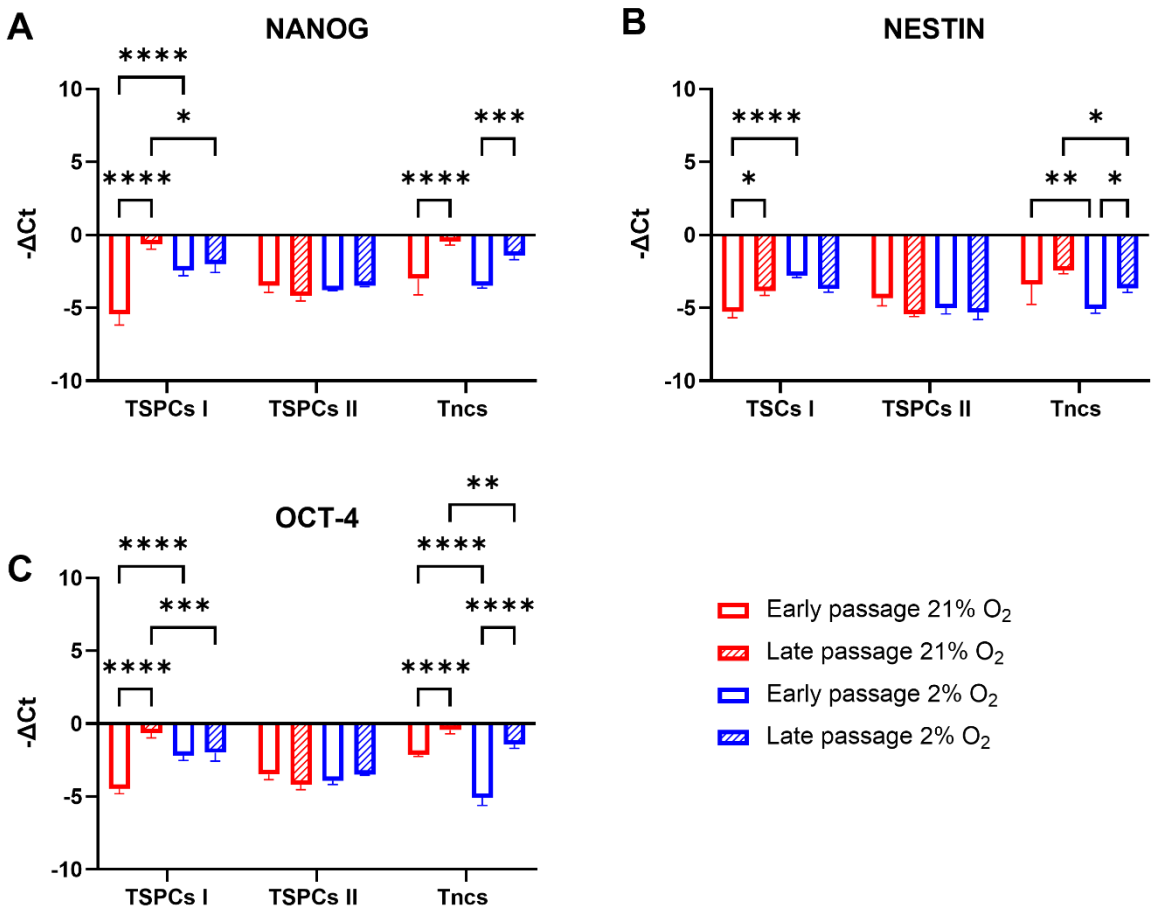


Figure 3-16. Gene expression of stem cell markers in tendon-derived cell populations. Early and late passage TSPCs I, TSPCs II, and Tncs were analysed for the expression of (A) *NANOG*, (B) *NESTIN*, and (C) *OCT-4* under 21% and 2% O_2 conditions. Gene expression data are presented as −ΔCt, with normalisation to *ACTβ* (housekeeping gene). Statistical analysis: two-way ANOVA, followed by Tukey's HSD multiple-comparison post-hoc test; '*' for $p < 0.05$, '**' for $p < 0.01$, '***' for $p < 0.001$, and '****' for $p < 0.0001$, n=3. Image adapted from Clerici et al., 2023[9] under CC BY 4.0 License.

When examining tendon-specific markers, TSPCs I showed significant variations in *TNMD* expression between early and late-passage cells. The expression of *TNMD* was higher in 2% O_2 compared to 21% O_2 ($p = 0.0379$ for 2% O_2, $p = 0.0473$ for 21% O_2) (Figure 3-17A). A 2-fold increase in *TNMD* expression was observed between early-passage cells cultured in different oxygen conditions, with 2% O_2 showing significantly higher expression ($p < 0.0001$). *SCX* expression increased 1.5-fold in TSPCs I in 21% O_2 ($p = 0.0035$), remaining stable in 2% O_2 across passages. Early-passage TSPCs I cultured in 2% O_2 showed 1.4-fold higher *SCX* expression than those in 21% O_2 ($p = 0.0233$) (Figure 3-17B). *THBS4* expression increased

by 1.4-fold in early-passage TSPCs I cultured in 2% O_2 compared to 21% O_2 ($p = 0.0021$), while late-passage cells in 21% O_2 exhibited 1.8-fold higher *THBS4* expression compared to 2% O_2 ($p < 0.0001$) (Figure 3-17C). TSPCs I showed a significant increase in *TNC* expression in 21% O_2, with a 13.5-fold increase ($p < 0.0001$), while a 1.7-fold decrease in 2% O_2 was observed ($p = 0.0041$). Late-passage TSPCs I in 21% O_2 exhibited 5.3-fold higher *TNC* expression compared to those cultured in 2% O_2 ($p < 0.0001$) (Figure 3-17d).

TSPCs II exhibited stable *TNMD* expression across all passages and oxygen conditions, with only slightly increasing late-passage cells cultured in 21% O_2 (1.2-fold, $p = 0.0500$) compared to 2% O_2 (Figure 3-17A). No significant changes in *SCX* expression were observed across passages and oxygen conditions (Figure 3-17B). *THBS4* expression showed a 1.3-fold increase in 2% O_2 ($p = 0.0356$) but decreased non-significantly in 21% O_2 ($p = 0.0356$). Late-passage TSPCs II cultured in 2% O_2 exhibited 1.4-fold higher *THBS4* expression than those cultured in 21% O_2 ($p = 0.0012$) (Figure 3-17C). *TNC* expression in TSPCs II decreased by 8.7-fold in 21% O_2 ($p < 0.0001$) and 2.4-fold in 2% O_2 ($p = 0.0446$), with late-passage cells in 2% O_2 showing 4.3-fold higher *TNC* expression than those in 21% O_2 ($p < 0.0001$) (Figure 3-17D).

For Tncs, a 1.9-fold increase in *TNMD* expression was observed between early and late-passage cells in 21% O_2 ($p = 0.0002$) and a 2.2-fold increase in 2% O_2 ($p < 0.0001$). Significant differences were also noted between early-passage Tncs cultured in different oxygen concentrations, with a 2-fold higher *TNMD* expression in 21% O_2 ($p < 0.0001$) and 1.6-fold higher expression in late-passage Tncs cultured in 21% O_2 ($p = 0.0036$) (Figure 3-17A). *SCX* expression in Tncs increased 1.5-fold in late-passage cells cultured in 21% O_2 compared to 2% O_2 ($p = 0.0146$) (Figure 3-17B). *THBS4* expression in Tncs remained stable across passages and oxygen conditions (Figure 3-17C). *TNC* expression decreased by 1.7-fold in 2% O_2 and 5.8-fold in 21% O_2 between early- and late-passage cells (Figure 3-17D).

To summarise, TSPCs I and Tncs showed gene expression profiles significantly influenced by oxygen concentration and passage number, suggesting that environmental factors can have

a strong impact on their differentiation and stem cell characteristics. In contrast, TSPCs II generally maintained a relatively stable gene expression profile across passages and oxygen conditions, particularly for *TNMD*, *SCX*, and stem cell markers. However, some variability was observed, most notably in *TNC* expression, which decreased under 21% O_2 and at later passages compared with 2% O_2 and earlier passages (Figure 3-17D). This indicates that while TSPCs II are less sensitive than TSPCs I and Tncs, not all markers are uniformly stable under extended culture.

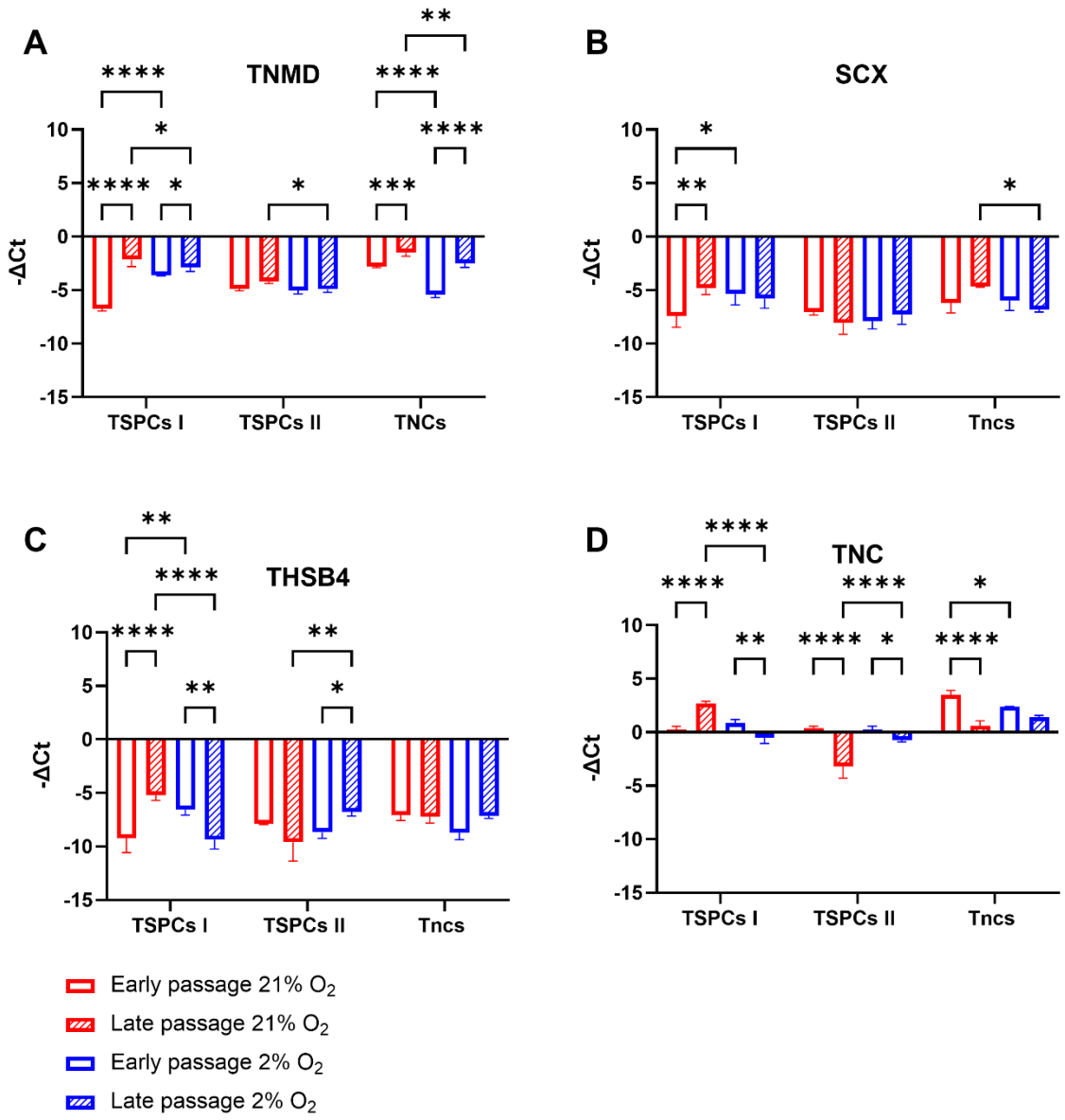


Figure 3-17. Gene expression of tenogenic markers in tendon-derived cell populations. Early and late passage TSPCs I, TSPCs II, and Tncs were analysed for the expression of (A) *TNMD*, (B) *SCX*, (C)

THSB4 and (D) *TNC* under 21% and 2% O_2 conditions. Gene expression data are presented as −ΔCt, with normalisation to *ACTβ* (housekeeping gene). Statistical analysis: two-way ANOVA, followed by Tukey's HSD multiple-comparison post-hoc test; '*' for $p < 0.05$, '**' for $p < 0.01$, '***' for $p < 0.001$, and '****' for $p < 0.0001$, n=3. Image adapted from Clerici et al., 2023[9] under CC BY 4.0 License.

3.4.7 Immunofluorescence analysis

Building on previous findings, endotenon-derived TSPCs II exhibited the highest proliferative potential and retained multipotency in the late passage. They demonstrated a positive immunophenotype for CD44 and CD90 markers and consistent expression of tenogenic (*TNMD*, *SCX*, *THBS4*, *TNC*) and stem (*NANOG*, *NESTIN*, *OCT-4*) markers. We selected this population for further investigation; specifically, we evaluated TNMD protein expression in TSPCs II at P2 over a 14-day period, cultured under 2% and 21% O_2, to assess the influence of oxygen conditions on their tenogenic profile over time.

Immunofluorescence analysis revealed a decrease in TNMD expression by day 7 in both oxygen conditions. In 21% O_2, TNMD levels remained stable from day 7 to day 14, whereas in 2% O_2, TNMD expression increased significantly by day 14 (Figure 3-18A). Semi-quantitative analysis of the immunofluorescence images was performed to track changes in MFI of TNMD expression over the 14 days. On day 1, TNMD expression in 21% O_2 was 1.4-fold higher than in 2% O_2 ($p=0.0019$). Between day 1 and day 7, a significant decrease in TNMD expression was observed, with a 50.3% reduction in 21% O_2 ($p<0.0001$) and a 63.6% reduction in 2% O_2 ($p<0.0001$). On day 7, TNMD levels in 21% O_2 were 1.9-fold higher than in 2% O_2 ($p=0.0080$). However, from day 7 to day 14, TNMD expression remained stable in 21% O_2 and increased by 69.7% in 2% O_2 ($p<0.0001$). After 14 days, TNMD expression in 2% O_2 was 1.6-fold higher than 21% O_2 ($p=0.0007$) (Figure 3-18B).

These results indicate that the physiological oxygen condition was optimal for preserving and enhancing the tenogenic profile of type II TSPCs. This finding aligns with the hypoxic environment of native tendon tissues, emphasising the importance of mimicking physiological conditions to maximise regenerative potential *in vitro*.

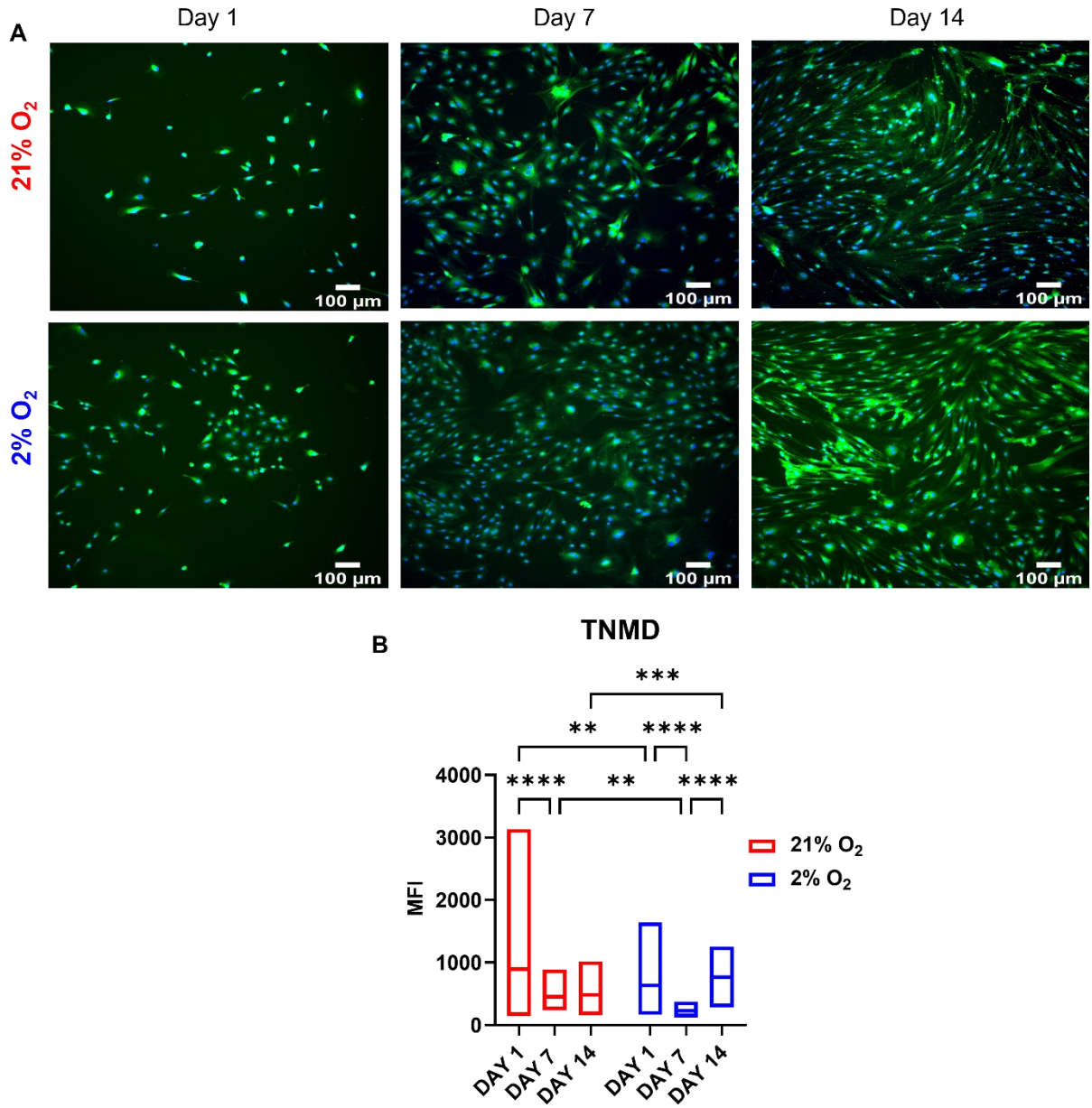


Figure 3-18. Immunofluorescence analysis of TNMD expression in TSPCs II over 14 days. (A) Representative immunofluorescence images of TNMD expression in TSPCs II cultured under 2% and 21% O_2 at days 1, 7, and 14. Scale bar = 100 µm. (B) Semi-quantitative analysis of mean fluorescence intensity (MFI) of TNMD expression in TSPCs II over the 14-day culture period under 2% and 21% O_2 conditions. Statistical analysis: two-way ANOVA, followed by Tukey's HSD multiple-comparison post-hoc test; '*' for $p < 0.05$, '***' for $p < 0.001$, and '****' for $p < 0.0001$, n=3. Image adapted from Clerici et al., 2023[9] under CC BY 4.0 License.

3.4.8 Porcine crude EVs characterisation

Conditioned medium was collected from porcine tendon cells, TSPCs II and Tncs, cultured under 21% and 2% oxygen conditions. The media was ultracentrifuged at 100,000 g for 90

minutes, and the resulting CP was subjected to morphological analysis using SEM and TEM and protein characterisation through Bradford assay, MACSPlex, and cytokine analysis.

TSPCs I were not included in this analysis due to their anatomical origin from the vascularised paratenon, which differs from the core tendon-derived TSPCs II and Tncs. Given their distinct microenvironment and function, TSPCs I may have a different EV secretion profile that was not the primary focus of this study. Additionally, their high sensitivity to prolonged culture and SF conditions resulted in reduced confluence, leading to insufficient CM for EV isolation.

3.4.8.1 SEM and TEM analysis

SEM analysis of the cEVs derived from TSPCs II indicated a monodisperse population, with particles uniformly measuring less than 200 nm in size under both oxygen conditions. No significant differences in particle size or overall morphology were observed between the two conditions. The surface of the EVs appeared smooth and intact, with no visible signs of aggregation or deformation, further confirming the quality of the isolated particles (Figure 3-19).

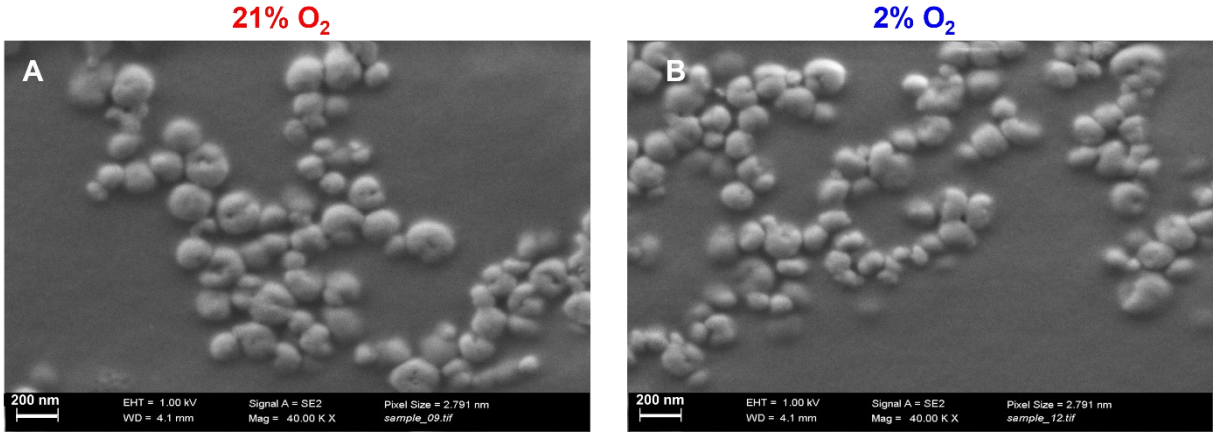


Figure 3-19. SEM analysis of porcine cEVs. SEM images of crude EVs isolated from TSPCs II cultured under 21% O_2 (A) and 2% O_2 (B) conditions. EVs exhibit generally spherical morphology, with particle sizes consistently smaller than 200 nm across both oxygen environments. Scale bar: 200 nm.

TEM further confirmed these observations for crude EVs derived from TSPCs II, revealing particles with a consistent round morphology and diameters within the same size range (50-

200 nm). Similarly, crude EVs derived from Tncs exhibited a round shape and uniform morphology, with a size distribution comparable to TSPCs II-derived EVs (50–200 nm). No apparent contaminants or aggregation were observed in either condition, highlighting the uniformity and purity of the EVs (Figure 3-20).

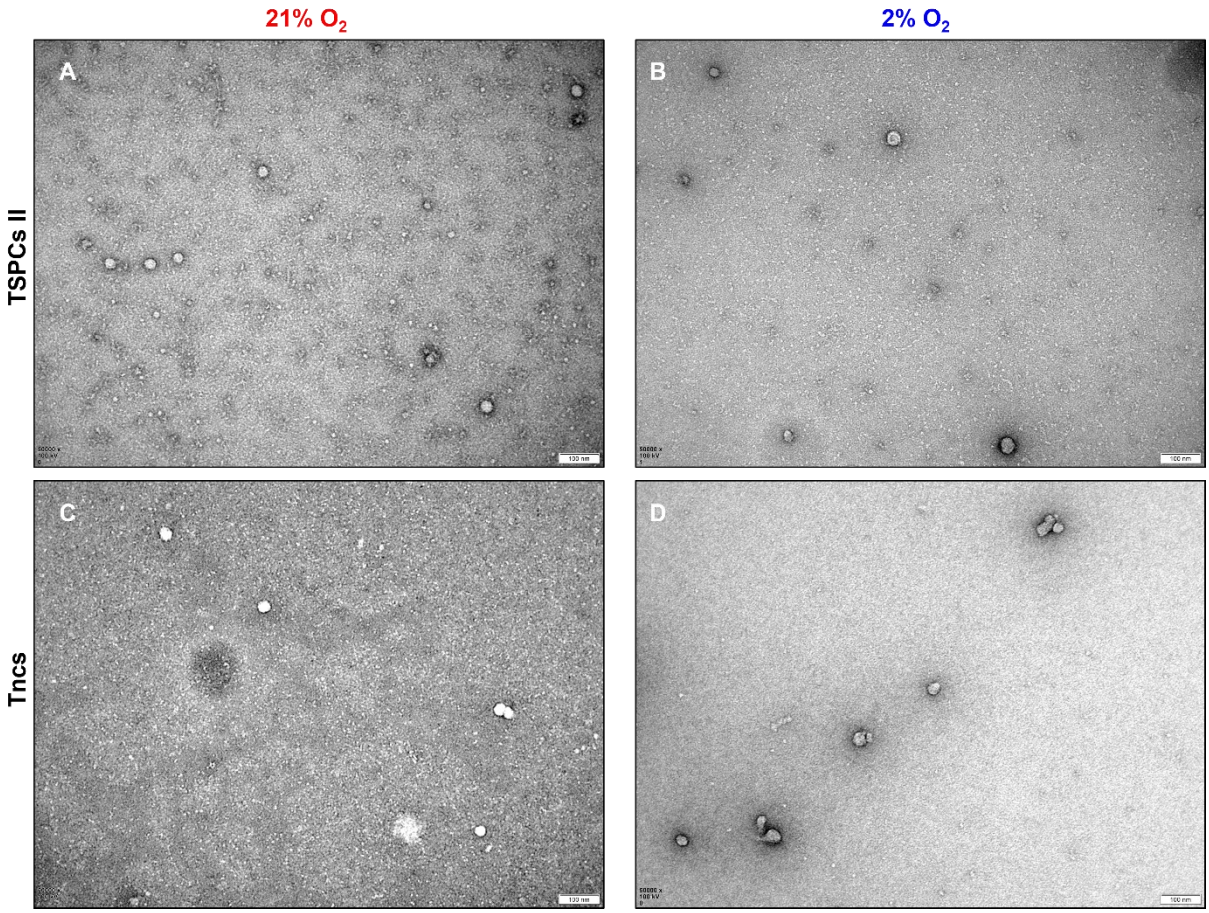


Figure 3-20. TEM analysis of porcine cEVs. TEM images of crude EVs isolated from TSPCs II cultured under 21% O_2 (A) and 2% O_2 (B) conditions and from Tncs under 21% O_2 (C) and 2% O_2 (D). EVs exhibit a round morphology with diameters ranging from 50-200 nm. Scale bar: 100 nm.

3.4.8.2 Total protein concentration

The Bradford assay was used to quantify protein concentration in both the CM and the CP. After the ultracentrifugation step, a decrease in protein concentration was observed, confirming

the initial separation between soluble and non-soluble proteins. Crude EV pellets were resuspended in 500 µL SF medium for analysis.

For TSPCs II-derived CM, the average protein concentration in 30 mL of media cultured at 21% O_2 was 30.4 ± 6.6 µg/mL, representing a 95-fold reduction in the resulting CP. At 2% O_2, the average protein concentration in the CM was 26.2 ± 2.3 µg/mL, corresponding to a 52.4-fold decrease in the CP. No significant differences in protein concentration were detected between the two oxygen conditions (Figure 3-21A).

In the case of Tnc-derived CM, the average protein concentration at 21% O_2 was 9.8 ± 2.8 µg/mL, with an 8.2-fold reduction in the CP. At 2% O_2, the CM protein concentration was slightly higher at 10.7 ± 6.4 µg/mL, corresponding to an 11.9-fold decrease in the CP. As with TSPCs II, no statistically significant differences were observed between Tnc-derived CM and CP oxygen conditions (Figure 3-21B).

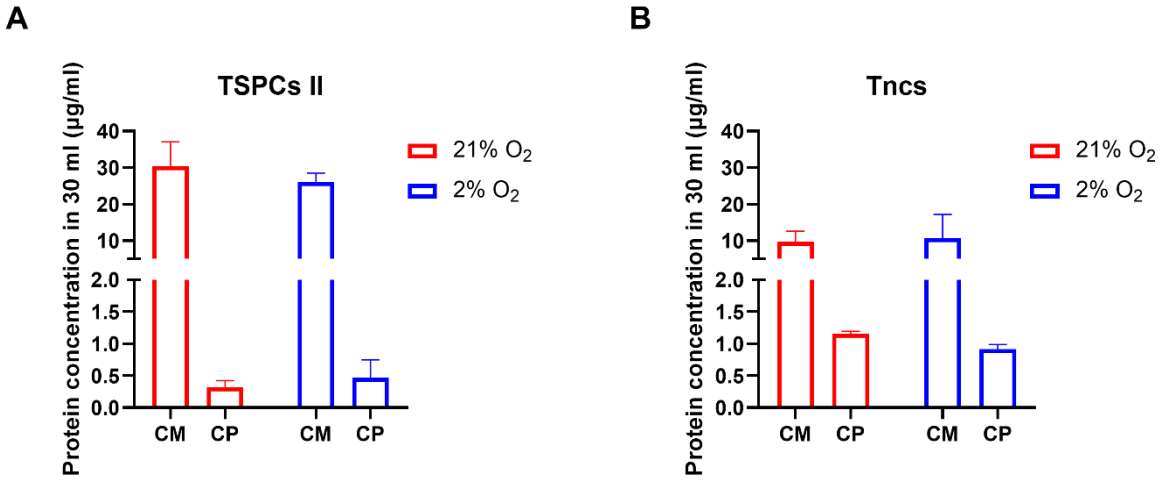


Figure 3-21. Total protein concentration in conditioned media and crude pellet. Bradford assay results show the protein concentration in CM and the corresponding CP derived from TSPCs II (A) and Tncs (B) cultured under 21% O_2 and 2% O_2 conditions. A notable decrease in protein concentration was observed in the CP after ultracentrifugation, confirming the separation of soluble and non-soluble proteins. Statistical analysis: unpaired *t*-tests comparing 21% vs 2% O_2 within each group. No significant differences were detected between oxygen conditions. Data are shown as mean ± SD, n=3.

3.4.8.3 Cytokine profiling

Cytokine analysis was performed on CM collected from TSPCs II and Tncs cultured under 21% and 2% O_2 conditions. The analysis included the following biomarkers: GM-CSF, IL-1RA, IL-1β, TNFα, IL-2, IL-4, IL-6, IL-8, IL-10, IL-12, IL-18, IFNγ, and IL-1α.

Among the cytokines assessed, GM-CSF, IL-1RA, IL-1β, IL-10, and IL-12 were either undetectable or consistently below the assay's detection limits, which were 0.040 ng/mL for GM-CSF, 0.021 ng/mL for IL-1RA, 0.079 ng/mL for IL-1β, 0.015 ng/mL for IL-10, and 0.010 ng/mL for IL-12, as reported by the manufacturer. The remaining cytokines exhibited varying expression levels depending on cell type and oxygen condition.

In TSPCs II-derived CM, the detected cytokines were IFNγ, IL-1α, IL-2, IL-4, IL-6, IL-8, IL-18, and TNFα. Most cytokines showed higher expression in 2% O_2 than 21% O_2, except for the pro-inflammatory TNFα, which was 1.4-fold higher in 21% O_2. Specifically, IFNγ was 1.6-fold higher, IL-1α was 57.7-fold higher, IL-2 was 1.1-fold higher, IL-4 was 1.8-fold higher, IL-6 was 7.3-fold higher, IL-8 was 11.8-fold higher, and IL-18 was 1.5-fold higher in 2% O_2 (Figure 3-22A).

In Tnc-derived CM, the detected cytokines included IFNγ, IL-2, IL-4, IL-6, IL-18, and TNFα. TNFα, IL-4, and IL-18 were expressed at higher levels in 21% O_2, with TNFα being 2.5-fold higher, IL-4 1.01-fold higher, and IL-18 1.3-fold higher than at 2% O_2. In contrast, IFNγ (1.01-fold), IL-2 (1.2-fold), and IL-6 (1.1-fold) showed higher expression under 2% O_2 conditions (Figure 3-22B). Despite trends observed in cytokine expression levels, the large variability across biological replicates prevented the overall detection of statistically significant differences.

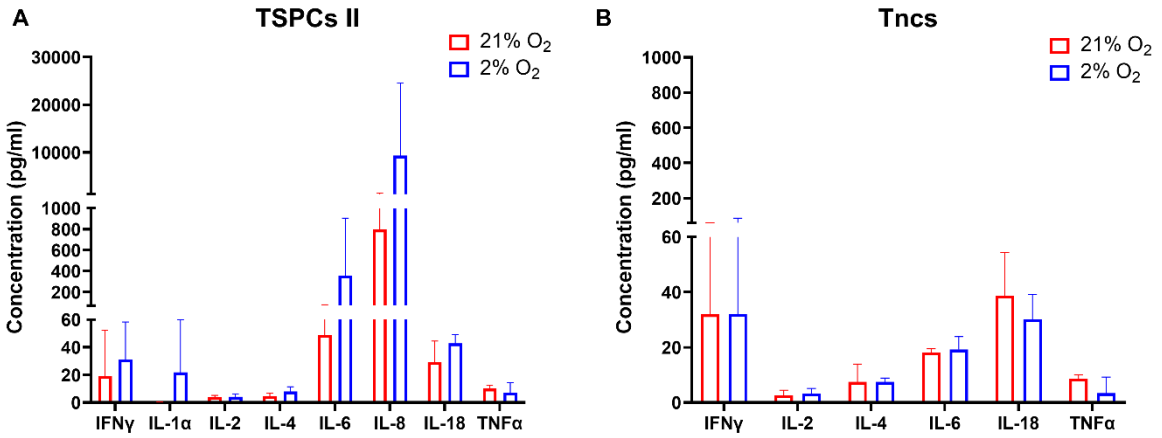


Figure 3-22. Cytokine profiling in CM from TSPCs II and Tncs. Expression levels of cytokines detected in CM collected from TSPCs II (A) and Tncs (B) cultured under 21% O_2 and 2% O_2 conditions. The analysis included GM-CSF, IL-1RA, IL-1β, TNFα, IL-2, IL-4, IL-6, IL-8, IL-10, IL-12, IL-18, IFNγ, and IL-1α. Statistical analysis: multiple unpaired *t*-tests were performed for 21% vs 2% O_2 for each cytokine. Data represent mean ± SD, n=3.

3.4.8.4 MACSPlex analysis

Flow cytometry analysis was performed using the MACSPlex Exosome kit to detect 37 exosomal surface epitopes on crude EVs derived from TSPCs II. The results showed that 30 out of 37 markers were detected in TSPCs II-derived EVs cultured under 21% and 2% O_2 conditions.

Among immune cell markers, CD4 (2-fold), CD25 (1.6-fold), CD69 (1.9-fold), CD19 (3.8-fold), CD1c (3.2-fold), CD11c (1.1-fold), and CD209 (1.2-fold) were higher in 21% O_2, while CD8 and CD14 were exclusively detected under 21% O_2 conditions. CD2 (1.5-fold), CD22 (1.2-fold), CD40 (3.4-fold), HLA-DRDPDQ (5.5-fold), and HLA-ABC (1.5-fold) were also expressed at higher levels in atmospheric oxygen (Figure 3-23A).

For stem cell/progenitor markers, CD44 (7.5-fold), CD105 (3.1-fold), and CD133/1 (1.7-fold) were more abundant in 21% O_2, whereas CD146 (1.03-fold) and SSEA-4 (14.2-fold) were elevated under 2% O_2 conditions (Figure 3-23B).

Regarding tumour/stem cell-associated markers, MCSP was exclusively detected in 21% O_2, and CD326 was 1.2-fold higher in this condition. ROR1 expression was 2.1-fold higher in 2% O_2 (Figure 3-23C).

Among platelet/endothelial markers, CD41b (3.6-fold) and CD42a (3.7-fold) were more highly expressed in 2% O_2, while CD31 (2.3-fold) showed increased expression in 21% O_2 (Figure 3-23D).

Finally, for EV-associated markers, the tetraspanins CD9 (2.6-fold), CD63 (2.2-fold), and CD81 (2.9-fold), which are widely recognized as exosomal markers[102], were more highly expressed under 21% O_2, along with the adhesion marker CD62P (2.9-fold). In contrast, CD49e was 3.8-fold higher in 2% O_2 (Figure 3-23E). Despite trends observed in surface marker expression, the large variability across biological replicates prevented the detection of statistically significant differences overall.

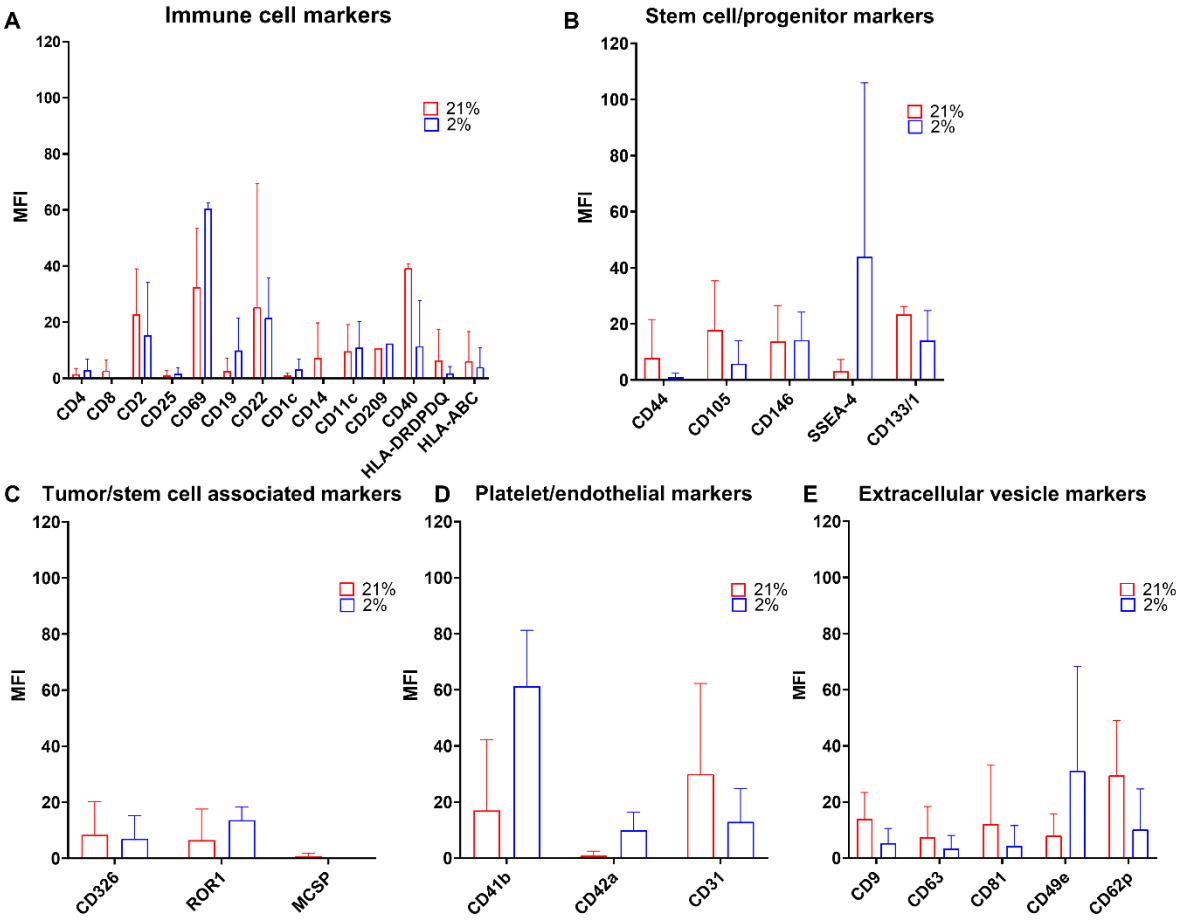


Figure 3-23. Surface marker expression on cEVs derived from TSPCs II. Flow cytometry-based MACSPlex analysis showing the expression of 30 surface markers on crude EVs cultured under 21% O_2 and 2% O_2 conditions. (A) Immune cell markers, (B) stem cell/progenitor markers, (C) tumour/stem cell-associated markers, (D) platelet/endothelial markers, and (E) extracellular vesicle-associated markers. Statistical analysis: multiple unpaired *t*-tests were performed for 21% vs 2% O_2 for each marker; no significant differences were detected due to variability across biological replicates. Data are presented as mean ± SD, n=3.

3.5 Discussion

Tendon injuries are a major clinical challenge due to the tissue's limited regenerative capacity[2,57]. Tendon-derived cells hold promise for regenerative therapies, but their biological properties vary by anatomical origin. TSPCs I, from the vascularised paratenon, play a role in injury response, while TSPCs II, located in the ECM-rich endotenon, contribute to tendon homeostasis and repair[23]. Tncs, the primary tendon cells in the interfascicular matrix, maintain tissue structure but have limited proliferative potential[9,20,23]. This study compared TSPCs I, TSPCs II, and Tncs under physiological and atmospheric oxygen conditions to evaluate their growth, morphology, gene and protein expression, and EV production. These findings offer insight into the most promising tendon-derived cell population for use in repair and tissue engineering applications.

TSPCs II demonstrated superior proliferative capacity and comparatively stable gene and protein expression across most markers and conditions, supporting their identification as the most promising tendon-derived population for in-vitro expansion. However, their definitive identity remains incompletely characterised, and conclusions about regenerative efficacy are preliminary in the absence of functional assays or in vivo validation. These findings are consistent with earlier studies on porcine Achilles tendons, demonstrating enhanced proliferative potential and multipotency in endotenon-derived cells[278,286]. However, this study extended previous work by directly comparing TSPCs II with TSPCs I and TNCs, incorporating sensitive methods such as flow cytometry and RT-qPCR, and analysing the effects of oxygen tension. The advantages of physiological oxygen in enhancing the proliferation and tenogenic potential of distinct tendon-derived populations were particularly emphasised, providing a more

comprehensive understanding of tendon cell dynamics compared to earlier studies that pooled tendon stem cells[283,284,293] or focused only on individual populations[294,295].

The enzymatic digestion method with type II collagenase was shown to be highly effective for isolating tendon stem cells, aligning with earlier protocols[9,296–298]. The explant method, supplemented by pre-scratched plates, efficiently isolated Tncs by promoting cell adherence and directional growth[299,300]. While tendon stem cells from various species, including rabbits[284], mice[28,283], rats[157], and horses[158] have been characterised, limited studies[278,286] have focused on porcine TSPCs I and II, particularly under varying oxygen tensions and compared them to Tncs. This study addressed this gap, providing valuable insights into the behaviour of tendon-derived populations.

Notable morphological differences were observed among the three populations. TSPCs II exhibited smaller, rounded morphologies, contrasting with the elongated spindle shapes of Tncs, consistent with previous studies in rabbit[284] and mouse[28,283] models. The aspect ratio of all cell types decreased with proliferative ageing, indicating a transition from spindle-shaped to rounder, flatter morphologies, as previously reported[9,284,301]. Proliferative potential varied significantly across the cell populations and oxygen conditions. Physiological oxygen enhanced the proliferation of all cell types, supporting earlier studies[175,255,285] suggesting that hypoxia mimics the native low-oxygen environment of tendons and promotes stem cell expansion. TSPCs II showed the highest cumulative population doublings (CPDs), being 1.8-fold higher than TSPCs I and 3.5-fold higher than Tncs in 21% O_2 after 120 days, and maintaining an advantage under 2% O_2. This resilience may reflect their native localisation within the endotenon, where oxygen fluctuations occur. By contrast, TSPCs I (paratenon-derived[286]) were more sensitive to oxygen tension, while Tncs showed the lowest proliferative potential, consistent with their differentiated status[284,286]. These results underline the influence of oxygen in shaping tendon cell behaviour and suggest TSPCs II are best suited for applications requiring long-term expansion.

All tendon-derived populations exhibited trilineage differentiation potential, although Tncs showed reduced adipogenic and chondrogenic differentiation compared to TSPCs I and II. These findings align with reports that tendon-derived fibroblasts can undergo adipogenesis[302], challenging earlier claims of absent differentiation potential in Tncs from rabbits[284] and mice[283]. TSPCs II maintained multipotency even at late passages, suggesting adaptability that could support future applications. At the same time, extended culture may promote selection of subpopulations within heterogeneous TSPCs II, potentially explaining reduced chondrogenic differentiation at later passages and trends in cytokine secretion. The minimal chondrogenic potential of Tncs, even at early passages, underscores the importance of understanding population dynamics over time. Future single-cell or clonal studies will be required to resolve this heterogeneity.

Although no specific immunophenotypic markers have been identified yet for TSPCs[303], the findings align with previous reports[24,255,304], where tendon-derived cell populations were negative for the haematopoietic markers (CD34 and CD45) and positive for CD90 and CD44, markers associated with stemness and adhesion. TSPCs II exhibited the highest number of CD44-positive cells, with almost 90% of the cells under both oxygen conditions. Physiological oxygen further enhanced CD90 expression in TSPCs II, with levels 1.1-fold higher than in atmospheric oxygen, supporting the hypothesis that hypoxia preserves stem-like characteristics, as previously reported[255,285]. However, Tncs displayed lower positivity for all markers, reflecting their differentiated status, apart from CD90 in atmospheric oxygen, where they reached the highest value (94%) compared to all the other cell populations, consistent with previous reports[283,285]. These distinctions are consistent with the functional differences observed. A limitation of the study is the absence of definitive markers distinguishing TSPCs I, TSPCs II, and Tncs. Populations were therefore defined operationally by anatomical origin and isolation method, in line with current practice, and compared primarily through functional characteristics. Future proteomic studies will be needed to refine these definitions.

As previously reported[283,285], tendon stem cells and tenocytes expressed tenogenic and stem markers. However, gene expression analysis further distinguished the populations, with TSPCs II maintaining stable levels of tenogenic markers (*TNMD*, *SCX*, *THBS4*, *TNC*) and stem cell markers (*NANOG*, *NESTIN*, *OCT-4*) across passages and oxygen conditions. In contrast, Tncs showed the highest expression of tenogenic markers (*TNMD*, *THBS4*), potentially indicating a terminally differentiated state, consistent with earlier findings[283].*THBS4* expression in Tncs was consistent across oxygen concentrations with no significant differences[285]. Higher transcript levels of *SCX* and *TNMD* were observed in proper tendon cells (TSPCs II and Tncs) compared to paratenon cells (TSPCs I) in atmospheric oxygen, as previously reported[28,305]. TSPCs I demonstrated sensitivity to oxygen tension, with early passages cultured under physiological oxygen showing significantly higher expression of tenogenic markers. Across all populations, ageing was associated with increased *TNMD* expression, underscoring its role as a tenogenic marker.

At the protein level, validation was limited to TNMD in early-passage TSPCs II, confirming its preservation under physiological oxygen. This observation aligns with earlier studies[9,175,255,256,306] demonstrating that hypoxia enhances the tenogenic profile of tendon stem cells. While this provided valuable support for transcript data, broader protein-level studies, including later passages, are needed to fully characterise phenotypic stability. The relatively consistent transcript and protein levels observed in TSPCs II suggest resilience that may be advantageous for therapeutic applications, though further validation is required.

The study also evaluated the potential for EV production by TSPCs II and Tncs to explore their role in intercellular communication and therapeutic applications. CEVs were successfully isolated from both populations, and their morphology was consistent across oxygen conditions, with sizes ranging between 50–200 nm, as confirmed by SEM and TEM. These findings align with previous studies on EVs derived from rat tendon cell populations, which similarly reported uniform morphologies and size ranges of isolated EVs under varying culture conditions[289,290]. Protein analysis using the Bradford assay showed that cEVs derived from TSPCs II contained

higher total protein levels than those from Tncs, consistent with the more active phenotype of TSPCs II. However, as NTA particle counts were not available for porcine samples, these results cannot distinguish whether the increased protein levels reflect a greater number of vesicles released or a higher protein load per vesicle. Consequently, while the data support differences in secretory activity between the two populations, further studies incorporating quantitative EV counting methods will be necessary to determine whether these differences reflect EV abundance, cargo composition, or both. Cytokine profiling revealed oxygen-dependent trends: in TSPCs II, most cytokines (e.g. IFNγ, IL-1α, IL-2, IL-4, IL-6, IL-8, IL-18) were elevated under 2% O_2, while TNFα was higher in 21% O_2. In Tncs, TNFα, IL-4, and IL-18 were more abundant in 21% O_2, while IFNγ, IL-2, and IL-6 increased slightly under 2% O_2. Although these patterns suggest oxygen-mediated modulation, variability across replicates and the abundance of IL-6 and IL-8, which are cytokines not strictly anti-inflammatory, limit interpretation. These results cannot be taken as evidence of an anti-inflammatory or regenerative profile, but they do indicate that oxygen tension affects EV secretory behaviour. Tnc-derived EVs showed generally lower activity, reflecting their differentiated status.

Flow cytometry-based MACSPlex analysis revealed surface marker expression profiles on cEVs, with distinct patterns modulated by oxygen tension. EVs from TSPCs II were enriched in markers associated with stemness and adhesion, including CD44, CD105, and CD49e. Hypoxic conditions promoted the expression of SSEA-4, a marker associated with progenitor characteristics, whereas atmospheric oxygen increased the abundance of tetraspanins, including CD9, CD63, and CD81, which are crucial for EV membrane integrity and function. These findings support the notion that oxygen tension influences the functional potential of EVs, with hypoxia-enhancing markers associated with stemness and regeneration. Similar studies have demonstrated that EV surface markers are modulated by microenvironmental factors, such as oxygen tension, influencing their cargo and therapeutic properties[260,261]. In addition, low-level expression of immune-associated markers (e.g., CD4, CD25, CD69, CD19) was detected in TSPCs II-derived EVs. While not tendon-specific, these markers may reflect

either broad expression patterns or minor contamination during isolation, highlighting the need for more refined characterisation strategies to confirm EV origin and purity.

Overall, this study highlights TSPCs II and their EVs as promising subjects for further investigation in tendon biology. TSPCs II displayed superior proliferative capacity, relative phenotypic stability, and generally consistent tenogenic features under different conditions, while their EVs exhibited oxygen-dependent variation in composition and surface markers. These findings underscore the importance of mimicking physiological oxygen *in vitro* and provide a foundation for future work exploring the functional and therapeutic potential of tendon-derived cells and their EVs.

3.6 Conclusion

This study comprehensively characterised tendon-derived cell populations, TSPCs I, TSPCs II, and Tncs, evaluating their growth, morphology, differentiation potential, and marker expression under physiological and atmospheric conditions. Among them, TSPCs II demonstrated the most favourable features for *in vitro* expansion, including superior proliferative capacity and comparatively stable gene and protein expression, with relatively consistent phenotypic characteristics across passages and oxygen conditions. These properties highlight TSPCs II as a promising population for further investigation in tendon research.

In addition to cellular properties, this study explored EV production by TSPCs II and Tncs, providing insights into their morphology, protein content, cytokine secretion, and surface marker expression. TSPCs II-derived cEVs showed oxygen-dependent variation, with hypoxia enhancing the expression of markers associated with stemness and adhesion, such as SSEA-4 and CD44. However, cytokine analyses exhibited variability and included factors not strictly anti-inflammatory, meaning functional implications remain to be determined. In contrast, Tnc-derived EVs generally reflected the more limited activity of their parental cells.

These findings underscore the importance of mimicking physiological oxygen conditions *in vitro* to preserve the phenotypic and secretory characteristics of tendon-derived cells. While TSPCs II and their EVs appear particularly promising, definitive conclusions about regenerative efficacy require functional validation and *in vivo* studies.

It should also be acknowledged that definitive phenotypic markers for tendon-derived subpopulations are still lacking; thus, populations were defined operationally by their isolation method and compared functionally. Future work employing single-cell or proteomic approaches will be needed to refine these definitions. Building on these results, subsequent studies will further investigate EV production and characterisation, extending the analysis to human tendon cells to explore their influence on stem cell behaviour.



Chapter 4

Enhancing EV production from human TSPCs through dynamic culture and GDF-5 supplementation

4. ENHANCING EV PRODUCTION FROM HUMAN TSPCS THROUGH DYNAMIC CULTURE AND GDF-5 SUPPLEMENTATION

4.1 Introduction

Tendon injuries remain a significant clinical challenge due to the tissue's limited regenerative capacity[307]. As covered in Chapter 3, the combination of poor vascularisation and low cellularity prevents complete healing, which leads to increased reinjury risk[2]. To overcome these challenges, new therapeutic strategies are under investigation to enhance tendon repair and improve clinical outcomes.

TSPCs have gained increasing attention as promising candidates for tendon regeneration owing to their self-renewal capacity, multipotency, and tenogenic differentiation potential[24,308]. They can be isolated from tendon tissue and characterised based on their proliferative and differentiation properties. Among biochemical regulators, GDF-5 is a key factor in tendon development and healing[279], promoting tenogenic differentiation in various stem cell types, including MSCs[309] and umbilical cord-derived cells[194]. However, the response of human TSPCs to GDF-5 remains incompletely defined, and clarifying its effects is important for optimising tendon-specific regenerative approaches.

Alongside biochemical factors, EVs secreted by stem/progenitor cells are emerging as important mediators of intercellular communication, with roles in modulating inflammation, ECM remodelling, and cell differentiation[310,311]. While EVs from MSCs have been investigated in tendon repair applications[182,184], EVs from hTSPCs remain poorly characterised, particularly in relation to culture-dependent changes in their production and cargo[279].

Environmental factors such as oxygen tension and mechanical cues strongly influence EV yield, composition, and function. Static culture provides a controlled and standardised

environment for cell growth[289–292] but lacks mechanical input. In contrast, dynamic culture systems, including perfusion bioreactors and rocker platforms, provide continuous nutrient exchange and mechanical stimulation, which improve cell viability and have been shown to enhance EV yield in other cell types[274,312–314]. Whether similar benefits occur in hTSPCs has not yet been systematically assessed.

Building upon the findings of Chapter 3, this chapter focuses on characterising hTSPCs and their EVs under static and dynamic culture conditions, providing key insights into how these environments influence their biological properties and secretory profile. By directly comparing these conditions, this study establishes a foundation for future investigations into the regenerative potential of hTSPC-derived EVs in tendon repair.

4.2 Aim

The primary objective of this chapter was to characterise hTSPCs and investigate the impact of different culture conditions, including static and dynamic environments, on their EV production and characteristics. Additionally, this study aimed to evaluate the potential of GDF-5 supplementation in enhancing the tenogenic properties of hTSPCs.

Specifically, the study aimed to:

1. Isolate and characterise hTSPCs from human tendon tissue using explant methods and assess their proliferative capacity, morphological characteristics, and stemness properties through flow cytometry, trilineage differentiation assays, and RT-qPCR.
2. Evaluate the tenogenic differentiation potential of hTSPCs by investigating the effects of GDF-5 supplementation on cellular morphology, collagen deposition, and the expression of tenogenic markers at early and late passages.
3. Characterise crude EVs derived from hTSPCs under static and dynamic culture conditions, including their morphology, size, concentration, protein content, surface

marker expression, and cytokine profile. Analytical techniques included SEM, TEM, NTA, Bradford assay, Western blot, MACSPlex, and multiplex cytokine analysis.

This chapter comprehensively characterises hTSPCs and their EVs by addressing these objectives and examining how static and dynamic culture conditions influence their biological properties and secretory profiles. These findings lay the foundation for future chapters, where the tenogenic potential of EVs will be further explored in Chapters 5 and 6.

4.3 Methods

Human TSPCs were isolated and characterised using the procedures described in Chapter 2, with an overview of the study design provided in Scheme 2. Briefly, cells were extracted from three patients with ethical approval (Section 2.3.3) and assessed for proliferative potential, trilineage differentiation, flow cytometry profile, and gene expression (Sections 2.4, 2.5, 2.6, 2.9, and 2.12). Flow cytometry data analysis was performed in collaboration with Dr. Valentina Giudice.

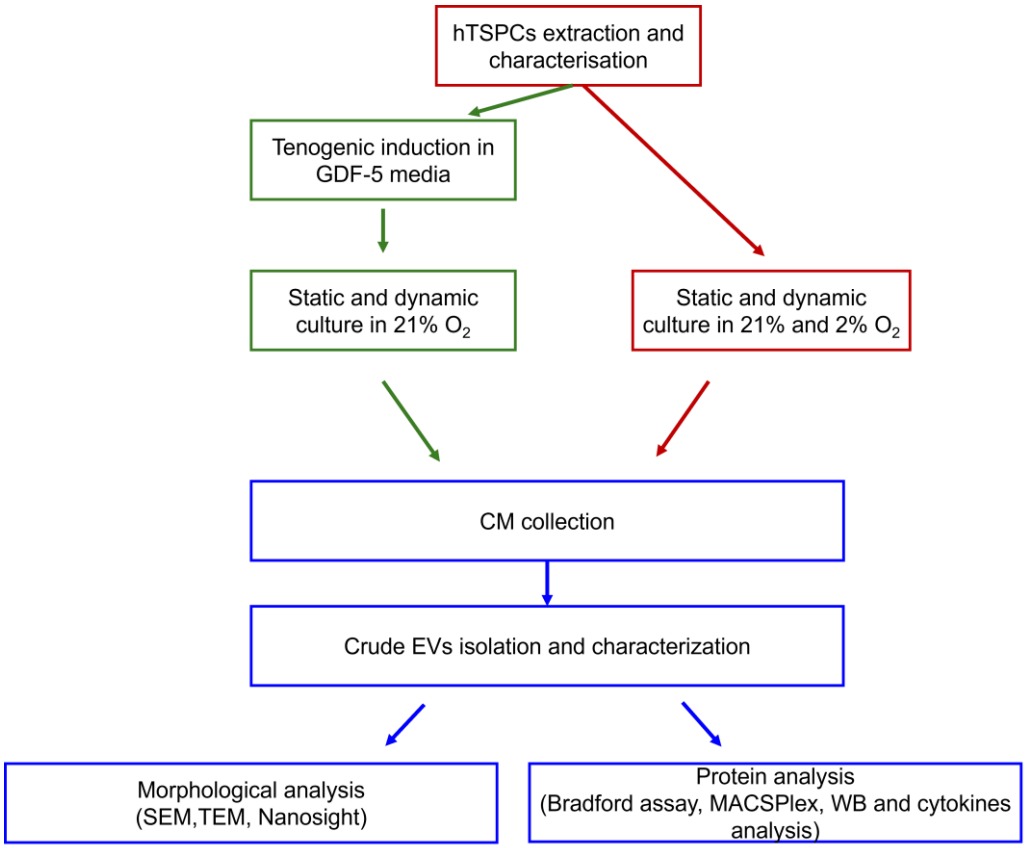
To evaluate tenogenic differentiation, early passage (P3) and late passage (P16) TSPCs were cultured in media supplemented with 100 ng/mL GDF-5 for 21 days (Section 2.8). Cells were subsequently analysed for aspect ratio, histological staining (Section 2.16), and tendon-related gene expression by RT-qPCR.

For EV experiments, hTSPCs were seeded at a density of 5,000 cells/cm² in static and dynamic culture environments. Dynamic culture was performed using a custom-made perfusion bioreactor operating at a constant flow rate of 1 mL/min (Section 2.18.1). Flow conditions were modelled using finite element simulations (Section 2.18.1.1) in collaboration with Dr. Joseph Lovecchio and Prof. Emanuele Giordano (University of Bologna). CM were collected at 70–90% confluence, and cEVs were isolated by ultracentrifugation (Section 2.19). Crude pellets were then characterised using SEM, TEM, and Nanosight analysis for morphology and size (Section 2.22), as well as protein analysis via Bradford assay, Western blot, and MACSPlex (Section 2.23).

Additional conditions were tested by culturing hTSPCs at two oxygen concentrations (2% and 21%) under static and dynamic environments. When the perfusion bioreactor was not available, dynamic conditions were simulated using a laboratory rocker system (Section 2.18.2). Conditioned media were collected at confluence, followed by cEV isolation and analysis by Bradford assay, MACSPlex, and cytokine profiling.

4.3.1 Statistical analysis

Data are presented as the mean ± SD from three biological replicates (n = 3). Statistical comparisons were conducted using the Mann–Whitney test, unpaired *t*-tests, or multiple unpaired *t*-tests, as appropriate. All analyses were performed using GraphPad Prism software (version 10.2.2), with significance thresholds set as '*' for $p < 0.05$, '**' for $p < 0.01$, '***' for $p < 0.001$, and '****' for $p < 0.0001$.



Scheme 2. Summary of the methodology adopted in Chapter 4.

4.4 Results

4.4.1 Human tendon-derived cell characterisation

Using an explant method, followed by enzymatic digestion, human TSPCs were isolated from healthy semitendinosus tendon tissue samples. The cells were harvested in 21% O_2 and characterised to assess their biological properties. Proliferative potential was evaluated at early (P3) and late (P16) passages. Stemness properties were confirmed through flow cytometry analysis and trilineage differentiation assays, while the tenogenic profile was assessed using RT-qPCR.

4.4.1.1 Cell proliferative capacity and aspect ratio

Human TSPCs were cultured over a 120-day period under 21% O_2 conditions to monitor their proliferation rates, expressed as CPDs. The growth curve demonstrated continuous proliferation throughout the entire culture period, with the cells achieving 29.6 CPD without reaching a growth plateau (Figure 4-1A).

Morphological analysis revealed significant changes between P3 and P16 passages. A 1.08-fold decrease in the aspect ratio was observed ($p < 0.0001$), indicating a shift from the characteristic spindle-shaped morphology to a rounder and flatter appearance at later passages (Figure 4-1B). Representative images illustrate these morphological differences, with early passage cells displaying elongated, spindle-like shapes, whereas late passage cells appear more rounded and flattened (Figure 4-1B). These findings align with previously observed changes in porcine tendon-derived cells described in Chapter 3.

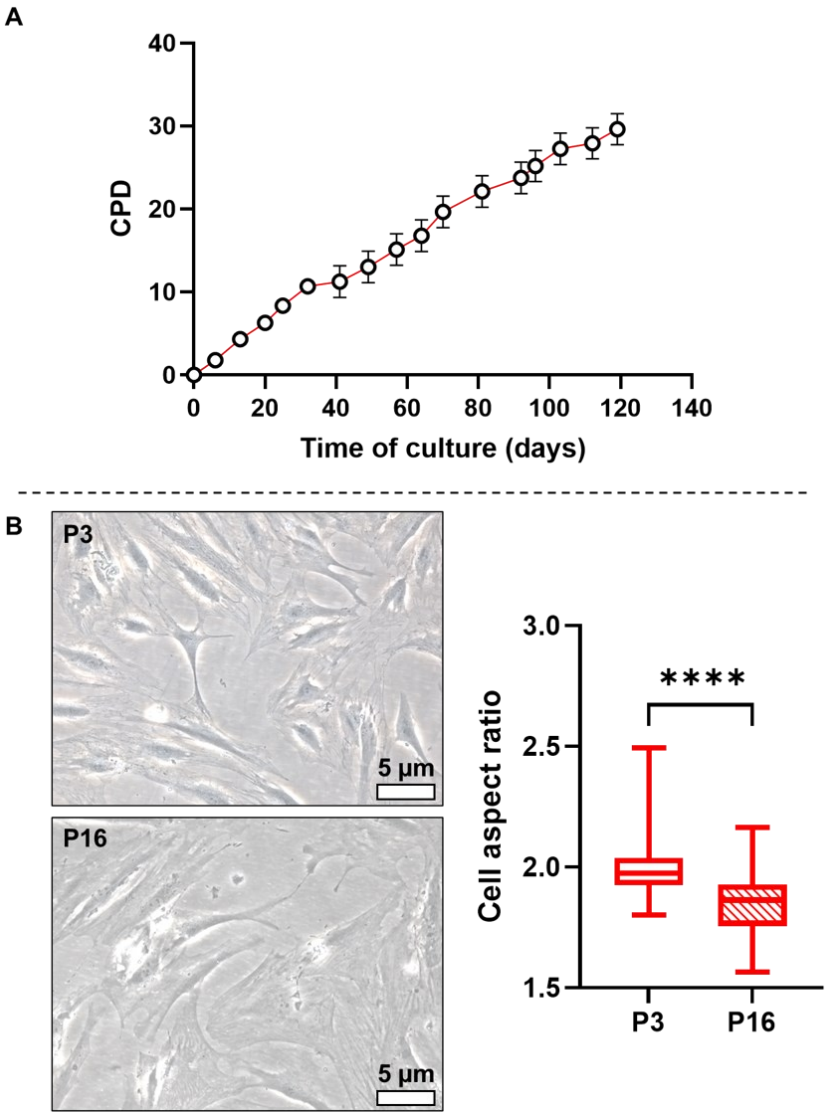


Figure 4-1. Proliferative capacity and cell aspect ratio of human TSPCs. (A) The CPD curve of human TSPCs cultured under 21% O_2 conditions over 120 days shows continuous proliferation without a growth plateau. (B) Morphological differences between human TSPCs at early passage (P3) and late passage (P16) were observed using optical microscopy and quantified by measuring cell aspect ratios. Scale bar = 5 µm. Statistical analysis: Mann–Whitney test comparing P3 vs P16; '****' for $p < 0.0001$, n=3. Image adapted from Clerici et al., 2025[279] under CC BY-NC 4.0 License.

4.4.1.2 Flow cytometry and trilineage differentiation

The immunophenotypic profile of human TSPCs was evaluated through flow cytometry to analyse the expression of MSC surface markers CD90, CD73, and CD105 while confirming the absence of haematopoietic markers HLA-DR, CD34, and CD14. Histograms of fluorescence intensity for each marker at early and late passages are presented in Figure 4-2A.

The immunophenotypic profile remained consistent across early and late passages. Positive MSC markers were highly expressed at both stages, with CD90, CD105, and CD73 showing over 98% positivity. A slight but measurable increase was observed at the late passage, with a 1.003-fold increase in CD90 (99.6% at P3 and 99.9% at P16), a 1.01-fold increase in CD105 (98.7% at P3 and 99.8% at P16), and a similar increase in CD73 (99.3% at P3 and 99.8% at P16). Conversely, the expression of negative haematopoietic markers declined with passage. At P16, HLA-DR showed an 8-fold decrease, CD14 exhibited a 6-fold decrease, and CD34 demonstrated a 3.8-fold decrease, shifting from 25% positivity at P3 to 6.5% at P16 (Figure 4-2B).

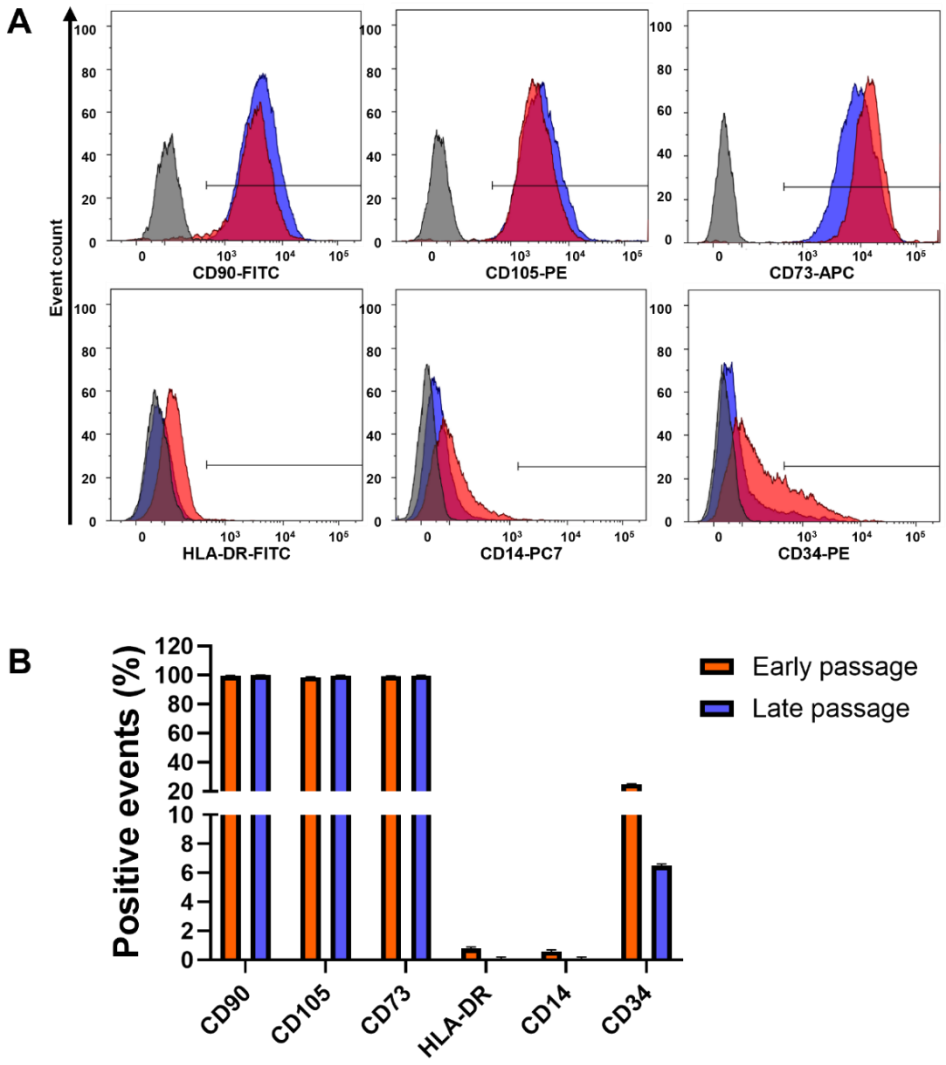


Figure 4-2. Immunophenotype of hTSPCs. hTSPCs cultured in 21% O_2 were analysed by flow cytometry using a panel of MSC markers. (A) Overlay histograms show each antibody marker, with grey

fill representing the isotype control, orange fill representing the antibody marker for early passage cells, and light blue fill representing the antibody marker for late passage cells. (B) Percentage of positively stained cells at early and late passage compared to the corresponding isotype control. Image adapted from Clerici et al., 2025[279] under CC BY-NC 4.0 License.

In addition to immunophenotypic analysis, the multipotency of TSPCs was assessed through trilineage differentiation assays. At both early and late passage, TSPCs were induced to differentiate into osteogenic, adipogenic, and chondrogenic lineages. Successful differentiation was confirmed by Alizarin Red staining for mineralised deposits (osteogenesis), Oil Red O staining for lipid vacuoles (adipogenesis), and Alcian Blue staining for glycosaminoglycans (chondrogenesis). Visual inspection of the staining results suggested that the adipogenic differentiation capacity of hTSPCs was maintained or slightly increased at later passages (P16), as indicated by the presence of lipid vesicle-containing cells, although the intensity of Oil Red O staining appeared reduced. In contrast, osteogenic differentiation appeared slightly less pronounced in later-passage cells, as indicated by a possible decrease in Alizarin Red staining (Figure 4-3).

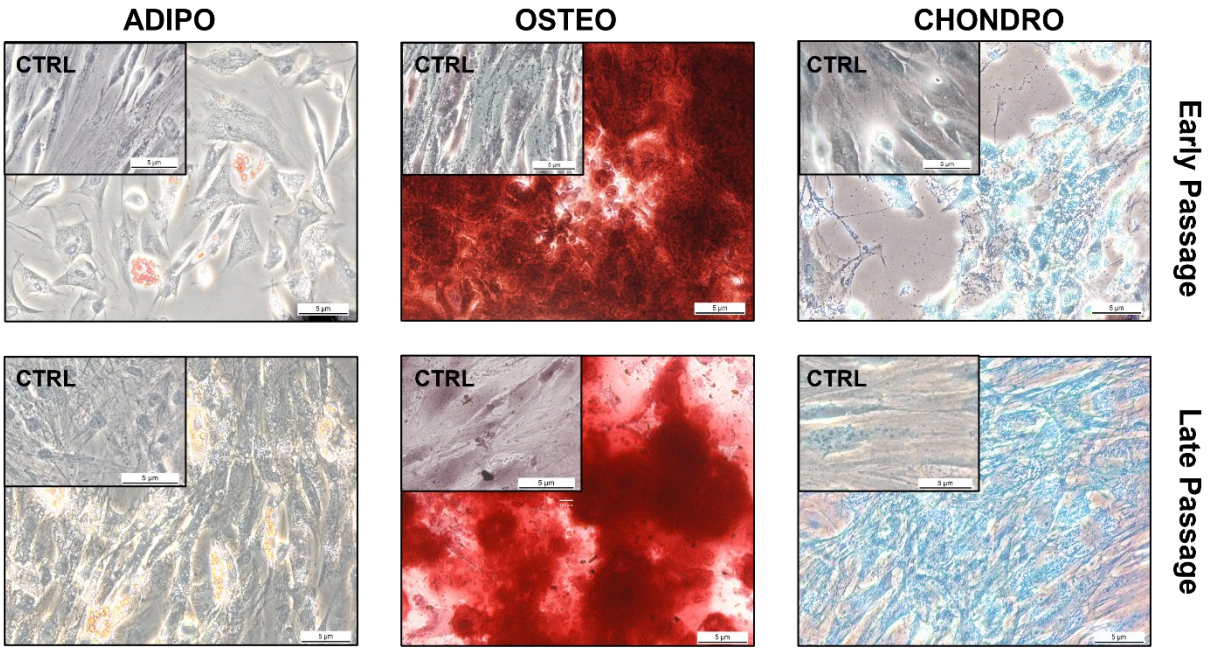


Figure 4-3. Trilineage differentiation of hTSPCs. Images of P3 and P16 TSPCs cultured in monolayers for 21 days in 21% O_2 conditions, with pro-differentiation media supplements, followed by fixation and histological staining. Scale bar = 5 µm. Image adapted from Clerici et al., 2025[279] under CC BY-NC 4.0 License.

4.4.1.3 Gene expression

The gene expression profile of TSPCs was analysed at P3 and P16, showing distinct changes in tenogenic gene expression. Most tested tenogenic genes (*SCX-A*, *DCN*, *TNC*, *TNMD*, and *COL3A1*) were downregulated in late-passage cells compared to early-passage cells. Notably, significant reductions were observed in *SCX-A* (20-fold decrease, <0.0001), *DCN* (2-fold decrease, p <0.0001), *TNC* (3.4-fold decrease, p<0.0001), and *COL3A1* (1.5-fold decrease, p=0.0002). In contrast, COL1A1 was upregulated at late passage, showing a 1.2-fold increase (p=0.0441) (Figure 4-4).

These findings suggest that the ageing process alters the tenogenic gene expression profile of TSPCs, with a general decline in key tenogenic markers, except for *COL1A1*, which may reflect changes in the cells' ECM production during prolonged culture.

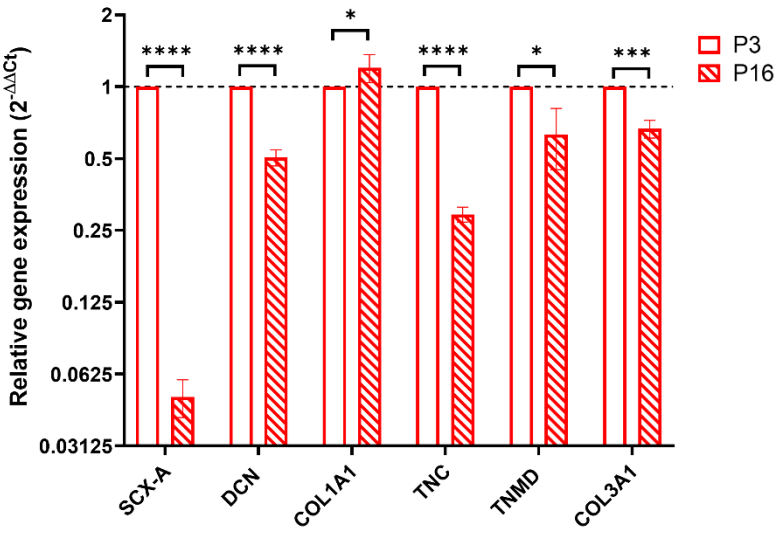


Figure 4-4. Gene expression of tenogenic markers in hTSPCs. Early (P3) and late (P16) passage TSPCs were analysed for the expression of *SCX-A*, *DCN*, *COL1A1*, *TNC*, *TNMD*, and *COL3A1* under 21% O_2 condition. Gene expression data are presented as relative levels over early passage = 1. Statistical analysis: multiple unpaired *t*-tests comparing P3 vs P16 for each gene; '*' for p < 0.05, '***' for p < 0.001, and '****' for p < 0.0001, n=3. Image adapted from Clerici et al., 2025[279] under CC BY-NC 4.0 License.

4.4.2 GDF-5 effect on hTSPCs

TSPCs were cultured in GDF-5 supplemented media (100 ng/mL) for 21 days to evaluate the tenogenic potential of this treatment on early (P3) and late (P17) passage TSPCs. Then, characterisation was performed using histological staining, RT-qPCR, and IF analysis.

4.4.2.1 Picro-Sirius Red staining and quantification

Early (P3) and late passage (P17) TSPCs were stained with Picro-Sirius Red to detect collagen fibres. Visual inspection revealed morphological changes and an increased presence of collagen in GDF-5-treated samples compared to controls, particularly on day 14 (Figures 4-5A). To quantify collagen production, staining intensity was measured as described in Section 2.16.1 over a 21-day culture period, with results normalised to day 0 samples. In early passage cells, GDF-5 treatment resulted in a 1.1-fold increase in collagen production at day 7 ($p = 0.094$) and a significant 1.2-fold increase at day 14 ($p = 0.0015$). Late passage cells also showed significant increases in collagen production following GDF-5 treatment, with a 1.2-fold increase at day 7 ($p=0.0009$), a 1.4-fold increase at day 14 ($p<0.0001$), and a 1.2-fold increase at day 21 ($p=0.0005$) (Figure 4-5B). These findings demonstrate that GDF-5 supplementation effectively enhances collagen deposition in TSPCs, with both early- and late-passage cells showing a positive response, particularly at day 14.

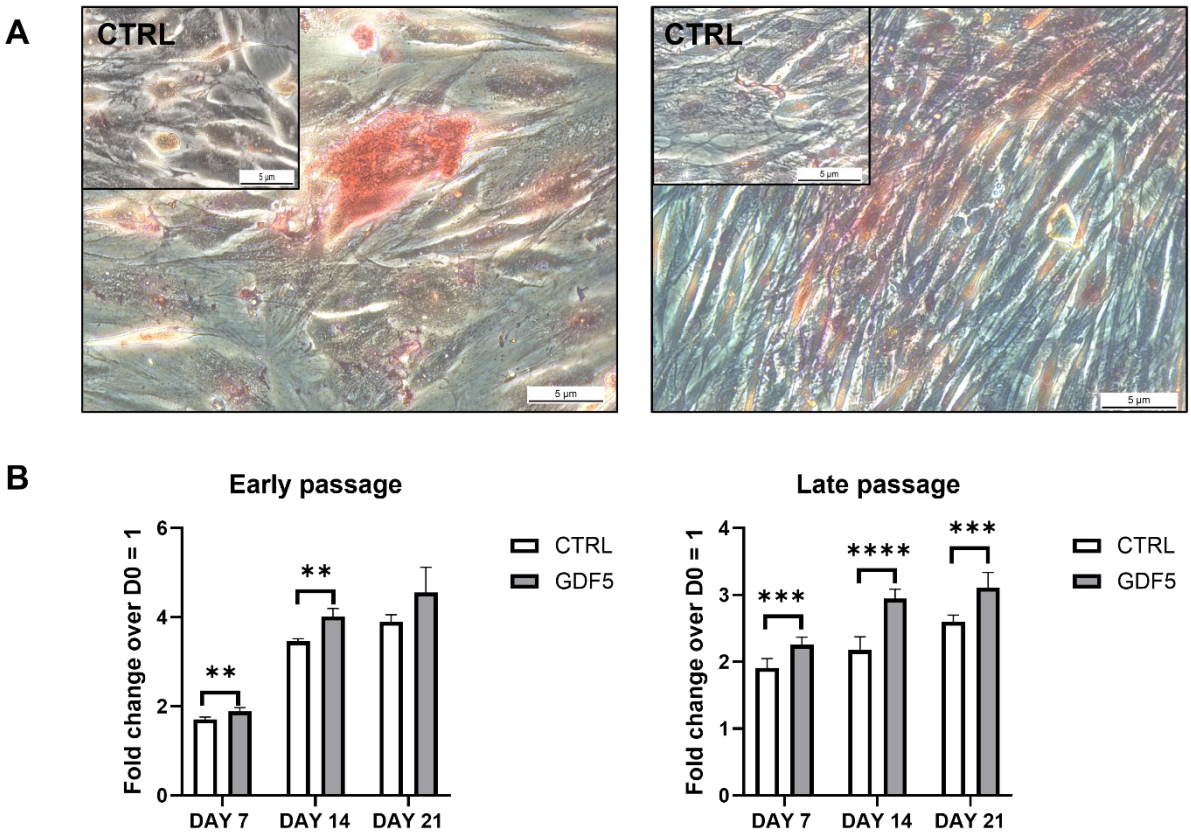


Figure 4-5. Collagen deposition in GDF-5-treated human TSPCs, assessed by Picro-Sirius Red staining. (A) Representative images of day 14 early passage (P3) and late passage (P17) TSPCs stained with Picro-Sirius Red, showing increased collagen deposition in GDF-5 treated samples compared to controls. Scale bar: 5 µm. (B) Quantification of staining intensity normalised to day 0 samples. GDF-5 treatment significantly increased collagen deposition in both early- and late-passage cells compared to the control group. Statistical analysis: unpaired *t*-tests comparing control vs GDF-5 treatment within each passage; '**' for $p < 0.01$, '***' for $p < 0.001$, and '****' for $p < 0.0001$, n=3. Image adapted from Clerici et al., 2025[279] under CC BY-NC 4.0 License.

4.4.2.2 Gene expression

Based on the histological results, RT-qPCR was performed to assess the expression of key tenogenic markers (*TNMD*, *SCX-A*, *TNC*, *DCN*, *COL1A1*, and *COL3A1*) in samples collected on days 7 and 14 following GDF-5 treatment.

After 7 days of GDF-5 treatment, TSPCs exhibited a 1.5-fold decrease in *SCX-A* (p=0.0052), a 2.7-fold decrease in *DCN* (p=0.0031), and a significant 1.7-fold increase in *COL1A1* (p=0.0256). Conversely, after 14 days of treatment, a significant upregulation of tenogenic

markers was observed. Specifically, *SCX-A* increased by 2.2-fold (p<0.0001), *COL1A1* by 2.1-fold (p=0.0085), *TNMD* by 9-fold (p=0.3308), and *COL3A1* by 2.3-fold (p=0.0003). In contrast, *DCN* showed a 1.2-fold decrease (p = 0.0294) (Figure 4-6).

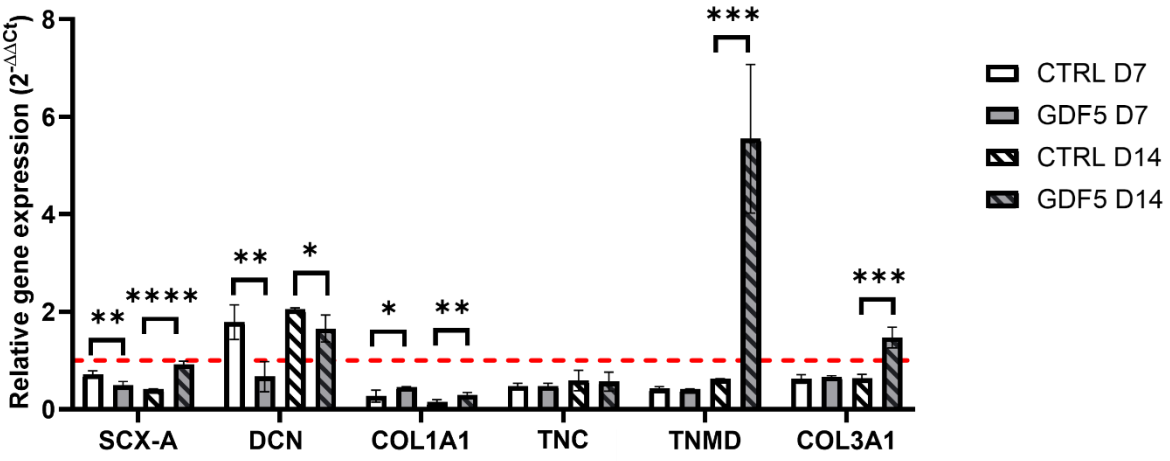


Figure 4-6. Gene expression of tenogenic markers in GDF-5-treated TSPCs. RT-qPCR analysis shows the expression levels of tenogenic markers (*SCX-A*, *DCN*, *COL1A1*, *TNC*, *TNMD*, and *COL3A1*) in early passage TSPCs cultured with GDF-5 (100 ng/mL) for 7 and 14 days. Gene expression data are presented as relative levels over day 0 = 1. Statistical analysis: unpaired *t*-tests comparing control vs GDF-5 treatment for each gene at each timepoint; '*' for p < 0.05, '**' for p < 0.01, '***' for p < 0.001, and '****' for p < 0.0001, n=3. Image adapted from Clerici et al., 2025[279] under CC BY-NC 4.0 License.

4.4.2.3 Immunofluorescence analysis

Immunofluorescence analysis was conducted to evaluate the expression of TNMD and COL1 in day 14 samples from both control and GDF-5-treated TSPCs. TNMD was labelled with a green-fluorescent signal, while COL1 was labelled with red fluorescence to allow for visualisation.

Visual inspection of the IF images revealed an apparent increase in the expression of both TNMD and COL1 in GDF-5-treated cells compared to control samples, suggesting an enhanced tenogenic differentiation response to GDF-5 stimulation. This increase in marker

expression was accompanied by noticeable morphological changes in treated cells, which displayed a more elongated and spindle-like shape, indicative of tenocyte-like morphology.

Cell aspect ratio analysis was performed to support these observations quantitatively. The results demonstrated a 1.4-fold increase in the aspect ratio of GDF-5-treated cells compared to controls. This elongation in cell shape aligns with the visual findings and further confirms that GDF-5 treatment promotes a phenotypic shift towards a tenogenic lineage (Figure 4-7). Overall, the combination of increased TNMD and COL1 expression, along with the morphological changes observed in GDF-5-treated samples, highlights GDF-5's positive effect on driving tenogenic differentiation in TSPCs.

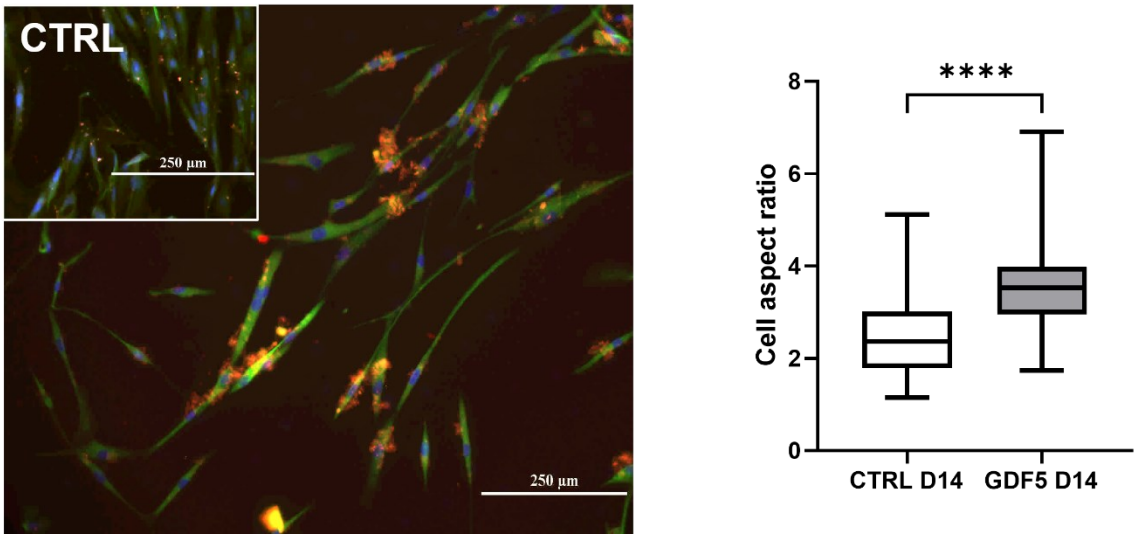


Figure 4-7. Immunofluorescence analysis and cell aspect ratio of GDF-5-treated TSPCs. Morphological differences between human TSPCs cultured in standard media and GDF-5 supplemented media under 21% O_2 at P3 were observed using fluorescence microscopy and quantified by measuring cell aspect ratios. Immunofluorescence images on day 14 show the expression of Tenomodulin (TNMD, green) and Collagen Type I (COL1, red). Scale bar = 250 µm. Statistical analysis: Mann–Whitney test comparing control vs GDF-5; '****' for $p < 0.0001$. Image adapted from Clerici et al., 2025[279] under CC BY-NC 4.0 License.

4.4.3 Perfusion bioreactor-derived human cEVs characterisation

Following the findings on the tenogenic potential of GDF-5-supplemented media, human TSPCs were cultured in this optimised medium for EV isolation. Cells were expanded until they reached 70-90% confluence, and cultures were performed under static and dynamic

conditions. A custom-made perfusion bioreactor was used to simulate a dynamic environment, operating at a constant flow rate of 1 mL/min to provide mechanical stimulation.

FEM analysis was conducted to evaluate the impact of the flow conditions on the cell culture environment. The results demonstrated a uniform medium velocity distribution across the horizontal cross-section, with an average flow velocity of 8.28×10^{-6} m/s, indicating stable and homogenous conditions within the bioreactor (Figure 4-8).

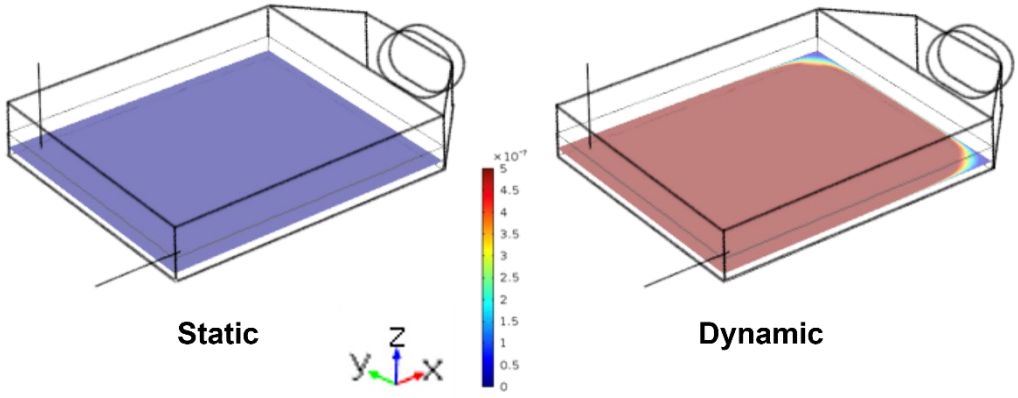


Figure 4-8. Finite Element Method analysis of medium flow in a custom-made perfusion bioreactor. FEM analysis was performed to assess the flow distribution within a T-175 flask used for static and dynamic culture. The horizontal cross-section demonstrates a uniform medium velocity distribution with an average flow velocity of 8.28×10^{-6} m/s across the surface, indicating minimal variations within the culture area. Image adapted from Clerici et al., 2025[279] under CC BY-NC 4.0 License.

After 24 hours of conditioning, the CM was collected, and cEVs were isolated via ultracentrifugation. The resulting crude pellet was subjected to comprehensive characterisation, including morphological analysis using SEM, TEM, and NTA. In addition, protein analysis was performed using the Bradford assay for total protein content, MACSPlex

to detect surface marker expression, and Western blot to validate the presence of EV-associated proteins.

4.4.3.1 Morphological and size analysis

The morphology and size of cEVs isolated from human TSPCs cultured in GDF-5-supplemented media under static and dynamic conditions were analysed using SEM, TEM, and NTA.

SEM analysis revealed a polydisperse population of EVs, with a significant proportion of particles measuring below 200 nm in diameter. However, regions of particle aggregation were observed, likely due to the drying process during SEM sample preparation. Drying-induced surface tension forces can lead to the clustering of vesicles, a common artefact in SEM imaging of EVs (Figure 4-9A).

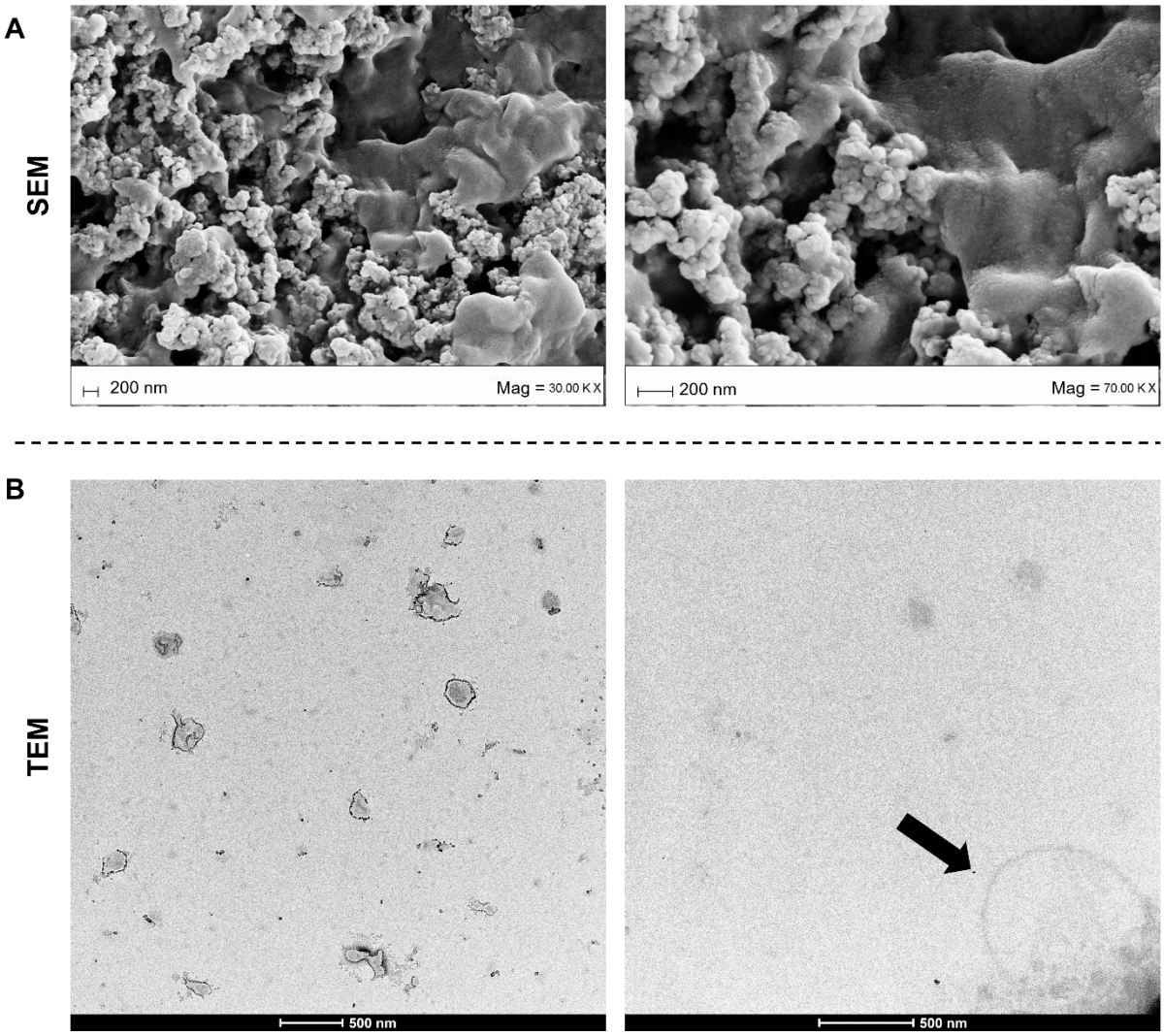
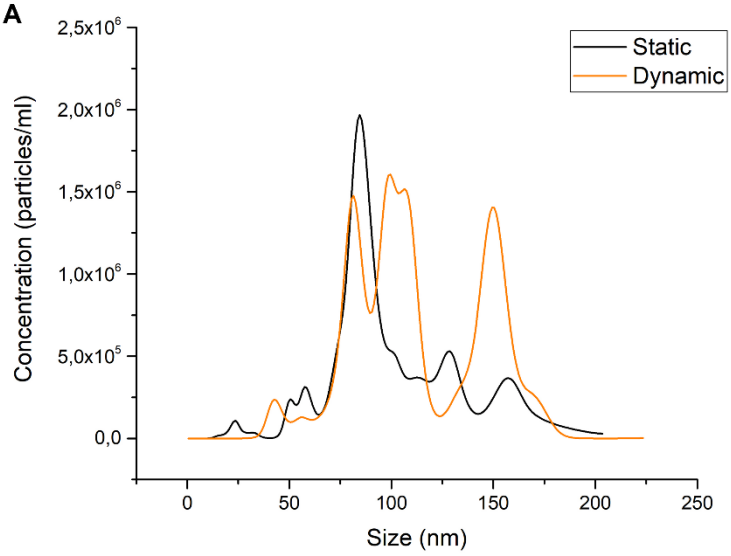


Figure 4-9. Morphological analysis of human TSPC-derived cEVs using SEM and TEM. (A) SEM images show a polydisperse population of EVs with particles below 200 nm, though aggregation is observed, likely due to drying artefacts during sample preparation. Scale bar: 200 nm. (B) TEM images confirm the presence of spherical EVs (50–200 nm) with an intact bilayer membrane and a more uniform, well-dispersed population. Scale bar: 500 nm. Image adapted from Clerici et al., 2025[279] under CC BY-NC 4.0 License.

TEM analysis provided enhanced visualisation of the EVs, confirming the presence of spherical particles with diameters predominantly within the 50–200 nm range. TEM images displayed a more uniform and well-dispersed population, further supporting the observed size and morphology. The vesicles exhibited an intact bilayer membrane structure, a hallmark feature of EVs (Figure 4-9B, pointed by the black arrow). Compared to SEM, TEM offered better resolution of smaller particles and highlighted a more homogenous population.

The size and concentration of EVs were quantified using NTA, with results indicating a particle concentration between 1.5 × 10^6 and 2 × 10^6 particles/mL across all conditions (Figure 4-10A). The size distribution profiles revealed a polydisperse population of EVs, with distinct peaks below 200 nm in both static and dynamic cultures.

A



B

Static	Dynamic
Mean size (nm)	
112.3 +/- 7.4	143.6 +/- 6.5
150.5 +/- 2.3	151.6 +/- 14.0
121.5 +/- 0.8	122.1 +/- 8.2

Figure 4-10. Size and concentration analysis of human TSPC-derived cEVs using NTA. (A) Representative NTA profiles comparing particle size and concentration between static and dynamic culture conditions. Both conditions exhibit polydisperse particle populations with distinct peaks below 200 nm in diameter. (B) Mean particle sizes derived from three biological replicates for static and dynamic culture conditions. Data are presented as mean ± standard deviation. Image adapted from Clerici et al., 2025[279] under CC BY-NC 4.0 License.

The mean particle size was calculated from three biological replicates for each condition, showing subtle but consistent differences between static and dynamic environments (Figure 4-10B). EVs from static cultures had an average size of 128.1 ± 16 nm, while EVs from dynamic cultures displayed a slightly larger average size of 139.1 ± 12 nm. However, some variability was observed across patients, with the most pronounced increase in particle size under

dynamic conditions noted in one patient. These findings suggest that the mechanical stimulation provided by dynamic culture conditions might influence the physical characteristics of EVs, potentially leading to the production of slightly larger vesicles.

4.4.3.2 Protein analysis

The total protein content of EVs was measured, showing that CM derived from dynamic culture conditions contained 4.3-fold more protein (normalised to the number of harvested cells) compared to static conditions. Similarly, the CP obtained from dynamic conditions exhibited a 1.3-fold higher protein content than the CP from static cultures (Figure 4-11A). Consistent with findings from porcine-derived samples, a marked decrease in protein concentration was observed following the ultracentrifugation step, further confirming the effective separation of soluble and non-soluble proteins.

Western blot analysis was conducted to evaluate the presence of EV-associated protein markers, including CD9, CD63, CD81, TSG101, HSP70, and Calnexin. Among these, only CD81 and TSG101 were detected in the EV pellet derived from dynamic culture conditions, likely due to the relatively low protein yield in the EV samples (<0.5 µg/mL) (Figure 4-11B).

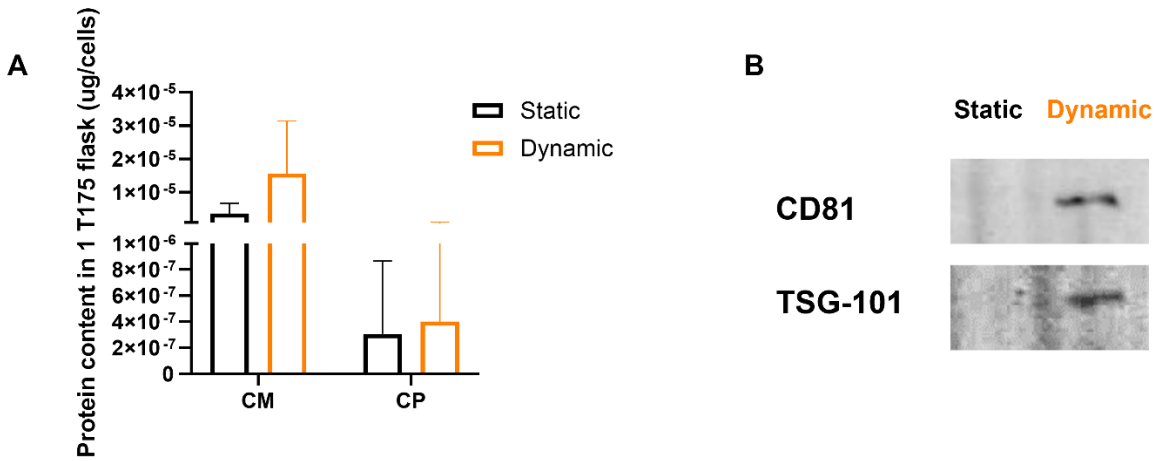


Figure 4-11. Total protein content and western blot analysis of EVs isolated from human TSPCs. (A) Total protein content of CM and CP collected from static and dynamic culture conditions. (B) Western blot analysis of EV-associated protein markers, including CD81 and TSG101, detected in the crude pellet from dynamic culture conditions. Statistical analysis: unpaired *t*-tests were performed for CM and CP (static vs dynamic). Data are presented as mean ± SD, n=3. Image adapted from Clerici et al., 2025[279] under CC BY-NC 4.0 License.

Flow cytometry analysis using the MACSPlex Exosome Kit, which detects 37 exosomal surface epitopes plus two isotype controls, revealed the presence of 13 surface markers: CD45, CD63, CD81, CD1c, CD41b, MCSP, HLA-DR/DP/DQ, CD25, CD9, CD2, CD3, CD326, and CD56. Notably, the surface expression of almost all markers was higher in the EV pellet obtained from dynamic culture conditions, with CD63 exhibiting the highest level of expression.

Among immune cell markers, CD2 (301-fold) and CD25 (291-fold) exhibited the most substantial increases in dynamic culture-derived EV pellets. Moderate increases were observed for HLA-DR/DP/DQ (3.94-fold), CD45 (1.96-fold), and CD3 (2-fold), while CD1c showed a more modest increase (1.66-fold) compared to static conditions (Figure 4-12A).

For EV-associated markers, CD63 showed the highest increase (4.93-fold) in dynamic culture, while CD81 was exclusively detected in dynamic culture-derived EV pellets. In contrast, CD9 was 3-fold higher in static culture-derived pellets, indicating possible differences in EV subpopulations between the two conditions (Figure 4-12B).

Regarding platelet markers, CD41b was the only marker detected, exhibiting similar expression levels in both static and dynamic conditions, which suggests minimal platelet-derived EV contamination in both environments (Figure 4-12C).

For tumour and stem cell-associated markers, CD326 was detected only in static culture-derived pellets, whereas MCSP was uniquely found in dynamic culture-derived pellets, indicating potential shifts in EV cargo influenced by culture conditions (Figure 4-12D).

Among other functional markers, CD56, a neural cell adhesion molecule, was dramatically higher (184-fold) in dynamic culture-derived EV pellets, suggesting a strong culture-dependent enrichment (Figure 4-12E).

Although trends in marker expression were evident, biological replicate variability prevented the detection of statistically significant differences, highlighting the need for additional samples to confirm these findings.

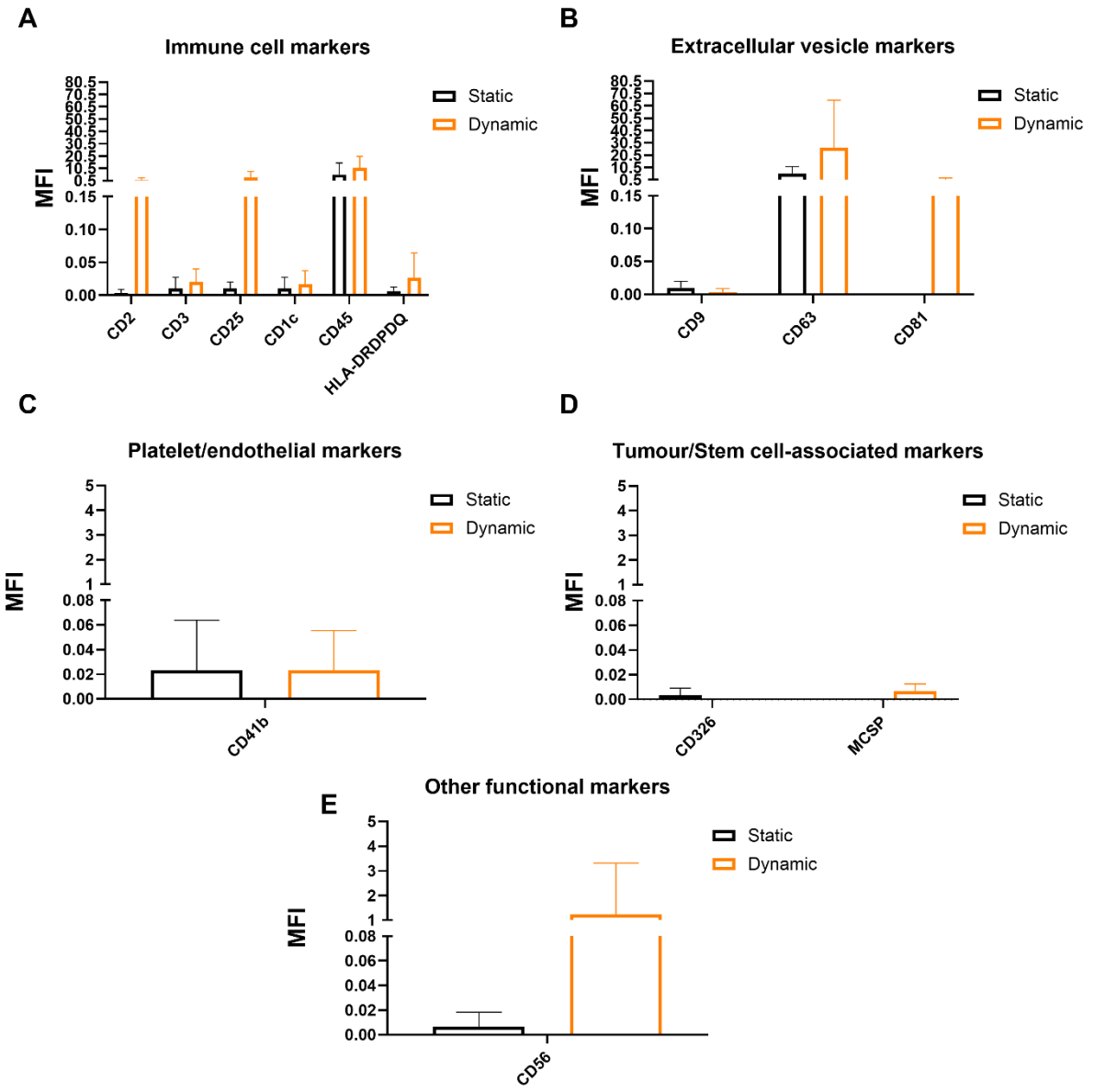


Figure 4-12. Surface marker expression on crude EVs derived from hTSPCs. Flow cytometry-based MACSPlex analysis showing the expression of 13 surface markers on cEVs cultured under static and dynamic conditions. (A) Immune cell markers, (B) extracellular vesicle-associated markers, (C) platelet/endothelial markers, (D) tumour/stem cell-associated markers, and (E) other functional markers. Dynamic culture conditions generally resulted in substantially higher marker expression levels than static conditions, as indicated by the fold-change values. Statistical analysis: unpaired *t*-tests were performed for each marker (static vs dynamic). Data are presented as mean ±SD, n=3.

4.4.4 Lab-rocker system-derived human cEVs characterisation

Human TSPCs obtained from three patients were cultured under two oxygen conditions (2% and 21%) and in static and dynamic environments to encompass all experimental variables. As the custom-made perfusion bioreactor could not be replicated for this setup, flasks

containing hTSPCs were placed on a lab rocker system (section 2.18.2) to simulate dynamic culture conditions. Once the cells reached confluence, CM was collected, subjected to ultracentrifugation, and subsequently characterised through Bradford assay, MACSPlex analysis, and cytokine profiling.

4.4.4.1 Total protein concentration

The Bradford assay was used to quantify the protein concentration in both the CM and the CP. The CM was collected and normalised to the number of cells harvested from a T-175 cm² flask, with protein concentration expressed in µg. In 21% O_2, the average total protein content in CM obtained from dynamic culture was 1.6-fold higher than in static culture. Conversely, in 2% O_2, the values were nearly identical, with CM from static culture showing a slightly higher protein content (1.04-fold) (Figure 4-13A). However, no statistically significant differences were observed due to the substantial variability between biological replicates. To better illustrate this variability, the average values for each sample across replicates were reported for both dynamic and static culture conditions. In 21% O_2, the total protein normalised to cell number in CM from dynamic culture was higher in sample #1 (5.2-fold, $p = 0.001004$) and sample #3 (1.2-fold), while sample #2 exhibited a significantly higher protein content in static culture (3.1-fold, $p = 0.003218$) (Figure 4-13B). In 2% O_2, while sample #1 showed a significantly higher protein concentration in dynamic culture (1.8-fold, $p = 0.000570$), sample #2 (1.3-fold, $p = 0.008103$) and sample #3 (1.6-fold, $p = 0.001373$) displayed higher protein levels in static culture, differing from the trend seen in 21% O_2 (Figure 4-13C).

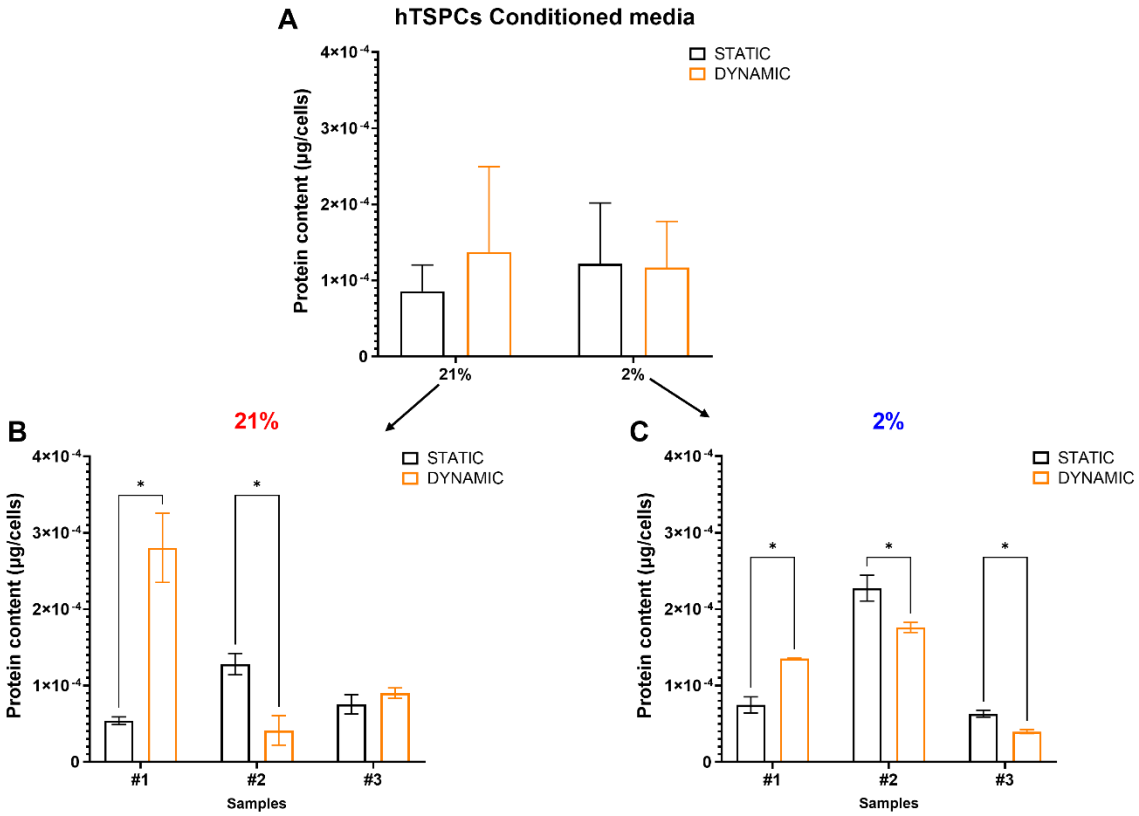


Figure 4-13. Total protein concentration of CM from human TSPCs under static and dynamic conditions at 21% and 2% oxygen. (A) The average total protein content, normalised to cell number, shows higher protein levels in dynamic culture at 21% O_2, while no significant differences were observed at 2% O_2. Individual sample analysis reveals variability in protein content across conditions, with (B) dynamic culture generally yielding higher protein levels in 21% O_2, whereas (C) static culture showed comparable or higher levels in 2% O_2. Statistical analysis: multiple unpaired *t*-tests were performed comparing static vs dynamic at each oxygen level; '*' for $p < 0.05$, n=3.

For the CP, protein concentration followed a similar pattern to that of CM. In atmospheric oxygen, the average protein content in CP from dynamic culture was 1.5-fold higher compared to static culture. Conversely, in physiological oxygen, the CP from static culture exhibited a 1.7-fold higher protein content than in dynamic conditions (Figure 4-14A). Due to the high variability across biological replicates, no statistically significant differences were found; therefore, the average values for each sample were reported separately. In 21% O_2, sample #1 exhibited a 1.3-fold higher protein content in static culture, while samples #2 and #3 showed a 2.1-fold and 2.4-fold higher protein content, respectively, in dynamic culture (Figure 4-14B). In 2% O_2, like atmospheric oxygen, sample #1 exhibited a 3.4-fold higher protein content in

static culture compared to dynamic culture, while sample #2 (1.7-fold) and sample #3 (1.1-fold) also displayed higher protein content in static conditions (Figure 4-14C).

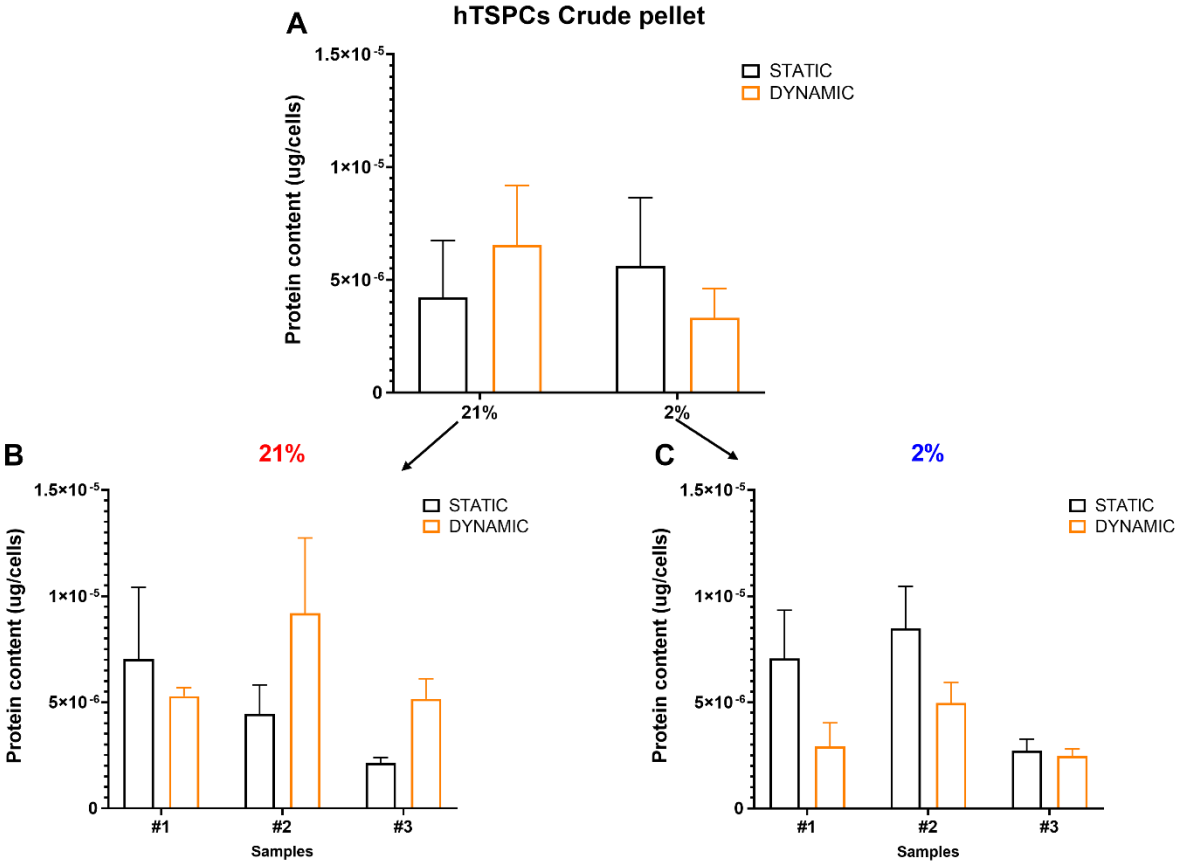


Figure 4-14. Total protein concentration of CP from human TSPCs under static and dynamic conditions at 21% and 2% oxygen. (A) The average total protein content, normalised to cell number, shows higher protein levels in the dynamic culture at 21% O_2, whereas at 2% O_2, the static culture exhibits higher protein content. Individual sample analysis highlights variability among conditions, with (B) dynamic culture yielding higher protein levels in 21% O_2 for some samples, while (C) static culture showed higher levels in 2% O_2. Statistical analysis: multiple unpaired *t*-tests were performed comparing static vs dynamic at each oxygen level. Data are presented as mean ± SD, n=3.

4.4.4.2 MACSPlex analysis

The surface marker profile of cEVs derived from hTSPCs cultured under static and dynamic conditions at 21% and 2% oxygen levels was assessed using the MACSPlex Exosome Kit.

This kit is designed to detect 37 exosomal surface epitopes and includes two isotype controls to determine non-specific binding.

In this analysis, a total of 33 surface markers were detected under each oxygen condition, with 31 markers common between both conditions, including CD3, CD105, CD56, HLA-DRDPDQ, ROR1, CD49e, HLA-ABC, CD25, CD2, CD40, CD63, CD9, CD62P, SSEA-4, CD81, CD11c, MCSP, CD146, CD41b, CD133/1, CD326, CD44, CD86, CD42a, CD24, CD29, CD20, CD14, CD45, CD142, and CD69. Two markers, CD209 and CD8, were detected exclusively in 21% O_2, whereas CD19 and CD31 were uniquely detected in 2% O_2.

Among immune cell markers, most exhibited moderate changes in expression between conditions. For example, CD3 was 1.9-fold higher in static culture-derived EV pellets under 21% O_2 and 1.5-fold higher under 2% O_2. Similar moderate increases were observed for CD2 (1.6-fold) and HLA-ABC (1.1-fold) in static conditions across both oxygen levels. CD11c expression was also moderately higher in static culture, with a 3.1-fold increase at 21% O_2 and 1.4-fold at 2% O_2. Conversely, HLA-DR/DP/DQ expression was moderately increased in dynamic culture-derived pellets, with a 3.9-fold increase under 21% O_2 and a 2.7-fold increase under 2% O_2. CD40 followed a similar pattern, with 1.5- and 1.2-fold increases in dynamic conditions under 21% and 2% O_2, respectively. CD20 and CD86 also showed modest variations, while CD25 and CD209 were expressed exclusively under specific conditions (Figure 4-15A).

Among markers with larger differences, CD24 expression was 3.8-fold higher in static culture-derived pellets under 21% O_2, whereas CD69 showed a 2.8-fold increase in dynamic culture under 2% O_2. CD14 and CD45 exhibited mild increases (1.7-fold and 1.4-fold, respectively) under dynamic conditions. CD8 and CD19 were detected exclusively in dynamic (21% O_2) and static (2% O_2) cultures, respectively, highlighting condition-specific expression.

For EV-associated markers, tetraspanins generally showed moderately higher expression in dynamic culture. CD63 was 1.5-fold and 1.2-fold higher under 21% and 2% O_2, respectively; CD9 increased by 1.2-fold and 2.1-fold, and CD81 by 1.1-fold and 1.6-fold. Among adhesion

markers, CD49e was moderately upregulated in dynamic culture (1.6-fold in 21% O_2 and 2.1-fold in 2% O_2), while CD62P was more highly expressed in static conditions under 21% O_2 (1.8-fold) but reversed under 2% O_2 (1.6-fold dynamic) (Figure 4-15B).

Platelet/endothelial markers showed variable trends. CD41b had a substantial 4.1-fold increase in dynamic culture under 21% O_2, while CD42a was moderately higher in static culture in both conditions (1.7- and 1.8-fold). CD31 was exclusively detected in static culture under 2% O_2 (Figure 4-15C).

Most stem/progenitor cell markers were moderately higher in the dynamic culture. CD105 increased by 1.8-fold (21% O_2) and 3.3-fold (2% O_2), SSEA-4 by 1.9-fold, and CD146 showed a 4-fold increase under 21% O_2 and was exclusively detected under 2% O_2. CD29 expression also showed moderate upregulation (2- to 2.2-fold). CD133/1 was slightly higher in static culture under 2% O_2 (1.2-fold), while CD44 displayed small variations depending on condition (Figure 4-15D).

Regarding tumour/stem cell-associated markers, MCSP was upregulated in dynamic culture by 1.3-fold (21% O_2) and 3.5-fold (2% O_2), while CD326 was only detected in static culture. ROR1 exhibited minor shifts in response to varying oxygen concentrations (Figure 4-15E).

Lastly, functional markers CD56 and CD142 displayed only modest changes, with no consistent trend across conditions (Figure 4-15F).

Although clear trends were observed in surface marker expression between static and dynamic cultures across different oxygen conditions, the high biological variability between patient-derived samples precluded the detection of statistically significant differences. Therefore, future studies with a larger sample size will be necessary to validate these findings and more accurately define the expression patterns of EV markers under various culture conditions.

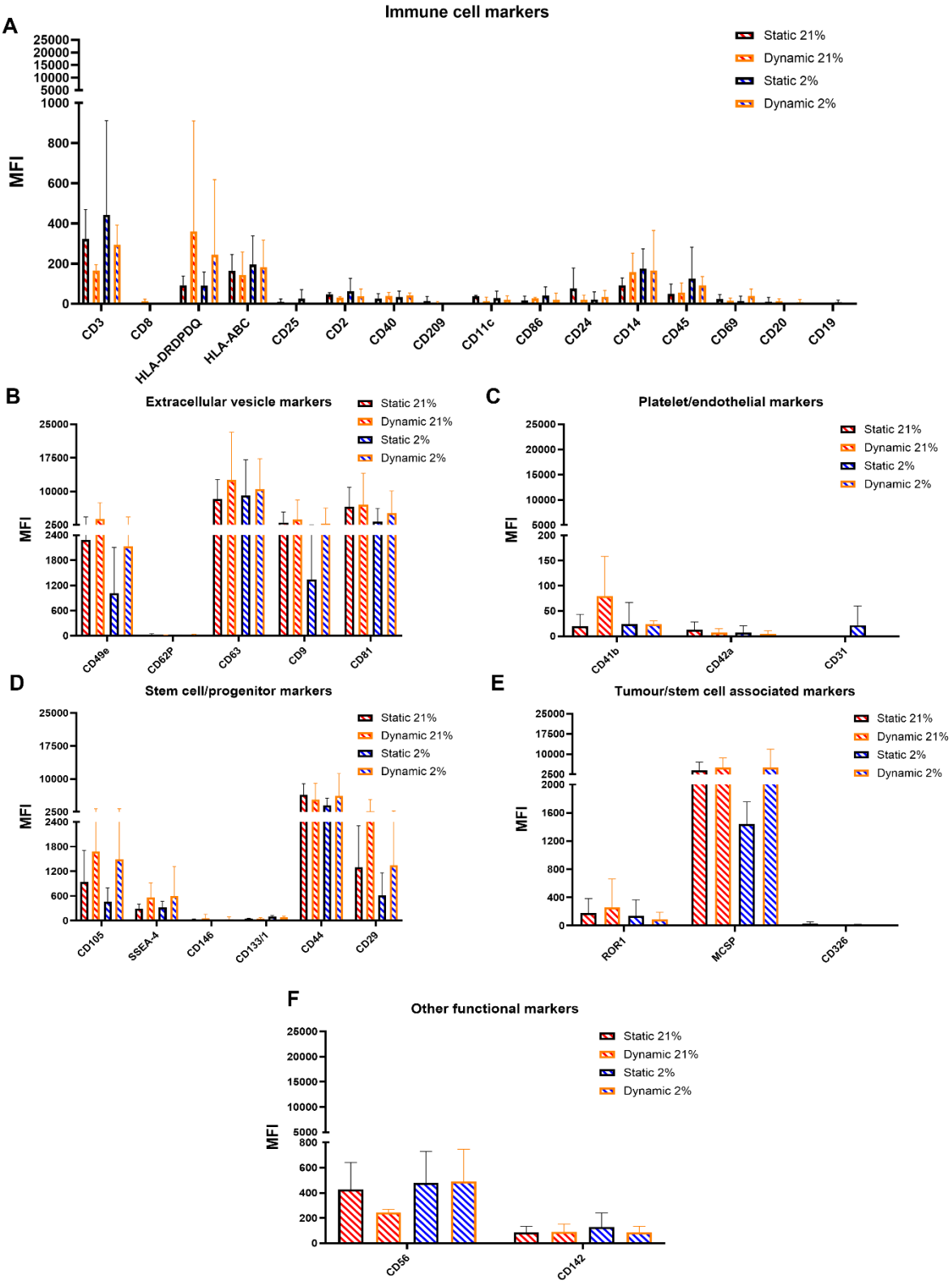


Figure 4-15. Surface marker expression on cEVs derived from hTSPCs cultured under static and dynamic conditions at 21% and 2% O_2. Flow cytometry-based MACSPlex analysis showing the expression of 33 surface markers on cEVs cultured under static and dynamic conditions at 21% (red lines) or 2% (blue lines) oxygen. (A) Immune cell markers, (B) extracellular vesicle-associated markers, (C) platelet/endothelial markers, (D) stem cell/progenitor markers, (E) tumour/stem cell-associated

markers, and (e) other functional markers. Statistical analysis: unpaired *t*-tests were performed for static vs dynamic at each oxygen level for each marker. Data are presented as MFI ± SD, n=3.

4.4.4.3 Cytokine profiling

Cytokine analysis was performed on cEVs collected from hTSPCs cultured under 21% and 2% O_2 conditions in static and dynamic environments using the lab-rocker system. The analysis was conducted using the Human Focused 15-Plex Discovery Assay® from Eve Technologies, which included the following biomarkers: IFN-γ, GM-CSF, IL-1RA, IL-1β, TNFα, IL-2, IL-4, IL-5, IL-6, IL-8, IL-10, IL-12p40, IL-12p70, IL-13, and MCP-1.

No detectable levels of GM-CSF, IL-1β, IL-2, IL-4, or IL-12p70 were found in any of the samples. According to the manufacturer's specifications, using the overnight protocol, the assay sensitivity limits for these cytokines are 2.05 pg/mL for GM-CSF, 0.79 pg/mL for IL-1β, 0.46 pg/mL for IL-2, 0.29 pg/mL for IL-4, and 1.20 pg/mL for IL-12p70. The absence of detectable signals suggests that the concentrations of these analytes in the EV samples were below the assay's minimum detection thresholds (Figure 4-16).

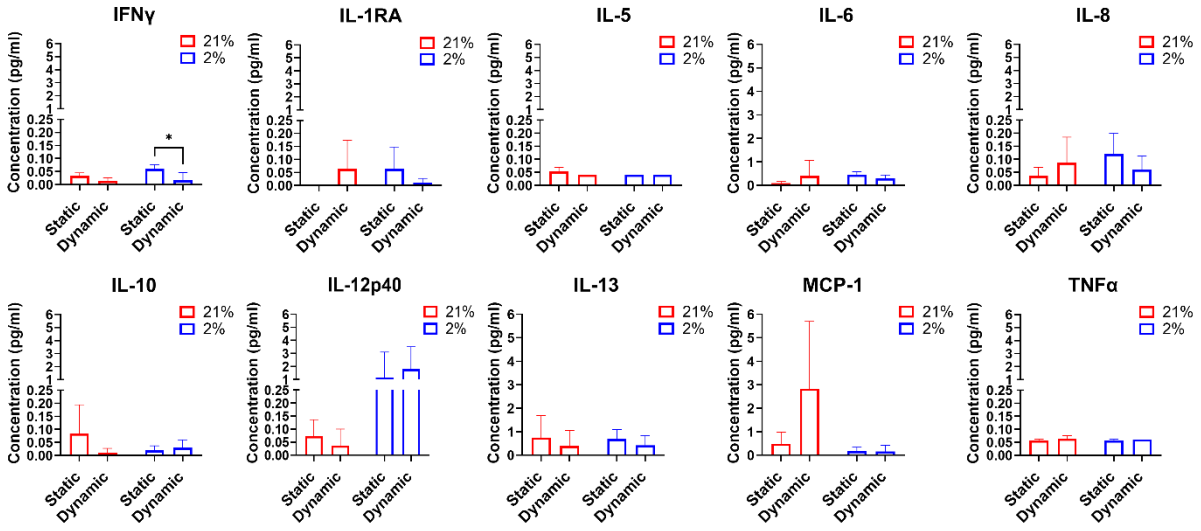


Figure 4-16. Cytokine profiling of cEVs from hTSPCs under static and dynamic conditions at 21% and 2% O_2. CEVs were isolated from hTSPCs cultured under static and dynamic conditions at 21% and 2% O_2, and cytokine levels were assessed using the Human Focused 15-Plex Discovery Assay, detecting IFN-γ, IL-1RA, TNFα, IL-5, IL-6, IL-8, IL-10, IL-12p40, IL-13, and MCP-1. Statistical analysis: multiple unpaired *t*-tests were performed for static vs dynamic at each oxygen level for each cytokine. Data are presented as mean ± SD, n=3.

Among detectable cytokines, IFN-γ levels were higher in static culture-derived cEVs under both oxygen conditions, with a 2.5-fold increase in 21% O_2 and a statistically significant 3.75-fold increase ($p = 0.0219$) in 2% O_2 compared to dynamic culture-derived EVs, reaching the highest concentration in 2% O_2. A similar trend was observed for IL-13, IL-5, and IL-12p40, all of which exhibited increased expression in static culture-derived EVs under atmospheric oxygen conditions. Conversely, IL-6, IL-8, and MCP-1 were more highly expressed in dynamic culture-derived EVs under 21% O_2. IL-10 expression followed a variable pattern depending on oxygen conditions.

Although several cytokines displayed notable fold changes between conditions, most comparisons did not reach statistical significance. This was likely due to high variability across the three biological replicates, which limited the statistical power of the analysis. The biological differences between patient-derived samples, combined with the inherently low abundance of some cytokines in EV preparations, may have contributed to this variability. These findings underscore the need to increase the number of patient samples and consider alternative normalisation strategies, such as adjusting cytokine concentrations based on total EV protein content, particle number (via NTA), or housekeeping EV markers like CD9/CD63/CD81, to reduce inter-sample variation and improve analytical consistency in future studies.

The cytokine profiling revealed condition- and oxygen-specific trends. Pro-inflammatory cytokines such as IFNγ and IL-13 were more abundant in static culture-derived EVs, particularly under 2% O_2. In contrast, dynamic culture conditions appeared to favour the secretion of immune-modulatory and tissue repair-associated cytokines, such as IL-6 and IL-8, particularly under atmospheric oxygen.

4.5 Discussion

Tendon injuries pose significant clinical challenges due to tendons' limited intrinsic healing capacity, primarily attributed to their low cellularity and restricted vascular supply[307]. Conventional treatment strategies, including surgical and conservative approaches, often fail

to fully restore tendon function, leading to high recurrence rates and prolonged rehabilitation periods[7]. Consequently, research efforts have shifted towards alternative strategies, such as stem cell-based therapies, to enhance tendon regeneration[8]. However, concerns regarding stem cell-based approaches, including donor variability, genetic instability, and the potential risk of ectopic tissue formation, have led to an increased focus on EVs as a promising cell-free therapeutic alternative[2,217]. EVs play a crucial role in intercellular communication by transporting bioactive molecules, including proteins, lipids, and nucleic acids, which influence tissue repair processes[136].

In this study, human TSPCs were successfully isolated from healthy tendon biopsies using an optimised explant method[53,279]. The isolated cells exhibited a MSC immunophenotype, as confirmed by their expression of CD73, CD90, and CD105 and the absence of haematopoietic markers, in accordance with ISCT guidelines[164] (Figure 4-2). While these markers confirm MSC identity, stemness was further supported by their demonstrated trilineage differentiation capacity. These findings align with previous reports on TSPCs isolated from human[24,53] and animal[2,278,284] tendons, further validating the reliability of the explant technique.

However, hTSPCs are distinct from general MSCs due to their intrinsic commitment to the tenogenic lineage. While MSCs from various tissues have been shown to express tendon-associated markers such as *SCX*, *TNMD*, and *DCN* under specific conditions[162], hTSPCs reside within the tendon niche[23] and are inherently primed for tenogenic differentiation, responding to tendon-specific biochemical and mechanical cues[24,315]. This distinction highlights their specialised regenerative potential for tendon repair applications. It should be noted that MSCs from another tissue source were not included as a direct control in this study, which represents a limitation. The distinction between hTSPCs and general MSCs is therefore based on published evidence rather than side-by-side comparison, and future studies including such controls would provide stronger experimental support for these observations.

While the MSC immunophenotype was retained across multiple passages, a progressive decline in multipotency, particularly towards adipogenic and osteogenic lineages, was

observed with increasing passage number (Figure 4-3). This observation aligns with previous studies reporting reduced multipotency in aged tendon-derived cells, supporting the notion that prolonged *in vitro* culture may lead to cellular ageing and functional decline[2,29,316].

Morphological analysis of hTSPCs revealed a transition from an elongated, spindle-like shape in early passages to a more flattened and rounded morphology in later passages (Figure 4-1b). This observation corresponds with reports on TSPCs from different species[9,284,301], which describe similar changes in cell shape with prolonged culture. The significant reduction in aspect ratio with increasing passage suggests cytoskeletal remodelling and a potential shift towards a senescent-like phenotype, which may contribute to the observed decline in tenogenic marker expression[317]. However, alternative mechanisms, such as dedifferentiation rather than senescence, may also explain these changes. Gene expression analysis confirmed the downregulation of critical tenogenic markers, such as *SCX-A* and *TNMD*, in late passage cells, consistent with previous studies[9,316] that reported age-associated declines in tendon-related gene expression profiles (Figure 4-4). Despite these transcriptional changes, the CPD results confirmed that hTSPCs continued to proliferate over 120 days without reaching a growth plateau (Figure 4-1A). While a senescent phenotype is typically associated with reduced proliferation, the sustained growth observed here suggests that late-passage hTSPCs may undergo phenotypic drift or dedifferentiation rather than complete senescence instead. Similar trends have been reported in other studies of tendon-derived cells[21,301,318] where extended culture led to alterations in gene expression without complete growth arrest. Further analyses, such as senescence-associated β-galactosidase staining or p16/p21 expression profiling, would be required to definitively distinguish between cellular senescence and dedifferentiation in this context.

To counteract the effects of cellular ageing and enhance the tenogenic differentiation potential of hTSPCs, the effect of GDF-5 supplementation was investigated. Treatment with 100 ng/mL of GDF-5 resulted in a significant increase in collagen deposition, with the most pronounced effects observed at day 14, as confirmed by Picro-Sirius Red staining and quantitative analysis

(Figures 4-5). These findings align with previous studies on MSCs from various origins[194–196], demonstrating enhanced tendon-related gene expression upon GDF-5 treatment. Notably, the upregulation of key tenogenic markers such as *SCX-A*, *TNMD*, and *COL3A1* further supports the role of GDF-5 in promoting a tendon-specific phenotype. However, differences in response to GDF-5 treatment between early and late passage cells suggest that cell ageing influences the efficiency of tenogenic differentiation, underscoring the importance of optimising treatment protocols for clinical applications. Some discrepancies were noted compared to studies reporting peak *TNMD* and *COL3A1* expression at earlier time points, such as 6 to 8 days post-treatment in adipose-derived MSCs[197] and bone marrow MSCs[194]. This is in contrast with our results, which described 14 days as the most effective time point (Figure 4-6). This variation underscores the cell-type-specific responses to GDF-5 and highlights the need for further optimisation of treatment duration and concentration specific to hTSPCs. Additionally, GDF-5 treatment resulted in a phenotypic shift, with cells adopting a more elongated, tenocyte-like morphology, which is a key indicator of tendon-specific differentiation, as previously described in murine[319] and human[194,196] cells (Figure 4-7).

Beyond biochemical stimulation, the effects of mechanical stimuli on hTSPC-derived EV production were examined using dynamic culture systems. CEVs were successfully isolated and characterised under different culture conditions, with a distinction made between results obtained from the custom-made perfusion bioreactor and the lab rocker system, both of which simulated dynamic conditions. Consistent with findings from previous studies on MSCs and other stem cell types, dynamic culture conditions enhanced EV production and altered their characteristics compared to static conditions[274,312–314].

The perfusion bioreactor, operating at a constant flow rate of 1 mL/min, provided continuous nutrient exchange and mechanical stimulation, leading to a notable increase in EV production compared to static conditions. This flow rate was selected to enhance cell viability and EV production while minimising shear stress, as demonstrated in previous optimisation studies[205,276,277,320]. Specifically, the dynamic culture in the perfusion bioreactor resulted in a

4.3-fold higher total protein content in CM and a 1.3-fold increase in CP protein content, consistent with findings in other dynamic culture systems used for MSC-derived EV production, which have shown a higher protein content in dynamic culture products[274,321]. Consistent with previous studies[235,322], morphological analysis using SEM and TEM confirmed the presence of a heterogeneous EV population, with an average particle size of approximately 139 nm, slightly larger than that observed in static culture, suggesting that dynamic flow conditions may influence vesicle biogenesis and release (Figure 4-10). Additionally, Western blot analysis revealed the presence of EV-associated markers CD81 and TSG101, confirming the successful isolation of EVs from perfusion-based cultures. While these findings are consistent with the MISEV 2023 guidelines for EV characterisation[112], full compliance would require the inclusion of additional markers, as well as complementary purification methods (Figure 4-11B).

In contrast, the lab rocker system, which provided continuous bidirectional tilting, may have generated greater mechanical stimulation compared to the low flow-rate (1 mL/min) perfusion bioreactor. While both systems introduced dynamic conditions, the fluid motion induced by the rocker likely exposed cells to more frequent fluctuations in shear stress, potentially influencing EV release differently. Notably, dynamic conditions using the lab rocker yielded higher protein content in CM at 21% O_2 compared to static conditions; however, under 2% O_2, both static and dynamic cultures showed increased protein levels relative to atmospheric conditions, suggesting that physiological oxygen tension had a stronger influence on EV production than mechanical stimulation alone. The variability in results across different biological replicates highlights the complex interplay between oxygen levels and mechanical cues in regulating EV production.

The MACSPlex analysis provided key insights into the surface marker profiles of EVs derived from dynamic culture conditions. Immune-related markers, including CD2, CD25, and CD45, were detected at higher levels under dynamic conditions. These markers are typically associated with immune cells rather than MSCs/TSPCs, and their presence may therefore reflect residual immune cells in the cultures or technical limitations of the assay, rather than

intrinsic features of TSPC-derived EVs. As discussed in Chapter 3, the lack of tendon-specific EV markers and the overlap of many markers across cell types complicate interpretation. Dynamic culture may also have contributed to their higher detection, possibly by influencing the behaviour of rare contaminating cells. In light of these considerations, the detection of immune-related markers should be interpreted with caution. While they cannot be directly taken as evidence of an immunomodulatory EV profile, their presence highlights the importance of careful interpretation and the need for further validation in future work.

HLA-DR/DP/DQ upregulation further supports this immunomodulatory trend, as these molecules are involved in antigen presentation and immune regulation. However, in this context they are more cautiously interpreted as reflecting either marker overlap or potential minor contamination, rather than definitive evidence of immune-modulatory activity. Similar trends have been observed in MSC-derived EVs, where physical and mechanical stimulation enhances their immunosuppressive or immune-balancing effects through both protein cargo and surface marker modulation[323,324].

Platelet/endothelial markers, such as CD41b, were detected in EVs derived from both static and dynamic cultures in the perfusion bioreactor system. The presence of this marker suggests a potential role in coagulation-related functions, consistent with previous findings in platelet-derived EVs[325]. However, its expression remained unchanged between culture conditions, indicating that mechanical stimulation in the perfusion system did not significantly alter the expression of platelet-associated markers in hTSPC-derived EVs. CD56, a neural adhesion molecule, was highly upregulated in dynamic culture-derived EVs, indicating a potential enhancement in neurotrophic and regenerative properties, which aligns with studies demonstrating the role of neural cell adhesion molecules in tissue repair[326]. For EV-associated markers, CD63 and CD81 (detected only in dynamic culture) were significantly upregulated, reinforcing the notion that mechanical stimuli enhance EV biogenesis[327]. The exclusive detection of CD81 in dynamic conditions suggests a shift in EV subpopulation characteristics, while CD9 (3-fold higher in static conditions) may indicate a distinct vesicle profile. Among

stem/progenitor cell markers, the melanoma-associated chondroitin sulfate proteoglycan (MCSP), a marker associated with stem and progenitor cells, was exclusively detected in EVs derived from dynamic culture, whereas it was absent in EVs from static culture. This suggests that mechanical stimulation may enhance the release of EVs from stem-like hTSPCs or selectively promote the production of EVs enriched with stem/progenitor cell characteristics. In contrast, CD326, a marker associated with epithelial and tumour cells, was exclusively detected in static culture-derived EVs, indicating potential variations in cellular origin under different mechanical stimuli.

In comparison, EVs derived from the lab rocker system displayed a broader range of markers, with 33 surface proteins identified across oxygen conditions. Under 21% O_2, immune-related markers such as CD3, CD2, and CD11c were upregulated in static cultures, whereas HLA-DR/DP/DQ and CD40 were more prominent in dynamic conditions. This trend suggests that gentle mechanical stimulation through rocking may offer some immunomodulatory benefits, albeit to a lesser extent than those observed with the perfusion bioreactor. At 2% O_2, differences in CD86, CD45, and CD14, all of which were higher in dynamic culture, suggested a potential interaction between hypoxia and mechanical forces in modulating EV composition. In contrast, static cultures at 2% O_2 exhibited a higher expression of CD24 and CD69, indicating a more pro-inflammatory or activated EV profile under these conditions. These findings align with previous research suggesting that mechanical stimulation can enhance the immunomodulatory properties of MSC-EVs[328]. Furthermore, the observed variations under different oxygen tensions are consistent with studies demonstrating that hypoxic conditions can influence the composition and function of MSC-EVs[329]. Culturing MSCs under low-oxygen conditions has been reported to enhance the angiogenic properties of their EVs, suggesting that oxygen tension plays a crucial role in determining the function of EVs.

For platelet/endothelial markers, CD41b was higher in dynamic culture at 21% O_2, whereas CD42a and CD31 (detected only in static 2% O_2) were more enriched in static cultures, particularly under physiological oxygen. This finding suggests that while dynamic conditions

may enhance certain adhesion-related factors such as CD41b, static cultures might favour the retention of endothelial-associated markers, especially under hypoxia. Regarding EV markers, CD63, CD81 and CD9 were consistently upregulated in dynamic cultures, reinforcing findings from the perfusion bioreactor system and further confirming the impact of mechanical stimulation on EV properties. Additionally, CD49e, an adhesion-associated integrin, was more enriched in dynamic conditions, suggesting that mechanical stimulation may influence EV cargo related to cell adhesion and matrix interactions. Among stem/progenitor cell markers, CD105 and SSEA-4 were upregulated in dynamic cultures, while CD133/1 showed no significant variation between static and dynamic cultures in 21% O_2 but was higher in static culture at 2% O_2. Interestingly, CD146, a pericyte-associated marker, was upregulated in dynamic culture at 21% O_2 and detected only in dynamic culture under 2% O_2. These findings suggest that mechanical forces may enhance the secretion of EVs enriched in stem/progenitor cell-associated proteins, potentially improving their regenerative capabilities. Finally, among other functional markers, differential expression patterns of CD56 and CD142 suggest that both oxygen tension and mechanical stimulation may shape the functional phenotype of EVs. The higher levels of CD56 in static cultures at 21% O_2 and in dynamic cultures at 2% O_2 may reflect environment-specific regulation of EV cargo linked to cell-cell interaction or neurogenic signalling[330]. Similarly, the variable expression of CD142, a coagulation-associated marker, under different conditions, suggests that the haemostatic properties of EVs might also be influenced by culture parameters, with possible implications for their application in regenerative or inflammatory contexts[331]. These findings highlight the role of mechanical forces and oxygen tension in modulating the molecular composition of EVs derived from hTSPCs. While this aligns with existing evidence on MSC-derived EVs[332], limited studies are currently available on TSPC-derived EVs, warranting further investigation.

Cytokine profiling of hTSPC-derived EVs further demonstrated the impact of oxygen levels and mechanical stimulation on their cargo composition. Static culture conditions favoured an inflammatory cytokine profile, particularly under physiological oxygen levels, with IFN-γ and IL-

13 significantly elevated. These findings align with previous research, indicating that hypoxia can induce a pro-inflammatory response in stem cells.[333]. Additionally, IL-5 and IL-12p40 were also upregulated, suggesting a Th2-mediated immune response. In contrast, dynamic culture conditions promoted the secretion of cytokines associated with immune modulation and tissue repair. IL-6, IL-8, and MCP-1 were upregulated in dynamic culture-derived EVs, particularly under atmospheric oxygen. These cytokines play key roles in tendon healing by promoting cell recruitment and extracellular matrix remodelling[334]. IL-10, an anti-inflammatory cytokine, was enriched in static culture at 21% O_2, whereas under 2%, its expression was higher in dynamic culture-derived EVs. This finding appears to contrast with previous literature, where hypoxic preconditioning of MSCs has been shown to increase IL-10 secretion, thereby enhancing their immunomodulatory capacity[335]. The differential expression of IL-1RA and TNFα further highlights the role of mechanical stimuli in shaping EV function. IL-1RA was not detected in static culture-derived EVs at 21% O_2 but showed an increase in static culture under 2% O_2, possibly as a compensatory response to inflammatory conditions[336]. In contrast, TNFα levels were only slightly higher in dynamic culture-derived EVs, reinforcing previous findings that mechanical stimulation does not significantly alter TNFα levels[337].

These findings demonstrate that EVs derived from dynamic culture conditions, particularly at 21% O_2, exhibit a cytokine profile that favours immune modulation, tissue repair, and angiogenesis, as previously shown with MSCs-derived EVs[334]. Future studies should investigate the therapeutic implications of these cytokine-enriched EVs in preclinical models of tendon injury.

To our knowledge, this is the first study to comprehensively isolate and characterise EVs derived from human TSPCs under different culture conditions. While EVs from MSCs have been extensively investigated for tendon repair applications, the potential of hTSPC-derived EVs remains largely unexplored. Our findings provide a foundational characterisation of these vesicles, demonstrating how dynamic culture conditions influence their composition and

functional properties. These insights lay the groundwork for further studies evaluating their regenerative capacity in tendon healing models.

However, despite these promising findings, several limitations should be acknowledged. The variability observed across patient samples underscores the inherent heterogeneity of primary hTSPCs, necessitating larger sample sizes for more robust conclusions. Additionally, while *in vitro* characterisation provided valuable insights into EV production and tenogenic potential, future studies should focus on *in vivo* validation to assess the functional relevance of hTSPC-derived EVs in tendon repair. The long-term effects of GDF-5 treatment on maintaining the tenogenic phenotype also warrant further investigation.

In summary, this study highlights the role of culture conditions in shaping the production and potential functionality of hTSPC-derived EVs. The dynamic culture, particularly in a perfusion bioreactor, influenced the secretion profile and surface marker expression of EVs, suggesting an altered capacity for cellular communication and tissue interaction. The cytokine and surface marker profiles indicate that mechanical stimulation modulates EV cargo in ways that could impact immune responses and regenerative processes.

4.6 Conclusion

This chapter characterised human TSPCs and their EVs under static and dynamic culture conditions. hTSPCs retained an MSC-like immunophenotype across passages but showed progressive morphological changes and reduced expression of tendon-related genes at later passages, suggesting a decline in tenogenic potential over time. Supplementation with GDF-5 enhanced collagen deposition and tendon-specific gene expression, supporting its role as a biochemical stimulus for tenogenic differentiation.

In parallel, culture environment strongly influenced EV production and composition. Dynamic systems, particularly the perfusion bioreactor, increased EV yield and altered their marker and cytokine profiles, while oxygen tension further modulated these effects. The detection of immune-related markers was interpreted cautiously, as they may reflect assay limitations or

rare contaminating cells rather than intrinsic features of TSPC-derived EVs. Overall, these findings demonstrate that both biochemical and mechanical cues shape the functional properties of hTSPCs and their EVs, providing a basis for optimising culture strategies and guiding future validation in tendon repair models.

Chapter 5

Evaluating the tenogenic potential of porcine TSPC-derived CM and cEVs

5. EVALUATING THE TENOGENIC POTENTIAL OF PORCINE TSPC-DERIVED CM AND CEVS

5.1 Introduction

In recent years, MSC-derived CM and EVs have emerged as promising regenerative strategies for tendon repair. These cell-free therapies offer an alternative to traditional stem cell transplantation by harnessing the paracrine effects of bioactive factors secreted by MSCs. MSC-derived CM and EVs have demonstrated the ability to modulate inflammation, remodel the ECM, and enhance tenocyte proliferation[131,182,184,223,229,230]. However, MSC-based therapies still face challenges, including phenotypic instability and cell source variability, which may hinder their clinical application[167].

Given these limitations, as detailed in previous chapters, TSPCs represent an attractive alternative due to their intrinsic tenogenic properties and crucial role in tendon homeostasis[338]. Their secretome and EVs have been shown to enhance tenocyte proliferation, balance matrix synthesis and degradation, and modulate inflammatory responses[235,289,292,339,340]. However, despite their potential, TSPC-derived CM and EVs remain relatively unexplored compared to MSCs. Another critical factor influencing stem cell behaviour and secretome composition is oxygen tension. Physiological oxygen levels have been shown to enhance stem cell differentiation and ECM maturation in various tissues[215,255,258], including tendons, yet their role in regulating the tenogenic effects of TSPC-derived CM and EVs remains poorly characterised. Understanding how oxygen tension modulates the bioactivity of CM and EVs could provide key insights for optimising their therapeutic potential in tendon regeneration.

This chapter investigates the tenogenic potential of CM and cEVs derived from porcine tendon TSPCs II and their effects on both TSPCs and human bone marrow-derived MSCs under different oxygen conditions (21% vs 2%). While previous studies have focused on MSC-derived secretomes in tendon repair, this study is the first to specifically compare porcine

TSPC-derived CM and cEVs in the context of tenogenic differentiation, providing new insights into their role in tendon regeneration. Additionally, by evaluating the impact of hypoxia on tenogenic differentiation, this work aims to determine optimal culture conditions that enhance the regenerative potential of CM and cEVs, thereby contributing to the development of cell-free regenerative therapies for tendon injuries.

Two cell populations were selected for this study to provide complementary insights. TSCPs II represent tendon-resident progenitors and therefore reflect tissue-specific responses relevant to tendon biology. Human BM-MSCs were included as a clinically relevant and widely used multipotent cell source in regenerative medicine. Comparing these populations allowed us to assess both intrinsic tendon-specific effects and broader translational potential of TSPC-derived CM and EVs.

5.2 Aim

The primary aim of this chapter was to evaluate the tenogenic potential of CM and cEVs derived from porcine TSPCs II under different oxygen concentrations (21% and 2%). The study investigated their effects on cell proliferation, morphology, and tenogenic differentiation, focusing on key markers such as *TNMD*, *SCX*, *MKX*, and *COL1A2*, *COL3A1*.

Specifically, this study aimed to:

1. Optimise CM dilution and source by determining the most effective CM dilution ratio and comparing CM derived from TSPCs II and tenocytes regarding their ability to support cell viability and morphology under physiological and atmospheric oxygen conditions.
2. Assess CM cytotoxicity by evaluating the biocompatibility of TSPCs II-derived CM using murine fibroblasts, ensuring its suitability for cell-based applications.

3. Investigate the long-term effects of CM on TSPCs II by analysing its impact on proliferation, ECM organisation, and tenogenic differentiation over 14 days, using RT-qPCR and immunofluorescence to assess tenogenic marker expression.

4. Examine the tenogenic potential of CM and cEVs on hBM-MSCs by assessing their effects on proliferation, ECM deposition, and tenogenic marker expression, with and without GDF-5 supplementation (10 ng/mL and 100 ng/mL), to determine whether GDF-5 enhances tenogenic differentiation and influences tenogenic differentiation differently in CM- and cEV-treated cells.

5. Compare oxygen conditions by investigating the influence of oxygen tension (2% vs 21%) on the effects of CM and cEVs, focusing on cell proliferation, collagen synthesis, ECM organisation, and tenogenic gene expression.

By addressing these objectives, this study aimed to evaluate the mechanisms through which CM and cEVs modulate tenogenic differentiation, ECM formation, and oxygen-dependent responses. These findings could provide a foundation for their potential application in tendon tissue engineering and regenerative medicine, advancing the field.

5.3 Methods

The study design is summarised in Scheme 3, with detailed materials and methods provided in Chapter 2.

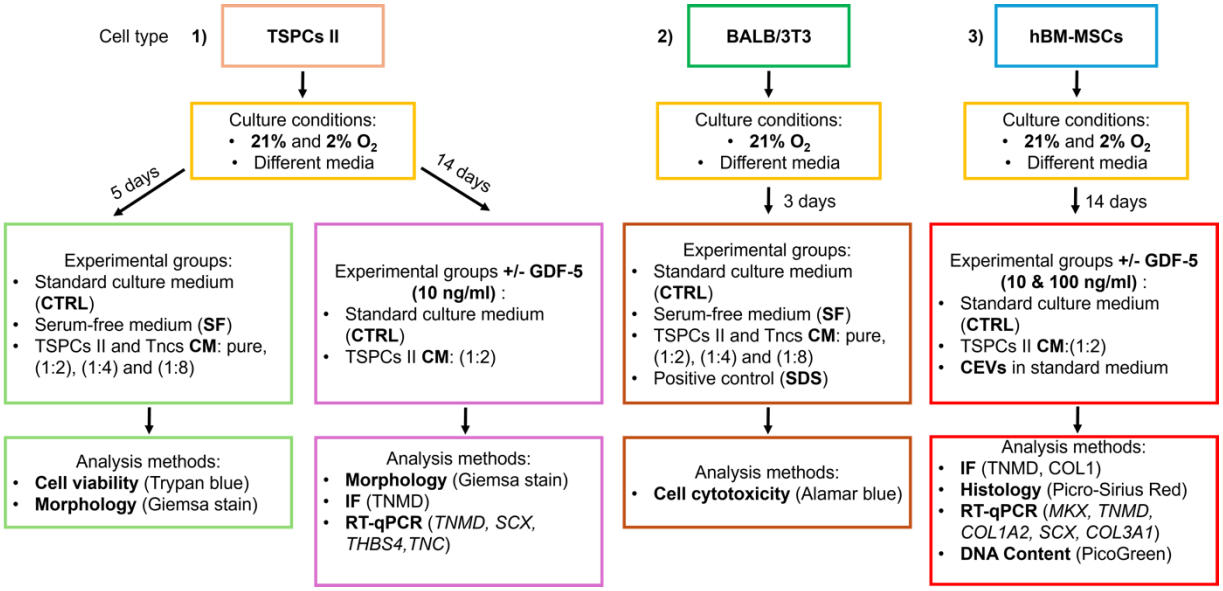
To evaluate the effect of CM on TSPCs II, cells were seeded at 5,000 cells/cm² and cultured under six media conditions. Standard culture medium (high-glucose DMEM supplemented with 10% FBS, 1% L-glut, and 1% NEAA) and SF medium (high-glucose DMEM with 1% L-glutamine and 1% NEAA) served as controls. CM was tested at pure (10 µg/mL protein concentration) and diluted concentrations (1:2, 1:4, 1:8) with standard medium. Experiments were conducted under 21% and 2% oxygen using CM collected from Tncs and TSPCs II cultured under static conditions.

Cell viability was assessed by trypan blue exclusion (Section 2.2.2), and cell morphology by Giemsa staining (Section 2.15).

The cytotoxicity of porcine TSPCs II CM was further evaluated using the Alamar Blue assay (Section 2.20). Assays were performed at Fidia Farmaceutici S.p.A. (Abano Terme, Italy) with technical assistance from Dr Alba Di Lucia and Dr Anna Marchetti. BALB/3T3 clone A31 murine fibroblasts were cultured in different CM dilutions (pure, 1:2, 1:4, 1:8) or control media (standard medium, SF medium at equivalent dilutions, and 0.5 mM SDS as positive control) and analysed at 24, 48, and 72 h under 21% O_2.

The tenogenic effect of CM on TSPCs II was evaluated over 14 days at three time points (day 0, 7, 14). Four conditions were tested: standard medium and 1:2 TSPCs II-derived CM, each with or without 10 ng/mL GDF-5, under 2% and 21% oxygen. Cells were seeded on day –1 in standard medium, then switched to experimental media at day 0. Morphology (Section 2.15), TNMD expression (Section 2.14), and gene expression (Section 2.12) were analysed.

To further assess tenogenic potential, hBM-MSCs (P3) were cultured for 14 days under 2% and 21% oxygen in standard medium, 1:2 porcine TSPCs II CM (5 µg/mL protein), or CM-derived cEVs (1 µg/mL EVs). Each condition was tested with or without GDF-5 (10 or 100 ng/mL). After 14 days, samples were analysed for TNMD and COL1 expression (Section 2.14), collagen deposition (Section 2.16), gene expression (Section 2.12), and DNA content (Section 2.13).



Scheme 3. Summary of the methodology adopted in Chapter 5.

5.3.1 Statistical analysis

All experiments in this chapter were performed using a single preparation of porcine TSPCs II–derived CM. Data are presented as mean ± SD from technical triplicates (n = 3); statistical tests therefore describe within-assay variation only, and p-values are descriptive rather than evidence of biological replication.

Analyses were carried out in GraphPad Prism (v10.2.2). Depending on the design, data were analysed by two-way ANOVA followed by either Dunnett's test (comparisons against control or day 0) or Tukey's test (comparisons across all treatments within oxygen levels, including intra-group contrasts for CM vs CM+GDF-5 and cEVs vs cEVs+GDF-5). Significance thresholds were set as '*' for $p < 0.05$, '**' for $p < 0.01$, '***' for $p < 0.001$, and '****' for $p < 0.0001$.

5.4 Results

5.4.1 Short-term evaluation of CM effect on TSPCs II (5 days)

TSPCs II were cultured for 5 days in six different media types, using CM derived from both TSPCs II and Tncs that had been previously cultured in static conditions. The objective was to

assess cell viability and morphology using Giemsa staining. The experiment was conducted under both physiological and atmospheric oxygen conditions, using standard culture medium as a positive control and SF as a negative control.

In addition to these controls, cells were cultured in pure CM, where the medium consisted entirely of CM with a final protein concentration of 10 μg/mL. To assess the effect of different CM dilutions, cells were also cultured in 1:2 CM, 1:4 CM, and 1:8 CM, where the conditioned medium was diluted at respective ratios in standard culture medium.

5.4.1.1 Cell viability

Live and dead cells were quantified using the trypan blue exclusion assay. Cell viability in TSPCs cultured in their CM remained above 85% in all media types, irrespective of oxygen concentration (Figure 5-1A). The lowest viability was observed in the negative control (SF medium), though values were still relatively high, at 88% in 21% oxygen and 87% in 2% oxygen. The second lowest viability was recorded in pure CM, with 89% in 21% oxygen and 94% in 2% oxygen. Cell viability exceeded 90% in all cases among the diluted CM samples. Except for the SF condition, cell viability appeared generally higher under physiological oxygen conditions across all media types.

Cell viability remained high for TSPCs cultured in Tncs-derived CM but was slightly lower than TSPCs-derived CM, with all values exceeding 80% (Figure 5-1B). As observed in TSPCs CM, the lowest viability was recorded in the SF medium, but only under 2% oxygen conditions, where it was significantly lower (84% in 2% O_2 vs. 94% in 21% O_2). The pure CM condition showed the second lowest viability, but only under 21% oxygen conditions (85%). Among the diluted CM samples, all viability values were above 90%, indicating they were still compatible with cell survival.

Unlike the trend observed with TSPCs CM, where higher viability was generally measured in 2% oxygen, no clear trend was observed in Tncs CM. In this case, higher viability was observed only in the CTRL and pure CM groups under 2% oxygen conditions, whereas in all other conditions, higher viability was recorded under 21% oxygen conditions.

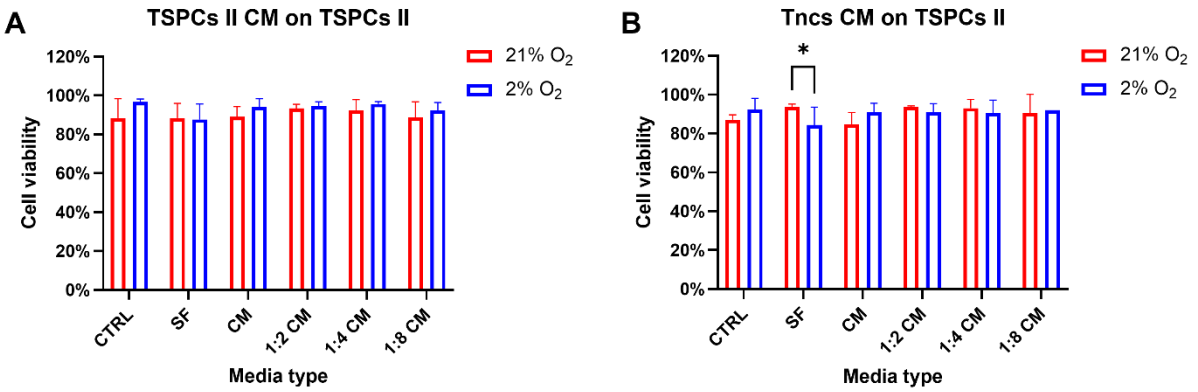


Figure 5-1. Cell viability of TSPCs II cultured in different conditioned media for 5 days. The graph illustrates the percentage of viable cells after 5 days of culture in various media conditions, as determined by the trypan blue exclusion assay. (A) TSPCs II cultured in TSPCs II-derived CM under 2% and 21% oxygen conditions. (B) TSPCs II cultured in Tncs-derived CM under 2% and 21% oxygen conditions. Statistical analysis: two-way ANOVA followed by Tukey's multiple comparisons test within each oxygen level; '*' for $p < 0.05$, n=3.

5.4.1.2 Giemsa staining

Giemsa staining was performed after 5 days of culture to assess potential differences in cell morphology. Figure 5-2 shows that TSPCs II cultured in a SF medium exhibited a more elongated morphology and lower cell density, indicating a stressed phenotype, which aligns with the cell viability measurements.

In contrast, TSPCs II cultured in their CM maintained a well-spread, spindle-shaped morphology across all tested dilutions, comparable to that of the positive control (standard culture medium). This suggests that TSPCs II CM preserves cell morphology and supports viability, reinforcing its role in maintaining a stable phenotype.

Oxygen concentration also influenced cell morphology and confluence levels. At 2% oxygen, cells exhibited a denser, more compact arrangement, whereas conditions with 21% oxygen resulted in a slightly more elongated morphology, which may be attributed to increased metabolic activity or cellular adaptation to atmospheric oxygen levels. These findings further support the hypothesis that physiological oxygen levels may help maintain a more stable cellular environment by promoting a denser culture with reduced stress.

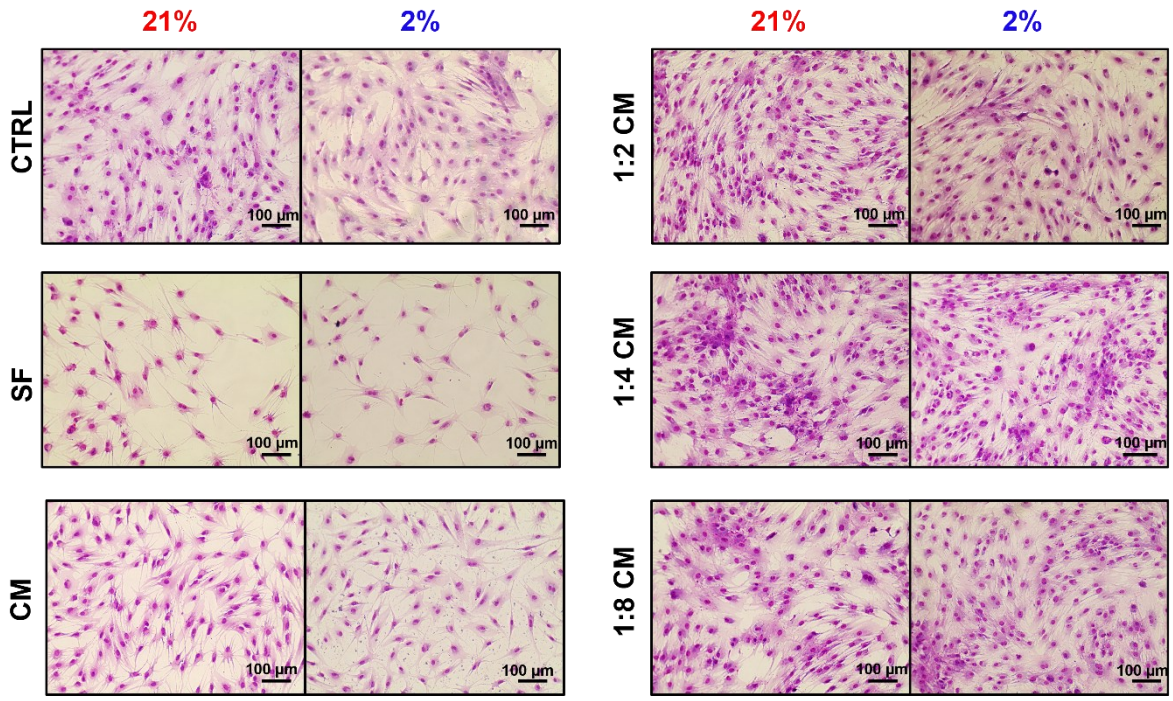


Figure 5-2. Giemsa staining of TSPCs II cultured in TSPCs II-derived CM under different oxygen conditions. Representative images of TSPCs II cultured for 5 days in standard culture medium (CTRL), SF medium, pure CM, 1:2 CM, 1:4 CM, and 1:8 CM, under 21% and 2% oxygen conditions. Cells in SF medium exhibit a more elongated and stressed morphology, whereas those in TSPCs II CM maintain a spindle-shaped morphology comparable to the CTRL condition. Cells in 2% oxygen appear denser and more compact, while those in 21% oxygen show a more elongated morphology and slightly lower confluence levels. Scale bar: 100 µm.

Similarly, TSPCs II cultured in Tncs-derived CM exhibited a viable morphology, although with notable differences from TSPCs II CM (Figure 5-3). Cells appeared more elongated and showed a slightly reduced density, particularly under 21% oxygen conditions, where the lower cell confluence was more evident. This suggests that Tncs CM may provide less support for proliferation than TSPCs II CM, potentially due to differences in the composition of secreted factors, such as growth factors, EVs, or matrix components, which may play a role in modulating cell behaviour.

Moreover, while TSPCs II CM promoted a morphology that closely resembled the standard culture condition, cells in Tncs CM displayed a more elongated, loosely packed arrangement, possibly indicating a weaker influence on maintaining TSPCs II characteristics. The impact of oxygen concentration was also less pronounced than that of TSPCs II CM, as no clear trend

was observed in cell density across the 2% and 21% oxygen conditions. Nonetheless, despite these differences, TSPCs II maintained an elongated, fibroblast-like morphology across all conditions, reinforcing the idea that both types of CM are compatible with cell survival. However, they may have distinct biological effects on proliferation and morphology.

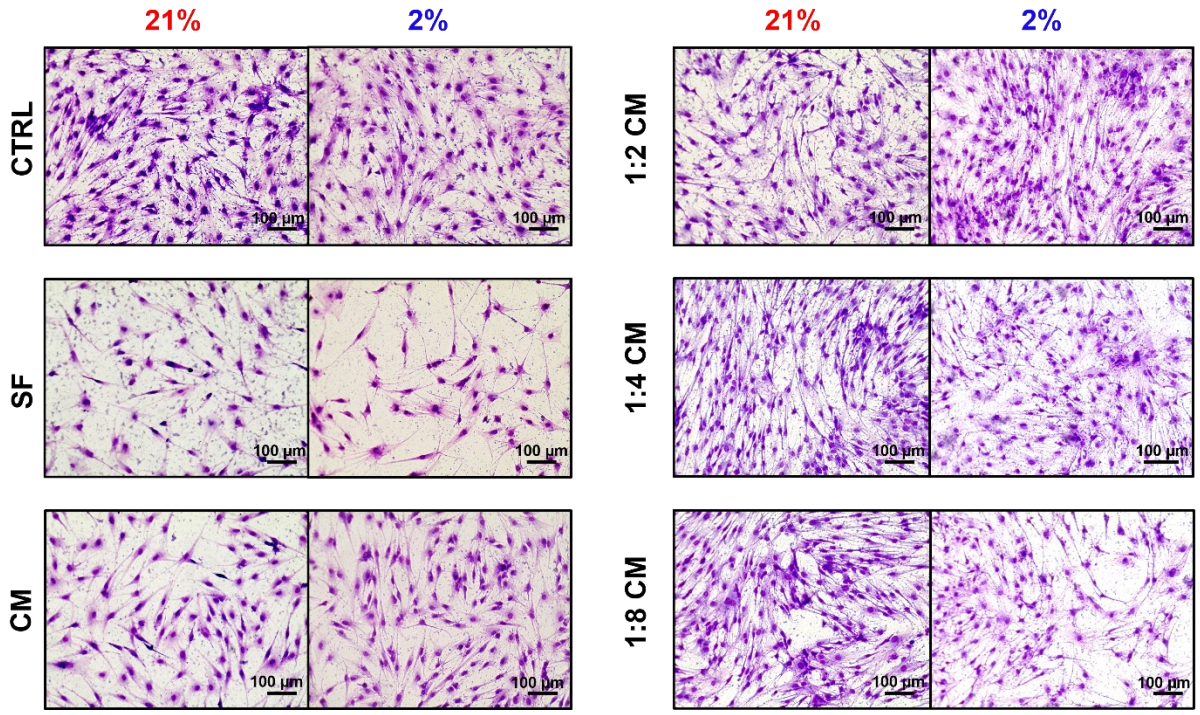


Figure 5-3. Giemsa staining of TSPCs II cultured in Tncs-derived CM under different oxygen conditions. Representative images of TSPCs II cultured for 5 days in standard culture medium (CTRL), SF medium, pure CM, 1:2 CM, 1:4 CM, and 1:8 CM, under 21% and 2% oxygen conditions. Cells in the SF medium appear stressed and elongated. At the same time, those in Tncs-derived CM maintain a fibroblast-like morphology, though slightly more elongated and with lower density than TSPCs II CM. Scale bar: 100 µm.

5.4.2 Cytotoxicity assessment of CM

Based on the results obtained from the cell viability assay and Giemsa staining, TSPCs II CM at a 1:2 dilution was considered suitable for further experiments evaluating its tenogenic potential, as it was non-toxic and maintained a morphology comparable to standard culture conditions. This dilution was therefore chosen as the working concentration, providing a favourable environment for cell survival while ensuring sufficient CM volume for subsequent experiments.

An Alamar Blue assay was performed to further confirm the suitability of this method in assessing the cytotoxicity of TSPCs II CM under the same conditions previously tested. The CM used in this experiment was previously obtained from a static culture of TSPCs II under 21% and 2% oxygen conditions. However, due to equipment constraints at Fidia Farmaceutici S.p.A., which did not allow for cell culture under hypoxic conditions (2% oxygen), the cytotoxicity assay was performed on cells maintained at 21% oxygen.

The experiment was conducted using BALB/3T3 clone A31 murine fibroblast cell lines, with CM tested at different dilutions: pure (non-diluted), 1:2, 1:4, and 1:8, each diluted with standard culture medium. Control samples were prepared by substituting CM with SF culture medium at the same dilution ratios. Standard culture medium (CTRL) also served as a negative control, while 0.5 mM SDS was used as a positive control for cytotoxicity. Cells were cultured under these conditions for three days, and Alamar Blue assays were performed at 24, 48, and 72 hours.

In samples cultured with CM obtained from 21% oxygen condition, statistical differences were observed only between the control samples and pure CM, as well as SF medium. Pure CM showed only 24% cell viability after 24 hours, while SF reached 29% viability at 24 hours; both further declined after 72 hours, likely due to the absence of serum, causing high cellular stress. Similarly, the positive control (SDS) exhibited a substantial decrease in viability over time. In contrast, all diluted CM samples (1:2, 1:4, and 1:8) and their respective controls maintained viability above 90%, even after 72 hours of culture (Figure 5-4A). The 1:2 CM ratio was confirmed as a strong candidate, showing 90% viability at 24 hours, which increased to 94% at 48 and 72 hours.

In samples cultured with CM obtained from 2% oxygen condition, cell viability was generally slightly lower across all conditions compared to 21% oxygen, yet remained above 70% in all cases (Figure 5-4B). Like the 21% oxygen group, statistical differences were observed between control samples and pure CM, where viability dropped to 38% at 24 hours, further decreasing to 15% at 72 hours. SF exhibited a similar trend, with 30% viability at 24 hours,

decreasing to 17% at 72 hours, alongside the positive control, which showed a comparable pattern. Notably, at 72 hours, statistical differences emerged between the control and the 1:2 CM and 1:2 CTRL conditions, with viability reaching 57% and 69%, respectively.

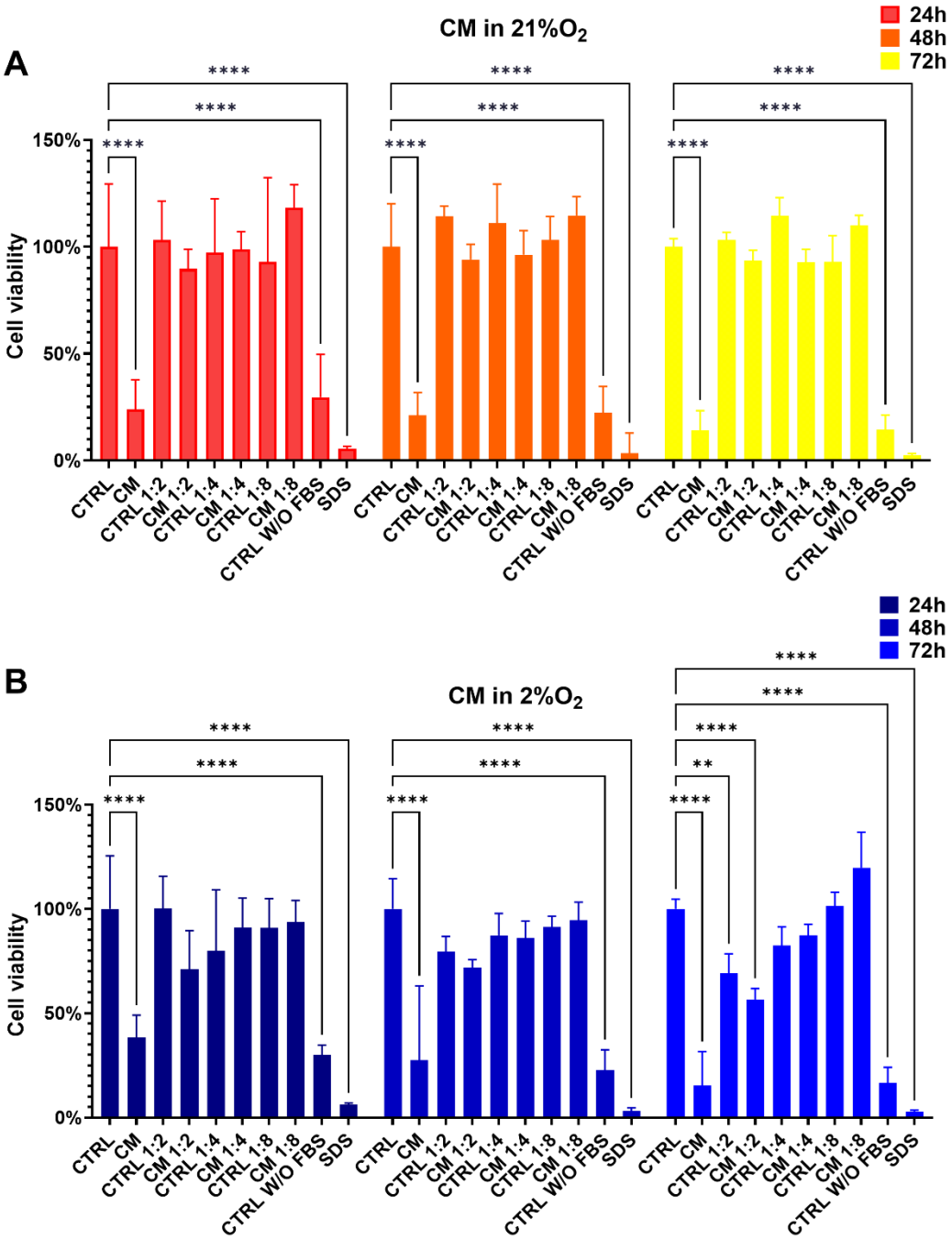


Figure 5-4. Cytotoxicity assessment of TSPCs II-CM using Alamar blue assay. Cell viability of BALB/3T3 murine fibroblasts cultured in TSPCs II CM at different dilutions (pure, 1:2, 1:4, and 1:8) and controls (CTRL, SF) under 21% (A) and 2% (B) oxygen conditions. SDS (0.5 mM) served as a positive control. Pure CM and SF exhibited a significant decline in viability over time, whereas diluted CM samples maintained high viability, typically above 90% at 21% oxygen and 70% at 2% oxygen. Statistical

analysis: two-way ANOVA followed by Dunnett's multiple comparisons test; '**' for $p < 0.01$, '***' for $p < 0.001$, and '****' for $p < 0.0001$, n=3.

5.4.3 Long-term evaluation of CM effect on TSPCs II (14 days)

TSPCs II were cultured for 14 days under 2% and 21% oxygen conditions in either standard culture medium (CTRL) or TSPCs II-CM (1:2 ratio, diluted in standard medium) obtained from static culture, with and without 10 ng/mL GDF-5. At each time point (days 0, 7, and 14), cells were analysed for morphology using Giemsa staining, TNMD expression by IF, and gene expression using RT-qPCR.

5.4.3.1 Giemsa staining

Giemsa staining was performed to assess morphological differences between cells cultured in different media types under both oxygen conditions. As shown in Figure 5-5, TSPCs II maintained an elongated, fibroblast-like shape across all media conditions, with no drastic morphological alterations observed between treatments.

After 24 hours, cells in 2% oxygen exhibited faster proliferation, reaching confluence earlier than 14 days. By day 7, all conditions displayed high confluency, with a notably denser cell arrangement under 2% oxygen than 21% oxygen, suggesting that lower oxygen tension may promote a more compact cell organisation. By day 14, some cultures appeared less confluent than on day 7, likely due to overgrowth and subsequent detachment from the plates, a phenomenon more evident in 2% oxygen conditions.

Additionally, cells cultured in TSPCs II CM with GDF-5 supplementation appeared to maintain a more uniform morphology over time, whereas those in standard culture medium exhibited slightly more variation in density. Despite minor differences in confluency and arrangement, no significant morphological abnormalities were observed, indicating that TSPCs II CM provides a supportive environment for long-term culture and preserves the characteristic morphology of tendon stem cells. These findings suggest that TSPCs II CM may contribute to maintaining cell viability and a stable phenotype throughout extended culture periods.

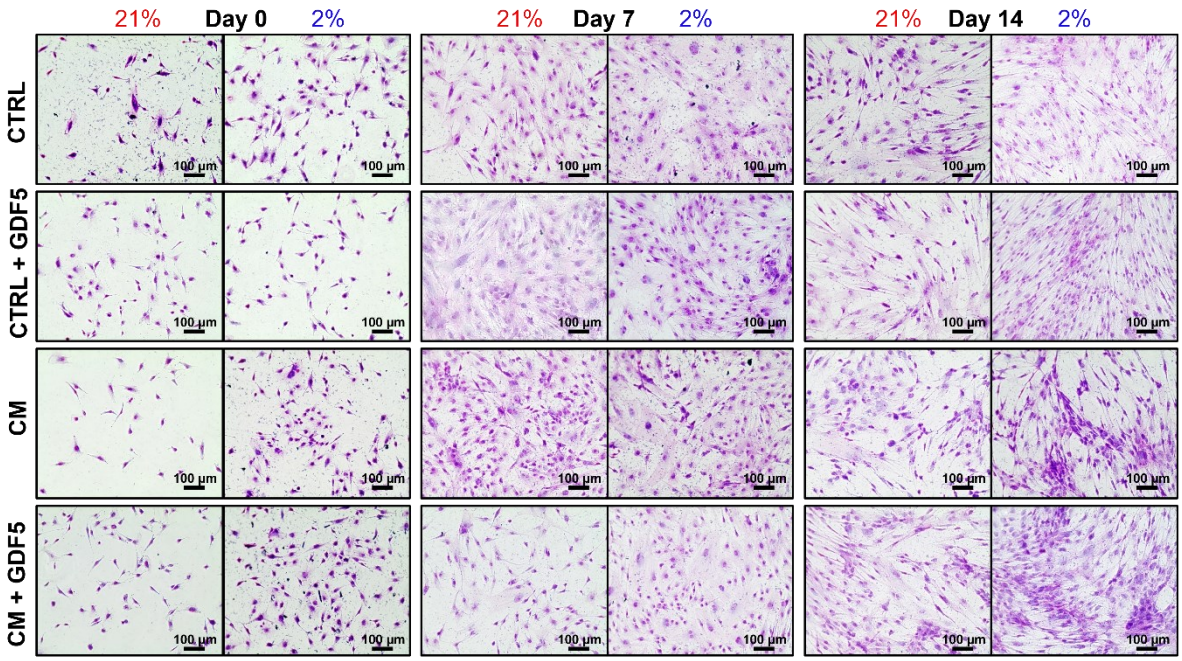


Figure 5-5. Giemsa staining of TSPCs II cultured for 14 days in different media conditions. Representative images of TSPCs II cultured under 21% and 2% oxygen conditions in standard culture medium (CTRL) and TSPCs II-conditioned medium (1:2 ratio), with and without 10 ng/mL GDF-5. Images were taken on days 0, 7, and 14. Cells in 2% oxygen exhibited higher proliferation, reaching confluence earlier than 14 days, while some detachment was observed at day 14 due to overgrowth. Morphological similarities were observed across conditions, with TSPCs II maintaining an elongated, fibroblast-like shape. Scale bar: 100 µm.

5.4.3.2 Immunofluorescence analysis

To confirm and quantify TNMD expression, immunofluorescence staining was performed, and the MFI was measured across different time points (Figure 5-6). The results provided insights into the temporal changes in TNMD expression under various media conditions and oxygen concentrations.

In atmospheric oxygen at day 0 (24 hours after seeding and media replacement), no significant differences in TNMD expression were observed between the control sample and the control media or conditioned media supplemented with 10 ng/mL GDF-5. However, TNMD expression was significantly lower in the CM alone, showing a 2.2-fold decrease compared to the control sample ($p < 0.0001$). By day 7, the control media with GDF-5 supplementation exhibited a 1.5-fold increase in TNMD expression relative to the control sample ($p = 0.0199$), while the CM samples demonstrated a substantial 1.9-fold increase ($p < 0.0001$). At day 14, a significant

reduction in MFI was noted for the control sample with GDF-5, with a 2.7-fold decrease ($p = 0.0021$). In contrast, TNMD expression significantly increased in the CM and CM supplemented with GDF-5, showing 2-fold and 1.5-fold increases, respectively ($p < 0.0001$ and $p = 0.0382$).

Examining the temporal trends, the control sample displayed the highest MFI at day 0, followed by a decrease at day 7, which plateaued at day 14. Similarly, the control media supplemented with GDF-5 peaked at day 0 but declined over time. On the other hand, the MFI of samples cultured in CM alone increased steadily across all time points. At the same time, the MFI of CM with GDF-5 supplementation decreased slightly on day 7 before rising again on day 14.

In physiological oxygen, the trends varied. At day 0, the control media with GDF-5 supplementation showed a significant 1.7-fold increase in TNMD expression compared to the control sample ($p < 0.0001$). However, both CM and CM supplemented with GDF-5 demonstrated substantial decreases in TNMD expression, with 2.6-fold and 2.2-fold reductions, respectively ($p < 0.0001$). By day 7, all media types exhibited significant increases in MFI relative to the control sample: the control media with GDF-5 showed a 2.3-fold increase ($p < 0.0001$), the CM had a 1.6-fold increase ($p = 0.0478$), and the CM with GDF-5 supplementation showed a 2.3-fold increase ($p < 0.0001$). At day 14, a reversal was noted, with significant decreases in TNMD expression across all samples compared to the control: the control media with GDF-5 decreased by 2.5-fold ($p < 0.0001$), CM decreased by 1.4-fold ($p = 0.0006$), and CM with GDF-5 showed a 1.7-fold decrease ($p < 0.0001$).

When analysing the trends over time, the control sample displayed a decrease in TNMD expression at day 7, followed by a peak at day 14. The control media with GDF-5 showed a continuous decline in MFI over the entire period. Conversely, TNMD expression in CM alone consistently increased at each time point, while CM supplemented with GDF-5 saw an increase at day 7, stabilising through day 14.

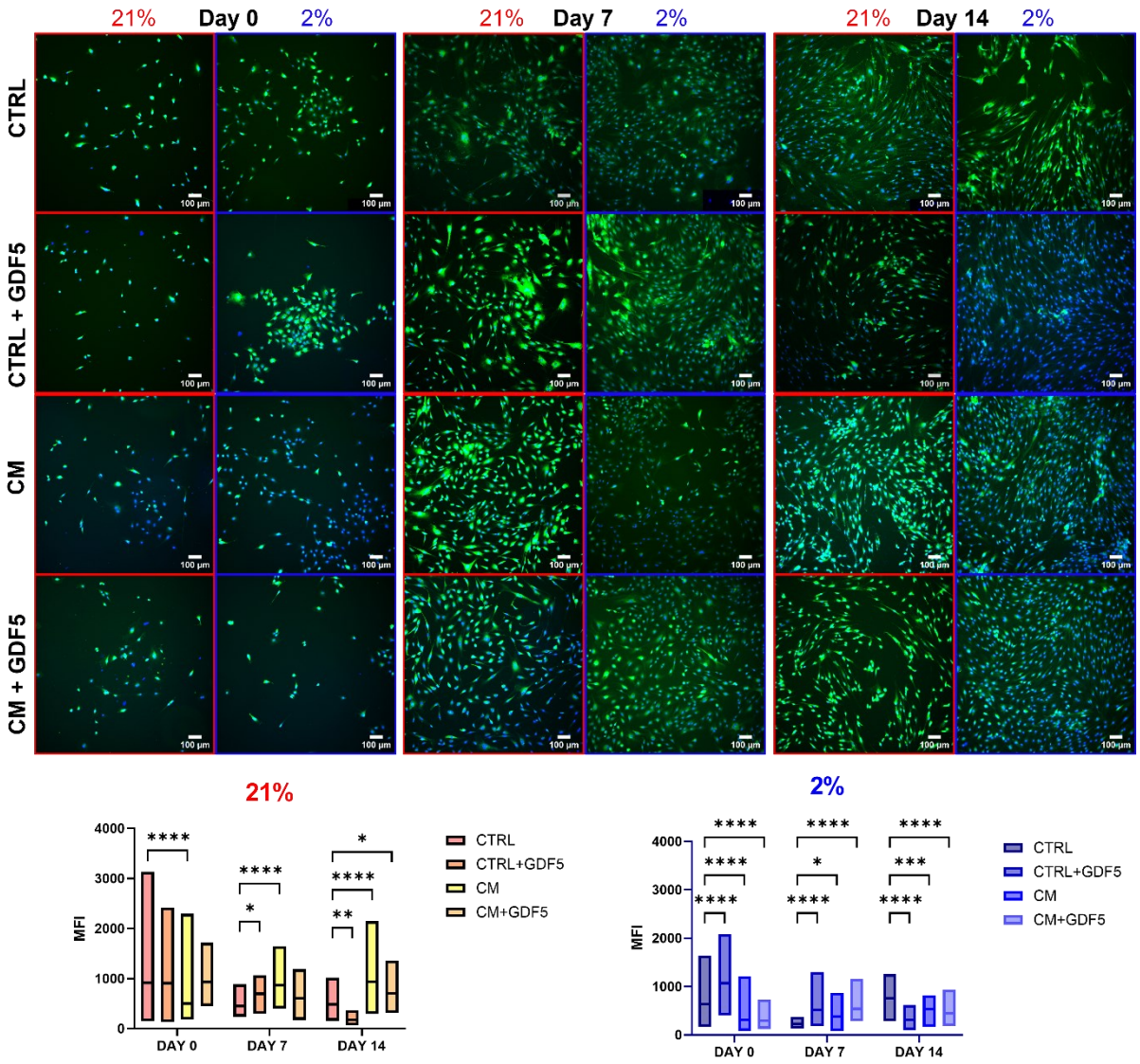


Figure 5-6. Immunofluorescence analysis of TNMD expression in TSPCs II cultured for 14 days under different media conditions. Representative images of TNMD staining (green) in TSPCs II cultured in standard culture medium (CTRL), CM (1:2 dilution), and CM supplemented with 10 ng/mL GDF-5 under 21% and 2% oxygen conditions at 3 time points (day 0, 7, and 14). Nuclei are counterstained with DAPI (blue). The lower panel shows the quantification of MFI of TNMD expression across the experimental conditions in 21% and 2% oxygen conditions. Scale bar: 100 µm. Statistical analysis: two-way ANOVA followed by Dunnett's multiple comparisons test; '*' for $p < 0.05$, '**' for $p < 0.01$, '***' for $p < 0.001$, and '****' for $p < 0.0001$, n=3.

5.4.3.3 Gene expression

RT-qPCR was performed to assess the expression levels of key tenogenic markers: *TNMD*, *SCX*, *THBS4*, and *TNC*. Gene expression was normalised to the housekeeping gene *YWHAZ*,

and results were expressed as fold-changes relative to the control sample at day 0, allowing for a comparative evaluation of the impact of different culture conditions over time.

SCX expression in 21% O_2 followed a common trend across all samples, with a downregulation at day 7 and a general upregulation at day 14, resulting in no significant differences between the control and the other conditions. In 2% O_2, a similar trend was observed at day 0, with no significant differences. However, by day 7, the control and GDF-5-supplemented control samples showed reduced expression, with CTRL+GDF-5 being 1.9-fold lower than the control ($p = 0.0223$). In contrast, CM and CM+GDF-5 samples were significantly upregulated, with a 3.8-fold ($p = 0.0031$) and 2-fold ($p = 0.0417$) increase, respectively, compared to the control. By day 14, all samples exhibited *SCX* upregulation, with a 2.1-fold increase in CTRL+GDF-5 ($p = 0.0034$), a 2.8-fold increase in CM ($p = 0.0001$), and a 2.2-fold increase in CM+GDF-5 ($p = 0.0017$) (Figure 5-7A).

Regarding *TNC* expression, in 21% O_2, all samples were downregulated across all time points, except at day 14, where CM+GDF-5 exhibited a 7.7-fold increase relative to the control ($p = 0.0041$), despite remaining downregulated overall. A similar trend was observed in 2% O_2, where all conditions exhibited downregulation. However, at day 0, CM+GDF-5 was significantly lower than the control (2.4-fold, $p = 0.0175$), and by day 7, CTRL+GDF-5 showed a 5-fold lower expression than the control ($p = 0.0107$). By day 14, CM+GDF-5 displayed a 4.1-fold increase in expression relative to the control ($p = 0.0480$) despite overall downregulation (Figure 5-7B).

TNMD expression in 21% O_2 showed no significant differences at day 0, except for CTRL+GDF-5, which was 1.5-fold lower than the control ($p = 0.0313$). On day 7, all samples were upregulated, with CM+GDF-5 exhibiting the highest *TNMD* expression, which was 1.4-fold higher than the control ($p = 0.0309$). This upregulation was sustained at day 14 across all conditions. A similar pattern was observed in 2% O_2, with no significant differences at day 0 and a general upregulation at day 7, particularly in CM and CM+GDF-5, which exhibited *TNMD* expression levels comparable to or slightly higher than the control. In contrast, CTRL+GDF-5

showed a 1.7-fold decrease compared to the control ($p = 0.0255$). By day 14, all samples remained upregulated, with *TNMD* expression levels becoming comparable across conditions (Figure 5-7C).

THBS4 expression in 21% O_2 followed a dynamic trend. At day 0, CTRL+GDF-5 exhibited a 1.9-fold lower expression than the control ($p = 0.0426$). At day 7, all samples were upregulated, particularly CM and CM+GDF-5, which showed a 2.1-fold ($p = 0.0237$) and 2.9-fold ($p = 0.0018$) increase, respectively. By day 14, CTRL and CM+GDF-5 remained upregulated, whereas CTRL+GDF-5 and CM were significantly downregulated, showing 2.6-fold ($p = 0.0080$) and 3.2-fold ($p = 0.0029$) lower expression than the control. In 2% O_2, all samples were downregulated at day 0, particularly CTRL+GDF-5, which exhibited a 2.5-fold reduction compared to the control ($p = 0.0400$). By day 7, CM and CM+GDF-5 showed expression levels comparable to the control, while CTRL+GDF-5 remained significantly downregulated, showing a 3.3-fold decrease compared to the control ($p = 0.0090$). At day 14, all samples exhibited an upregulation, and *THBS4* expression became comparable across conditions (Figure 5-7D).

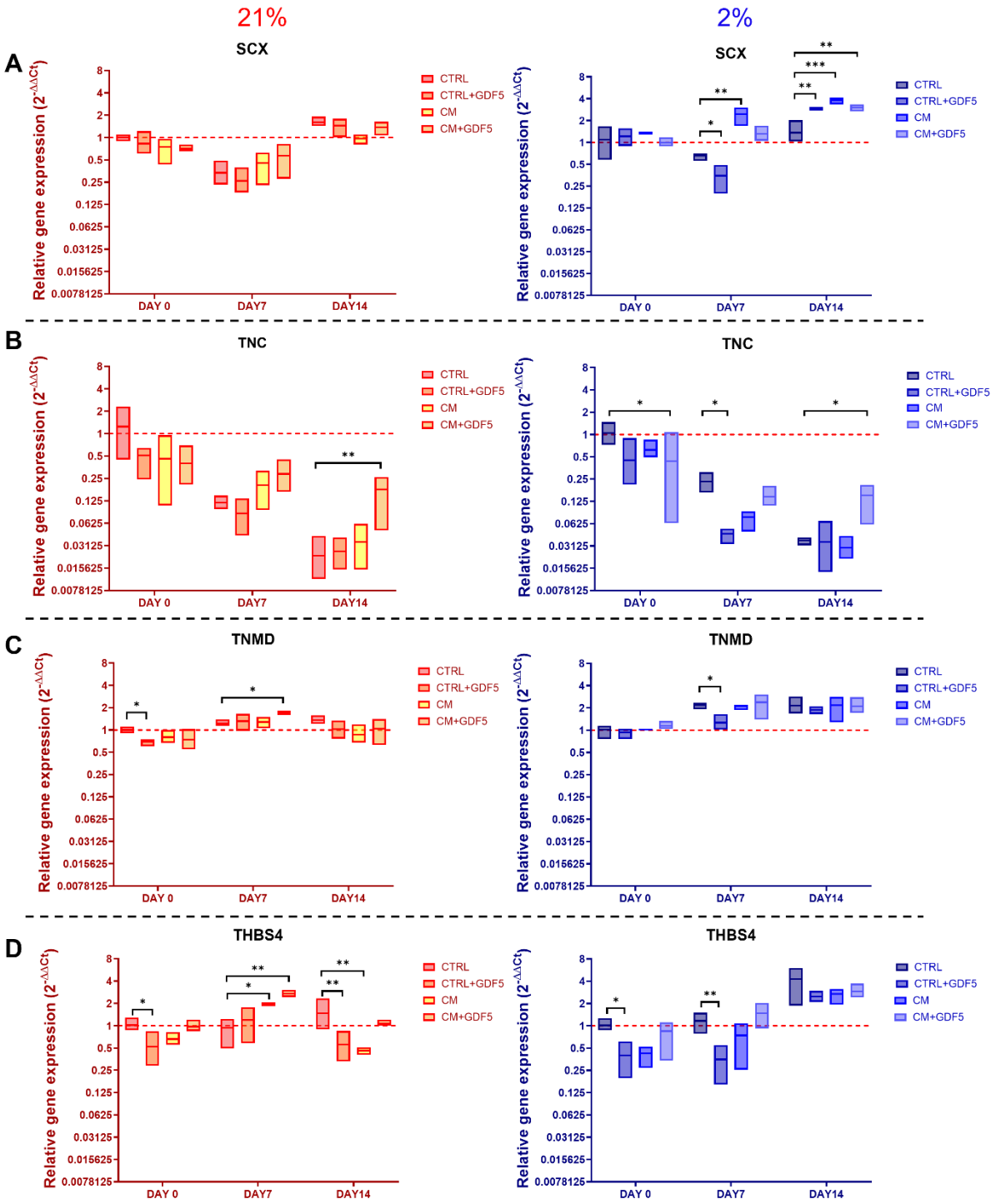


Figure 5-7. Gene expression of tenogenic markers in TSPCs II cultured for 14 days under different media conditions. RT-qPCR analysis of (A) *SCX*, (B) *TNC*, (C) *TNMD*, and (D) *THBS4* expression in TSPCs II cultured in standard culture medium (CTRL), CTRL supplemented with GDF-5 (CTRL+GDF5), conditioned medium (CM), and CM supplemented with GDF-5 (CM+GDF5) under 21% and 2% oxygen conditions. Gene expression levels are presented as fold changes relative to the control at day 0. Data illustrate trends across days 0, 7, and 14. Statistical analysis: two-way ANOVA followed by Dunnett's multiple comparisons test; '*' for $p < 0.05$, '**' for $p < 0.01$, '***' for $p < 0.001$, n=3.

5.4.4 Long-term evaluation of CM and cEVs on hBM-MSCs (14 days)

Human BM-MSCs were cultured for 14 days under 2% and 21% oxygen conditions in standard culture medium and TSPCs II-CM (1:2 dilution) obtained from static culture, with a final protein concentration of 5 µg/mL. Additionally, cEVs were isolated from the same CM via ultracentrifugation and resuspended in standard culture medium at a final EV concentration of 1 µg/mL. Both CM and cEVs were tested with and without the supplementation of 10 ng/mL or 100 ng/mL of GDF-5. These concentrations were selected based on previous findings demonstrating the role of GDF-5 in promoting tenogenic differentiation[189,194,195,341]. On day 14, cells were analysed for TNMD and COL1 expression by immunofluorescence, histological assessment by Picro-Sirius Red staining, gene expression by RT-qPCR, and DNA content quantification using the PicoGreen assay.

5.4.4.1 Immunofluorescence analysis

To confirm and quantify the expression of tenogenic markers, immunofluorescence staining was performed, and the MFI was measured across various media conditions under both 21% and 2% oxygen concentrations.

TNMD expression significantly increased in CM-treated samples, particularly in physiological oxygen (Figure 5-8). On day 14, in 21% oxygen, no significant differences were observed between the control and the control supplemented with either 10 ng/mL or 100 ng/mL of GDF-5. However, a slight increase in MFI correlated with the increasing GDF-5 concentration. CM-treated samples showed a significant increase in TNMD expression, with an MFI 1.6-fold higher than the control ($p = 0.0201$), while supplementation with GDF-5 did not further enhance TNMD expression. The highest TNMD expression was detected in cEVs, with MFI values 2-fold ($p < 0.0001$), 1.6-fold ($p = 0.0454$), and 1.8-fold ($p = 0.0009$) higher than the control for pure cEVs, cEVs + 10 ng/mL GDF-5, and cEVs + 100 ng/mL GDF-5, respectively. Direct intra-group comparisons (CM vs CM+GDF-5 and cEVs vs cEVs+GDF-5) revealed no significant differences, indicating that GDF-5 supplementation did not significantly enhance CM- or cEV-induced TNMD expression at 21% oxygen.

In 2% oxygen, a similar trend was observed, with no significant differences between the control and control samples supplemented with GDF-5, although an increasing MFI was visible with higher GDF-5 concentrations. All CM-treated samples showed significantly increased TNMD expression, with CM alone 1.8-fold ($p < 0.0001$) higher, CM + 10 ng/mL GDF-5 1.9-fold ($p < 0.0001$) higher, and CM + 100 ng/mL GDF-5 2.2-fold ($p < 0.0001$) higher than the control. A significant increase was also observed in pure cEVs and cEVs + 10 ng/mL GDF-5, both showing a 1.8-fold ($p < 0.0001$) increase compared to the control, while cEVs + 100 ng/mL GDF-5 did not show significant differences. Intra-group comparisons confirmed that CM vs CM+GDF-5 and cEVs vs cEVs+GDF-5 did not show significant differences, except for cEVs + 100 ng/mL GDF-5, which was significantly lower than pure cEVs (1.4-fold decrease, $p = 0.028$).

When comparing oxygen conditions, TNMD expression was generally higher in 2% oxygen across all samples, except for cEVs + 100 ng/mL GDF-5, which displayed the highest MFI in 21% oxygen. CM-treated samples demonstrated the highest TNMD fluorescence intensity in 2% oxygen, particularly with 100 ng/mL GDF-5 supplementation, suggesting that physiological oxygen enhances the tenogenic effect of CM.

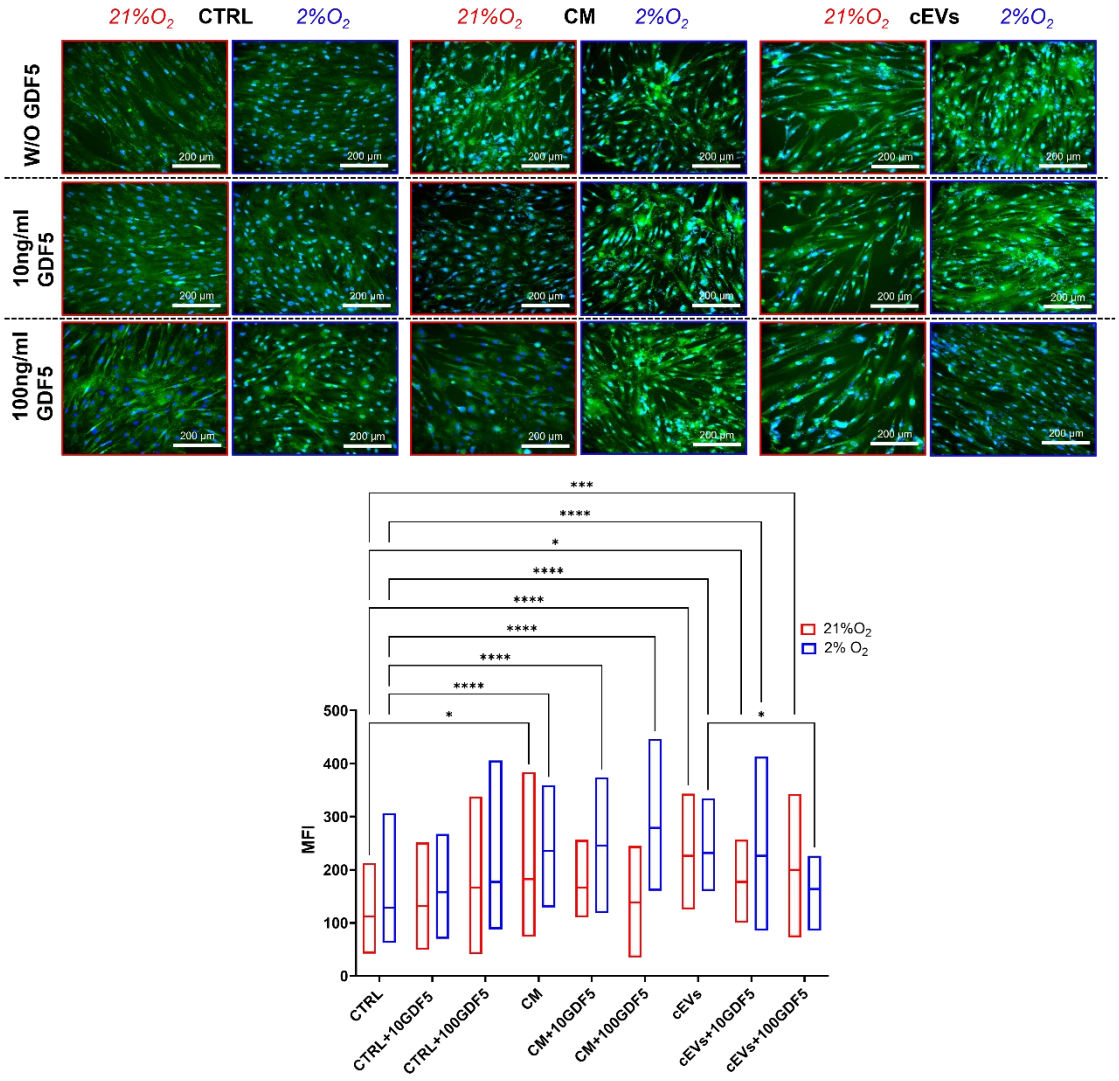


Figure 5-8. Immunofluorescence analysis of TNMD expression in hBM-MSCs cultured for 14 days under different media conditions. Representative images and MFI quantification of TNMD expression in hBM-MSCs cultured in standard culture medium (CTRL), TSPCs II-CM, and cEVs, with or without GDF-5 supplementation (10 ng/mL or 100 ng/mL), under 21% and 2% oxygen conditions. Scale bar: 200 µm. Statistical analysis: two-way ANOVA followed by Tukey's multiple comparisons test across all treatment groups, within each oxygen level, including intra-group comparisons (CM vs CM+GDF5 and cEVs vs cEVs+GDF5); '*' for $p < 0.05$, '**' for $p < 0.01$, '***' for $p < 0.001$, '****' for $p < 0.0001$, n=3.

Similarly, IF staining and MFI quantification were performed to assess COL1 expression across different media conditions. At day 14 in 21% oxygen, significant differences were detected between the control and control samples supplemented with GDF-5, where 10 ng/mL and 100 ng/mL GDF-5 increased COL1 MFI by 1.6-fold ($p = 0.009$) and 2.1-fold ($p < 0.0001$), respectively. CM-treated samples displayed a general increase in COL1 fluorescence intensity, with significance observed for CM + 10 ng/mL GDF-5 (1.9-fold, $p < 0.0001$) and CM

+ 100 ng/mL GDF-5 (1.7-fold, $p = 0.0013$). A similar trend was observed in cEV-treated samples, where pure cEVs and cEVs + 10 ng/mL GDF-5 showed 2.3-fold ($p < 0.0001$) and 1.6-fold ($p = 0.011$) higher COL1 expression, respectively. Intra-group comparisons (CM vs CM+GDF-5 and cEVs vs cEVs+GDF-5) revealed that pure cEVs had significantly higher COL1 expression than both cEVs + 10 ng/mL GDF-5 (1.4-fold, $p = 0.008$) and cEVs + 100 ng/mL GDF-5 (1.7-fold, $p < 0.0001$).

In 2% oxygen, although a visible increase in COL1 fluorescence was noted in control samples supplemented with GDF-5, no significant differences were detected. A significant increase was measured in CM-treated samples, where pure CM exhibited a 2.3-fold ($p < 0.0001$) higher COL1 MFI compared to the control. Among cEV-treated samples, no significant increase in COL1 expression was observed. Intra-group comparisons (CM vs CM+GDF-5 and cEVs vs cEVs+GDF-5) did not show any significant differences at 2% oxygen.

When comparing oxygen conditions, COL1 fluorescence intensity was generally higher in 21% oxygen than in 2%, except in CM-treated samples, which exhibited the highest COL1 MFI in 2% oxygen. Microscopic images further revealed that cells in 2% oxygen had begun producing extracellular collagen, whereas in 21% oxygen, collagen appeared primarily intracellular despite showing higher fluorescence intensity (Figure 5-9).

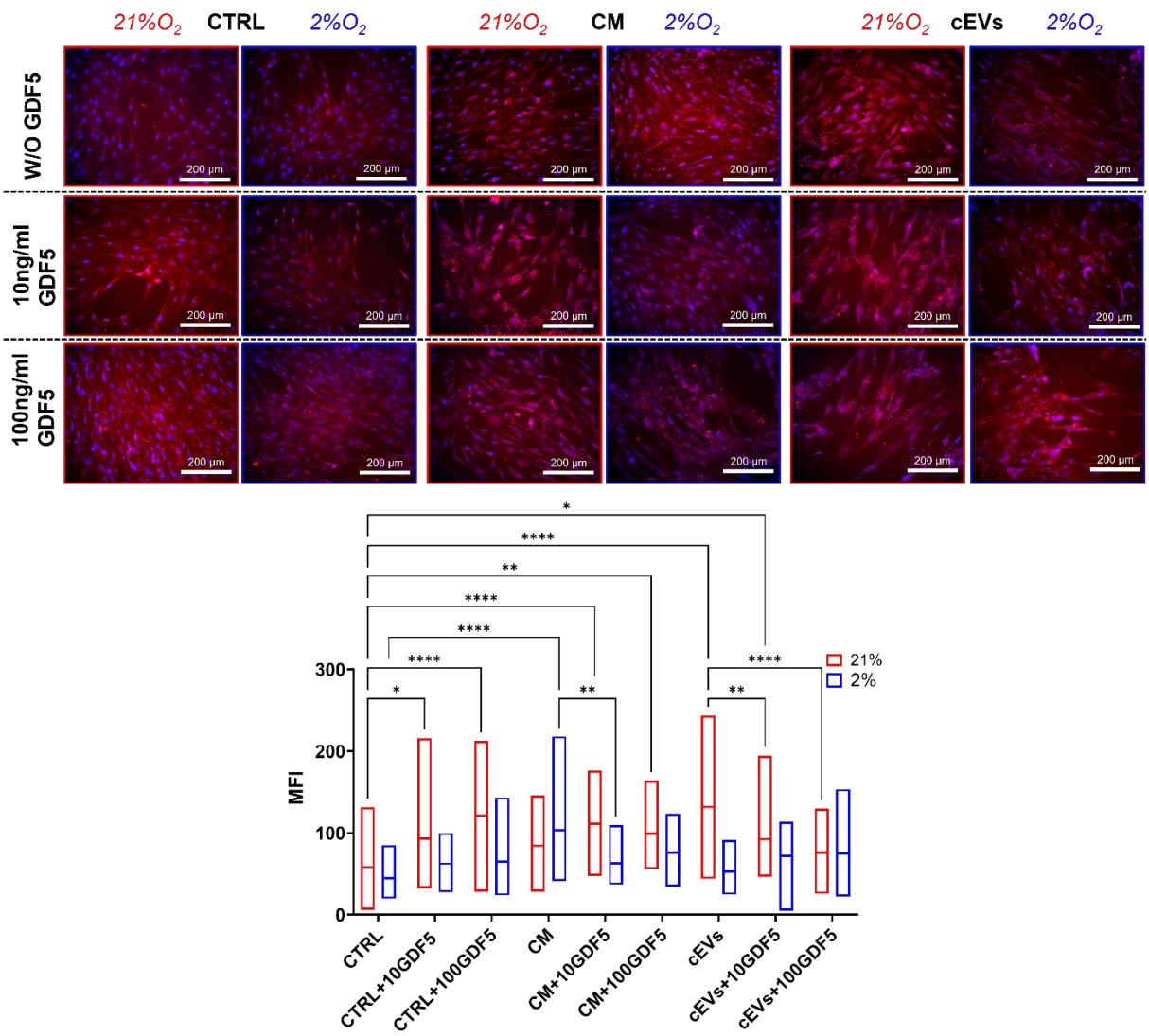


Figure 5-9. Immunofluorescence analysis of COL1 expression in hBM-MSCs cultured for 14 days under different media conditions. Representative images and MFI quantification of COL1 expression in hBM-MSCs cultured in standard culture medium (CTRL), TSPCs II-CM, and cEVs, with or without GDF-5 supplementation (10 ng/mL or 100 ng/mL), under 21% and 2% oxygen conditions. Compared to the control, COL1 expression increased in CM- and cEV-treated samples, with higher fluorescence intensity in 21% oxygen, while 2% oxygen promoted extracellular matrix deposition. Scale bar: 200 µm. Statistical analysis: two-way ANOVA followed by Tukey's multiple comparisons test across all treatment groups, within each oxygen level, including intra-group comparisons (CM vs CM+GDF5 and cEVs vs cEVs+GDF5); '*' for $p < 0.05$, '**' for $p < 0.01$, '***' for $p < 0.001$, '****' for $p < 0.0001$, n=3.

When comparing TNMD and COL1 results, TNMD expression was generally more responsive to CM treatment, with stronger upregulation in 2% oxygen, particularly with 100 ng/mL GDF-5. By contrast, COL1 expression was more pronounced in 21% oxygen, suggesting that these markers are regulated by distinct oxygen-dependent mechanisms. CM treatment effectively

enhanced both TNMD and COL1 expression, although cEVs exerted a stronger effect on TNMD. Notably, GDF-5 supplementation had a greater influence on COL1 expression, especially in CM-treated samples.

5.4.4.2 Histological analysis

Picro-Sirius Red staining was performed to evaluate collagen deposition and ECM organisation in hBM-MSCs cultured for 14 days under different media conditions and oxygen concentrations. As shown in Figure 5-10, distinct differences in collagen staining intensity and distribution were observed between conditions.

In 21% oxygen, collagen staining appeared predominantly red and intracellular, suggesting increased collagen synthesis but limited secretion into the ECM. An increase in collagen intensity was observed in CM-treated samples, particularly in the presence of GDF-5, where a more organised fibrillar structure was apparent. cEV treatments also promoted collagen deposition, with GDF-5 supplementation further enhancing ECM production.

In 2% oxygen, collagen staining appeared more orange and diffusely distributed, indicating enhanced secretion and integration into the ECM. CM-treated samples exhibited improved collagen organisation, especially with GDF-5 supplementation, while cEV-treated samples displayed a more scattered collagen distribution, suggesting a less structured but still active ECM formation.

A comparison between oxygen conditions highlights that 21% oxygen favoured stronger intracellular collagen deposition, while 2% oxygen promoted a more extracellularly organised matrix structure, as shown in immunofluorescence COL1 results.

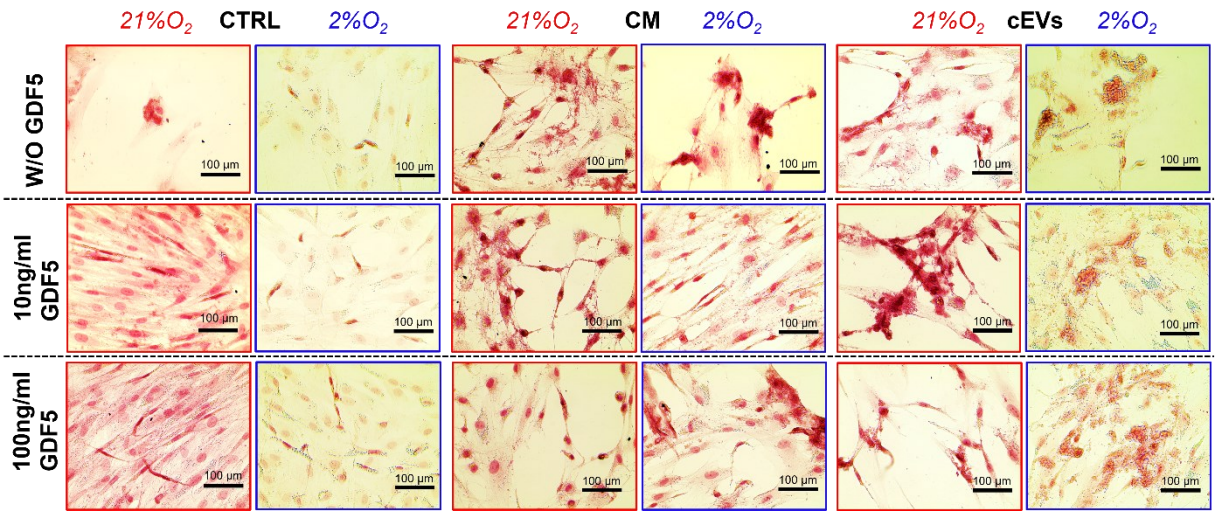


Figure 5-10. Picro-Sirius Red staining of collagen deposition in hBM-MSCs cultured for 14 days under different media conditions. Representative images of collagen distribution in hBM-MSCs cultured in standard culture medium (CTRL), TSPCs II-CM, and cEVs, with or without GDF-5 supplementation (10 ng/mL or 100 ng/mL), under 21% and 2% oxygen conditions. Collagen appears predominantly red and intracellular in 21% oxygen, indicating increased synthesis with limited extracellular deposition. In contrast, in 2% oxygen, collagen staining is more orange and diffusely distributed, suggesting enhanced secretion and ECM organisation. Scale bar: 100 µm.

5.4.4.3 Gene expression analysis

RT-qPCR was performed to assess the expression levels of key tenogenic markers: *SCX*, *MKX*, *TNMD*, *COL1A2*, and *COL3A1*. Gene expression was measured as fold changes relative to the control sample at day 0, allowing for a comparative evaluation of the impact of different culture conditions over time.

In 21% oxygen, *SCX* expression was significantly upregulated in most conditions, with the highest increases in CTRL+10GDF-5 (10.9-fold, $p < 0.0001$) and CM+10GDF-5 (20.4-fold, $p < 0.0001$). Pure CM also induced a robust upregulation (6.7-fold, $p < 0.0001$), while cEV-treated samples showed a non-significant trend toward increase. Intra-group comparisons revealed that CM was 3.1-fold lower than CM+10GDF-5 ($p = 0.0027$) and 4.9-fold higher than CM+100GDF-5 ($p < 0.0001$), while no significant differences were detected among cEV groups. A similar trend was observed in 2% oxygen, with the strongest increases in CTRL+10GDF-5 (8.4-fold, $p < 0.0001$) and pure CM (5.5-fold, $p < 0.0001$). By contrast, cEVs supplemented with GDF-5 were significantly lower than pure cEVs ($p < 0.01$) (Figure 5-11A).

MKX expression showed a distinct profile. In 21% oxygen, control and CM-treated samples were upregulated, with CTRL+10GDF-5 (8.5-fold, $p < 0.0001$), CTRL+100GDF-5 (3.6-fold, $p = 0.0153$), and CM+10GDF-5 (9.2-fold, $p < 0.0001$) showing the strongest increases. All cEV-treated samples were significantly downregulated compared to control ($p < 0.0001$). Intra-group comparisons indicated that CM was 6.4-fold lower than CM+10GDF-5 ($p = 0.0001$), with no significant differences among cEV groups. In 2% oxygen, upregulation was observed across most conditions, with the highest increases in CTRL+10GDF-5 (11.3-fold, $p < 0.0001$) and CM (3.9-fold, $p = 0.0122$). However, CM+GDF-5 samples were significantly lower than pure CM ($p < 0.05$), and cEVs+10GDF-5 was significantly reduced compared to control ($p = 0.0220$) (Figure 5-11B).

For *TNMD*, all conditions in 21% oxygen showed increased expression, most notably CTRL+100GDF-5 (12.1-fold, $p < 0.0001$), pure CM (7.6-fold, $p < 0.0001$), and CM+10GDF-5 (13.6-fold, $p < 0.0001$). Intra-group comparisons revealed that supplementation with 100 ng/mL GDF-5 reduced expression relative to unsupplemented CM (3.4-fold lower, $p = 0.0318$) and cEVs (5.3-fold lower, $p = 0.0014$). In 2% oxygen, *TNMD* expression was also upregulated, with CTRL+100GDF-5 (9.1-fold, $p < 0.0001$) and CM (5.6-fold, $p = 0.0010$) showing the highest values. However, CM+GDF-5 samples were significantly lower than CM alone ($p < 0.05$) (Figure 5-11C).

COL1A2 expression exhibited strong variability. In 21% oxygen, all groups were upregulated except CTRL+10GDF-5 and cEVs+100GDF-5, the latter being significantly reduced compared to control ($p = 0.0004$). The highest expression was in cEVs+10GDF-5 (18.5-fold, $p = 0.0086$). Intra-group comparisons showed no significant differences among CM groups, while pure cEVs was 273-fold higher than cEVs+100GDF-5 ($p < 0.0001$). In 2% oxygen, upregulation was observed in most conditions, with the strongest increases in CTRL+100GDF-5 (17.6-fold, $p = 0.0041$) and CM (12.3-fold, $p = 0.0072$). CM was significantly higher than CM+10GDF-5 (30.8-fold, $p = 0.0062$), and cEVs were strongly higher than both cEV+GDF-5 groups ($p < 0.0001$) (Figure 5-11D).

Finally, *COL3A1* was generally upregulated. In 21% oxygen, the strongest effects were in CTRL+10GDF-5 (4.9-fold, $p = 0.0032$), CM (5.6-fold, $p = 0.0015$), CM+10GDF-5 (5.7-fold, $p < 0.0001$), and pure cEVs (5.5-fold, $p = 0.0047$). By contrast, cEVs+100GDF-5 was significantly downregulated compared to control ($p = 0.0107$). CM was 7.1-fold higher than CM+100GDF-5 ($p = 0.0003$), and pure cEVs was 25-fold higher than cEVs+100GDF-5 ($p < 0.0001$). In 2% oxygen, all conditions except cEVs+100GDF-5 were upregulated, with the strongest increases in CTRL+10GDF-5 (21.9-fold, $p < 0.0001$), CTRL+100GDF-5 (6.2-fold, $p = 0.0008$), and CM (9.8-fold, $p < 0.0001$). CM was significantly higher than both CM+GDF-5 groups ($p < 0.01$), while pure cEVs was 10.9-fold higher than cEVs+100GDF-5 ($p < 0.0001$) (Figure 5-11E).

Overall, CM and cEVs generally promoted upregulation of tenogenic markers, with 2% oxygen enhancing expression in most cases. GDF-5 supplementation had differential effects: it boosted *SCX* and *COL1A2* in some conditions but reduced *TNMD* and *COL3A1* when combined with CM or cEVs, particularly at the higher dose.

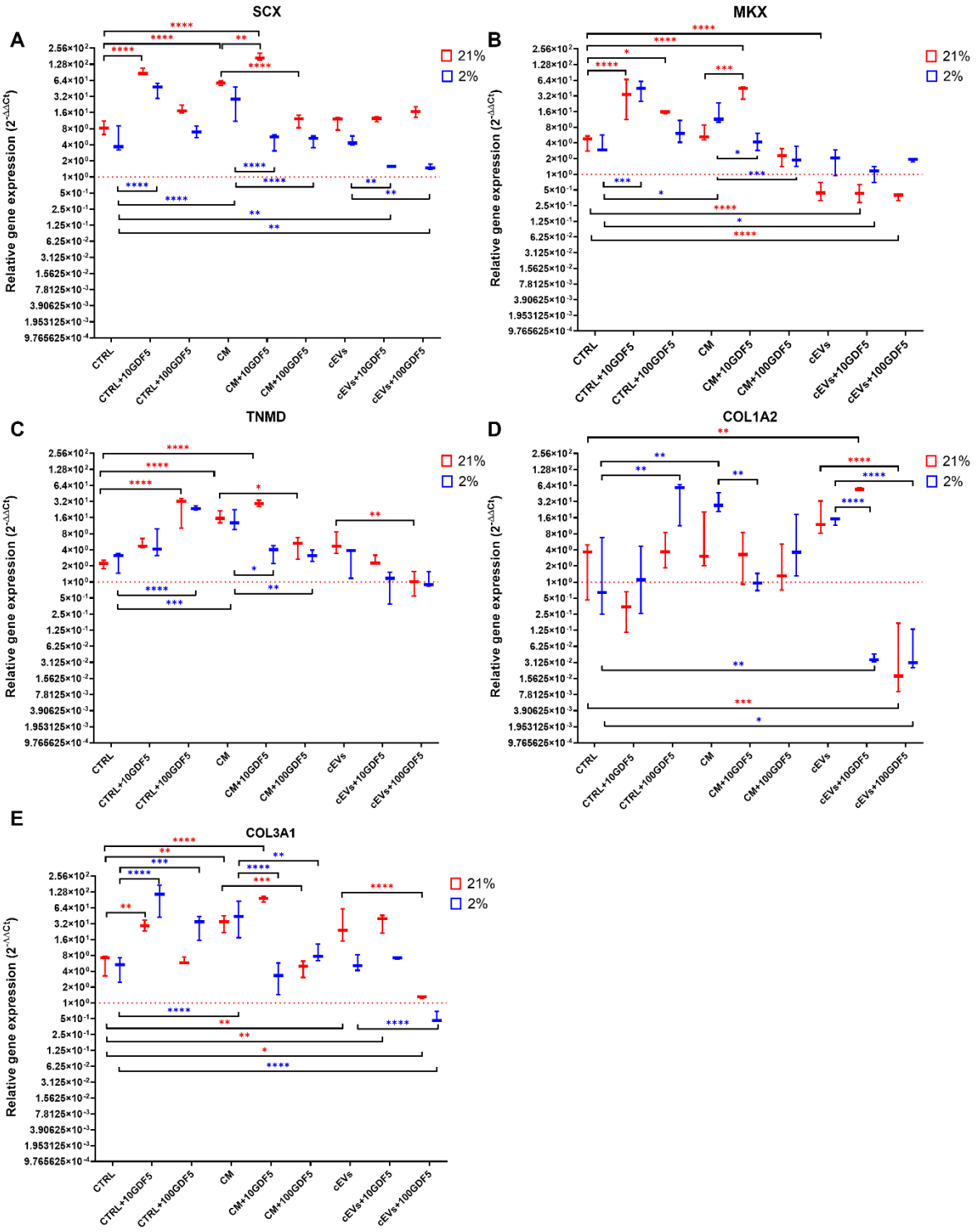


Figure 5-11. Gene expression of tenogenic marker expression in hBM-MSCs cultured for 14 days under different media conditions. Expression of *SCX*, *MKX*, *TNMD*, *COL1A2*, and *COL3A1* is shown as fold changes relative to the control at day 0. hBM-MSCs were cultured in standard culture medium (CTRL), TSPCs II-CM, and cEVs, with or without GDF-5 supplementation (10 ng/mL or 100 ng/mL), under 21% and 2% oxygen conditions. Gene expression levels were normalised to *YWHAZ*. Statistical analysis: two-way ANOVA followed by Tukey's multiple comparisons test, comparing all treatments within each oxygen level, including intra-group comparisons (CM vs CM+GDF5 and cEVs vs cEVs+GDF5); '*' for $p < 0.05$, '**' for $p < 0.01$, '***' for $p < 0.001$, '****' for $p < 0.0001$, n=3.

5.4.4.4 DNA quantification

To estimate cell proliferation at each time point across different media conditions, total DNA content was quantified using the PicoGreen assay.

In atmospheric oxygen, DNA content remained relatively stable across all conditions, with no statistically significant differences observed between the control and experimental groups. A slight increase in DNA content was noted at day 7 in samples supplemented with 10 ng/mL or 100 ng/mL of GDF-5 and in CM- and cEV-treated samples, suggesting a moderate proliferative effect. However, by day 14, DNA levels plateaued, indicating that cell proliferation had slowed as cultures reached confluence. At this time point, cEV-treated samples exhibited the highest DNA content among all conditions (Figure 5-12A).

A different trend was observed in physiological oxygen, where a substantial increase in DNA content was measured at day 7 compared to day 0 across multiple conditions. Control samples supplemented with 10 ng/mL and 100 ng/mL of GDF-5 exhibited a marked increase in DNA content on day 7, though their levels were significantly lower than the control on day 14. Similarly, CM- and cEV-treated samples displayed a continuous increase in DNA content through days 7 and 14, suggesting that 2% oxygen enhances cellular proliferation. By day 14, DNA content remained elevated, with cEV-treated samples showing the highest values, particularly in the pure cEV group, indicating that cEVs may provide more sustained cell growth than CM (Figure 5-12B).

Comparing the final DNA quantification values at day 14 across both oxygen concentrations, physiological oxygen appeared to promote higher overall cell proliferation over time. At day 0, DNA levels in 21% oxygen were 1.6-fold higher than in 2% despite the same initial seeding density. However, by day 7, all samples in 2% oxygen surpassed 0.250 μg/cm², whereas in 21%, values ranged from 0.197 μg/cm² to 0.300 μg/cm², with most samples below the 0.250 μg/cm² threshold. By day 14, the highest DNA content measured in 21% oxygen (0.300 μg/cm²) was 1.4-fold lower than the maximum value recorded in 2% oxygen (0.430 μg/cm²), further supporting the role of physiological oxygen in enhancing cell proliferation.

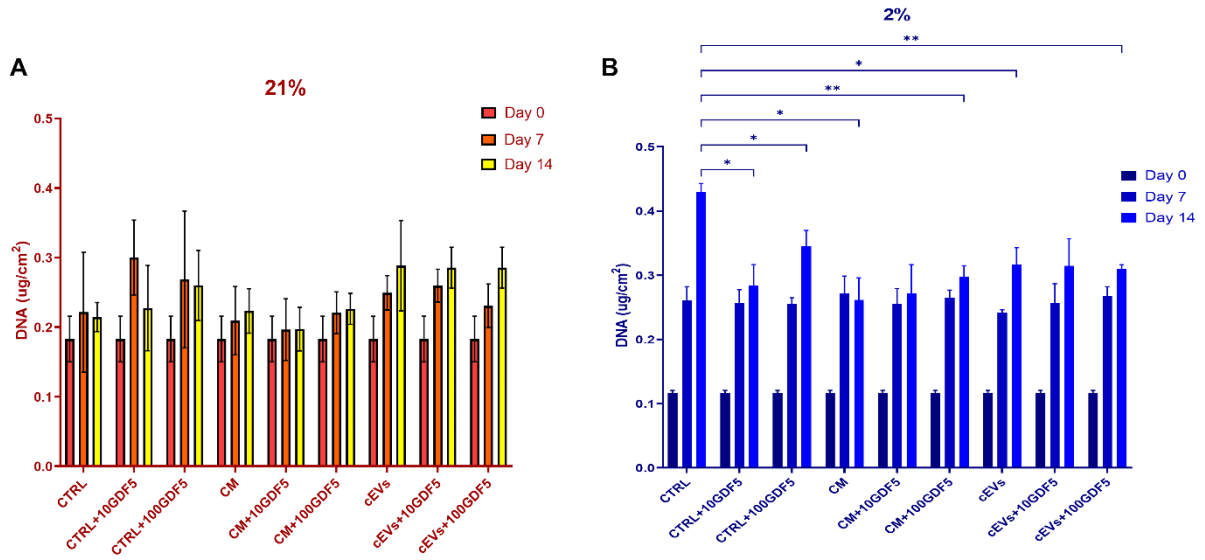


Figure 5-12. Total DNA quantification in hBM-MSCs cultured for 14 days under different media conditions. DNA content was measured using the PicoGreen assay at days 0, 7, and 14 in hBM-MSCs cultured in standard culture medium (CTRL), CTRL supplemented with GDF-5 (10 ng/ml or 100 ng/ml), TSPCs II- CM, and cEVs with or without GDF-5, under 21% oxygen (A) and 2% oxygen (B) conditions. Statistical analysis: two-way ANOVA followed by Tukey's multiple comparisons test across timepoints and treatments within each oxygen level; '*' for $p < 0.05$, '**' for $p < 0.01$, n=3.

5.5 Discussion

This study investigated the tenogenic potential of CM and cEVs derived from porcine TSPCs II on both TSPCs II and hBM-MSCs under different oxygen concentrations (21% and 2%). The findings demonstrated that CM and cEVs significantly influenced cell viability, proliferation, ECM organisation, and tenogenic differentiation, with oxygen concentration playing a crucial modulatory role. Previous studies have investigated the role of conditioned medium and EVs derived from tenocytes[290], TSPCs[235,289,292,339,340,342] and MSCs[131,182,184,223,229,230,343,344] derived EVs from different species in promoting tendon healing by stimulating the proliferation and migration of tenocytes or tendon stem cells, reducing inflammation and improving biomechanical properties and the tendon-bone interface. While previous studies have explored separately CM and EVs derived from different cell types in the context of tendon healing, our study is, to the best of our knowledge, the first to specifically examine the tenogenic differentiation potential of porcine TSPC-derived CM and cEVs, with a focus on the role of oxygen tension, making it a novel contribution to the field of tendon tissue engineering.

Across all experiments, 2% oxygen provided a more favourable environment for tenogenic differentiation and ECM organisation. Cells cultured in hypoxia exhibited higher viability, denser morphology, and sustained expression of key tenogenic markers, including *SCX*, *TNMD*, and *MKX*. Gene expression trends and histological analysis confirmed that ECM synthesis and remodelling were enhanced under low oxygen conditions, particularly in CM-treated samples. Our findings align with previous studies[9,175,255,256,306] demonstrating that physiological oxygen levels enhance tenogenic differentiation and ECM maturation, while atmospheric oxygen may lead to oxidative stress and incomplete ECM remodelling.

Short-term culture experiments confirmed the feasibility of using tendon-derived CM, as TSPCs II maintained high viability across all tested conditions. While cell viability remained above 85%, it was slightly lower in pure CM and SF medium, particularly under 21% oxygen, likely due to the absence of essential nutrients; in 2% oxygen, cells exhibited higher viability, reinforcing hypoxia's role in reducing oxidative stress, as previously reported[9,249,258] (Figure 5-1).

Morphological analysis revealed that TSPCs II cultured in their own CM maintained a spindle-shaped, well-spread morphology comparable to cells in standard culture medium. In contrast, SF-treated cells exhibited a more elongated, stressed appearance with lower density. A similar effect has been reported for amniotic epithelial cells, where tendon explant derived-CM supported a fibroblast-like phenotype, promoting viability and maintaining cellular morphology[30]. Additionally, tenocyte-derived CM was also compatible with cell survival but exhibited slightly lower viability and a more elongated morphology, suggesting that the TSPCs II secretome provides a broader range of bioactive factors crucial for cell homeostasis. This aligns with the characterisation of TSPCs II-derived EVs (Chapter 3), which demonstrated enrichment in stemness and adhesion markers (CD44, CD105, CD49e) and a regenerative cytokine profile, supporting their role in maintaining cellular morphology and function. The effect of oxygen tension was evident in cell morphology, as cultures in 2% oxygen formed a denser, more compact arrangement compared to the more elongated and loosely packed

morphology in 21% oxygen. This observation corresponds with findings in Chapter 3, where hypoxia enhanced the tenogenic properties of TSPCs II and modulated their EV secretion, reinforcing the importance of oxygen tension in optimising regenerative potential.

Cytotoxicity assessment further confirmed the biocompatibility of TSPCs II CM. While pure CM reduced fibroblast viability, likely due to an imbalance in nutrient concentration or pH, which could induce cellular stress, as seen in the trypan blue exclusion assay on TSPCs II, diluted CM samples (1:2, 1:4, and 1:8) maintained high viability (Figure 5-4). The 1:2 CM dilution was selected for further experiments as it provided a balance between bioactivity and biocompatibility, as reported in other studies[30,345]. Notably, under 2% oxygen, fibroblasts exhibited slightly lower viability than in 21%, suggesting that while hypoxia supports TSPCs II, fibroblast sensitivity to low oxygen conditions may differ[346,347]. Similar cytotoxic effects have been observed in MSC-derived CM studies, where undiluted CM reduced viability due to an accumulation of proteolytic enzymes or metabolic by-products over time[348,349].

Long-term culture experiments further demonstrated that CM supports TSPCs II proliferation and phenotype maintenance over 14 days. Cells remained elongated and fibroblast-like across conditions, confirming that CM preserves tendon stem cell morphology. Proliferation was enhanced in 2% oxygen, where cells reached confluence earlier than in 21%, aligning with our previous results. PicoGreen analysis further confirmed this trend, showing that cEVs promote sustained proliferation, particularly under hypoxia, where continuous growth was observed compared to the plateau seen on day 14 in 21% oxygen (Figure 5-12). GDF-5 supplementation contributed to a more uniform morphology among different conditions, suggesting that it may stabilise cellular organisation while promoting tenogenic differentiation, consistent with prior studies[189,195] demonstrating GDF-5's role in tenogenic differentiation and ECM synthesis, and in agreement with our findings in Chapter 4 on its tenogenic effect.

Immunofluorescence analysis of TNMD expression provided key insights into the effect of CM and oxygen tension on tenogenic differentiation. In 21% oxygen, TNMD expression followed a pattern of early upregulation at day 0, a decline at day 7, and a plateau at day 14, suggesting

transient upregulation followed by stabilisation. In contrast, CM-treated samples, with and without GDF-5 supplementation, showed sustained TNMD expression, supporting the hypothesis that CM contains bioactive factors that prolong tenogenic commitment. Under 2% oxygen, TNMD expression was initially lower at day 0 and decreased by day 7 before increasing at day 14 without any supplementation. This trend suggests an initial adaptation phase under hypoxia before tenogenic differentiation is activated. In contrast, after rising on day 7, CM-treated samples decreased again on day 14. GDF-5 supplementation had a transient effect, enhancing TNMD expression at day 7 in 2% oxygen but not sustaining it long-term. These results highlight the complex interplay between oxygen tension, CM, and tenogenic differentiation, where physiological oxygen promotes sustained TNMD expression over time without supplementation. Meanwhile, atmospheric oxygen requires CM and GDF-5 supplementation for prolonged TNMD expression (Figure 5-6). These results align with previous reports demonstrating that hypoxia supports tendon-like matrix deposition and upregulates tenogenic markers[9,215,255].

Gene expression analysis confirmed that CM enhances tenogenic differentiation, with 2% oxygen providing a more stable regulatory environment for tendon-related gene expression, as previously reported[9,30,255]. *SCX* expression followed a biphasic trend, with downregulation at day 7 and upregulation at day 14, particularly in CM-treated samples, indicating a progressive tenogenic commitment. *TNMD* was consistently upregulated across conditions, reinforcing CM's role in promoting differentiation. *THBS4* exhibited variable trends, with an initial increase followed by a decline in 21% oxygen, whereas in 2% oxygen, it was initially downregulated but later increased, suggesting that hypoxia may suppress early ECM remodelling before facilitating it at later stages. *TNC* remained consistently downregulated except in the CM+GDF-5 condition at day 14, indicating that while CM alone may not strongly induce *TNC*, GDF-5 enhances its late-stage activation. These findings agree with studies on tenogenic differentiation of adipose-derived stem cells, and tendon stem cells in response to hypoxia, which reported that 2% oxygen enhances *SCX* and *TNMD* expression[255,350].

Further confirmation of the tenogenic potential of CM and cEVs was obtained from the 14-day culture of hBM-MSCs. The concentrations used were selected based on both feasibility and comparability. The 1:2 dilution of CM (5 µg/mL protein) was chosen because cytotoxicity assays (Section 5.4.2) showed this dilution to be non-toxic and suitable for long-term culture, while the EV concentration (1 µg/mL protein) was selected in line with commonly reported ranges in the literature, ensuring consistency with previous studies[182,289]. Both CM and cEVs promoted TNMD expression, but cEVs had the strongest effect, likely due to their microRNA and protein cargo[351]. This effect was most pronounced in hypoxia, reinforcing the role of vesicle-mediated signalling in tendon differentiation in low oxygen. Interestingly, GDF-5 supplementation did not further enhance TNMD expression in 21% oxygen but significantly increased it in 2% oxygen, particularly at 100 ng/mL (Figure 5-8).

COL1, a major structural component of tendon tissue, exhibited a different trend than TNMD. COL1 expression was generally more pronounced in 21% oxygen, particularly in CM-treated samples, suggesting that atmospheric oxygen supports collagen synthesis but potentially limits its secretion and extracellular organisation. In contrast, 2% oxygen promoted ECM deposition, as evidenced by the more diffuse and extracellular collagen staining observed in microscopic images (Figure 5-9). Notably, in 21% oxygen, COL1 expression significantly increased in CM and cEV-treated samples, especially with GDF-5 supplementation, indicating that GDF-5 plays a stronger role in regulating COL1 than TNMD, potentially influencing collagen fibrillogenesis. However, in 2% oxygen, COL1 expression was upregulated in CM-treated samples, while only cEVs supplemented with 100 ng/mL GDF-5 showed a significant increase. This suggests that CM alone provides sufficient stimuli for collagen synthesis under hypoxia, whereas cEVs may require additional GDF-5 to enhance this effect[229].

The different TNMD and COL1 responses suggest separate regulatory mechanisms for tenogenesis and ECM formation under various oxygen conditions. As previously stated, TNMD expression was more responsive to CM treatment in 2% oxygen, like most of the tenogenic

markers, while COL1 expression was higher in 21% oxygen, suggesting that atmospheric oxygen favours collagen synthesis but may limit its extracellular deposition.

Histological analysis confirmed that collagen deposition patterns varied with oxygen levels (Figure 5-10). In 21% oxygen, collagen was primarily intracellular (red staining), indicating active synthesis but limited secretion. In contrast, in 2% oxygen, collagen appeared more diffusely distributed (orange staining), suggesting enhanced secretion and ECM integration. This aligns with the hypothesis that hypoxia upregulates ECM remodelling enzymes, such as lysyl oxidase, facilitating collagen crosslinking and organisation[352]. A notable increase in collagen intensity was observed in 21% of CM and cEVs-treated samples, enhanced even more by GDF-5 supplementation. In comparison, in 2%, CM-treated samples showed higher collagen organisation, and cEVs-treated samples showed more scattered collagen distribution and were less structured.

Gene expression analysis in hBM-MSCs revealed distinct trends in tenogenic differentiation influenced by CM, cEVs, oxygen concentration, and GDF-5 supplementation. *SCX* and *MKX* were consistently upregulated by CM, particularly in 2% oxygen, reinforcing the role of soluble factors in tenogenesis. The highest expression was observed in CM+10GDF-5, suggesting a synergistic effect between CM-derived factors and GDF-5. While cEVs promoted moderate upregulation, as previously reported in BM-MSCs-derived EVs[182], their combination with high-dose (100 ng/mL) GDF-5 led to reduced *SCX* and *MKX* expression, suggesting a possible saturation of tenogenic signalling pathways. One hypothesis is that excess soluble GDF-5 competes with EV-associated growth factors for receptor binding, thereby altering downstream signalling.

TNMD was consistently upregulated across all conditions, confirming the tenogenic potential of CM and cEVs, in agreement with previous reports[30,182,290,344]. In both oxygen concentrations, CM and GDF-5 independently enhanced *TNMD* expression, especially in 100 ng/mL GDF-5 concentration, while cEVs-treated samples showed higher upregulation in the absence of any GDF-5 supplementation.

COL1A2 and *COL3A1* were upregulated in CM-treated samples under both oxygen levels, with CM alone promoting ECM production more effectively than cEVs. Low-dose GDF-5 (10 ng/ml) enhanced *COL1A2* and *COL3A1*, particularly with cEVs, but high-dose GDF-5 (100 ng/ml) reached a high expression comparable to that of the CM-treated samples.

In summary, this study demonstrated that porcine TSPC-derived CM and cEVs significantly enhance tenogenic differentiation, with 2% oxygen providing a more favourable environment for cell viability, ECM organisation, and sustained tenogenic marker expression. CM exhibited strong bioactivity, supporting cell proliferation, morphology, and tenogenic differentiation. At the same time, cEVs had a more significant effect on TNMD expression, suggesting a key role for vesicle-mediated signalling in tendon repair. Additionally, GDF-5 supplementation influenced tenogenic differentiation differently in CM- and cEV-treated samples, highlighting the complex regulatory interactions between soluble factors and EV cargo in tendon regeneration. This chapter, focusing on the tenogenic potential of porcine-derived CM and cEVs, lays the foundation for the next chapter, which will extend the analysis to human-derived CM and cEVs.

When comparing the two cell populations, distinct yet complementary responses were observed. TSPCs II primarily showed enhanced proliferation and maintenance of their progenitor phenotype in response to CM and EVs, particularly under hypoxia. In contrast, hBM-MSCs exhibited stronger induction of tenogenic markers such as TNMD, SCX, and COL1, especially in response to EVs. These findings suggest that TSPC-derived CM and EVs act through different mechanisms depending on the target cell population: sustaining the activity of resident tendon progenitors while also promoting tenogenic differentiation in exogenous MSCs. This dual effect highlights their potential to support both intrinsic tendon repair and cell-based regenerative therapies. Despite these promising results, some limitations should be acknowledged. First, all results in this chapter were based on a single preparation of porcine TSPCs II-derived CM, and statistical analysis was therefore performed on technical replicates only. In addition, the control condition used in the long-term CM experiments (Section 5.4.3)

consisted of undiluted standard medium, which does not fully account for the serum dilution introduced by CM treatment; therefore, part of the observed differences may reflect serum reduction rather than CM bioactivity alone. Accordingly, these findings should be considered preliminary and will require confirmation using multiple independent CM batches. Second, this study was conducted *in vitro*, which may not fully replicate the complex physiological environment of tendon healing *in vivo*. Third, the mechanisms underlying the tenogenic effects of CM and cEVs, mainly their molecular cargo (e.g., microRNAs, proteins), require further exploration to optimise their therapeutic potential. Fourth, Picro-Sirius Red staining was presented qualitatively and not quantified; images were obtained under bright-field rather than polarised microscopy, which is required for reliable quantification and collagen subtype discrimination.

5.6 Conclusion

This study demonstrated that porcine TSPC-derived CM and cEVs exert beneficial effects on both tendon-resident progenitors (TSPCs II) and human BM-MSCs, with oxygen tension emerging as a major regulatory factor. Under physiological oxygen, cells showed enhanced viability, sustained tenogenic marker expression, and improved ECM organisation, whereas atmospheric oxygen favoured initial collagen synthesis but limited extracellular integration.

Distinct yet complementary effects were observed across the two cell populations. In TSPCs II, CM and cEVs primarily supported proliferation and maintenance of their progenitor phenotype. In hBM-MSCs, they induced tenogenic differentiation, particularly through EV-mediated signalling. GDF-5 further modulated these outcomes, enhancing collagen synthesis under selected conditions.

Together, these findings highlight the dual regenerative role of TSPC-derived secretome products: sustaining tendon-resident progenitors while promoting differentiation of exogenous MSCs. This dual activity underscores their promise as cell-free therapeutics for tendon repair

and provides a rationale for optimising oxygen culture conditions to maximise their translational potential.

Chapter 6

Investigating the tenogenic potential of human TSPC-derived CM and cEVs in 2D and 3D cultures

6. INVESTIGATING THE TENOGENIC POTENTIAL OF HUMAN TSPC-DERIVED CM AND CEVS IN 2D AND 3D CULTURES

6.1 Introduction

Following the characterisation of hTSPC-derived secretomes under varied oxygen and mechanical conditions (Chapter 4) and the evaluation of porcine TSPC-derived products in tenogenic differentiation (Chapter 5), this chapter focuses on assessing the regenerative potential of hTSPC-derived CM and cEVs. Specifically, their effects are evaluated on human bone marrow-derived MSCs cultured in both two-dimensional (2D) and three-dimensional (3D) environments.

Three-dimensional culture systems, particularly those based on collagen scaffolds, more accurately replicate the biochemical and structural complexity of native tendon tissue, facilitating cell–matrix interactions and guiding ECM organisation[353–355]. These models provide a more physiologically relevant platform for evaluating the functional activity of paracrine factors in tissue regeneration. Additionally, the application of key microenvironmental stimuli, such as low oxygen tension[9,175,255,256,306] (2% O_2) and mechanical stimulation[274,312–314] through dynamic culture, has been shown to enhance stem cell function, promote ECM production, and increase the yield and activity of secretome components, including EVs.

To mimic the structural and biomechanical complexity of native tendon tissue[355,356], a 3D collagen scaffold model was employed in which hBM-MSCs were embedded together with cEVs and cultured in hTSPC-derived CM. This setup integrated biomechanical cues, biochemical signals, and ECM support in a single system. By combining hypoxia, dynamic culture, and 3D scaffolds, the present study provides a multifaceted evaluation of tendon-like differentiation, clarifying the contributions of both soluble and vesicle-associated factors to tenogenic responses.

6.2 Aim

This chapter aimed to investigate the ability of CM and cEVs derived from human TSPCs to promote tenogenic differentiation in hBM-MSCs.

The specific objectives were to:

1. Compare the tenogenic effects of hTSPC-derived CM and cEVs obtained from static versus dynamic culture conditions.
2. Assess the influence of a 3D microenvironment on tenogenic differentiation by embedding hBM-MSCs in collagen-based scaffolds.
3. Investigate the effect of CM, cEVs, and GDF-5 supplementation on tendon-like tissue formation, with CM applied in 2D cultures and crude EVs embedded within 3D scaffolds cultured in CM.
4. Determine whether dynamic culture conditions enhance the regenerative properties of hTSPC-derived secretomes.

Overall, the chapter aimed to evaluate how CM, cEVs, and 3D culture conditions may be used to support tenogenic differentiation, thereby informing strategies for tendon tissue engineering.

6.3 Methods

The study design is summarised in Scheme 4, with detailed materials and methods provided in Chapter 2.

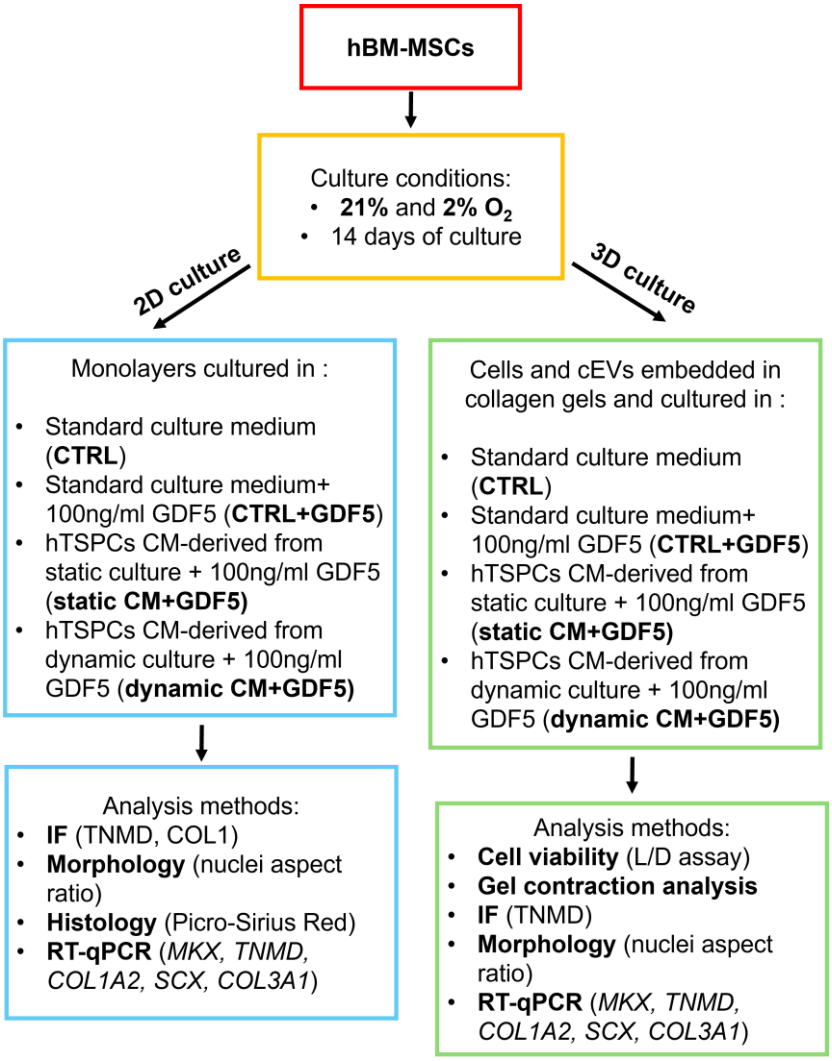
Human bone marrow MSCs (P3) were cultured for 14 days under different media conditions and oxygen concentrations (21% and 2%) in both 2D and 3D environments. Control groups consisted of standard culture medium (CTRL) and CTRL supplemented with 100 ng/mL GDF-5 (CTRL+GDF-5). Conditioned medium was collected from hTSPCs (n = 3 donors) cultured under static or dynamic conditions (Section 2.18.2).

In 2D culture, hBM-MSCs were seeded as monolayers (5,000 cells/cm²) and maintained in CTRL, CTRL+GDF-5, or hTSPC-derived CM (static or dynamic), each supplemented with 100 ng/mL GDF-5. After 14 days, cells were analysed by immunofluorescence (TNMD, COL1), Picro-Sirius Red staining, nuclear aspect ratio analysis, and RT-qPCR of tenogenic markers (*SCX*, *TNMD*, *MKX*, *COL1A2*, *COL3A1*).

In 3D culture, collagen scaffolds (Section 2.25) were prepared with hBM-MSCs embedded together with crude EVs (1 µg/mL). Scaffolds were cultured in CTRL, CTRL+GDF-5, or CM (static or dynamic), supplemented with 100 ng/mL GDF-5. Viability (Live/Dead, days 1 and 14), collagen gel contraction (days 0, 3, 14), TNMD immunofluorescence, nuclear aspect ratio, and RT-qPCR analysis of tenogenic markers were performed (Section 2.12).

6.3.1 Statistical analysis

Data are presented as mean ± SD from three biological replicates (n = 3). Normality was assessed prior to analysis. For non-normally distributed datasets, the Kruskal–Wallis test followed by Dunn's multiple comparisons test was applied, or the Mann–Whitney U test was used for two-group comparisons. For normally distributed datasets, two-way ANOVA was used, followed by Šídák's or Tukey's multiple comparisons test as appropriate. All analyses were performed using GraphPad Prism software (version 10.2.2), with significance thresholds set as '*' for $p < 0.05$, '**' for $p < 0.01$, '***' for $p < 0.001$, and '****' for $p < 0.0001$.



Scheme 4. Summary of the methodology adopted in Chapter 6.

6.4 Results

6.4.1 2D culture: hBM-MSCs in hTSPCs-CM

For the 2D culture, hBM-MSCs were seeded as monolayers and maintained for 14 days in either a control medium (CTRL or CTRL+GDF-5) or a conditioned medium derived from hTSPCs cultured under static or dynamic conditions, supplemented with GDF-5.

To assess the effects of these culture conditions, IF analysis was performed to evaluate the expression of TNMD and COL1. Morphological changes were examined by measuring the nuclear aspect ratio, while histological assessment was conducted using Picro-Sirius Red staining to analyse collagen deposition. Gene expression analysis was also performed using RT-qPCR to investigate the regulation of key tenogenic markers.

6.4.1.1 Immunofluorescence analysis

To confirm and quantify the expression of the tenogenic marker TNMD, immunofluorescence staining was performed, and mean fluorescence intensity (MFI) was measured across different media conditions under both atmospheric and physiological oxygen concentrations (Figure 6-1).

For TNMD expression under atmospheric oxygen, all experimental groups showed higher MFI than the control, with the strongest effect in the CTRL+GDF-5 group (1.4-fold vs CTRL, $p < 0.0001$). Static CM+GDF-5 and dynamic CM+GDF-5 were modestly upregulated relative to CTRL (1.1-fold, $p = 0.0123$; 1.2-fold, $p = 0.0002$, respectively), but both were significantly lower than CTRL+GDF-5 (1.2-fold, $p < 0.0001$).

At physiological oxygen, TNMD expression was also elevated compared to CTRL across all conditions. CTRL+GDF-5 and static CM+GDF-5 were 1.3-fold higher than CTRL ($p < 0.0001$), while dynamic CM+GDF-5 was 1.2-fold higher ($p < 0.0001$). No significant differences were observed between CM+GDF-5 groups and CTRL+GDF-5 at this oxygen level.

When comparing oxygen concentrations, TNMD expression tended to be higher at 2% O_2 in control and CM-treated groups. However, CTRL+GDF-5 at 21% O_2 remained the single highest condition overall.

The representative images (Figure 6-1) illustrate increased TNMD staining in all GDF-5-supplemented and CM+GDF-5 conditions compared with CTRL, in agreement with MFI quantification. Cells cultured under 2% O_2 appeared more elongated, particularly in CM+GDF-5 groups, suggesting that hypoxia enhances tenocyte-like morphology. Under 21% O_2, TNMD expression was dominated by the CTRL+GDF-5 condition, while CM+GDF-5 groups showed intermediate levels.

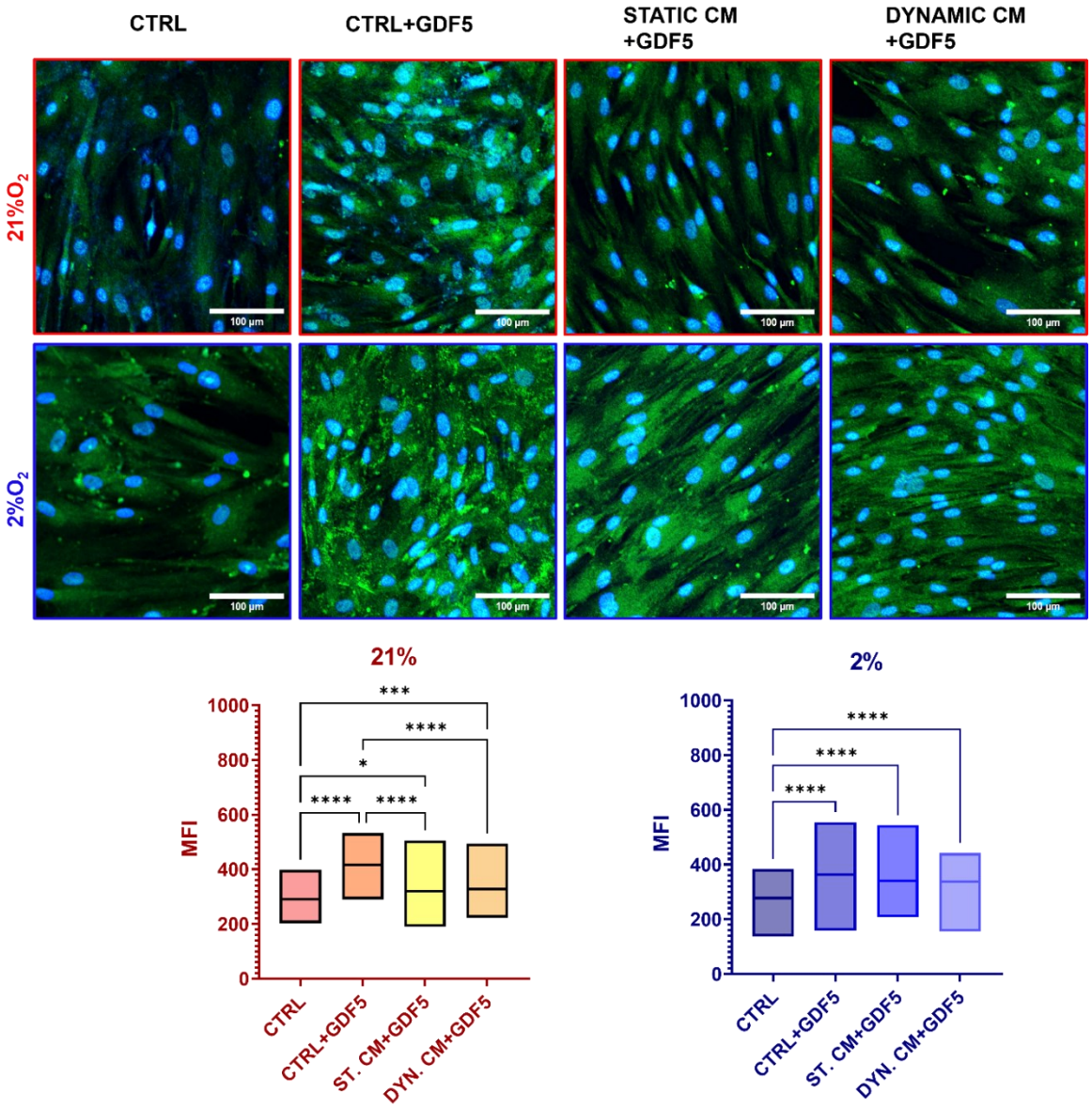


Figure 6-1. Immunofluorescence analysis of TNMD expression in hBM-MSCs cultured in 2D under different oxygen concentrations and media conditions. Representative images show TNMD (green) expression in hBM-MSCs cultured for 14 days under 21% O_2 and 2% O_2, with nuclei counterstained with DAPI. Scale bars = 100 µm. Box plots represent MFI across conditions: CTRL, CTRL+GDF5, ST.CM+GDF5, and DYN. CM+GDF5 in 21% O_2 and 2% O_2. Statistics: Kruskal–Wallis followed by Dunn's multiple comparisons within each oxygen level; '**' for $p < 0.01$, '***' for $p < 0.001$, and '****' for $p < 0.0001$, n=3.

The same analysis was performed for COL1 expression (Figure 6-2). Under atmospheric oxygen, both CM+GDF-5 groups exhibited higher MFI than the control, with static CM+GDF-5 and dynamic CM+GDF-5 being 1.3-fold higher (p = 0.0004 and p = 0.0002, respectively). No significant difference was detected between CTRL and CTRL+GDF-5. Compared to

CTRL+GDF-5, static CM+GDF-5 and dynamic CM+GDF-5 were modestly but significantly higher (1.21-fold, $p = 0.0017$; and 1.24-fold, $p = 0.0007$, respectively).

Under physiological oxygen, all samples showed higher MFI than the control, with CTRL+GDF-5 being 1.4-fold higher ($p < 0.0001$), static CM+GDF-5 being 1.3-fold higher ($p < 0.0001$), and dynamic CM+GDF-5 being 1.2-fold higher ($p = 0.0104$). No significant differences were observed between the CM+GDF-5 groups.

When comparing oxygen conditions, COL1 expression was generally higher under 2% O_2, except for dynamic CM+GDF-5, which displayed greater expression under 21% O_2. The representative images confirm these quantitative results, showing increased COL1 fluorescence in all GDF-5-supplemented and CM+GDF-5 conditions compared with CTRL. Under 21% O_2, the strongest staining was observed in static and dynamic CM+GDF-5, while under 2% O_2, COL1 expression was particularly pronounced in CTRL+GDF-5 and static CM+GDF-5. This indicates that GDF-5 alone, as well as CM in combination with GDF-5, contributed to collagen synthesis, and that hypoxia further enhanced this effect across most conditions. Notably, CM was tested only in combination with GDF-5 in this experiment; therefore, the observed effects should be interpreted as a modulation of the GDF-5 response by secretome-derived factors.

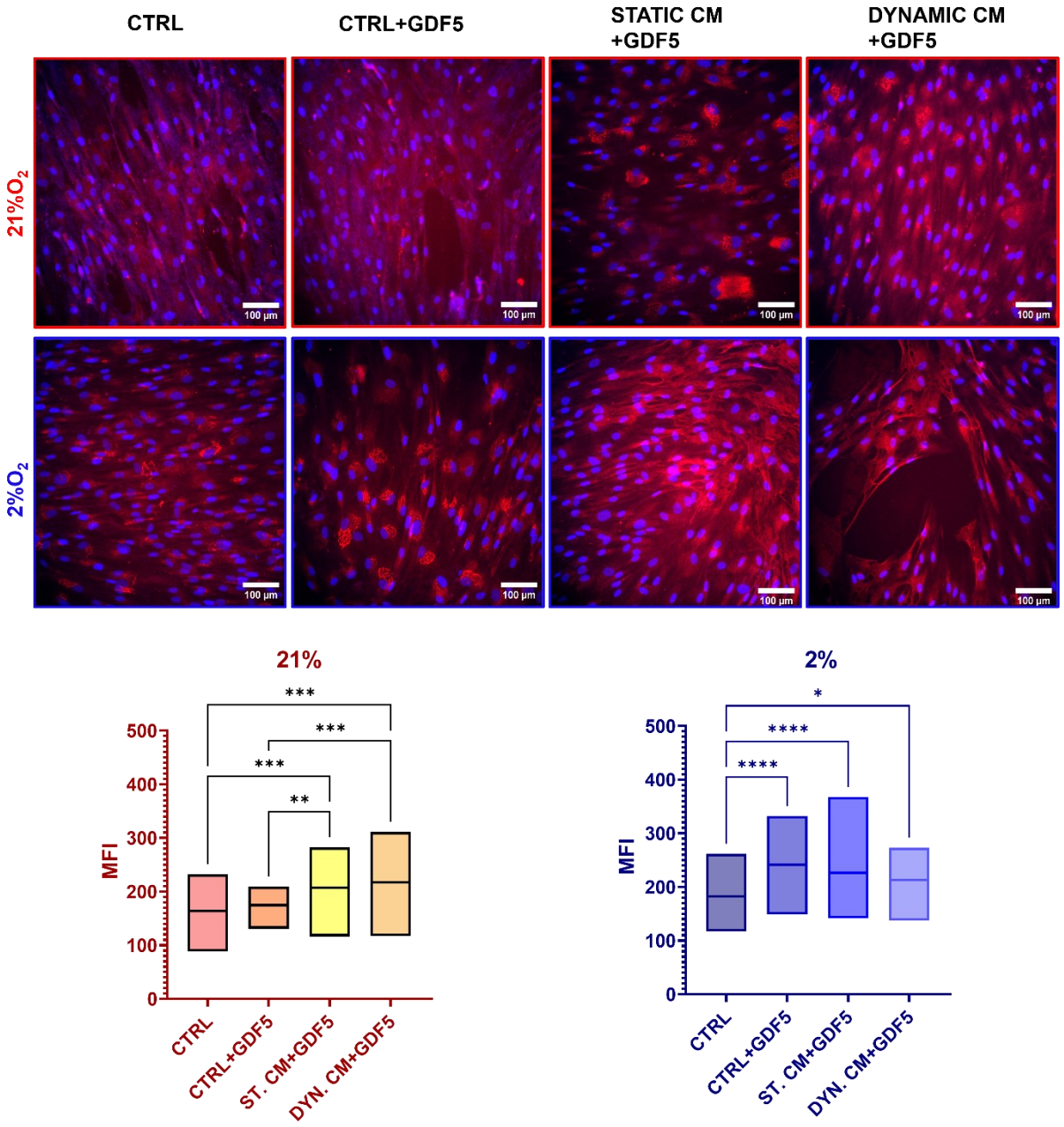


Figure 6-2. Immunofluorescence analysis of COL1 expression in hBM-MSCs cultured in 2D under different oxygen concentrations and media conditions. Representative images show COL1 (red) expression in hBM-MSCs cultured for 14 days under 21% O_2 and 2% O_2, with nuclei counterstained with DAPI. Scale bars = 100 µm. Box plots represent MFI across conditions: CTRL, CTRL+GDF5, ST.CM+GDF5, and DYN. CM+GDF5 in 21% O_2 and 2% O_2. Statistics: Kruskal–Wallis followed by Dunn's multiple comparisons within each oxygen level; '*' for $p < 0.05$, '**' for $p < 0.01$, '***' for $p < 0.001$, and '****' for $p < 0.0001$, n=3.

6.4.1.2 Nuclei aspect ratio

The nuclei aspect ratio of hBM-MSCs was analysed to assess the influence of GDF-5 and CM supplementation on nuclear elongation. A value closer to 1.0 corresponds to rounded nuclei, whereas values below 0.1 indicate entirely elongated nuclei[357].

Under atmospheric oxygen, all experimental groups exhibited significantly lower nuclei aspect ratio values than the control. Specifically, CTRL+GDF-5 and static CM+GDF-5 were 1.3-fold lower ($p < 0.0001$), while dynamic CM+GDF-5 was 1.2-fold lower ($p < 0.0001$) (Figure 6-3A). However, a significant difference was detected between the CM-treated samples, with static CM+GDF-5 showing a 1.1-fold higher aspect ratio than dynamic CM+GDF-5 ($p = 0.0062$).

As shown in Figure 6-3B, the frequency distribution of nuclei aspect ratio values revealed that in the control group, over 51% of nuclei had an aspect ratio above 0.7. In the CTRL+GDF-5, static CM+GDF-5, and dynamic CM+GDF-5 groups, 72.5%, 67.5%, and 55.7% of the nuclei, respectively, had aspect ratios ranging from 0.3 to 0.5.

A similar trend was observed under physiological oxygen, where all GDF-5- and CM-treated samples displayed significantly lower nuclei aspect ratio values than the control. Specifically, CTRL+GDF-5 was 1.12-fold lower ($p = 0.0026$), static CM+GDF-5 was 1.05-fold lower ($p = 0.0185$), and dynamic CM+GDF-5 was 1.06-fold lower ($p = 0.0147$). A significant difference was observed between static CM+GDF-5 and CTRL+GDF-5, with static CM+GDF-5 being 1.06-fold higher ($p = 0.0268$) (Figure 6-3C).

The frequency distribution in Figure 6-3D showed that in the control group, more than 86% of nuclei had aspect ratios above 0.5. In the CTRL+GDF-5, static CM+GDF-5, and dynamic CM+GDF-5 groups, 78%, 68%, and 67% of nuclei, respectively, had aspect ratios between 0.3 and 0.5, consistent with elongation induced by the respective treatments.

To further assess the role of oxygen tension in modulating nuclear morphology, a direct comparison of nuclei aspect ratios between 21% and 2% O_2 was conducted across all treatment groups (Figure 6-3E). Although differences were modest, physiological oxygen

generally induced lower aspect ratio values compared to atmospheric oxygen. This effect was particularly evident in the CTRL group, where the aspect ratio was 1.2-fold lower under 2% O_2 ($p < 0.0001$), and in the dynamic CM+GDF-5 group, where it was 1.1-fold lower ($p = 0.0087$). These findings suggest that hypoxia may further enhance nuclear elongation in combination with biochemical and mechanical cues.

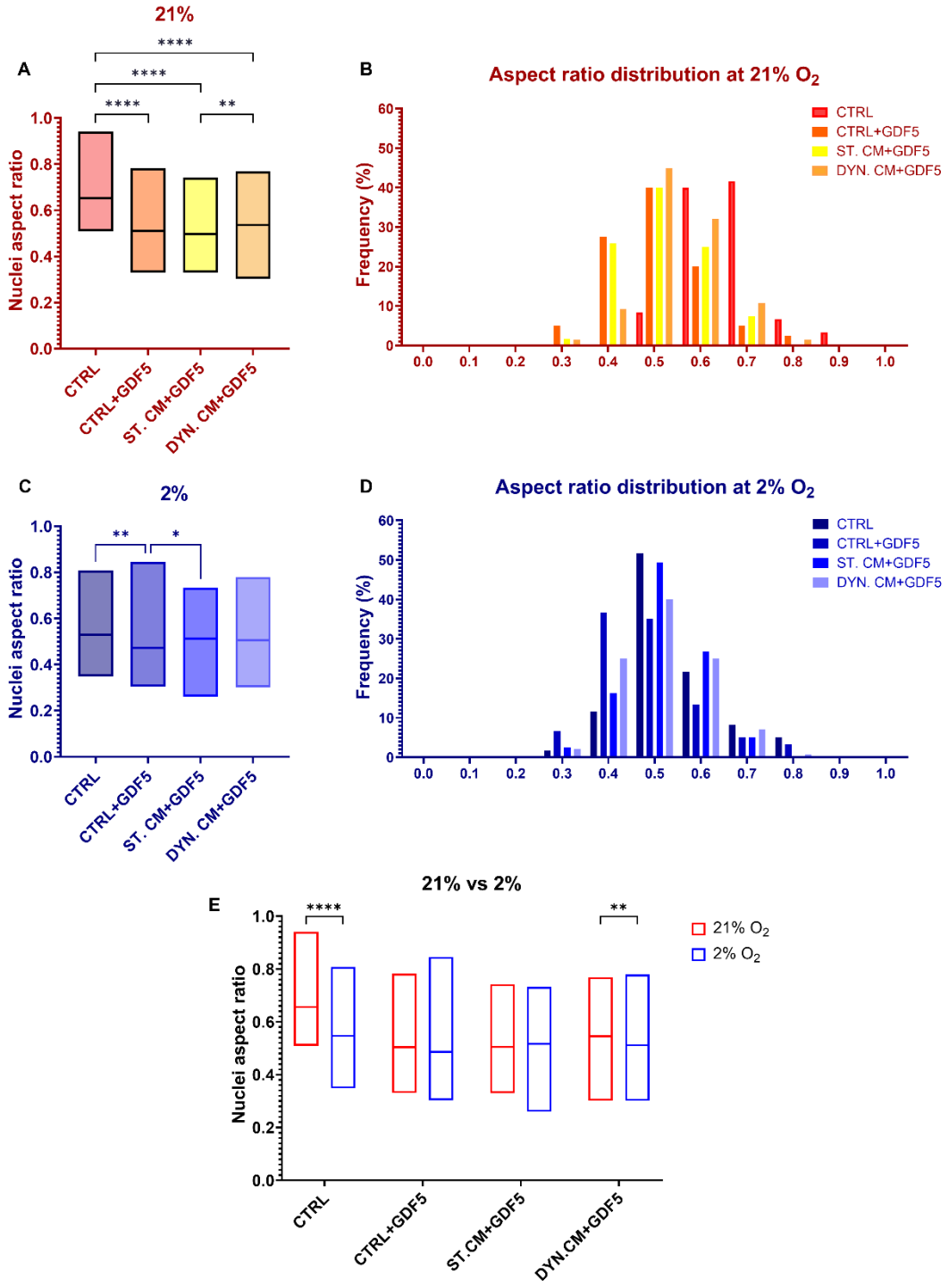


Figure 6-3. Nuclei aspect ratio analysis of hBM-MSCs cultured in 2D under different oxygen concentrations and media conditions. Box plots show the nuclei aspect ratio of hBM-MSCs cultured for 14 days under 21% O_2 (A) and 2% O_2 (C) across conditions: CTRL, CTRL+GDF5, ST.CM+GDF5, and DYN.CM+GDF5. Frequency distribution histograms illustrate the percentage of nuclei within different aspect ratio distribution at 21% O_2 (B) and 2% O_2 (D). Comparison of nuclei aspect ratios between 21% and 2% O_2 for each treatment group (E). Statistical analysis: Kruskal–Wallis test with Dunn's multiple comparisons for A–D; two-way ANOVA followed by Sidak's multiple comparisons test for E; '*' for $p < 0.05$, '**' for $p < 0.01$, '***' for $p < 0.001$, and '****' for $p < 0.0001$, n=3.

6.4.1.3 Histological analysis

Picro-Sirius Red staining was performed to evaluate collagen deposition and ECM organisation in hBM-MSCs cultured for 14 days under different media conditions and oxygen concentrations. As shown in Figure 6-4, distinct differences in collagen staining intensity and distribution were observed across conditions.

Under atmospheric oxygen, CTRL and CTRL+GDF-5 samples displayed a more fibrous ECM organisation, with collagen staining distributed homogeneously throughout the monolayer. In CTRL+GDF-5, an increase in collagen deposition was evident, suggesting that GDF-5 supplementation promoted ECM remodelling. The CM-treated groups (static and dynamic CM+GDF-5) exhibited an enhanced collagen network, with more intensely stained regions, particularly in the dynamic CM+GDF-5 group, indicating an increased fibrillar collagen deposition.

Under physiological oxygen, collagen deposition was generally more uniform across all conditions. The CTRL showed weaker staining, indicating lower collagen production. In contrast, CTRL+GDF-5, static CM+GDF-5, and dynamic CM+GDF-5 groups exhibited stronger collagen staining, suggesting that both GDF-5 supplementation and CM treatment enhanced ECM deposition. Interestingly, dynamic CM+GDF-5 samples exhibited a denser collagen network than their static counterparts, a trend similar to that observed under 21% O_2, which reinforces the role of mechanical stimuli in ECM organisation.

Comparing oxygen conditions, collagen deposition appeared more intense in 21% O_2, particularly in CM-treated groups, indicating oxygen availability influences ECM remodelling.

At 2% O_2, collagen staining patterns appeared more uniform and less fibrillar than at 21% O_2. These qualitative observations suggest that oxygen tension may modulate ECM organisation; however, quantitative image analysis was not performed in this study and should be included in future work to confirm these trends.

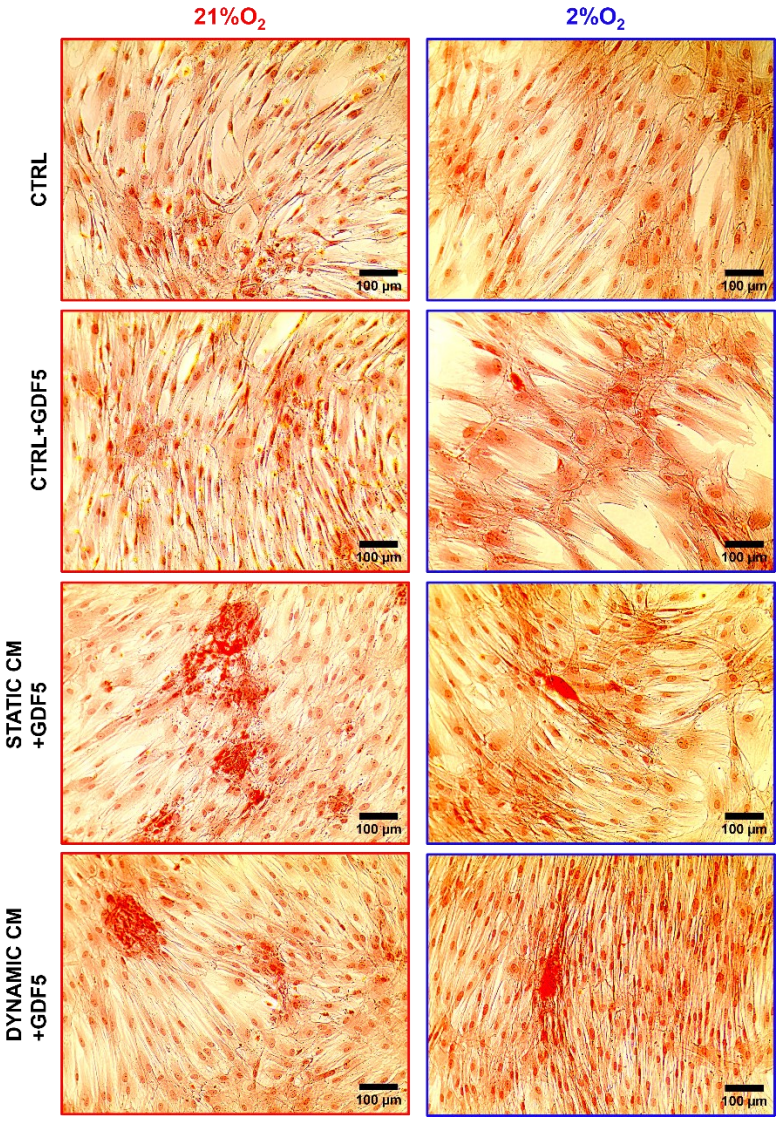


Figure 6-4. Picro-Sirius Red staining of collagen deposition in hBM-MSCs cultured in 2D under different oxygen concentrations and media conditions. Representative images show the distribution of collagen in hBM-MSCs cultured in standard culture medium (CTRL), CTRL+GDF5, static CM+GDF5, and dynamic CM+GDF5, under 21% O_2 and 2% O_2. Scale bar: 100 µm.

6.4.1.4 Gene expression

RT-qPCR was performed to assess the expression of key tenogenic markers: *SCX*, *MKX*, *TNMD*, *COL1A2*, and *COL3A1*. Gene expression was normalised to the housekeeping gene *YWHAZ* and presented as fold-changes relative to the control at day 0.

SCX expression increased in all conditions after 14 days. Under 21% O_2, upregulation was observed in GDF-5- and CM-treated samples, with the strongest effect in static CM+GDF-5 (1.6-fold vs CTRL). However, statistical significance was detected only under 2% O_2, where both static and dynamic CM+GDF-5 showed robust increases compared to CTRL (3.1-fold, $p = 0.0053$; $p = 0.0016$) and CTRL+GDF-5 (3.6-fold, $p = 0.0009$; $p = 0.0002$) (Figure 6-5A).

MKX expression showed distinct oxygen-dependent trends. In 21% O_2, CTRL+GDF-5 and dynamic CM+GDF-5 were elevated compared to CTRL, but both CM conditions were significantly lower than CTRL+GDF-5 (2.8-fold and 2.4-fold decreases, $p = 0.0043$ and $p = 0.0022$). Conversely, under 2% O_2, CM treatments were strongly upregulated, with static and dynamic CM+GDF-5 showing 10.4-fold and 6.4-fold increases over CTRL ($p < 0.0001$), and 3.4-fold and 2.1-fold increases over CTRL+GDF-5 ($p < 0.0001$, $p = 0.0016$). CTRL+GDF-5 also showed a moderate 3-fold increase vs CTRL ($p = 0.0996$) (Figure 6-5B).

TNMD expression was upregulated in all conditions relative to day 0. In 21% O_2, the strong CTRL response limited inter-group differences, with significance detected only between CTRL and CTRL+GDF-5 (1.9-fold, $p = 0.$ 0.0200). By contrast, under 2% O_2, all treatments showed marked increases compared to CTRL: CTRL+GDF-5 (6.2-fold), static CM+GDF-5 (7.1-fold), and dynamic CM+GDF-5 (11.4-fold), all $p < 0.0001$. Dynamic CM+GDF-5 was further elevated relative to CTRL+GDF-5 (1.8-fold, $p = 0.0263$) (Figure 6-5C).

COL1A2 expression followed divergent patterns. In 21% O_2, all groups were upregulated, with CTRL+GDF-5 showing the highest expression (4.9-fold vs CTRL, $p = 00.0171$). In 2% O_2, however, CTRL was dominant, showing 5.5-fold and 8.4-fold higher expression than static and

dynamic CM+GDF-5 ($p = 0.0004$ and $p < 0.0001$), while CTRL+GDF-5 was also elevated (4-fold and 6.1-fold higher vs CM-treated groups, $p = 0.0025$ and $p = 0.0004$) (Figure 6-5D).

COL3A1 expression was broadly upregulated under both oxygen conditions. In 21% O_2, CTRL+GDF-5 and static CM+GDF-5 showed higher expression than CTRL, while dynamic CM+GDF-5 displayed a similar trend without additional effect. In 2% O_2, all groups exhibited increased *COL3A1* expression compared to CTRL, but no significant differences were detected among treatments (Figure 6-5E).

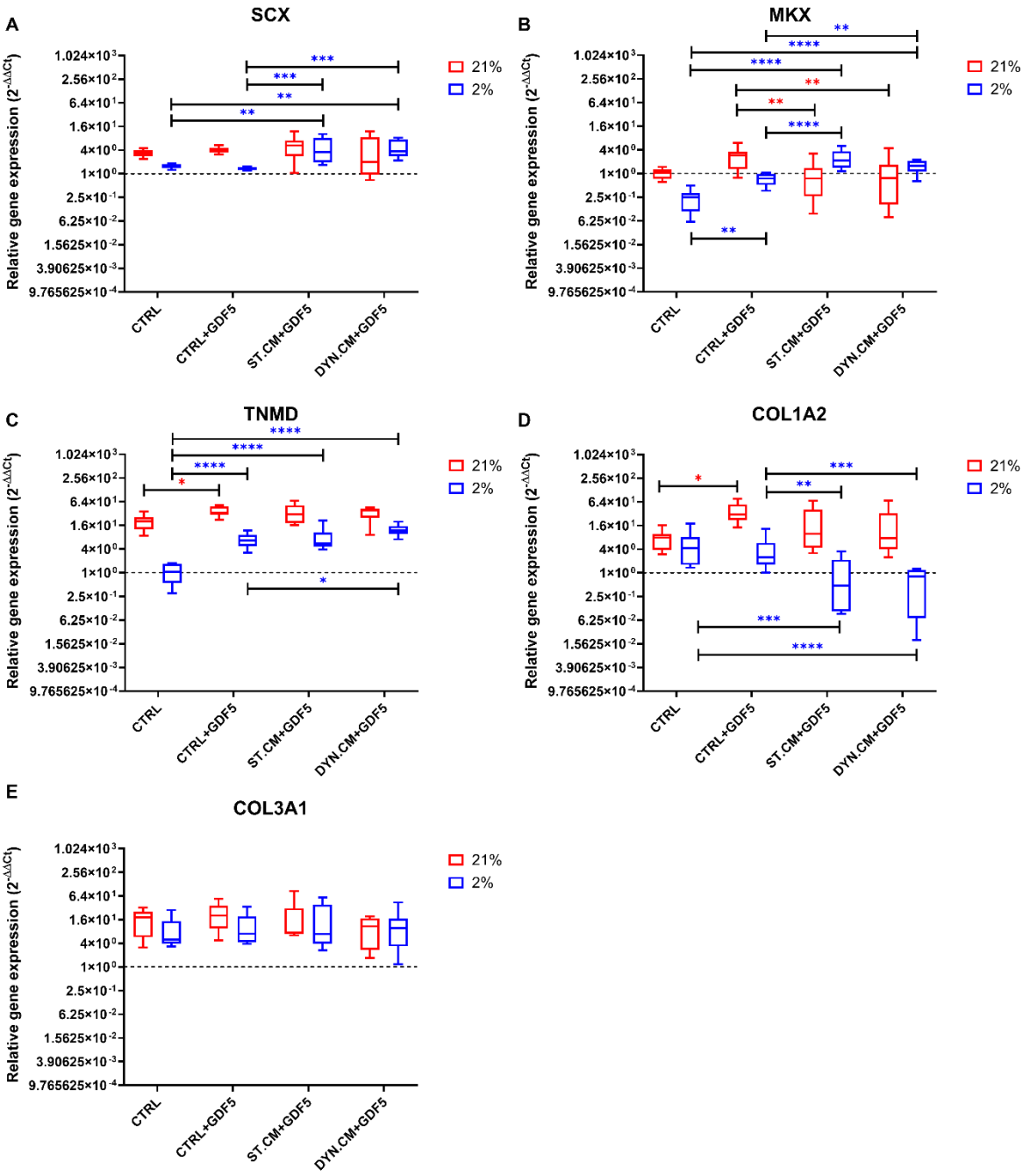


Figure 6-5. Gene expression of tenogenic markers in hBM-MSCs cultured in 2D for 14 days under different oxygen concentrations and media conditions. RT-qPCR analysis of (A) *SCX*, (B) *MKX*, (C) *TNMD*, (D) *COL1A2* and (E) *COL3A1* expression in hBM-MSCs cultured in standard culture medium (CTRL), CTRL supplemented with GDF-5 (CTRL+GDF5), conditioned medium (CM), derived from either static or dynamic culture, supplemented with GDF-5 (static or dynamic CM+GDF5) under 21% and 2% oxygen conditions. Gene expression levels are presented as fold changes relative to the control at day 0 and normalised to *YWHAZ*. Statistical analysis: two-way ANOVA followed by Tukey's multiple comparisons test across all treatment groups, within each oxygen level; '*' for $p < 0.05$, '**' for $p < 0.01$, '***' for $p < 0.001$, and '****' for $p < 0.0001$, n=3.

6.4.2 3D culture: hBM-MSCs embedded with cEVs and cultured in hTSPCs-CM

For all 3D experiments, collagen scaffolds contained hBM-MSCs embedded together with cEVs (final EV protein concentration: 1 µg/mL). Scaffolds were maintained in standard medium (±100 ng/mL GDF-5) or in hTSPC-derived CM from static or dynamic cultures (all CM groups supplemented with 100 ng/mL GDF-5).

To evaluate the effects of these conditions, a Live/Dead assay was performed to assess cell viability through semi-quantitative analysis. TNMD expression was analysed using immunofluorescence, while morphological changes were evaluated by measuring the nuclear aspect ratio. Gene expression analysis was also conducted using RT-qPCR to determine the impact of different culture conditions on tenogenic differentiation.

6.4.2.1 Live/Dead assay

After 1 day of culture, L/D staining revealed high cell viability in both oxygen conditions when cells were cultured in a standard medium. Despite the same initial seeding density, cells cultured under physiological oxygen exhibited faster growth, resulting in denser scaffolds compared to those cultured under atmospheric oxygen (Figure 6-6A). L/D quantification confirmed viability above 80% in both conditions, with no significant differences detected (Figure 6-6B).

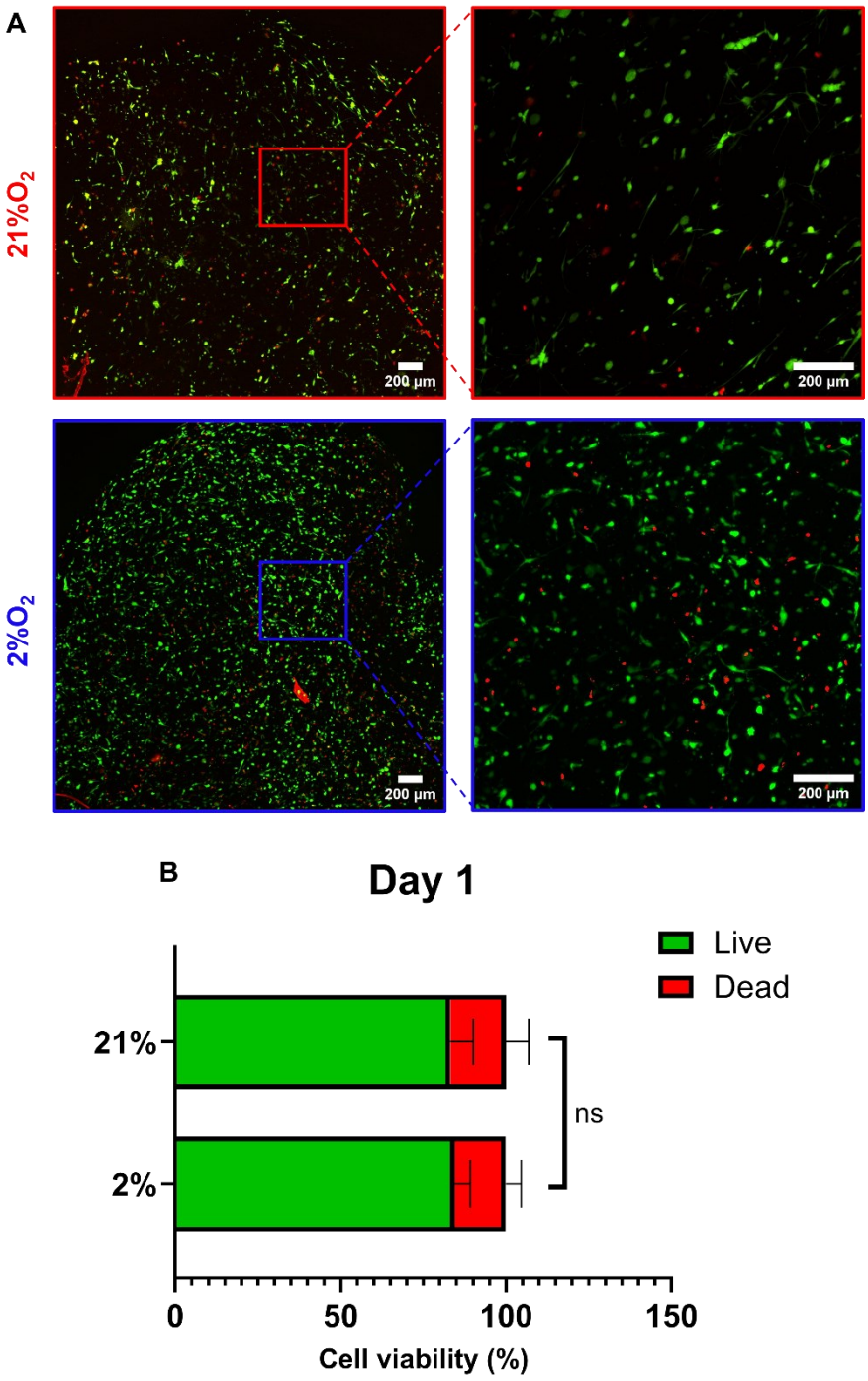


Figure 6-6. L/D assay at day 1 for hBM-MSCs embedded in collagen scaffolds with cEVs under different oxygen concentrations and media conditions. (A) Representative confocal fluorescence images show live (green) and dead (red) cells cultured in 21% O_2 and 2% O_2. Magnified insets highlight cell morphology and viability. (B) Quantification of cell viability (%) confirms high survival rates in both conditions. Scale bars = 200 µm. All 3D scaffolds contained cells and cEVs (1 µg/mL). Statistical analysis: Mann–Whitney test; no significant differences were detected, n=3.

After 14 days of culture, L/D staining confirmed high cell viability across all conditions, with CM-treated samples forming denser cellular layers compared to controls. In both 21% O_2 and 2% O_2, cells established well-distributed networks, particularly in CM groups, suggesting that hTSPC-derived factors support cell proliferation and matrix organisation. Although differences between oxygen conditions were observed at early time points, by day 14 these became less evident. Under hypoxic conditions, cells exhibited a more elongated and aligned morphology, especially in CM-treated groups. In transverse scaffold sections, cell density appeared lower in the central regions. Given the uniform initial cell distribution, this likely reflects increased peripheral proliferation and potentially outward migration from the core, possibly due to nutrient or oxygen gradients influencing cell behaviour (Figure 6-7A).

Quantification of cell viability showed >90% in CTRL and CTRL+GDF-5 groups under 21% O_2. Viability remained high in dynamic CM+GDF-5 (85%) and static CM+GDF-5 (82%), though both were significantly lower than CTRL ($p = 0.0493$). Under 2% O_2, slightly lower values were observed across all conditions, with CTRL and CTRL+GDF-5 reaching 81%, static CM+GDF-5 at 82%, and dynamic CM+GDF-5 at 78% (Figure 6-7B).

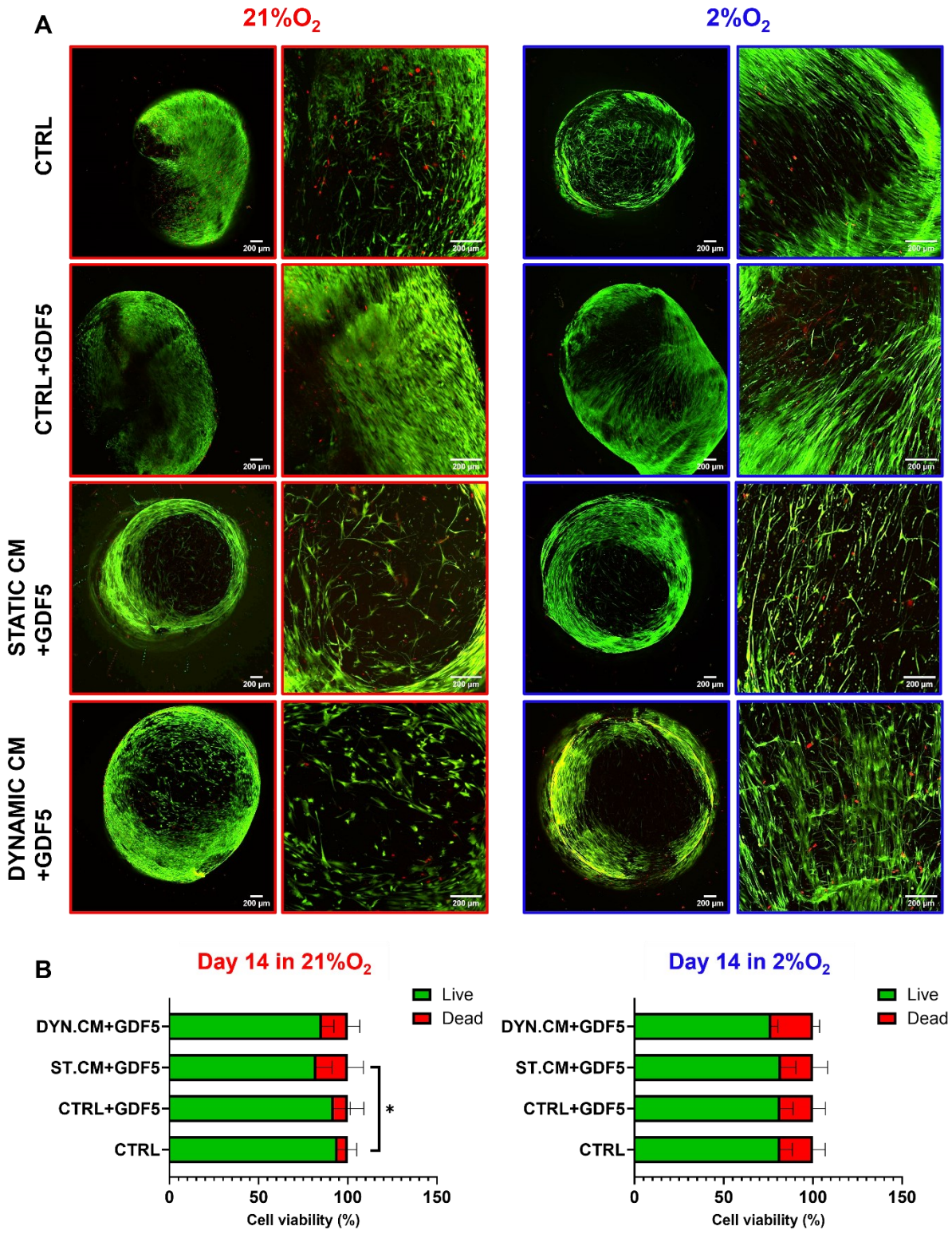


Figure 6-7. L/D assay at day 14 for hBM-MSCs embedded in collagen scaffolds with cEVs under different oxygen concentrations and media conditions. (A) Representative confocal fluorescence images show live (green) and dead (red) cells cultured in 21% O_2 and 2% O_2. Images were obtained from transverse sections of cut scaffolds. (B) Quantification of cell viability (%) demonstrates sustained survival across all conditions. Scale bars = 200 µm. All 3D scaffolds contained cells plus crude EVs (1 µg/mL). Statistical analysis: two-way ANOVA followed by Tukey's multiple comparisons test; '*' for $p < 0.05$, n=3.

6.4.2.2 Collagen gel contraction

Collagen gel contraction was monitored at three time points: day 0, day 3, and day 14. Gels were prepared with a seeding density of 10^5 cells/mL, following the method previously described by Lomas et al[282]. Significant contraction was observed in all conditions, particularly in the control sample, as early as day 3.

Under atmospheric oxygen, by day 3, CTRL gels exhibited a 55.1% reduction in length compared to their initial size, whereas CTRL+GDF5 showed only a 19.6% decrease. ST.CM+GDF5 and DYN.CM+GDF5 contracted by 25.5% and 26.5%, respectively (Figure 6-8A). Statistical analysis confirmed that both CM-treated groups contracted significantly less than CTRL (2.3-fold; $p < 0.0001$ and $p = 0.0043$) and CTRL+GDF5 (1.8-fold; $p = 0.0002$ and $p = 0.0169$) (Figure 6-8C). By day 14, further contraction was observed across all groups, with CTRL and DYN.CM+GDF5 showing the greatest reductions (69.6% and 62.7%, respectively), while CTRL+GDF5 and ST.CM+GDF5 contracted by 58.9% and 55.1% (Figure 6-8A). Both CM-treated groups remained significantly less contracted than CTRL and CTRL+GDF5: ST.CM+GDF5 was 1.65-fold longer than CTRL ($p = 0.0043$) and 1.7-fold longer than CTRL+GDF5 ($p = 0.0114$), while DYN.CM+GDF5 was 1.7-fold longer than CTRL ($p = 0.0045$) and 1.8-fold longer than CTRL+GDF5 ($p = 0.0083$) (Figure 6-8C).

Under physiological oxygen, by day 3, CTRL gels contracted by 48.5% and CTRL+GDF5 by 54.1%. ST.CM+GDF5 and DYN.CM+GDF5 showed smaller reductions of 27.3% and 40.1% (Figure 6-8B). ST.CM+GDF5 remained significantly longer than CTRL (2-fold; $p = 0.0034$) and CTRL+GDF5 (1.7-fold; $p = 0.0378$), while DYN.CM+GDF5 was 1.8-fold longer than CTRL ($p = 0.0158$) (Figure 6-8D). By day 14, CTRL and CTRL+GDF5 showed the greatest contraction (79.3%), while ST.CM+GDF5 and DYN.CM+GDF5 reduced by 68.1% and 74.1% (Figure 6-8B). At this timepoint, no statistically significant differences were detected (Figure 6-8D).

Despite identical seeding densities, gels cultured at 2% O_2 exhibited greater early contraction (day 3) than those at 21% O_2, likely reflecting higher proliferation rates observed in Live/Dead staining. By day 14, contraction progressed in all groups, and while overall gel size converged,

CM-treated gels remained consistently less contracted than CTRL and CTRL+GDF5. At this stage, all samples cultured at 2% O_2 were approximately 1.5-fold more contracted than their counterparts at 21% O_2.

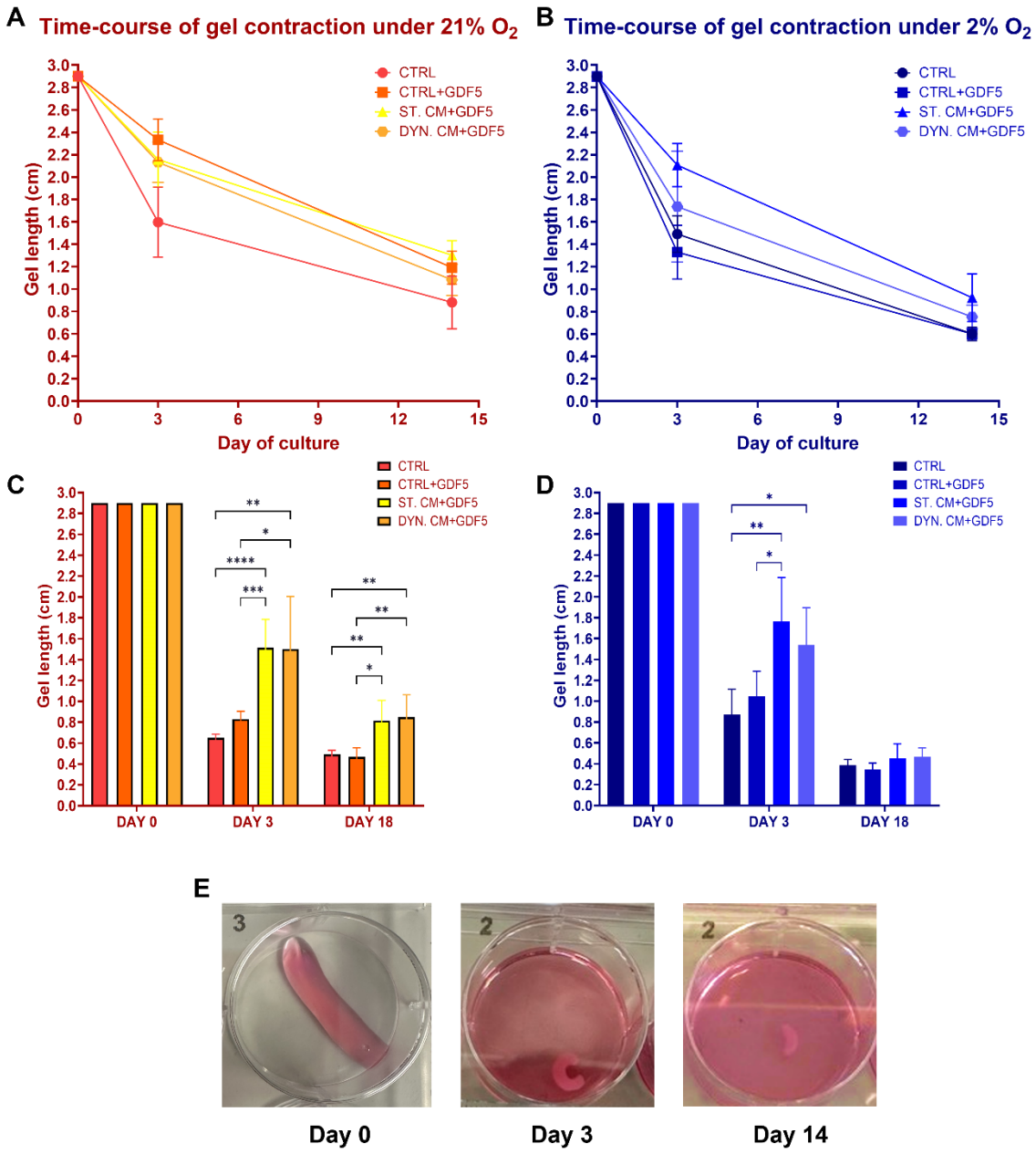


Figure 6-8. Collagen gel contraction over time under different oxygen concentrations and media conditions. (A–B) Time-course of gel length (cm) at days 0, 3, and 14 for hBM-MSC-seeded collagen gels cultured in 21% O_2 (A) and 2% O_2 (B). Conditions included standard medium (CTRL), CTRL supplemented with GDF-5 (CTRL+GDF5), and hTSPC-derived conditioned medium from static or dynamic cultures supplemented with GDF-5 (static CM+GDF5, dynamic CM+GDF5). (C–D) Bar graphs comparing gel length across conditions at each time point in 21% O_2 (C) and 2% O_2 (D). (E) Representative macroscopic images of gels at days 0, 3, and 14, illustrating visible matrix contraction. Images are illustrative and do not include all conditions. All gels contained hBM-MSCs embedded with

crude EVs (1 µg/mL). Statistical significance was determined by repeated-measures two-way ANOVA followed by Tukey's multiple comparisons test; '*' for $p < 0.05$, '**' for $p < 0.01$, '***' for $p < 0.001$, and '****' for $p < 0.0001$, n=3.

6.4.2.3 Immunofluorescence analysis of TNMD

To confirm and quantify the expression of the tenogenic marker TNMD, IF staining was performed, and the MFI was measured across different media conditions under both atmospheric and physiological oxygen concentrations (Figure 6-9).

Under atmospheric oxygen, no significant differences were observed between CTRL and CTRL+GDF-5. However, both CM-treated samples showed significantly higher MFI than the CTRL, with static CM+GDF-5 and dynamic CM+GDF-5 being 1.7-fold and 2.1-fold higher, respectively ($p < 0.0001$). Compared to CTRL+GDF-5, static CM+GDF-5 and dynamic CM+GDF-5 exhibited 1.3-fold ($p = 0.0107$) and 1.6-fold ($p < 0.0001$) higher MFI, respectively.

Under physiological oxygen, all conditions exhibited significantly higher TNMD expression than the CTRL, with CTRL+GDF-5 showing a 3-fold increase, while static CM+GDF-5 and dynamic CM+GDF-5 were both 3.7-fold higher (all $p < 0.0001$).

When comparing oxygen conditions, TNMD MFI was generally higher in GDF-5- and CM-treated samples under physiological oxygen, whereas in the untreated control sample, TNMD expression was higher in atmospheric oxygen.

The immunofluorescence images in Figure 6-9 visually support the quantified TNMD expression, showing increased staining intensity in CM-treated samples compared to the control. Under atmospheric oxygen, TNMD expression was highest in dynamic CM+GDF-5, aligning with the observed MFI data. In physiological oxygen, TNMD expression was further enhanced in CM-treated samples, characterised by stronger fluorescence intensity and more aligned cell morphology, which reinforces the role of hypoxia in promoting tenogenic differentiation. These findings complement the quantitative results, demonstrating that CM and

oxygen modulation synergistically enhance TNMD expression and tendon-like cell organisation.

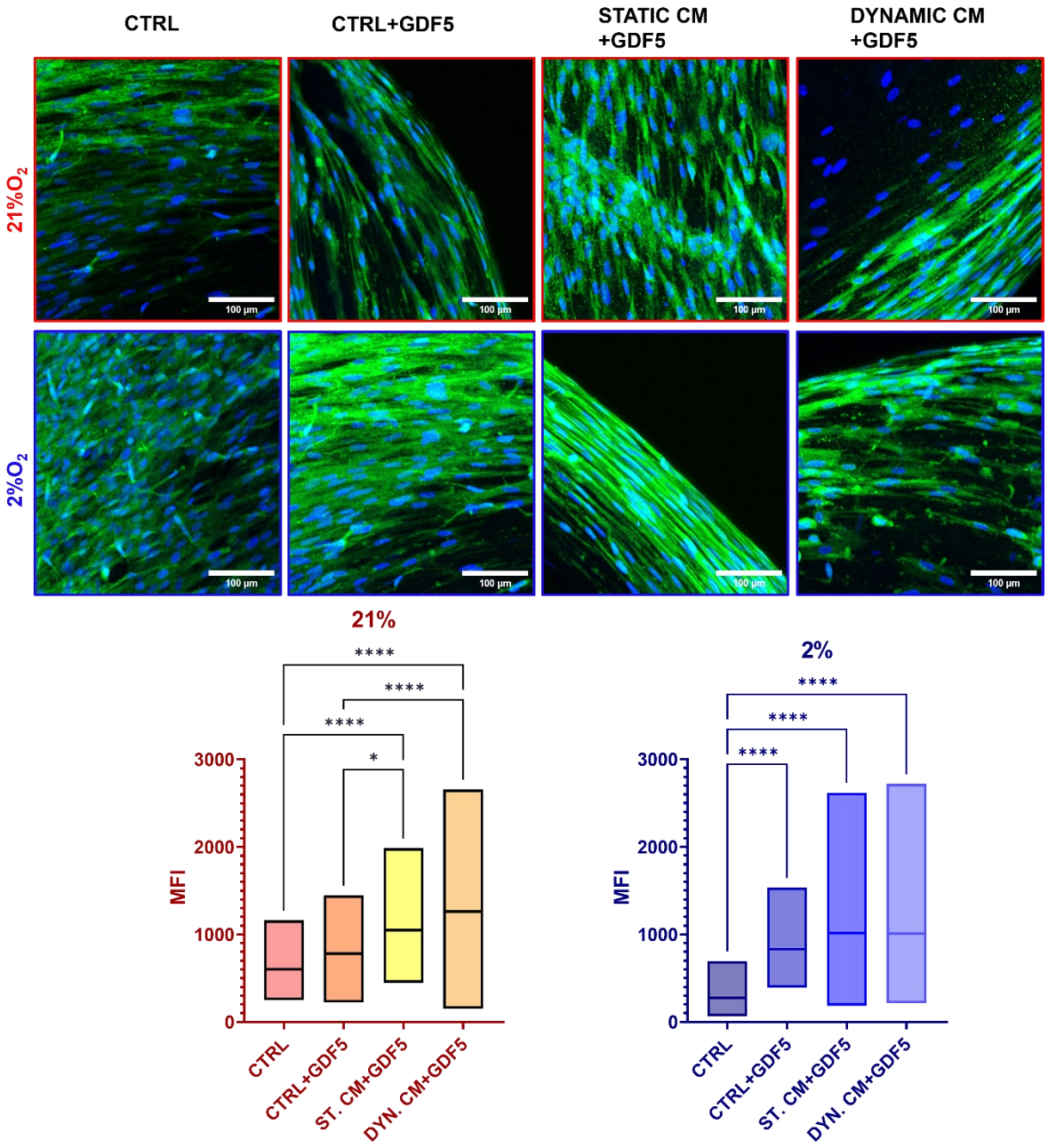


Figure 6-9. Immunofluorescence analysis of TNMD expression in hBM-MSCs cultured in 3D under different oxygen concentrations and media conditions. Representative immunofluorescence images show TNMD (green) expression in hBM-MSCs embedded in collagen scaffolds and cultured for 14 days under 21% O_2 and 2% O_2. Nuclei are counterstained with DAPI. Scale bars = 100 µm. Box plots represent MFI across CTRL, CTRL+GDF5, and ST.CM+GDF5, and DYN.CM+GDF5 in 21% O_2 and 2% O_2. All scaffolds contained hBM-MSCs embedded with cEVs (1 µg/mL). Statistical significance was determined by the Kruskal–Wallis test followed by Dunn's multiple comparisons test; '*' for $p < 0.05$, '**' for $p < 0.01$, '***' for $p < 0.001$, and '****' for $p < 0.0001$, n=3.

6.4.2.4 Nuclei aspect ratio

As in the 2D culture, the nuclei aspect ratio of hBM-MSCs was analysed to assess the influence of GDF-5 and CM supplementation on nuclear elongation.

Under atmospheric oxygen, all experimental groups exhibited lower nuclei aspect ratio values than the control. The most significant differences were observed in dynamic CM+GDF-5, which was 1.2-fold lower than both CTRL and static CM+GDF-5 ($p < 0.0001$) (Figure 6-10A).

As shown in Figure 6-10B, the frequency distribution of nuclei aspect ratio values revealed that 65% of nuclei had an aspect ratio above 0.5 in the control group. Additionally, 50% of CTRL+GDF-5-treated nuclei, 37% of static CM+GDF-5-treated nuclei, and 63.4% of dynamic CM+GDF-5-treated nuclei had aspect ratios ranging between 0.2 and 0.4.

A similar trend was observed under physiological oxygen,where all GDF-5- and CM-treated samples displayed significantly lower nuclei aspect ratio values than the control. Specifically, CTRL+GDF-5 and static CM+GDF-5 were 1.4-fold lower ($p < 0.0001$), while dynamic CM+GDF-5 was 1.2-fold lower ($p = 0.0156$). A significant difference was also observed between dynamic CM+GDF-5 and both CTRL+GDF-5 and static CM+GDF-5, with dynamic CM+GDF-5 being 1.1-fold and 1.2-fold lower than them ($p = 0.0156$ and $p = 0.0004$, respectively) (Figure 6-10C).

The frequency distribution in Figure 6-10D showed that over 85% of nuclei aspect ratios in the control group were above 0.4. 60% of CTRL+GDF-5-treated nuclei, 55% of static CM+GDF-5-treated nuclei, and 32% of dynamic CM+GDF-5-treated nuclei had aspect ratios between 0.2 and 0.3, indicating greater elongation following treatment.

To further evaluate the influence of oxygen tension, direct comparisons were made between 21% and 2% O_2 for each treatment group (Figure 6-10E). Overall, physiological oxygen levels resulted in lower aspect ratio values across all conditions. This effect was particularly evident in the CTRL+GDF-5 and static CM+GDF-5 groups, where nuclei were 1.4-fold more elongated

under 2% O_2 ($p < 0.0001$), suggesting a synergistic role of hypoxia in modulating nuclear morphology.

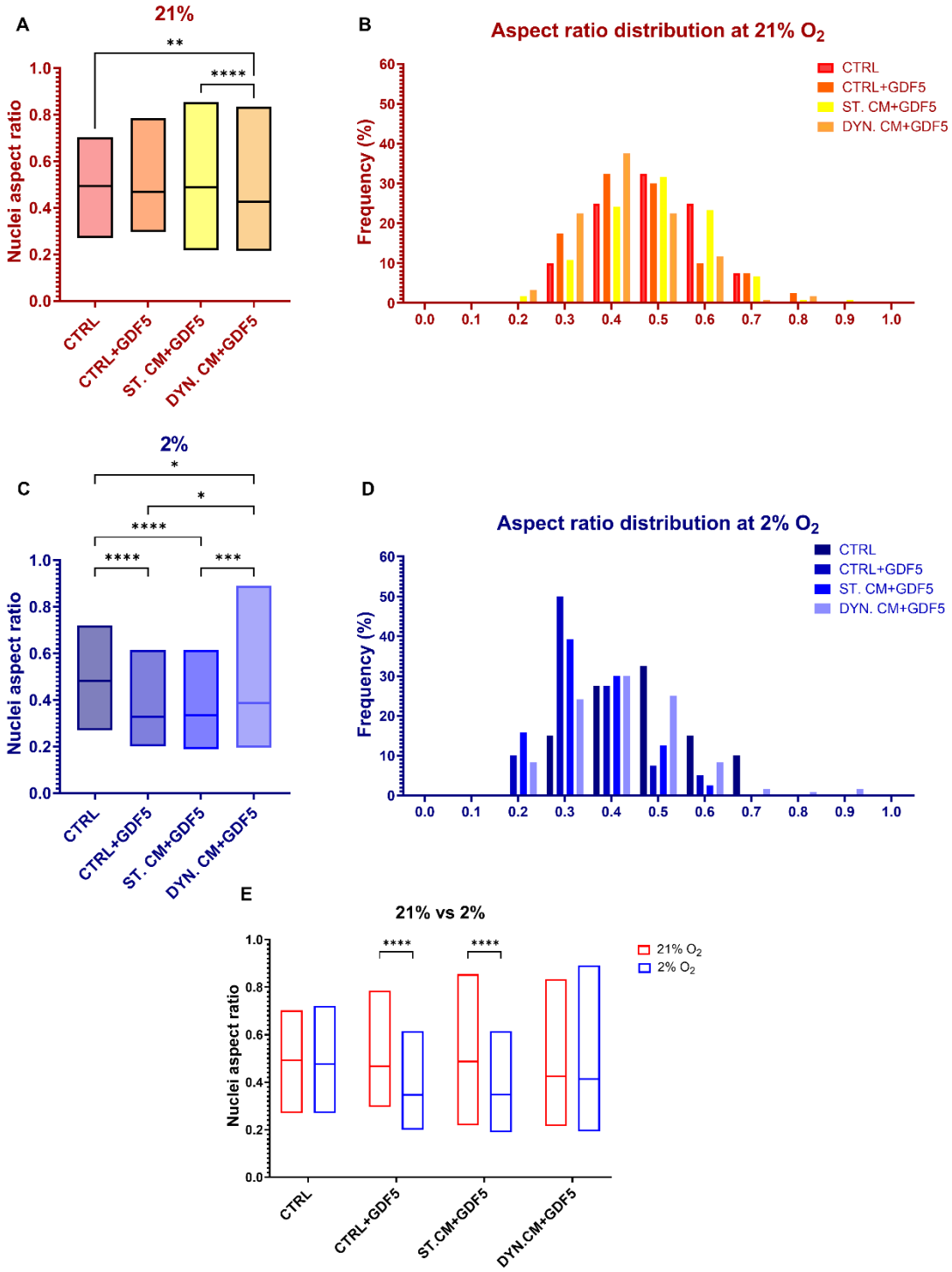


Figure 6-10. Nuclei aspect ratio analysis of hBM-MSCs cultured in 3D under different oxygen concentrations and media conditions. Box plots show the nuclei aspect ratio of hBM-MSCs cultured for 14 days under 21% O_2 (A) and 2% O_2 (C) across conditions: CTRL, CTRL+GDF5, ST.CM+GDF5, and DYN.CM+GDF5. Frequency distribution histograms illustrate aspect ratio distribution at 21% O_2 (B) and 2% O_2 (D). Comparison of nuclei aspect ratios between 21% and 2% O_2 for each treatment group

(E). All scaffolds contained hBM-MSCs embedded with cEVs (1 µg/mL). Statistical significance was determined by Kruskal–Wallis with Dunn's test (A, C) and two-way ANOVA with Sidak's test (E); '*' for $p < 0.05$, '**' for $p < 0.01$, '***' for $p < 0.001$, and '****' for $p < 0.0001$.

6.4.2.5 Gene expression

RT-qPCR was performed to assess the expression of key tenogenic markers, like *SCX*, *MKX*, *TNMD*, *COL1A2*, and *COL3A1*. Gene expression was normalised to the housekeeping gene *YWHAZ*, and results were expressed as fold-changes relative to the control sample at day 0, allowing for a comparative evaluation of the impact of different culture conditions over time.

SCX expression was upregulated in all samples under both oxygen conditions. Under 21% O_2, the highest expression was observed in CM-treated samples, with static CM+GDF-5 showing a 2.6-fold increase compared to CTRL, while dynamic CM+GDF-5 was 1.8-fold higher. However, no significant differences were measured. A similar trend was observed under 2% O_2, where CM-treated samples exhibited the highest *SCX* expression. Static CM+GDF-5 was 2.6-fold higher than CTRL ($p = 0.0292$) and 2.8-fold higher than CTRL+GDF-5 ($p = 0.0196$), while dynamic CM+GDF-5 was 2.9-fold ($p = 0.0464$) and 3.1-fold ($p = 0.0317$) higher than CTRL and CTRL+GDF-5, respectively (Figure 6-11A).

MKX expression was generally downregulated in most conditions. Under 21% O_2, the only upregulated sample was CTRL+GDF-5, which showed a 3.4-fold increase compared to CTRL ($p = 0.0013$), while CM-treated samples remained downregulated despite exhibiting higher expression than CTRL. Under 2% O_2, although GDF-5- and CM-treated samples were downregulated, their expression levels remained higher than those of CTRL (Figure 6-11B).

TNMD expression was upregulated across all conditions under both oxygen concentrations. Under 21% O_2, CTRL+GDF-5 was 3.5-fold higher than CTRL ($p = 0.0116$), while static CM+GDF-5 and dynamic CM+GDF-5 exhibited 2.4-fold and 2.5-fold increases, respectively. A similar trend was observed under 2% O_2, but CM-treated samples showed the highest expression levels, with static CM+GDF-5 being 2.6-fold higher than CTRL and 1.2-fold higher than CTRL+GDF-5. Dynamic CM+GDF-5 exhibited the strongest upregulation, with a 4.7-fold

increase compared to CTRL ($p = 0.0026$) and a 2.2-fold increase compared to CTRL+GDF-5 (Figure 6-11C).

COL1A2 expression was upregulated in all conditions, though CM-treated samples consistently showed lower expression than CTRL or CTRL+GDF-5 under both oxygen conditions. Under 21% O_2, CTRL+GDF-5 was the most upregulated sample, exhibiting a 5.5-fold increase compared to CTRL, a 17.9-fold increase compared to static CM+GDF-5 ($p < 0.0001$), and a 30.2-fold increase compared to dynamic CM+GDF-5 ($p < 0.0001$). Under 2% O_2, CTRL exhibited the highest expression, with a 2.3-fold increase compared to static CM+GDF-5 ($p = 0.0464$) and dynamic CM+GDF-5 (Figure 6-11D).

COL3A1 expression was upregulated across all conditions. Under 21% O_2, although no significant differences were observed, GDF-5- and CM-treated samples showed higher *COL3A1* expression than the control, with static CM+GDF-5 exhibiting the highest levels. Under 2% O_2, CM treatment appeared to be more effective than GDF-5 alone in promoting *COL3A1* expression, as both CM-treated samples showed higher expression than CTRL and CTRL+GDF-5. Dynamic CM+GDF-5 was significantly upregulated, with expression levels 1.5-fold higher than CTRL and 5.7-fold higher than CTRL+GDF-5 ($p = 0.0173$) (Figure 6-11E).

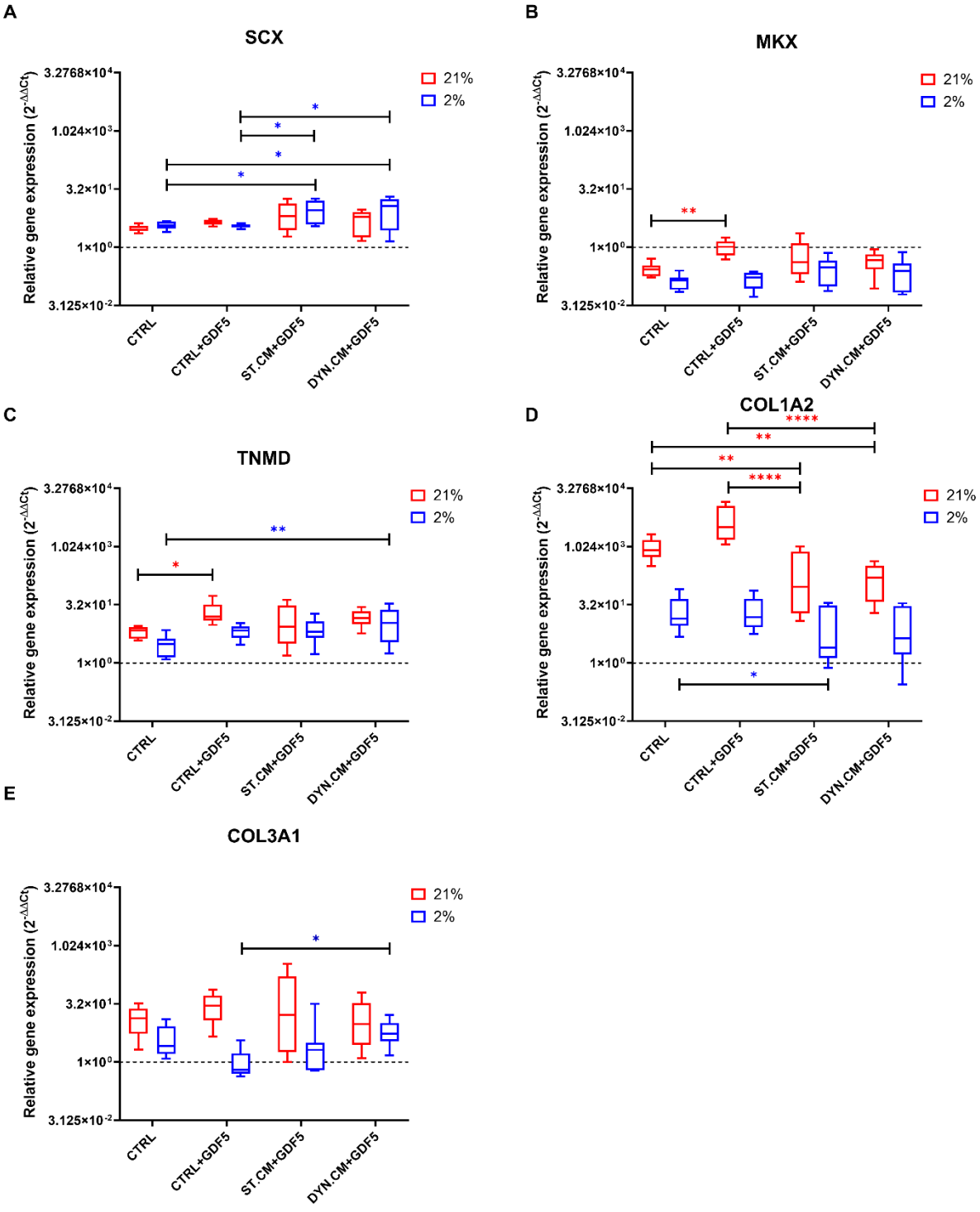


Figure 6-11. Gene expression of tenogenic markers in hBM-MSCs cultured in 3D for 14 days under different oxygen concentrations and media conditions. RT-qPCR analysis of (A) *SCX*, (B) *MKX*, (C) *TNMD*, (D) *COL1A2* and (E) *COL3A1* expression in hBM-MSCs cultured in standard culture medium (CTRL), CTRL supplemented with GDF-5 (CTRL+GDF5), conditioned medium (CM), derived from either static or dynamic culture, supplemented with GDF-5 (static or dynamic CM+GDF5) under 21% and 2% oxygen conditions. Gene expression levels are presented as fold changes relative to the control at day 0 and normalised to *YWHAZ*. All scaffolds contained hBM-MSCs embedded with cEVs (1 µg/mL). Statistical significance was determined by two-way ANOVA followed by Tukey's multiple

comparisons test, comparing all treatments within each oxygen level; '*' for $p < 0.05$, '**' for $p < 0.01$, '***' for $p < 0.001$, and '****' for $p < 0.0001$, n=3.

6.5 Discussion

This study builds upon our previous findings using porcine-derived CM and cEVs, where their tenogenic potential was demonstrated upon application in both porcine TSPCs and human bone marrow-MSCs. While the previous chapter confirmed the tenogenic effects of porcine-derived CM, the current study investigated whether human-derived CM and cEVs induce comparable or enhanced effects. By assessing tenogenic markers, morphological adaptations, ECM remodelling, and gene expression, this study explored the influence of oxygen concentration, dynamic culture conditions, and 2D versus 3D environments.

The evaluation of tenogenic commitment was first undertaken in a 2D environment, where IF analysis confirmed increased TNMD and COL1 expression under GDF-5 supplementation and CM+GDF-5 treatment (Figure 6-1 and 6-2). However, the extent of upregulation varied across treatment groups, oxygen concentrations, and culture conditions. The strongest TNMD expression was observed in the CTRL+GDF-5 group under both oxygen conditions, consistent with previous findings[189,195,196] and supporting GDF-5's established role in promoting tenogenesis, as also shown in Chapters 4 and 5. CM-treated groups (tested here only in combination with GDF-5) also displayed significant TNMD upregulation compared to the control, though at 21% O_2 their expression levels were lower than those of CTRL+GDF-5. This suggests that CM may act more as a modulator of the GDF-5 response, with its contribution being particularly evident under hypoxic conditions. The slightly higher TNMD expression in dynamic CM+GDF-5 compared to static CM+GDF-5 supports the idea that mechanical stimulation of hTSPCs enhances the release of bioactive factors, and that supplementing CM with GDF-5 further augments these effects, in line with previous reports[274,312–314], and with our observations in Chapter 4.

COL1 expression followed a similar pattern, with CM-treated groups exhibiting significantly higher fluorescence intensity than the CTRL and CTRL+GDF-5 groups, especially under 2% oxygen. Although CTRL+GDF-5 also enhanced COL1 expression, the addition of CM further supported ECM remodelling and collagen synthesis, indicating that secretome-derived cues can augment the GDF-5 response. Hypoxia amplified these effects across most conditions, in line with studies[9,175,255,256,306] demonstrating that low oxygen levels activate hypoxia-inducible factors and promote stem cell differentiation towards a tenogenic phenotype, as also observed in previous chapters.

Histological analysis further confirmed enhanced ECM organisation in CM+GDF-5 groups, with the most structured arrangement observed in dynamic CM+GDF-5 cultures (Figure 6-4). Both GDF-5 supplementation and CM contributed to collagen synthesis, but the addition of CM collected from mechanically stimulated hTSPCs and then supplemented with GDF-5 promoted more pronounced fibrillogenesis and ECM alignment, consistent with studies showing that dynamic stimulation enhances tendon ECM properties[358,359]. While CM+GDF-5 samples under 21% O_2 displayed well-structured fibrillar organisation, hypoxia instead appeared to facilitate ECM remodelling rather than fibrillogenesis, potentially through increased activity of matrix-modifying enzymes[352,360]. These findings suggest that dynamic culture enhances the secretion of bioactive factors in CM, which likely include both soluble proteins and vesicle-associated molecules[352,361]. However, since CM was used in its entirety, the specific contribution of EVs cannot be determined from these data.

The morphological analysis in 2D culture revealed a clear shift towards a more elongated nuclear phenotype in all CM-treated groups, indicating the induction of tenogenic differentiation[357]. This elongation was most prominent under physiological oxygen, particularly in the dynamic CM+GDF-5 group, where the lowest nuclear aspect ratio values were observed. These findings suggest a synergistic effect between hypoxia and dynamic culture of hTSPCs, resulting in a secretome capable of enhancing cytoskeletal reorganisation and nuclear remodelling, both recognised features of tenocyte-like morphology. The frequency distribution

of nuclear aspect ratios further reinforced these observations, with dynamic CM-treated samples under hypoxia showing a larger proportion of nuclei within lower aspect ratio ranges (0.2–0.4), indicative of spindle-shaped, elongated cells. This morphological shift is consistent with previous studies, which demonstrate that nuclear elongation correlates with tenogenic maturation and is influenced by both mechanical and biochemical signals in the microenvironment[274,312–314]. Together, these results indicate that CM, particularly from dynamically cultured hTSPCs under hypoxic conditions, can direct morphological changes in hBM-MSCs that are characteristic of tenogenic commitment in a 2D environment.

The upregulation of key tenogenic genes, including *SCX*, *TNMD*, *MKX*, *COL1A2*, and *COL3A1*, supports the tenogenic potential of hTSPC-derived CM, particularly under hypoxic conditions and with dynamic culture. *SCX* expression was highest in static CM+GDF-5-treated cells under 21% O_2, while a stronger increase under 2% O_2 indicates that low oxygen may promote early tenogenic commitment, in line with previous reports[256]. *MKX* also showed upregulation under hypoxia in CM-treated groups, suggesting that secretome-derived cues can complement GDF-5 stimulation[362]. *TNMD* expression was most strongly enhanced in dynamic CM+GDF-5 under hypoxia, consistent with studies reporting that mechanical culture conditions can influence matrix organisation and late-stage differentiation[274,312–314]. For collagen genes, *COL1A2* expression was stimulated mainly by GDF-5 under 21% O_2[363], whereas *COL3A1* was increased in CM-treated samples under hypoxia, reflecting patterns observed during early tendon remodelling. Taken together, these findings suggest that CM, in combination with oxygen modulation and dynamic culture, influences stage-specific tenogenic gene expression[72,249], though further work is required to confirm these mechanisms.

To further investigate the tenogenic potential of CM, hBM-MSCs were embedded in collagen scaffolds, previously optimised[282,364], with cEVs, and cultured under different oxygen and media conditions. L/D staining confirmed high cell viability (>80%) across all conditions after one day, demonstrating the biocompatibility of the collagen scaffold and the absence of cytotoxic effects from CM or GDF-5 (Figure 6-6). Cells cultured under 2% O_2 displayed faster

scaffold colonisation and early proliferation, consistent with our findings in Chapter 3 and previous studies[9,175,255,285].

By day 14, L/D staining revealed good overall viability (>78%) across all conditions, and CM-treated groups formed thicker cell layers and more significant scaffold infiltration, supporting the role of hTSPC-derived factors in promoting cell proliferation and ECM production, as seen in the 2D model. Similarly, a study utilising a porous collagen sponge scaffold for BM-MSC culture reported increased proliferation and tenogenic differentiation, emphasising the importance of biomaterial structure in supporting tendon-like differentiation[356]. Despite their enhanced matrix organisation, CM-treated groups exhibited slightly lower viability than controls, likely due to increased metabolic demands from higher cell density and active ECM synthesis. This highlights the delicate balance between proliferation and nutrient availability in 3D culture, reinforcing the role of oxygen modulation in supporting viable tendon constructs.

Collagen gel contraction measurements revealed that CM-treated gels exhibited significantly less contraction than controls, suggesting that components within CM, potentially including vesicle-associated factors, may help preserve matrix architecture or modulate remodelling activity (Figure 6-8). However, because cEVs were embedded together with hBM-MSCs and cultured in CM, both soluble and vesicle-associated cues were present, and their individual contributions could not be distinguished here. A previous study reported similar effects using platelet-derived EVs, which reduced gel contraction and helped maintain scaffold integrity, further supporting the role of EVs in regulating collagen matrix dynamics[365]. This observation supports the hypothesis that CM promotes ECM integrity rather than degradation, as observed in CM derived from different cell types[227,362,366]. The contraction was more pronounced under 2% O_2, likely due to increased cell proliferation and matrix turnover, a trend previously linked to hypoxia-induced MMP activity[360,367]. However, it should be acknowledged that scaffold volume reduction could also arise from collagen degradation in addition to cell-mediated contraction. Because acellular controls were not included, the contribution of medium composition to scaffold stability cannot be excluded. Future studies should incorporate cell-

free gels to help distinguish between scaffold degradation and contraction, as suggested by recent work. Future studies could also consider mechanically constraining the gels, such as by fixing the ends, to limit contraction directionally and encourage aligned matrix deposition, an approach often used in bioreactor-based tendon tissue models.

Immunofluorescence analysis demonstrated that TNMD expression was significantly higher in CM-treated samples than controls, with the most pronounced effect observed in dynamic CM+GDF-5 under 2% O_2 (Figure 6-9). This finding is consistent with the 2D results but more pronounced in the 3D model, where TNMD expression was generally higher across all conditions. This suggests that the collagen scaffold, by mimicking the structural and mechanical features of native tendon tissue, creates a more favourable environment for tenogenic maturation[368]. The 3D setting enables physiologically relevant cell–matrix interactions, likely enhancing ECM-integrin signalling, which contributes to the upregulation of tendon-specific markers like TNMD[369] and modulates cytoskeletal organisation[353]. This is further supported by the observed increase in nuclear elongation under CM treatment in 3D, particularly with dynamic CM+GDF-5, reinforcing the role of scaffold architecture and stiffness in guiding cell phenotype and function[370]. These findings support the use of biomaterial-based systems to replicate native tendon environments and potentiate tenogenic differentiation more effectively.

This is likely due to enhanced ECM-integrin signalling, which influences both gene expression and cytoskeletal dynamics[353]. The 3D model, based on cell-laden collagen scaffolds, more closely mimics the structural and mechanical properties of native tendon tissue. It provides not only physical support for cell growth and alignment but also facilitates more physiologically relevant cell–matrix interactions. These interactions are crucial for the upregulation of tendon-specific markers, such as TNMD, which are linked to matrix maturation and tissue functionality. Similarly, nuclear elongation was more pronounced in 3D cultures, particularly under CM treatment, reinforcing the role of matrix architecture and stiffness in modulating cytoskeletal tension and nuclear remodelling[370]. Together, these findings emphasise the relevance of

biomaterial-based systems in creating environments conducive to tenogenic commitment and maturation.

Gene expression analysis further confirmed the tenogenic effects of CM in the 3D model, where cells were co-embedded with crude EVs, indicating that both soluble and vesicle-associated components of the secretome likely contributed. *SCX* and *TNMD* were significantly upregulated in CM-treated groups, particularly under low-oxygen conditions. *SCX* expression was highest in the static CM+GDF-5 group, consistent with the 2D model, while *TNMD* showed the strongest upregulation in the dynamic CM+GDF-5 condition, suggesting that hypoxia and mechanical stimulation enhanced late-stage differentiation responses[355,371,372]. *MKX* expression also increased under hypoxia in CM-treated groups, though the changes were less pronounced than for *SCX* and *TNMD*, indicating a more gradual contribution to lineage progressio[373]. The expression of collagen genes varied with oxygen and treatment: under 21% O_2, *COL1A2* was highest in the CTRL+GDF-5 group, while under 2% O_2, *COL3A1* was markedly upregulated in CM-treated samples, particularly in the dynamic CM+GDF-5 group, as reported in previous studies[72,249,353].

Altogether, these findings show that CM and cEVs drive stage-specific gene expression patterns in 3D culture, with hypoxia and dynamic conditions amplifying these effects. Taken together, the data suggest that a combination of biochemical, mechanical, and oxygen-related cues is required to reproduce the sequential stages of tendon differentiation, aligning with reports that environmental conditioning shapes stem cell responses and ECM remodelling[308,372].

Both 2D and 3D models confirmed the tenogenic potential of hTSPC-derived CM and cEVs, with 3D culture more effectively replicating the native tendon microenvironment by providing a fibrillar collagen matrix, spatial cell organisation, and enhanced cell–matrix interactions, in agreement with previous studies[353–355], especially when incorporating cEVs, which provided sustained vesicle-mediated signalling alongside soluble bioactive factors[355]. Notably, 3D

cultures exhibited stronger tenogenic marker expression, greater nuclear elongation, and more structured ECM organisation than 2D models. Differences in ECM remodelling were also evident, as 2D cultures showed increased collagen deposition, whereas 3D cultures exhibited a more structured fibrillar ECM. The collagen gel contraction assay demonstrated that CM-treated gels contracted less than controls, further indicating that CM components contribute to scaffold stabilisation rather than excessive matrix contraction.

Despite demonstrating the tenogenic potential of hTSPC-derived CM and cEVs, this study has some limitations. A key limitation of this study is the variability in CM composition, as batch-to-batch differences may arise due to donor heterogeneity, passage number, and culture conditions. This variability could affect reproducibility and clinical translation, emphasising the need for standardised protocols. Additionally, while this study suggests a role for vesicle-associated factors in 3D cultures, the specific contribution of EVs versus soluble CM factors remains to be disentangled. As shown in Chapter 4, preliminary surface marker profiling of hTSPC-derived EVs revealed the presence of adhesion molecules and signalling-related markers such as CD29 and CD44, which may play a role in modulating cell–matrix interactions and downstream tenogenic responses. However, due to the low EV concentration and inter-donor variability, a definitive correlation could not be established, underscoring the need for deeper proteomic and transcriptomic analyses to identify key therapeutic components. Moreover, this study primarily focused on molecular and cellular markers of tenogenesis without assessing the mechanical properties of engineered constructs. Given the importance of tendon biomechanics, future studies should incorporate mechanical testing to determine whether observed differentiation translates into functional improvements. Lastly, while our research provided valuable mechanistic insights in an *in vitro* setting, *in vivo* models are essential to fully assess the regenerative potential of hTSPC-derived CM and cEVs. Studies[172,371] using amnion-derived secretomes in ovine models have demonstrated promising tendon regeneration outcomes, highlighting the need to translate *in vitro* findings into

preclinical settings. Future research should investigate whether hTSPC-derived CM induce similar effects *in vivo* and how it compares to alternative secretome-based therapies.

In addition, the study was performed with a limited number of biological replicates (n = 3 donors) and technical repeats, which may constrain statistical power. Although consistent trends were observed across independent experiments, future work should include larger sample sizes and validation across multiple donor cohorts to strengthen reproducibility and support clinical translation.

Overall, while 2D culture provided a controlled environment for assessing biochemical influences, 3D culture more effectively mimicked the native tendon microenvironment, integrating mechanical, biochemical, and structural cues. These findings emphasise the necessity of incorporating 3D models in tendon tissue engineering strategies to improve the translational potential of EV-based regenerative therapies.

6.6 Conclusion

This study provides evidence that hTSPC-derived CM and cEVs can support tenogenic differentiation in human BM-MSCs, as reflected by changes in morphology, ECM organisation, and gene expression. Dynamic culture conditions and hypoxia appeared to enhance these effects, although the contribution of specific soluble versus vesicle-associated factors could not be fully distinguished. While dynamic CM+GDF-5 tended to show stronger outcomes, these findings should be interpreted cautiously given the variability of donor-derived secretomes and the limited number of replicates.

The work addressed the main objectives of this chapter by assessing the impact of dynamic versus static culture, 3D versus 2D environments, and GDF-5 supplementation. The results suggest that human-derived CM may provide stronger support for ECM organisation and gene expression than porcine-derived CM in comparable settings, although species-specific differences in secretome composition require further investigation.

Embedding cEVs within collagen scaffolds may have contributed to sustained signalling in 3D culture, but this effect cannot yet be clearly distinguished from that of soluble CM factors. Similarly, reduced gel contraction in CM-treated groups points towards an influence on ECM remodelling, but future studies including acellular controls will be needed to separate scaffold degradation from true cell-mediated contraction.

Taken together, these findings support the potential of hTSPC-derived CM and cEVs as candidate tools for tendon regeneration. However, more comprehensive studies with larger sample sizes, deeper molecular analyses, and *in vivo* validation will be essential before firm conclusions can be drawn regarding their therapeutic applicability.



Chapter 7

Summative discussion, conclusions, and future perspectives

7. SUMMATIVE DISCUSSION, CONCLUSIONS AND FUTURE PERSPECTIVES

7.1 Summative discussion

Given their high risk of recurrence, prolonged healing times, and limited capacity for self-healing, tendon injuries pose a significant therapeutic challenge[31,56]. Since traditional therapies often do not entirely restore tendon function, interest in regenerative techniques that use cell-derived secretomes and purified EVs populations as potential remedies has grown[217,236,238]. While several studies have reported that EVs derived from various stem cell types and species can modulate inflammation, support cell proliferation, and promote ECM remodelling during tendon healing[292,344,374–376], important questions remain unanswered. In particular, the influence of tissue-specific EV sources, culture conditions, and bioengineering integration on EV bioactivity has yet to be fully elucidated.

This thesis aimed to address these gaps by investigating the tenogenic potential of porcine and human TSPC-derived CM and cEVs, with a focus on how oxygen tension, mechanical stimulation, and biomaterial integration affect their regenerative performance. Unlike many previous studies that used non-tendon-derived cells such as bone marrow or adipose-derived mesenchymal stem cells, this work concentrated on TSPCs due to their tissue-specific relevance and their natural involvement in tendon homeostasis and repair. Furthermore, the use of dynamic culture systems and 3D scaffolds aimed to mimic physiological conditions better and increase translational potential.

Across all experimental chapters, several unifying themes emerged. First, species origin influenced regenerative efficacy: porcine TSPCs provided a valuable initial model, but human TSPC-derived secretomes consistently showed stronger paracrine activity, particularly in 3D assays. This observation aligns with previous reports that human-derived factors can show superior compatibility and regenerative signalling compared to cross-species

applications[377,378]. Second, secretome composition determined functional outcomes: CM, which contains both EVs and soluble factors, induced robust tenogenic differentiation without supplementation, whereas purified cEVs required GDF-5 co-stimulation to achieve comparable effects. This distinction underscores the complementary nature of vesicular and non-vesicular fractions in tendon regeneration, consistent with other studies highlighting the synergistic role of cytokines and growth factors in secretome bioactivity[232,362,366].

Third, environmental modulation, through oxygen tension, dynamic culture, and scaffold integration, proved to be the most consistent driver of tenogenic responses. Hypoxia upregulated key markers (*SCX*, *TNMD*) and enhanced ECM organisation, while dynamic loading increased EV yield and altered cargo composition, reinforcing their mechanosensitive nature[274,312–314]. The introduction of 3D scaffolds further magnified these effects by providing spatial and mechanical cues that promoted aligned collagen deposition and cytoskeletal organisation, in line with other work showing the importance of biomimetic environments for tendon cell function[355,356]. These results demonstrate that recreating physiological microenvironments *in vitro* is central to unlocking the full potential of TSPC-derived secretomes.

Mechanistically, these findings suggest that hypoxia and mechanical stimulation converge on complementary pathways. Activation of HIF-1α under low oxygen and integrin/FAK–YAP/TAZ signalling under dynamic load have been shown to regulate EV biogenesis and selective cargo loading[252], thereby enriching vesicles with regenerative signals. This mechanistic link provides a framework for understanding how environmental and biochemical cues shape the regenerative potency of TSPC-derived CM and EVs.

Taken together, the findings demonstrate that tendon regeneration is not governed by a single parameter but by the integration of species-specific sources, secretome complexity, and environmental conditioning. This systems-level synthesis advances current knowledge by showing how these layers interact to enhance tenogenesis and matrix organisation, and it

provides a conceptual foundation for the conclusions and translational perspectives presented in the following sections.

7.2 Conclusions

Collectively, this thesis advances understanding of how tendon-derived EVs and CM can be potentially used for tendon repair. The findings confirm that TSPCs II serve as a valuable cell source due to their robust proliferative capacity, stable tenogenic profile, and ability to secrete bioactive EVs with regenerative properties. Notably, the roles of hypoxia and mechanical stimulation during culture have been established to enhance the bioactivity of tendon-derived secretomes, supporting their potential for clinical translation.

The comparative analysis of porcine- and human-derived CM and EVs revealed species-specific differences in their regenerative properties, with human-derived secretomes demonstrating superior effects in 3D cultures. Furthermore, integrating biomaterials with dynamic culture systems provided a more physiologically relevant environment, optimising cell-matrix interactions and promoting tenogenic differentiation. The influence of GDF-5 was evident in enhancing collagen deposition and tenogenic marker expression, particularly in combination with mechanically stimulated CM and EVs.

Overall, this thesis highlights the importance of optimising culture conditions to enhance the efficacy of cell-free regenerative approaches for tendon repair. This research contributes to advancing clinically viable regenerative strategies for tendon repair by optimising EV-based therapies through oxygen modulation and mechanical stimulation.

7.3 Future perspectives

Building on the integrated findings of this thesis, several avenues of future research emerge. Future work should focus on optimising EV isolation and characterisation to improve consistency and bioactivity across different experimental conditions. Donor variability, passage-dependent effects, and environmental factors remain key challenges in standardising CM and EV preparations. Further proteomic and transcriptomic analyses will be essential in

identifying the key bioactive molecules, such as proteins, lipids, and microRNAs, that drive tenogenic differentiation and ECM remodelling, enabling more targeted therapeutic applications.

A key area for further investigation is the integration of EVs with biomaterial scaffolds to enhance tendon repair strategies. While this thesis demonstrated EVs' ability to influence ECM organisation and tenogenic differentiation, future studies should assess the mechanical properties of engineered constructs and their ability to withstand physiological loading. Using bioreactors replicating tendon biomechanics could provide insights into the long-term stability of EV-based therapies in scaffold-assisted regeneration.

Furthermore, preclinical validation in tendon injury models is crucial for bridging the gap between *in vitro* findings and clinical applications. Investigating the regenerative potential of hTSPC-derived EVs *in vivo* by assessing their impact on tissue integration, inflammation, and functional recovery will be critical for establishing their therapeutic viability. Large animal models may be particularly important for evaluating EV efficacy under physiological conditions, thereby addressing key translational barriers before clinical testing. While previous *in vivo* studies have shown promising results[235,289,292], further research is required to confirm their long-term benefits in tendon repair.

Finally, addressing the challenges related to the scalability, storage stability, and regulatory compliance of EV-based therapies is crucial for their clinical implementation. The feasibility of allogeneic and autologous EV treatments presents opportunities and challenges, requiring optimised delivery methods and patient-specific treatment strategies. Regulatory frameworks for EV therapies are still evolving, necessitating the standardisation of isolation procedures, safety assessments, and large-scale production guidelines. Overcoming these barriers will be crucial for translating EV-based regenerative approaches into viable clinical treatments, providing a biologically driven alternative to conventional tendon repair strategies and enhancing patient outcomes in musculoskeletal medicine.



References

8. REFERENCES

1. Oliva, F., Gatti, S., Porcellini, G., Forsyth, N. R. & Maffulli, N. Growth factors and tendon healing. *Med Sport Sci* **57**, 53–64 (2012).
2. Citro, V. *et al.* Tendon tissue engineering: An overview of biologics to promote tendon healing and repair. *J Tissue Eng* **14**, 20417314231196275 (2023).
3. Snedeker, J. G. & Foolen, J. Tendon injury and repair – A perspective on the basic mechanisms of tendon disease and future clinical therapy. *Acta Biomaterialia* **63**, 18–36 (2017).
4. Ruiz-Alonso, S., Lafuente-Merchan, M., Ciriza, J., Saenz-del-Burgo, L. & Pedraz, J. L. Tendon tissue engineering: Cells, growth factors, scaffolds and production techniques. *Journal of Controlled Release* **333**, 448–486 (2021).
5. Liu, C.-F. *et al.* What We Should Know Before Using Tissue Engineering Techniques to Repair Injured Tendons: A Developmental Biology Perspective. *Tissue Engineering Part B: Reviews* **17**, 165–176 (2011).
6. Ackermann, P. W., Salo, P. & Hart, D. A. Tendon Innervation. in *Metabolic Influences on Risk for Tendon Disorders* (eds. Ackermann, P. W. & Hart, D. A.) 35–51 (Springer International Publishing, Cham, 2016). doi:10.1007/978-3-319-33943-6_4.
7. Citeroni, M. R. *et al.* In Vitro Innovation of Tendon Tissue Engineering Strategies. *Int J Mol Sci* **21**, 6726 (2020).
8. Docheva, D., Müller, S. A., Majewski, M. & Evans, C. H. Biologics for tendon repair. *Adv Drug Deliv Rev* **84**, 222–239 (2015).
9. Clerici, M. *et al.* Endotenon-Derived Type II Tendon Stem Cells Have Enhanced Proliferative and Tenogenic Potential. *Int J Mol Sci* **24**, 15107 (2023).
10. Kannus, P. Structure of the tendon connective tissue. *Scand J Med Sci Sports* **10**, 312–320 (2000).
11. Benjamin, M., Kaiser, E. & Milz, S. Structure-function relationships in tendons: a review. *J Anat* **212**, 211–228 (2008).

12. Elliott, D. H. Structure and Function of Mammalian Tendon. *Biological Reviews* **40**, 392–421 (1965).

13. Wang, J. H.-C. Mechanobiology of tendon. *J Biomech* **39**, 1563–1582 (2006).

14. Zafar, M. S., Mahmood, A. & Maffulli, N. Basic Science and Clinical Aspects of Achilles Tendinopathy. *Sports Medicine and Arthroscopy Review* **17**, 190 (2009).

15. Thorpe, C. T. *et al.* Distribution of proteins within different compartments of tendon varies according to tendon type. *Journal of Anatomy* **229**, 450–458 (2016).

16. Ellingson, A. J., Pancheri, N. M. & Schiele, N. R. Regulators of collagen crosslinking in developing and adult tendons. *Eur Cell Mater* **43**, 130–152 (2022).

17. Thorpe, C. T. & Screen, H. R. C. Tendon Structure and Composition. in *Metabolic Influences on Risk for Tendon Disorders* (eds. Ackermann, P. W. & Hart, D. A.) 3–10 (Springer International Publishing, Cham, 2016). doi:10.1007/978-3-319-33943-6_1.

18. Yoon, J. H. & Halper, J. Tendon proteoglycans: biochemistry and function. *J Musculoskelet Neuronal Interact* **5**, 22–34 (2005).

19. Artells, R., Pruna, R., Dellal, A. & Maffulli, N. Elastin: a possible genetic biomarker for more severe ligament injuries in elite soccer. A pilot study. *Muscles Ligaments Tendons J* **6**, 188–192 (2016).

20. Li, Y., Wu, T. & Liu, S. Identification and Distinction of Tenocytes and Tendon-Derived Stem Cells. *Front Cell Dev Biol* **9**, 629515 (2021).

21. Jo, C. H., Lim, H.-J. & Yoon, K. S. Characterization of Tendon-Specific Markers in Various Human Tissues, Tenocytes and Mesenchymal Stem Cells. *Tissue Eng Regen Med* **16**, 151–159 (2019).

22. Chuen, F. S. *et al.* Immunohistochemical Characterization of Cells in Adult Human Patellar Tendons. *J Histochem Cytochem.* **52**, 1151–1157 (2004).

23. Schneider, M., Angele, P., Järvinen, T. A. H. & Docheva, D. Rescue plan for Achilles: Therapeutics steering the fate and functions of stem cells in tendon wound healing. *Advanced Drug Delivery Reviews* **129**, 352–375 (2018).

24. Bi, Y. *et al.* Identification of tendon stem/progenitor cells and the role of the extracellular matrix in their niche. *Nat Med* **13**, 1219–1227 (2007).

25. Nourissat, G., Berenbaum, F. & Duprez, D. Tendon injury: from biology to tendon repair. *Nat Rev Rheumatol* **11**, 223–233 (2015).

26. Fuchs, E., Tumbar, T. & Guasch, G. Socializing with the Neighbors: Stem Cells and Their Niche. *Cell* **116**, 769–778 (2004).

27. Taichman, R. S. & Emerson, S. G. Human osteoblasts support hematopoiesis through the production of granulocyte colony-stimulating factor. *J Exp Med* **179**, 1677–1682 (1994).

28. Mienaltowski, M. J., Adams, S. M. & Birk, D. E. Regional Differences in Stem Cell/Progenitor Cell Populations from the Mouse Achilles Tendon. *Tissue Engineering Part A* **19**, 199–210 (2013).

29. Ruzzini, L. *et al.* Characterization of age-related changes of tendon stem cells from adult human tendons. *Knee Surg Sports Traumatol Arthrosc* **22**, 2856–2866 (2014).

30. Citeroni, M. R. *et al.* Amnion-Derived Teno-Inductive Secretomes: A Novel Approach to Foster Tendon Differentiation and Regeneration in an Ovine Model. *Frontiers in Bioengineering and Biotechnology* **9**, (2021).

31. Sharma, P. & Maffulli, N. Biology of tendon injury: healing, modeling and remodeling. *J Musculoskelet Neuronal Interact* **6**, 181–190 (2006).

32. Wang, J. H.-C., Guo, Q. & Li, B. Tendon Biomechanics and Mechanobiology—A Minireview of Basic Concepts and Recent Advancements. *Journal of Hand Therapy* **25**, 133–141 (2012).

33. Kyriakides, T. R. *et al.* Mice that lack thrombospondin 2 display connective tissue abnormalities that are associated with disordered collagen fibrillogenesis, an increased vascular density, and a bleeding diathesis. *J Cell Biol* **140**, 419–430 (1998).

34. Maganaris, C. N., Narici, M. V. & Maffulli, N. Biomechanics of the Achilles tendon. *Disabil Rehabil* **30**, 1542–1547 (2008).

35. Mosler, E. *et al.* Stress-induced molecular rearrangement in tendon collagen. *Journal of Molecular Biology* **182**, 589–596 (1985).

36. Matson, A., Konow, N., Miller, S., Konow, P. P. & Roberts, T. J. Tendon material properties vary and are interdependent among turkey hindlimb muscles. *J Exp Biol* **215**, 3552–3558 (2012).

37. Burgio, V. *et al.* Mechanical Properties of Animal Tendons: A Review and Comparative Study for the Identification of the Most Suitable Human Tendon Surrogates. *Processes* **10**, 485 (2022).

38. Wren, T. A., Yerby, S. A., Beaupré, G. S. & Carter, D. R. Mechanical properties of the human achilles tendon. *Clin Biomech (Bristol, Avon)* **16**, 245–251 (2001).

39. Shadwick, R. E. Elastic energy storage in tendons: mechanical differences related to function and age. *Journal of Applied Physiology* **68**, 1033–1040 (1990).

40. Komi, P. V., Fukashiro, S. & Järvinen, M. Biomechanical Loading of Achilles Tendon During Normal Locomotion. *Clinics in Sports Medicine* **11**, 521–531 (1992).

41. Fyfe, I. & Stanish, W. D. The Use of Eccentric Training and Stretching in the Treatment and Prevention of Tendon Injuries. *Clinics in Sports Medicine* **11**, 601–624 (1992).

42. Kjær, M. Role of Extracellular Matrix in Adaptation of Tendon and Skeletal Muscle to Mechanical Loading. *Physiological Reviews* **84**, 649–698 (2004).

43. Zhang, J. & Wang, J. H.-C. Mechanobiological response of tendon stem cells: Implications of tendon homeostasis and pathogenesis of tendinopathy. *Journal of Orthopaedic Research* **28**, 639–643 (2010).

44. Wang, J. H.-C. *et al.* Cyclic Mechanical Stretching of Human Tendon Fibroblasts Increases the Production of Prostaglandin E 2 and Levels of Cyclooxygenase Expression: A Novel In Vitro Model Study. *Connective Tissue Research* **44**, 128–133 (2003).

45. Zhang, J. & Wang, J. H.-C. The Effects of Mechanical Loading on Tendons - An In Vivo and In Vitro Model Study. *PLOS ONE* **8**, e71740 (2013).

46. Mousavizadeh, R. *et al.* Cyclic Strain Alters the Expression and Release of Angiogenic Factors by Human Tendon Cells. *PLOS ONE* **9**, e97356 (2014).

47. Yang, G., Crawford, R. C. & Wang, J. H.-C. Proliferation and collagen production of human patellar tendon fibroblasts in response to cyclic uniaxial stretching in serum-free conditions. *Journal of Biomechanics* **37**, 1543–1550 (2004).

48. Ventre, M., Causa, F. & Netti, P. A. Determinants of cell–material crosstalk at the interface: towards engineering of cell instructive materials. *Journal of The Royal Society Interface* **9**, 2017–2032 (2012).

49. Gomes, M. E., Reis, R. L. & Rodrigues, M. T. *Tendon Regeneration: Understanding Tissue Physiology and Development to Engineer Functional Substitutes*. (Academic Press, 2015).

50. Fleischhacker, V. *et al.* In Vivo and In Vitro Mechanical Loading of Mouse Achilles Tendons and Tenocytes-A Pilot Study. *Int J Mol Sci* **21**, 1313 (2020).

51. Zhang, J., Li, B. & Wang, J. H.-C. The role of engineered tendon matrix in the stemness of tendon stem cells in vitro and the promotion of tendon-like tissue formation in vivo. *Biomaterials* **32**, 6972–6981 (2011).

52. Maeda, T. *et al.* Conversion of Mechanical Force into TGF-β-Mediated Biochemical Signals. *Current Biology* **21**, 933–941 (2011).

53. Ciardulli, M. C. *et al.* Stem Cells from Healthy and Tendinopathic Human Tendons: Morphology, Collagen and Cytokines Expression and Their Response to T3 Thyroid Hormone. *Cells* **11**, 2545 (2022).

54. Morita, W., Dakin, S. G., Snelling, S. J. B. & Carr, A. J. Cytokines in tendon disease. *Bone Joint Res* **6**, 656–664 (2018).

55. Mora, M. V. *et al.* Stem cell therapy in the management of shoulder rotator cuff disorders. *World J Stem Cells* **7**, 691–699 (2015).

56. Thomopoulos, S., Parks, W. C., Rifkin, D. B. & Derwin, K. A. Mechanisms of tendon injury and repair. *Journal of Orthopaedic Research* **33**, 832–839 (2015).

57. Sharma, P. & Maffulli, N. Tendon injury and tendinopathy: healing and repair. *J Bone Joint Surg Am* **87**, 187–202 (2005).

58. Bestwick, C. S. & Maffulli, N. Reactive Oxygen Species and Tendon Problems: Review and Hypothesis. *Sports Medicine and Arthroscopy Review* **8**, 6 (2000).

59. Goodship, A. E., Birch, H. L. & Wilson, A. M. The pathobiology and repair of tendon and ligament injury. *Vet Clin North Am Equine Pract* **10**, 323–349 (1994).

60. Nigg, B. M. The Role of Impact Forces and Foot Pronation: A New Paradigm. *Clinical Journal of Sport Medicine* **11**, 2 (2001).

61. Selvanetti, A., Cipolla, M. & Puddu, G. Overuse tendon injuries: Basic science and classification. *Operative Techniques in Sports Medicine* **5**, 110–117 (1997).

62. Benazzo, F., Zanon, G. & Maffulli, N. An Operative Approach to Achilles Tendinopathy. *Sports Medicine and Arthroscopy Review* **8**, 96 (2000).

63. Arndt, A. N., Komi, P. V., Brüggemann, G.-P. & Lukkariniemi, J. Individual muscle contributions to the in vivo achilles tendon force. *Clin Biomech (Bristol)* **13**, 532–541 (1998).

64. Kleiner, D. M. Human Tendons: Anatomy, Physiology and Pathology. *J Athl Train* **33**, 185–186 (1998).

65. Khan, K. M., Cook, J. L., Bonar, F., Harcourt, P. & Astrom, M. Histopathology of common tendinopathies. Update and implications for clinical management. *Sports Med* **27**, 393–408 (1999).

66. Christensen, J., Alfredson, H. & Andersson, G. Protease-Activated Receptors in the Achilles Tendon–A Potential Explanation for the Excessive Pain Signalling in Tendinopathy. *Mol Pain* **11**, s12990-015-0007–4 (2015).

67. Kannus, P. & Józsa, L. Histopathological changes preceding spontaneous rupture of a tendon. A controlled study of 891 patients. *J Bone Joint Surg Am* **73**, 1507–1525 (1991).

68. Tallon, C., Maffulli, N. & Ewen, S. W. Ruptured Achilles tendons are significantly more degenerated than tendinopathic tendons. *Med Sci Sports Exerc* **33**, 1983–1990 (2001).

69. Maffulli, N., Moller, H. & Evans, C. Tendon healing: can it be optimised? *Br J Sports Med* **36**, 315–316 (2002).

70. Brebels, J. & Mignon, A. Polymer-Based Constructs for Flexor Tendon Repair: A Review. *Polymers* **14**, 867 (2022).

71. Rodrigues, M. T., Reis, R. L. & Gomes, M. E. Engineering tendon and ligament tissues: present developments towards successful clinical products. *Journal of Tissue Engineering and Regenerative Medicine* **7**, 673–686 (2013).

72. Millar, N. L., Murrell, G. A. C. & McInnes, I. B. Inflammatory mechanisms in tendinopathy – towards translation. *Nat Rev Rheumatol* **13**, 110–122 (2017).

73. Hu, J., Liu, S. & Fan, C. Applications of functionally-adapted hydrogels in tendon repair. *Front. Bioeng. Biotechnol.* **11**, (2023).

74. Harvey, T., Flamenco, S. & Fan, C.-M. A Tppp3+Pdgfra+ tendon stem cell population contributes to regeneration and reveals a shared role for PDGF signalling in regeneration and fibrosis. *Nat Cell Biol* **21**, 1490–1503 (2019).

75. Gomez-Florit, M., Labrador-Rached, C. J., Domingues, R. M. A. & Gomes, M. E. The tendon microenvironment: Engineered *in vitro* models to study cellular crosstalk. *Advanced Drug Delivery Reviews* **185**, 114299 (2022).

76. Andia, I., Sanchez, M. & Maffulli, N. Tendon healing and platelet-rich plasma therapies. *Expert Opin Biol Ther* **10**, 1415–1426 (2010).

77. Maffulli, N., Ewen, S. W., Waterston, S. W., Reaper, J. & Barrass, V. Tenocytes from ruptured and tendinopathic achilles tendons produce greater quantities of type III collagen than tenocytes from normal achilles tendons. An in vitro model of human tendon healing. *Am J Sports Med* **28**, 499–505 (2000).

78. Maffulli, N., Longo, U. G. & Denaro, V. Novel approaches for the management of tendinopathy. *J Bone Joint Surg Am* **92**, 2604–2613 (2010).

79. Aicale, R., Bisaccia, R. D., Oliviero, A., Oliva, F. & Maffulli, N. Current pharmacological approaches to the treatment of tendinopathy. *Expert Opin Pharmacother* **21**, 1467–1477 (2020).

80. Childress, M. A. & Beutler, A. Management of chronic tendon injuries. *Am Fam Physician* **87**, 486–490 (2013).

81. Gatz, M. *et al.* Multimodal Ultrasound Versus MRI for the Diagnosis and Monitoring of Achilles Tendinopathy: A Prospective Longitudinal Study. *Orthopaedic Journal of Sports Medicine* **9**, 23259671211006826 (2021).

82. Milankov, M. Z., Miljkovic, N. & Stankovic, M. Reconstruction of chronic patellar tendon rupture with contralateral BTB autograft: a case report. *Knee Surg Sports Traumatol Arthr* **15**, 1445–1448 (2007).

83. Schachter, A. K., White, B. J., Namkoong, S. & Sherman, O. Revision Reconstruction of a Pectoralis Major Tendon Rupture Using Hamstring Autograft: A Case Report. *Am J Sports Med* **34**, 295–298 (2006).

84. Kingma, J. J., de Knikker, R., Wittink, H. M. & Takken, T. Eccentric overload training in patients with chronic Achilles tendinopathy: a systematic review. *Br J Sports Med* **41**, e1–e5 (2007).

85. Prudêncio, D. A. *et al.* Eccentric exercise is more effective than other exercises in the treatment of mid-portion Achilles tendinopathy: systematic review and meta-analysis. *BMC Sports Science, Medicine and Rehabilitation* **15**, 9 (2023).

86. Kannus, P. Tendons--a source of major concern in competitive and recreational athletes. *Scand J Med Sci Sports* **7**, 53–54 (1997).

87. Yamamoto, E., Hayashi, K. & Yamamoto, N. Mechanical properties of collagen fascicles from stress-shielded patellar tendons in the rabbit. *Clinical Biomechanics* **14**, 418–425 (1999).

88. Akeson, W. H. *et al.* Collagen Cross-Linking Alterations in Joint Contractures: Changes in the Reducible Cross-Links in Periarticular Connective Tissue Collagen After Nine Weeks of Immobilization. *Connective Tissue Research* **5**, 15–19 (1977).

89. Kennedy, J. C. & Willis, R. B. The effects of local steroid injections on tendons: a biomechanical and microscopic correlative study. *Am J Sports Med* **4**, 11–21 (1976).

90. Dean, B. J. F. *et al.* The risks and benefits of glucocorticoid treatment for tendinopathy: a systematic review of the effects of local glucocorticoid on tendon. *Semin Arthritis Rheum* **43**, 570–576 (2014).

91. Wang, J. H.-C. Can PRP effectively treat injured tendons? *Muscles Ligaments Tendons J* **4**, 35–37 (2014).

92. Jeong, D. U. *et al.* Clinical Applications of Platelet-Rich Plasma in Patellar Tendinopathy. *Biomed Res Int* **2014**, 249498 (2014).

93. Lipman, K., Wang, C., Ting, K., Soo, C. & Zheng, Z. Tendinopathy: injury, repair, and current exploration. *DDDT* **12**, 591–603 (2018).

94. Hart, L. Shock-wave treatment was more effective than eccentric training for chronic insertional achilles tendinopathy. *Clin J Sport Med* **19**, 152–153 (2009).

95. Maffulli, G., Hemmings, S. & Maffulli, N. Assessment of the Effectiveness of Extracorporeal Shock Wave Therapy (ESWT) For Soft Tissue Injuries (ASSERT): An Online Database Protocol. *Transl Med UniSa* **10**, 46–51 (2014).

96. Bjordal, J. M., Lopes-Martins, R. a. B. & Iversen, V. V. A randomised, placebo controlled trial of low level laser therapy for activated Achilles tendinitis with microdialysis measurement of peritendinous prostaglandin E2 concentrations. *Br J Sports Med* **40**, 76–80; discussion 76-80 (2006).

97. Reddy, G. K., Stehno-Bittel, L. & Enwemeka, C. S. Laser photostimulation of collagen production in healing rabbit Achilles tendons. *Lasers Surg Med* **22**, 281–287 (1998).

98. Johnstone, R. M., Adam, M., Hammond, J. R., Orr, L. & Turbide, C. Vesicle formation during reticulocyte maturation. Association of plasma membrane activities with released vesicles (exosomes). *J Biol Chem* **262**, 9412–9420 (1987).

99. Zeng, Y. *et al.* Biological Features of Extracellular Vesicles and Challenges. *Front Cell Dev Biol* **10**, 816698 (2022).

100. Angulo, M. A., Royo, F. & Falcón-Pérez, J. M. Metabolic Nano-Machines: Extracellular Vesicles Containing Active Enzymes and Their Contribution to Liver Diseases. *Curr Pathobiol Rep* **7**, 119–127 (2019).

101. Colombo, M., Raposo, G. & Théry, C. Biogenesis, Secretion, and Intercellular Interactions of Exosomes and Other Extracellular Vesicles. *Annual Review of Cell and Developmental Biology* **30**, 255–289 (2014).

102. Théry, C. *et al.* Minimal information for studies of extracellular vesicles 2018 (MISEV2018): a position statement of the International Society for Extracellular Vesicles and update of the MISEV2014 guidelines. *J Extracell Vesicles* **7**, 1535750 (2018).

103. Piper, R. C. & Katzmann, D. J. Biogenesis and Function of Multivesicular Bodies. *Annual Review of Cell and Developmental Biology* **23**, 519–547 (2007).

104. Edgar, J. R., Eden, E. R. & Futter, C. E. Hrs- and CD63-Dependent Competing Mechanisms Make Different Sized Endosomal Intraluminal Vesicles. *Traffic* **15**, 197–211 (2014).

105. Petrovčíková, E., Vičíková, K. & Leksa, V. Extracellular vesicles – biogenesis, composition, function, uptake and therapeutic applications. *Biologia* **73**, 437–448 (2018).

106. Mittal, S., Gupta, P., Chaluvally-Raghavan, P. & Pradeep, S. Emerging Role of Extracellular Vesicles in Immune Regulation and Cancer Progression. *Cancers (Basel)* **12**, 3563 (2020).

107. Akers, J. C., Gonda, D., Kim, R., Carter, B. S. & Chen, C. C. Biogenesis of extracellular vesicles (EV): exosomes, microvesicles, retrovirus-like vesicles, and apoptotic bodies. *J Neurooncol* **113**, 1–11 (2013).

108. Muralidharan-Chari, V. *et al.* ARF6-Regulated Shedding of Tumor Cell-Derived Plasma Membrane Microvesicles. *Current Biology* **19**, 1875–1885 (2009).

109. Kerr, J. F. R., Wyllie, A. H. & Currie, A. R. Apoptosis: A Basic Biological Phenomenon with Wideranging Implications in Tissue Kinetics. *Br J Cancer* **26**, 239–257 (1972).

110. Ma, L. *et al.* Discovery of the migrasome, an organelle mediating release of cytoplasmic contents during cell migration. *Cell Res* **25**, 24–38 (2015).

111. Minciacchi, V. R., Freeman, M. R. & Di Vizio, D. Extracellular Vesicles in Cancer: Exosomes, Microvesicles and the Emerging Role of Large Oncosomes. *Seminars in Cell & Developmental Biology* **40**, 41–51 (2015).

112. Welsh, J. A. *et al.* Minimal information for studies of extracellular vesicles (MISEV2023): From basic to advanced approaches. *Journal of Extracellular Vesicles* **13**, e12404 (2024).

113. Shahi, S., Kang, T. & Fonseka, P. Extracellular Vesicles in Pathophysiology: A Prudent Target That Requires Careful Consideration. *Cells* **13**, 754 (2024).

114. Lakkaraju, A. & Rodriguez-Boulan, E. Itinerant exosomes: emerging roles in cell and tissue polarity. *Trends in Cell Biology* **18**, 199–209 (2008).

115. Heidarzadeh, M., Zarebkohan, A., Rahbarghazi, R. & Sokullu, E. Protein corona and exosomes: new challenges and prospects. *Cell Communication and Signaling* **21**, 64 (2023).

116. Musicò, A. *et al.* Extracellular vesicles of different cellular origin feature distinct biomolecular corona dynamics. *Nanoscale Horizons* **10**, 104–112 (2025).

117. Tóth, E. Á. *et al.* Formation of a protein corona on the surface of extracellular vesicles in blood plasma. *J Extracell Vesicles* **10**, e12140 (2021).

118. Kumar, M. A. *et al.* Extracellular vesicles as tools and targets in therapy for diseases. *Sig Transduct Target Ther* **9**, 1–41 (2024).

119. Nawaz, M. *et al.* Extracellular Vesicles and Matrix Remodeling Enzymes: The Emerging Roles in Extracellular Matrix Remodeling, Progression of Diseases and Tissue Repair. *Cells* **7**, 167 (2018).

120. Hakulinen, J., Sankkila, L., Sugiyama, N., Lehti, K. & Keski-Oja, J. Secretion of active membrane type 1 matrix metalloproteinase (MMP-14) into extracellular space in microvesicular exosomes. *Journal of Cellular Biochemistry* **105**, 1211–1218 (2008).

121. You, Y. *et al.* Matrix metalloproteinase 13-containing exosomes promote nasopharyngeal carcinoma metastasis. *Cancer Science* **106**, 1669–1677 (2015).

122. Yokoi, A. & Ochiya, T. Exosomes and extracellular vesicles: Rethinking the essential values in cancer biology. *Seminars in Cancer Biology* **74**, 79–91 (2021).

123. Huang, X. *et al.* Characterization of human plasma-derived exosomal RNAs by deep sequencing. *BMC Genomics* **14**, 319 (2013).

124. Yokoi, A. *et al.* Mechanisms of nuclear content loading to exosomes. *Science Advances* **5**, eaax8849 (2019).

125. Hessvik, N. P. *et al.* PIKfyve inhibition increases exosome release and induces secretory autophagy. *Cell. Mol. Life Sci.* **73**, 4717–4737 (2016).

126. Kowal, J., Tkach, M. & Théry, C. Biogenesis and secretion of exosomes. *Current Opinion in Cell Biology* **29**, 116–125 (2014).

127. Subra, C. *et al.* Exosomes account for vesicle-mediated transcellular transport of activatable phospholipases and prostaglandins [S]. *Journal of Lipid Research* **51**, 2105–2120 (2010).

128. Skotland, T. *et al.* Molecular lipid species in urinary exosomes as potential prostate cancer biomarkers. *European Journal of Cancer* **70**, 122–132 (2017).

129. Qu, Y. *et al.* P2X7 Receptor-Stimulated Secretion of MHC Class II-Containing Exosomes Requires the ASC/NLRP3 Inflammasome but Is Independent of Caspase-1 1. *The Journal of Immunology* **182**, 5052–5062 (2009).

130. N.M. Nolte-'t Hoen, E. & H.M. Wauben, M. Immune Cell-derived Vesicles: Modulators and Mediators of Inflammation. *Current Pharmaceutical Design* **18**, 2357–2368 (2012).

131. Huang, Y. *et al.* Bone marrow mesenchymal stem cell-derived exosomes promote rotator cuff tendon-bone healing by promoting angiogenesis and regulating M1 macrophages in rats. *Stem Cell Research & Therapy* **11**, 496 (2020).

132. Muraca, M. *et al.* Mesenchymal stromal cells and their secreted extracellular vesicles as therapeutic tools for COVID-19 pneumonia? *Journal of Controlled Release* **325**, 135–140 (2020).

133. Takahashi, A. *et al.* Exosomes maintain cellular homeostasis by excreting harmful DNA from cells. *Nat Commun* **8**, 15287 (2017).

134. Chen, C. C. *et al.* Elucidation of Exosome Migration Across the Blood–Brain Barrier Model In Vitro. *Cel. Mol. Bioeng.* **9**, 509–529 (2016).

135. McGough, I. J. & Vincent, J.-P. Exosomes in developmental signalling. *Development* **143**, 2482–2493 (2016).

136. EL Andaloussi, S., Mäger, I., Breakefield, X. O. & Wood, M. J. A. Extracellular vesicles: biology and emerging therapeutic opportunities. *Nat Rev Drug Discov* **12**, 347–357 (2013).

137. Takeuchi, T. & Nagai, Y. Emerging roles of extracellular vesicles in polyglutamine diseases: Mutant protein transmission, therapeutic potential, and diagnostics. *Neurochemistry International* **157**, 105357 (2022).

138. Bano, R., Ahmad, F. & Mohsin, M. A perspective on the isolation and characterization of extracellular vesicles from different biofluids. *RSC Adv* **11**, 19598–19615.

139. Sunkara, V., Woo, H.-K. & Cho, Y.-K. Emerging techniques in the isolation and characterization of extracellular vesicles and their roles in cancer diagnostics and prognostics. *Analyst* **141**, 371–381 (2016).

140. Wang, S., Wang, J., Wei, W. & Ma, G. Exosomes: The Indispensable Messenger in Tumor Pathogenesis and the Rising Star in Antitumor Applications. *Advanced Biosystems* **3**, 1900008 (2019).

141. Shao, H. *et al.* New Technologies for Analysis of Extracellular Vesicles. *Chem Rev* **118**, 1917–1950 (2018).

142. Massey, A. *et al.* Clinical Implications of Exosomes: Targeted Drug Delivery for Cancer Treatment. *International Journal of Molecular Sciences* **22**, 5278 (2021).

143. Théry, C., Zitvogel, L. & Amigorena, S. Exosomes: composition, biogenesis and function. *Nat Rev Immunol* **2**, 569–579 (2002).

144. Muller, L., Hong, C.-S., Stolz, D. B., Watkins, S. C. & Whiteside, T. L. Isolation of biologically-active exosomes from human plasma. *Journal of Immunological Methods* **411**, 55–65 (2014).

145. Böing, A. N. *et al.* Single-step isolation of extracellular vesicles by size-exclusion chromatography. *Journal of Extracellular Vesicles* **3**, 23430 (2014).

146. Crescitelli, R., Lässer, C. & Lötvall, J. Isolation and characterization of extracellular vesicle subpopulations from tissues. *Nat Protoc* **16**, 1548–1580 (2021).

147. Youssef El Baradie, K. B. & Hamrick, M. W. Therapeutic application of extracellular vesicles for musculoskeletal repair & regeneration. *Connective Tissue Research* **62**, 99–114 (2021).

148. Lötvall, J. *et al.* Minimal experimental requirements for definition of extracellular vesicles and their functions: a position statement from the International Society for Extracellular Vesicles. *J Extracell Vesicles* **3**, 10.3402/jev.v3.26913 (2014).

149. Gurunathan, S., Kang, M.-H., Jeyaraj, M., Qasim, M. & Kim, J.-H. Review of the Isolation, Characterization, Biological Function, and Multifarious Therapeutic Approaches of Exosomes. *Cells* **8**, 307 (2019).

150. Necochea-Campion, R. de *et al.* A practical approach to extracellular vesicle characterization among similar biological samples. *Biomed. Phys. Eng. Express* **4**, 065013 (2018).

151. Gercel-Taylor, C., Atay, S., Tullis, R. H., Kesimer, M. & Taylor, D. D. Nanoparticle analysis of circulating cell-derived vesicles in ovarian cancer patients. *Analytical Biochemistry* **428**, 44–53 (2012).

152. Kreimer, S. *et al.* Mass-Spectrometry-Based Molecular Characterization of Extracellular Vesicles: Lipidomics and Proteomics. *J. Proteome Res.* **14**, 2367–2384 (2015).

153. Rupert, D. L. M. *et al.* Determination of Exosome Concentration in Solution Using Surface Plasmon Resonance Spectroscopy. *Anal. Chem.* **86**, 5929–5936 (2014).

154. Pol, E. van der, Coumans, F., Varga, Z., Krumrey, M. & Nieuwland, R. Innovation in detection of microparticles and exosomes. *Journal of Thrombosis and Haemostasis* **11**, 36–45 (2013).

155. Lui, P. P. Y. Stem cell technology for tendon regeneration: current status, challenges, and future research directions. *Stem Cells and Cloning: Advances and Applications* **8**, 163–174 (2015).

156. Carstairs, A. & Genever, P. Stem cell treatment for musculoskeletal disease. *Current Opinion in Pharmacology* **16**, 1–6 (2014).

157. Rui, Y.-F. *et al.* Isolation and characterization of multipotent rat tendon-derived stem cells. *Tissue Eng Part A* **16**, 1549–1558 (2010).

158. Lovati, A. B. *et al.* Characterization and differentiation of equine tendon-derived progenitor cells. *J Biol Regul Homeost Agents* **25**, S75-84 (2011).

159. Soncini, M. *et al.* Isolation and characterization of mesenchymal cells from human fetal membranes. *Journal of Tissue Engineering and Regenerative Medicine* **1**, 296–305 (2007).

160. Girolamo, L. de *et al.* Mesenchymal Stem/Stromal Cells: A New '"Cells as Drugs"' Paradigm. Efficacy and Critical Aspects in Cell Therapy. *Current Pharmaceutical Design* **19**, 2459–2473 (2013).

161. Huang, Y.-Z. *et al.* Mesenchymal Stem/Progenitor Cells Derived from Articular Cartilage, Synovial Membrane and Synovial Fluid for Cartilage Regeneration: Current Status and Future Perspectives. *Stem Cell Rev and Rep* **13**, 575–586 (2017).

162. Costa-Almeida, R., Calejo, I. & Gomes, M. E. Mesenchymal Stem Cells Empowering Tendon Regenerative Therapies. *International Journal of Molecular Sciences* **20**, 3002 (2019).

163. Jiang, L. *et al.* Mesenchymal stem cells: An efficient cell therapy for tendon repair (Review). *International Journal of Molecular Medicine* **52**, 1–21 (2023).

164. Dominici, M. *et al.* Minimal criteria for defining multipotent mesenchymal stromal cells. The International Society for Cellular Therapy position statement. *Cytotherapy* **8**, 315–317 (2006).

165. Wilson, A., Webster, A. & Genever, P. Nomenclature and Heterogeneity: Consequences for the Use of Mesenchymal Stem Cells in Regenerative Medicine. *Regenerative Medicine* **14**, 595–611 (2019).

166. Oliva, A. A., McClain-Moss, L., Pena, A., Drouillard, A. & Hare, J. M. Allogeneic mesenchymal stem cell therapy: A regenerative medicine approach to geroscience. *Aging Med (Milton)* **2**, 142–146 (2019).

167. Ramaswamy Reddy, S. H., Reddy, R., Babu, N. C. & Ashok, G. N. Stem-cell therapy and platelet-rich plasma in regenerative medicines: A review on pros and cons of the technologies. *Journal of Oral and Maxillofacial Pathology* **22**, 367 (2018).

168. Wilson, A., Hodgson-Garms, M., Frith, J. E. & Genever, P. Multiplicity of Mesenchymal Stromal Cells: Finding the Right Route to Therapy. *Front. Immunol.* **10**, (2019).

169. González-González, A., García-Sánchez, D., Dotta, M., Rodríguez-Rey, J. C. & Pérez-Campo, F. M. Mesenchymal stem cells secretome: The cornerstone of cell-free regenerative medicine. *World J Stem Cells* **12**, 1529–1552 (2020).

170. Chen, J. L. *et al.* Efficacy of hESC-MSCs in knitted silk-collagen scaffold for tendon tissue engineering and their roles. *Biomaterials* **31**, 9438–9451 (2010).

171. Xu, W. *et al.* Human iPSC-Derived Neural Crest Stem Cells Promote Tendon Repair in a Rat Patellar Tendon Window Defect Model. *Tissue Engineering Part A* **19**, 2439–2451 (2013).

172. Russo, V. *et al.* Assessing the functional potential of conditioned media derived from amniotic epithelial stem cells engineered on 3D biomimetic scaffolds: An in vitro model for tendon regeneration. *Materials Today Bio* **25**, 101001 (2024).

173. Barboni, B. *et al.* Therapeutic potential of hAECs for early Achilles tendon defect repair through regeneration. *Journal of Tissue Engineering and Regenerative Medicine* **12**, e1594–e1608 (2018).

174. Liang, W. *et al.* The current status of various preclinical therapeutic approaches for tendon repair. *Annals of Medicine* **56**, 2337871 (2024).

175. Zhang, J. & Wang, J. H.-C. Human Tendon Stem Cells Better Maintain Their Stemness in Hypoxic Culture Conditions. *PLOS ONE* **8**, e61424 (2013).

176. Harris, M. T. *et al.* Mesenchymal stem cells used for rabbit tendon repair can form ectopic bone and express alkaline phosphatase activity in constructs. *Journal of Orthopaedic Research* **22**, 998–1003 (2004).

177. Pas, H. I. M. F. L., Moen, M. H., Haisma, H. J. & Winters, M. No evidence for the use of stem cell therapy for tendon disorders: a systematic review. *Br J Sports Med* **51**, 996–1002 (2017).

178. Bagnaninchi, P., Yang, Y., Haj, A. J. E. & Maffulli, N. Tissue engineering for tendon repair. *Br J Sports Med* **41**, e1–e5 (2007).

179. Rajpar, I. & Barrett, J. G. Optimizing growth factor induction of tenogenesis in three-dimensional culture of mesenchymal stem cells. *J Tissue Eng* **10**, 2041731419848776 (2019).

180. Sandonà, M. *et al.* Mesenchymal Stromal Cells and Their Secretome: New Therapeutic Perspectives for Skeletal Muscle Regeneration. *Front. Bioeng. Biotechnol.* **9**, (2021).

181. Kuntin, D. & Genever, P. Mesenchymal stem cells from biology to therapy. *Emerging Topics in Life Sciences* **5**, 539–548 (2021).

182. Yu, H. *et al.* Bone marrow mesenchymal stem cell-derived exosomes promote tendon regeneration by facilitating the proliferation and migration of endogenous tendon stem/progenitor cells. *Acta Biomaterialia* **106**, 328–341 (2020).

183. Ludlow, J. & Buehrer, B. Mesenchymal Stem Cell Exosomes - Potential Regenerative Medicine Application for Tendinopathy. *The FASEB Journal* **29**, 1018.3 (2015).

184. Li, J., Liu, Z.-P., Xu, C. & Guo, A. TGF-β1-containing exosomes derived from bone marrow mesenchymal stem cells promote proliferation, migration and fibrotic activity in rotator cuff tenocytes. *Regenerative Therapy* **15**, 70–76 (2020).

185. Li, J., Wang, Z.-H. & Sun, Y.-H. TGF-β1 stimulated mesenchymal stem cells-generated exosomal miR-29a promotes the proliferation, migration and fibrogenesis of tenocytes by targeting FABP3. *Cytokine* **162**, 156090 (2023).

186. Wei, X. *et al.* Local administration of TGFβ-1/VEGF165 gene-transduced bone mesenchymal stem cells for Achilles allograft replacement of the anterior cruciate ligament in rabbits. *Biochem Biophys Res Commun* **406**, 204–210 (2011).

187. Francis-West, P. H. *et al.* Mechanisms of GDF-5 action during skeletal development. *Development* **126**, 1305–1315 (1999).

188. P, B., C, E., Cw, A. & P, F.-W. Growth/differentiation factor-5 (GDF-5) and skeletal development. *The Journal of bone and joint surgery. American volume* **83-A Suppl 1**, (2001).

189. Li, H. *et al.* Therapeutic potential of GDF-5 for enhancing tendon regenerative healing. *Regenerative Therapy* **26**, 290–298 (2024).

190. Guzman, A. *et al.* SMAD versus Non-SMAD Signaling Is Determined by Lateral Mobility of Bone Morphogenetic Protein (BMP) Receptors. *The Journal of Biological Chemistry* **287**, 39492 (2012).

191. Wolfman, N. M. *et al.* Ectopic induction of tendon and ligament in rats by growth and differentiation factors 5, 6, and 7, members of the TGF-beta gene family. *J Clin Invest* **100**, 321–330 (1997).

192. Keller, T. C. *et al.* Growth/differentiation factor-5 modulates the synthesis and expression of extracellular matrix and cell-adhesion-related molecules of rat Achilles tendon fibroblasts. *Connective Tissue Research* **52**, 353–364 (2011).

193. Raabe, O. *et al.* Tenogenic differentiation of equine adipose-tissue-derived stem cells under the influence of tensile strain, growth differentiation factors and various oxygen tensions. *Cell Tissue Res* **352**, 509–521 (2013).

194. Ciardulli, M. C. *et al.* Dose-Response Tendon-Specific Markers Induction by Growth Differentiation Factor-5 in Human Bone Marrow and Umbilical Cord Mesenchymal Stem Cells. *Int J Mol Sci* **21**, 5905 (2020).

195. Tan, S. L. *et al.* Growth differentiation factor 5(GDF5)-induced mesenchymal stromal cells enhances tendon healing. *Tissue Engineering Part C: Methods* (2024) doi:10.1089/ten.TEC.2024.0230.

196. Tan, S.-L. *et al.* Effect of Growth Differentiation Factor 5 on the Proliferation and Tenogenic Differentiation Potential of Human Mesenchymal Stem Cells in vitro. *Cells Tissues Organs* **196**, 325–338 (2012).

197. Park, A. *et al.* Adipose-Derived Mesenchymal Stem Cells Treated with Growth Differentiation Factor-5 Express Tendon-Specific Markers. *Tissue Eng Part A* **16**, 2941–2951 (2010).

198. Farng, E., Urdaneta, A. R., Barba, D., Esmende, S. & McAllister, D. R. The Effects of GDF-5 and Uniaxial Strain on Mesenchymal Stem Cells in 3-D Culture. *Clin Orthop Relat Res* **466**, 1930–1937 (2008).

199. Wu, J. *et al.* Hierarchical porous ECM scaffolds incorporating GDF-5 fabricated by cryogenic 3D printing to promote articular cartilage regeneration. *Biomaterials Research* **27**, 7 (2023).

200. Sun, Y., You, Y., Jiang, W., Zhai, Z. & Dai, K. 3D-bioprinting a genetically inspired cartilage scaffold with GDF5-conjugated BMSC-laden hydrogel and polymer for cartilage repair. *Theranostics* **9**, 6949–6961 (2019).

201. Huang, L. *et al.* Biomimetic Scaffolds for Tendon Tissue Regeneration. *Biomimetics* **8**, 246 (2023).

202. Ma, P. X. Scaffolds for tissue fabrication. *Materials Today* **7**, 30–40 (2004).

203. Zhang, H. *et al.* Physical Microenvironment-Based Inducible Scaffold for Stem Cell Differentiation and Tendon Regeneration. *Tissue Engineering Part B: Reviews* **24**, 443–453 (2018).

204. Breidenbach, A. P. *et al.* Fibrin Gels Exhibit Improved Biological, Structural, and Mechanical Properties Compared with Collagen Gels in Cell-Based Tendon Tissue-Engineered Constructs. *Tissue Engineering Part A* **21**, 438–450 (2015).

205. Ciardulli, M. C. *et al.* Fibrin Scaffolds Perfused with Transforming Growth Factor-β1 as an In Vitro Model to Study Healthy and Tendinopathic Human Tendon Stem/Progenitor Cells. *International Journal of Molecular Sciences* **25**, 9563 (2024).

206. Liu, Y., Ramanath, H. S. & Wang, D.-A. Tendon tissue engineering using scaffold enhancing strategies. *Trends in Biotechnology* **26**, 201–209 (2008).

207. Ning, C. *et al.* Recent advances in tendon tissue engineering strategy. *Front. Bioeng. Biotechnol.* **11**, (2023).

208. Zhang, B. *et al.* Construction of tendon replacement tissue based on collagen sponge and mesenchymal stem cells by coupled mechano-chemical induction and evaluation of its tendon repair abilities. *Acta Biomater* **74**, 247–259 (2018).

209. Sahoo, S., Cho-Hong, J. G. & Siew-Lok, T. Development of hybrid polymer scaffolds for potential applications in ligament and tendon tissue engineering. *Biomed. Mater.* **2**, 169 (2007).

210. Jiang, Y.-H. *et al.* Cross-linking methods of type I collagen-based scaffolds for cartilage tissue engineering. *American Journal of Translational Research* **14**, 1146 (2022).

211. Kew, S. J. *et al.* Regeneration and repair of tendon and ligament tissue using collagen fibre biomaterials. *Acta Biomaterialia* **7**, 3237–3247 (2011).

212. Hakimi, O., Knight, D. P., Vollrath, F. & Vadgama, P. Spider and mulberry silkworm silks as compatible biomaterials. *Composites Part B: Engineering* **38**, 324–337 (2007).

213. Vasiliadis, A. V. & Katakalos, K. The Role of Scaffolds in Tendon Tissue Engineering. *Journal of Functional Biomaterials* **11**, 78 (2020).

214. Cribb, A. M. & Scott, J. E. Tendon response to tensile stress: an ultrastructural investigation of collagen:proteoglycan interactions in stressed tendon. *J Anat* **187**, 423–428 (1995).

215. Cheng, X. *et al.* Hypoxia-Mimicking Microenvironment Scaffold for Enhanced Tendon Regeneration. *ACS Appl. Mater. Interfaces* (2025) doi:10.1021/acsami.4c18082.

216. Tsiapalis, D. *et al.* The synergistic effect of low oxygen tension and macromolecular crowding in the development of extracellular matrix-rich tendon equivalents. *Biofabrication* **12**, 025018 (2020).

217. Fang, W. H., Agrawal, D. K. & Thankam, F. G. “Smart Exosomes”: A Smart Approach for Tendon Regeneration. *Tissue Engineering Part B: Reviews* **28**, 613–625 (2022).

218. Liu, H.-M., Zhu, M., Ding, W., Ning, L.-J. & Qin, T.-W. The role of extracellular vesicles in the treatment of tendinopathy by regulating the pathological immune microenvironment. *Chemical Engineering Journal* **499**, 156489 (2024).

219. Valanti, E.-K. *et al.* Reconstituted HDL-apoE3 promotes endothelial cell migration through ID1 and its downstream kinases ERK1/2, AKT and p38 MAPK. *Metabolism* **127**, 154954 (2022).

220. Fu, G., Lu, L., Pan, Z., Fan, A. & Yin, F. Adipose-Derived Stem Cell Exosomes Facilitate Rotator Cuff Repair by Mediating Tendon-Derived Stem Cells. *Regenerative Medicine* **16**, 359–372 (2021).

221. Li, X. *et al.* Eugenol-Preconditioned Mesenchymal Stem Cell-Derived Extracellular Vesicles Promote Antioxidant Capacity of Tendon Stem Cells In Vitro and In Vivo. *Oxidative Medicine and Cellular Longevity* **2022**, 3945195 (2022).

222. Cargnoni, A. *et al.* Extracellular Vesicles From Perinatal Cells for Anti-inflammatory Therapy. *Front. Bioeng. Biotechnol.* **9**, (2021).

223. Shi, Y. *et al.* Exosomes Derived from Bone Marrow Stromal Cells (BMSCs) Enhance Tendon-Bone Healing by Regulating Macrophage Polarization. *Med Sci Monit* **26**, (2020).

224. Chamberlain, C. S. *et al.* Extracellular Vesicle-Educated Macrophages Promote Early Achilles Tendon Healing. *Stem Cells* **37**, 652–662 (2019).

225. Ye, T. *et al.* Large extracellular vesicles secreted by human iPSC-derived MSCs ameliorate tendinopathy *via* regulating macrophage heterogeneity. *Bioactive Materials* **21**, 194–208 (2023).

226. Chen, W. *et al.* Immunomodulatory effects of mesenchymal stromal cells-derived exosome. *Immunol Res* **64**, 831–840 (2016).

227. Pawitan, J. A. Prospect of Stem Cell Conditioned Medium in Regenerative Medicine. *BioMed Research International* **2014**, 965849 (2014).

228. S, R. *et al.* Prospect of stem cells conditioned medium (secretome) in ligament and tendon healing: A systematic review. *Stem cells translational medicine* **9**, (2020).

229. Soukup, R. *et al.* Mesenchymal Stem Cell Conditioned Medium Modulates Inflammation in Tenocytes: Complete Conditioned Medium Has Superior Therapeutic Efficacy than Its Extracellular Vesicle Fraction. *Int J Mol Sci* **24**, 10857 (2023).

230. Chen, W. *et al.* Conditioned medium of human bone marrow-derived stem cells promotes tendon-bone healing of the rotator cuff in a rat model. *Biomaterials* **271**, 120714 (2021).

231. Papait, A. *et al.* Comparison of EV-free fraction, EVs, and total secretome of amniotic mesenchymal stromal cells for their immunomodulatory potential: a translational perspective. *Front. Immunol.* **13**, (2022).

232. He, C. *et al.* Comparison of two cell-free therapeutics derived from adipose tissue: small extracellular vesicles versus conditioned medium. *Stem Cell Research & Therapy* **13**, 86 (2022).

233. Derwin, K. A., Galatz, L. M., Ratcliffe, A. & Thomopoulos, S. Enthesis Repair. *J Bone Joint Surg Am* **100**, e109 (2018).

234. Wang, C., Hu, Q., Song, W., Yu, W. & He, Y. Adipose Stem Cell–Derived Exosomes Decrease Fatty Infiltration and Enhance Rotator Cuff Healing in a Rabbit Model of Chronic Tears. *Am J Sports Med* **48**, 1456–1464 (2020).

235. Zhang, M. *et al.* Tendon stem cell-derived exosomes regulate inflammation and promote the high-quality healing of injured tendon. *Stem Cell Res Ther* **11**, 402 (2020).

236. Kasula, V. *et al.* The Use of Extracellular Vesicles in Achilles Tendon Repair: A Systematic Review. *Biomedicines* **12**, 942 (2024).

237. Xue, M. & Jackson, C. J. Extracellular Matrix Reorganization During Wound Healing and Its Impact on Abnormal Scarring. *Advances in Wound Care* **4**, 119–136 (2015).

238. Connor, D. E. *et al.* Therapeutic Potential of Exosomes in Rotator Cuff Tendon Healing. *J Bone Miner Metab* **37**, 759–767 (2019).

239. Olejarz, W., Kubiak-Tomaszewska, G., Chrzanowska, A. & Lorenc, T. Exosomes in Angiogenesis and Anti-angiogenic Therapy in Cancers. *Int J Mol Sci* **21**, 5840 (2020).

240. Gupta, A. *et al.* Cell-free Stem Cell-Derived Extract Formulation for Regenerative Medicine Applications. *Int J Mol Sci* **21**, 9364 (2020).

241. Bahr, M. M., Amer, M. S., Abo-El-Sooud, K., Abdallah, A. N. & El-Tookhy, O. S. Preservation techniques of stem cells extracellular vesicles: a gate for manufacturing of clinical grade therapeutic extracellular vesicles and long-term clinical trials. *International Journal of Veterinary Science and Medicine* **8**, 1–8 (2020).

242. Qazi, R. e M. *et al.* Lyophilization Based Isolation of Exosomes. *Int J Mol Sci* **24**, 10477 (2023).

243. Tsintou, M. *et al.* The use of hydrogel-delivered extracellular vesicles in recovery of motor function in stroke: a testable experimental hypothesis for clinical translation including

behavioral and neuroimaging assessment approaches. *Neural Regen Res* **16**, 605–613 (2020).

244. Ma, Y., Brocchini, S. & Williams, G. R. Extracellular vesicle-embedded materials. *Journal of Controlled Release* **361**, 280–296 (2023).

245. Abdollahi, H. *et al.* The Role of Hypoxia in Stem Cell Differentiation and Therapeutics. *J Surg Res* **165**, 112–117 (2011).

246. Carreau, A., Hafny-Rahbi, B. E., Matejuk, A., Grillon, C. & Kieda, C. Why is the partial oxygen pressure of human tissues a crucial parameter? Small molecules and hypoxia. *Journal of Cellular and Molecular Medicine* **15**, 1239–1253 (2011).

247. Johnson, R. W., Sowder, M. E. & Giaccia, A. J. Hypoxia and Bone Metastatic Disease. *Current osteoporosis reports* **15**, 231 (2017).

248. Richardson, R. S. *et al.* Human skeletal muscle intracellular oxygenation: the impact of ambient oxygen availability. *The Journal of Physiology* **571**, 415–424 (2006).

249. Shahid, H., Morya, V. K., Oh, J.-U., Kim, J.-H. & Noh, K.-C. Hypoxia-Inducible Factor and Oxidative Stress in Tendon Degeneration: A Molecular Perspective. *Antioxidants (Basel)* **13**, 86 (2024).

250. Dale, T. P. Investigating the chondrogenic phenotype in clinically relevant cells: the effect of hTERT expression. (2016).

251. Strowitzki, M. J., Cummins, E. P. & Taylor, C. T. Protein Hydroxylation by Hypoxia-Inducible Factor (HIF) Hydroxylases: Unique or Ubiquitous? *Cells* **8**, 384 (2019).

252. Zhang, J., Yao, M., Xia, S., Zeng, F. & Liu, Q. Systematic and comprehensive insights into HIF-1 stabilization under normoxic conditions: implications for cellular adaptation and therapeutic strategies in cancer. *Cellular & Molecular Biology Letters* **30**, 2 (2025).

253. Csete, M. Oxygen in the Cultivation of Stem Cells. *Annals of the New York Academy of Sciences* **1049**, 1–8 (2005).

254. Keith, B. & Simon, M. C. Hypoxia-Inducible Factors, Stem Cells, and Cancer. *Cell* **129**, 465–472 (2007).

255. Lee, W. Y. W., Lui, P. P. Y. & Rui, Y. F. Hypoxia-Mediated Efficient Expansion of Human Tendon–Derived Stem Cells In Vitro. *Tissue Eng Part A* **18**, 484–498 (2012).

256. Zulkifli, A. *et al.* The potential mechanism of hypoxia-induced tenogenic differentiation of mesenchymal stem cell for tendon regeneration. *Tissue and Cell* **82**, 102075 (2023).

257. Pezzi, A. *et al.* Effects Of Hypoxia in Long-Term In Vitro Expansion of Human Bone Marrow Derived Mesenchymal Stem Cells. *Journal of Cellular Biochemistry* **118**, 3072–3079 (2017).

258. Ma, T., Grayson, W. L., Fröhlich, M. & Vunjak-Novakovic, G. Hypoxia and Stem Cell-Based Engineering of Mesenchymal Tissues. *Biotechnol Prog* **25**, 32–42 (2009).

259. Kwon, S. Y. *et al.* Hypoxia Enhances Cell Properties of Human Mesenchymal Stem Cells. *Tissue Eng Regen Med* **14**, 595–604 (2017).

260. Bister, N. *et al.* Hypoxia and extracellular vesicles: A review on methods, vesicular cargo and functions. *J Extracell Vesicles* **10**, e12002 (2020).

261. Jiang, H. *et al.* Hypoxia Induced Changes of Exosome Cargo and Subsequent Biological Effects. *Front Immunol* **13**, 824188 (2022).

262. Järvinen, T. A. Neovascularisation in tendinopathy: from eradication to stabilisation? *British Journal of Sports Medicine* **54**, 1 (2019).

263. Chen, G. *et al.* Hypoxia-Induced Mesenchymal Stem Cells Exhibit Stronger Tenogenic Differentiation Capacities and Promote Patellar Tendon Repair in Rabbits. *Stem Cells International* **2020**, 8822609 (2020).

264. Benage, L. G., Sweeney, J. D., Giers, M. B. & Balasubramanian, R. Dynamic Load Model Systems of Tendon Inflammation and Mechanobiology. *Front Bioeng Biotechnol* **10**, 896336 (2022).

265. Wu, S. Y., Kim, W. & Kremen, T. J. In Vitro Cellular Strain Models of Tendon Biology and Tenogenic Differentiation. *Front Bioeng Biotechnol* **10**, 826748 (2022).

266. Janvier, A. J., Canty-Laird, E. & Henstock, J. R. A universal multi-platform 3D printed bioreactor chamber for tendon tissue engineering. *J Tissue Eng* **11**, 2041731420942462 (2020).

267. Banik, B. L. & Brown, J. L. 3D-Printed Bioreactor Enhances Potential for Tendon Tissue Engineering. *Regen. Eng. Transl. Med.* **6**, 419–428 (2020).

268. Donderwinkel, I., Tuan, R. S., Cameron, N. R. & Frith, J. E. Tendon tissue engineering: Current progress towards an optimized tenogenic differentiation protocol for human stem cells. *Acta Biomaterialia* **145**, 25–42 (2022).

269. Youngstrom, D. W., LaDow, J. E. & Barrett, J. G. Tenogenesis of bone marrow-, adipose-, and tendon-derived stem cells in a dynamic bioreactor. *Connective Tissue Research* **57**, 454–465 (2016).

270. Ciardulli, M. C. *et al.* Tendon and Cytokine Marker Expression by Human Bone Marrow Mesenchymal Stem Cells in a Hyaluronate/Poly-Lactic-Co-Glycolic Acid (PLGA)/Fibrin Three-Dimensional (3D) Scaffold. *Cells* **9**, 1268 (2020).

271. Lindbergh, C. A. AN APPARATUS FOR THE CULTURE OF WHOLE ORGANS. *J Exp Med* **62**, 409–431 (1935).

272. Youngstrom, D. W. & Barrett, J. G. Engineering Tendon: Scaffolds, Bioreactors, and Models of Regeneration. *Stem Cells International* **2016**, 3919030 (2016).

273. Yeatts, A. B. & Fisher, J. P. Bone tissue engineering bioreactors: dynamic culture and the influence of shear stress. *Bone* **48**, 171–181 (2011).

274. Kang, H., Bae, Y., Kwon, Y., Kim, S. & Park, J. Extracellular Vesicles Generated Using Bioreactors and their Therapeutic Effect on the Acute Kidney Injury Model. *Advanced Healthcare Materials* **11**, 2101606 (2022).

275. Almeria, C., Kreß, S., Weber, V., Egger, D. & Kasper, C. Heterogeneity of mesenchymal stem cell-derived extracellular vesicles is highly impacted by the tissue/cell source and culture conditions. *Cell Biosci* **12**, 51 (2022).

276. Scala, P. *et al.* Myogenic commitment of human stem cells by myoblasts Co-culture: a static vs. a dynamic approach. *Artificial Cells, Nanomedicine, and Biotechnology* **50**, 49–58 (2022).

277. Lamparelli, E. P. *et al.* Chondrogenic Commitment of Human Bone Marrow Mesenchymal Stem Cells in a Perfused Collagen Hydrogel Functionalized with hTGF-β1-Releasing PLGA Microcarrier. *Pharmaceutics* **13**, 399 (2021).

278. Yang, J. *et al.* Isolation, culture and biological characteristics of multipotent porcine tendon-derived stem cells. *Int J Mol Med* **41**, 3611–3619 (2018).

279. Clerici, M. *et al.* Human tendon stem/progenitor cell-derived extracellular vesicle production promoted by dynamic culture. *Artificial Cells, Nanomedicine, and Biotechnology* **53**, 1–16 (2025).

280. Aaronson, S. A. & Todaro, G. J. Development of 3T3-like lines from Balb/c mouse embryo cultures: Transformation susceptibility to SV40. *Journal of Cellular Physiology* **72**, 141–148 (1968).

281. Schneider, C. A., Rasband, W. S. & Eliceiri, K. W. NIH Image to ImageJ: 25 years of image analysis. *Nat Methods* **9**, 671–675 (2012).

282. Lomas, A. J. *et al.* Poly (3-Hydroxybutyrate-co-3-Hydroxyhexanoate)/Collagen Hybrid Scaffolds for Tissue Engineering Applications. *Tissue Eng Part C Methods* **19**, 577–585 (2013).

283. Lee, K. J., Clegg, P. D., Comerford, E. J. & Canty-Laird, E. G. A comparison of the stem cell characteristics of murine tenocytes and tendon-derived stem cells. *BMC Musculoskelet Disord* **19**, 116 (2018).

284. Zhang, J. & Wang, J. H.-C. Characterization of differential properties of rabbit tendon stem cells and tenocytes. *BMC Musculoskeletal Disorders* **11**, 10 (2010).

285. Williamson, K. A. *et al.* Restricted differentiation potential of progenitor cell populations obtained from the equine superficial digital flexor tendon (SDFT). *Journal of Orthopaedic Research* **33**, 849–858 (2015).

286. Zhang, J. *et al.* Characterization of the structure, vascularity, and stem/progenitor cell populations in porcine Achilles tendon (PAT). *Cell Tissue Res* **384**, 367–387 (2021).

287. Ye, Y. *et al.* The pig as a potential organ donor for man. A study of potentially transferable disease from donor pig to recipient man. *Transplantation* **57**, 694–703 (1994).

288. Lyu, K. *et al.* A “cell-free treatment” for tendon injuries: adipose stem cell-derived exosomes. *European Journal of Medical Research* **27**, 75 (2022).

289. Song, K., Jiang, T., Pan, P., Yao, Y. & Jiang, Q. Exosomes from tendon derived stem cells promote tendon repair through miR-144-3p-regulated tenocyte proliferation and migration. *Stem Cell Research & Therapy* **13**, 80 (2022).

290. Xu, T. *et al.* Tenocyte-derived exosomes induce the tenogenic differentiation of mesenchymal stem cells through TGF-β. *Cytotechnology* **71**, 57–65 (2019).

291. Wang, Y. *et al.* Exosomes from tendon stem cells promote injury tendon healing through balancing synthesis and degradation of the tendon extracellular matrix. *Journal of Cellular and Molecular Medicine* **23**, 5475–5485 (2019).

292. He, Y. *et al.* Exosomes derived from tendon stem/progenitor cells enhance tendon-bone interface healing after rotator cuff repair in a rat model. *Bioactive Materials* **40**, 484–502 (2024).

293. Yang, J. *et al.* Isolation and biological characterization of tendon-derived stem cells from fetal bovine. *In Vitro Cell.Dev.Biol.-Animal* **52**, 846–856 (2016).

294. Mazzocca, A. D. *et al.* In vitro changes in human tenocyte cultures obtained from proximal biceps tendon: multiple passages result in changes in routine cell markers. *Knee Surg Sports Traumatol Arthrosc* **20**, 1666–1672 (2012).

295. Bernard-Beaubois, K., Hecquet, C., Houcine, O., Hayem, G. & Adolphe, M. Culture and characterization of juvenile rabbit tenocytes. *Cell Biol Toxicol* **13**, 103–113 (1997).

296. Wei, B. & Lu, J. Characterization of Tendon-Derived Stem Cells and Rescue Tendon Injury. *Stem Cell Rev and Rep* **17**, 1534–1551 (2021).

297. Tello, R. P. *et al.* Fabrication of hydrogel microspheres via microfluidics using inverse electron demand Diels–Alder click chemistry-based tetrazine-norbornene for drug delivery and cell encapsulation applications. *Biomater. Sci.* **11**, 4972–4984 (2023).

298. Chen, P. *et al.* Intramuscular injection of Botox causes tendon atrophy by induction of senescence of tendon-derived stem cells. *Stem Cell Research & Therapy* **12**, 38 (2021).

299. Okonkwo, C. & Singh, M. Recovery of fibroblast-like cells from refrigerated goat skin up to 41 d of animal death. *In Vitro Cell.Dev.Biol.-Animal* **51**, 463–469 (2015).

300. Kapoor, A., Caporali, E. H. G., Kenis, P. J. A. & Stewart, M. C. Microtopographically patterned surfaces promote the alignment of tenocytes and extracellular collagen. *Acta Biomaterialia* **6**, 2580–2589 (2010).

301. Yao, L., Bestwick, C. S., Bestwick, L. A., Maffulli, N. & Aspden, R. M. Phenotypic drift in human tenocyte culture. *Tissue Eng* **12**, 1843–1849 (2006).

302. de Mos, M. *et al.* Intrinsic differentiation potential of adolescent human tendon tissue: an in-vitro cell differentiation study. *BMC Musculoskeletal Disorders* **8**, 16 (2007).

303. Lui, P. P. Y. Markers for the identification of tendon-derived stem cells in vitro and tendon stem cells in situ – update and future development. *Stem Cell Research & Therapy* **6**, 106 (2015).

304. Tsai, C.-C., Huang, T.-F., Ma, H.-L., Chiang, E.-R. & Hung, S.-C. Isolation of Mesenchymal Stem Cells from Shoulder Rotator Cuff: A Potential Source for Muscle and Tendon Repair. *Cell Transplant* **22**, 413–422 (2013).

305. Cadby, J. A., Buehler, E., Godbout, C., Weeren, P. R. van & Snedeker, J. G. Differences between the Cell Populations from the Peritenon and the Tendon Core with Regard to Their Potential Implication in Tendon Repair. *PLOS ONE* **9**, e92474 (2014).

306. Spanoudes, K., Gaspar, D., Pandit, A. & Zeugolis, D. I. The biophysical, biochemical, and biological toolbox for tenogenic phenotype maintenance *in vitro*. *Trends in Biotechnology* **32**, 474–482 (2014).

307. Maffulli, N., Cuozzo, F., Migliorini, F. & Oliva, F. The tendon unit: biochemical, biomechanical, hormonal influences. *J Orthop Surg Res* **18**, 311 (2023).

308. Zhang, C., Zhu, J., Zhou, Y., Thampatty, B. P. & Wang, J. H.-C. Tendon Stem/Progenitor Cells and Their Interactions with Extracellular Matrix and Mechanical Loading. *Stem Cells International* **2019**, e3674647 (2019).

309. Tan, S.-L. *et al.* Identification of Pathways Mediating Growth Differentiation Factor5-Induced Tenogenic Differentiation in Human Bone Marrow Stromal Cells. *PLOS ONE* **10**, e0140869 (2015).

310. Zhu, Z. *et al.* The Therapeutic Effect of iMSC-Derived Small Extracellular Vesicles on Tendinopathy Related Pain Through Alleviating Inflammation: An in vivo and in vitro Study. *J Inflamm Res* **15**, 1421–1436 (2022).

311. Abels, E. R. & Breakefield, X. O. Introduction to Extracellular Vesicles: Biogenesis, RNA Cargo Selection, Content, Release, and Uptake. *Cell Mol Neurobiol* **36**, 301–312 (2016).

312. Patel, D. B., Luthers, C. R., Lerman, M. J., Fisher, J. P. & Jay, S. M. Enhanced extracellular vesicle production and ethanol-mediated vascularization bioactivity via a 3D-printed scaffold-perfusion bioreactor system. *Acta Biomaterialia* **95**, 236–244 (2019).

313. Yuan, X. *et al.* Engineering extracellular vesicles by three-dimensional dynamic culture of human mesenchymal stem cells. *Journal of Extracellular Vesicles* **11**, e12235 (2022).

314. Artuyants, A. *et al.* Production of Extracellular Vesicles Using a CELLine Adherent Bioreactor Flask. in *Bioreactors in Stem Cell Biology: Methods and Protocols* (ed. Turksen, K.) 183–192 (Springer US, New York, NY, 2022). doi:10.1007/7651_2021_413.

315. Walia, B. & Huang, A. H. Tendon Stem Progenitor Cells: Understanding the biology to inform therapeutic strategies for tendon repair. *J Orthop Res* **37**, 1270–1280 (2019).

316. Tan, Q., Lui, P. P. Y. & Rui, Y. F. Effect of In Vitro Passaging on the Stem Cell-Related Properties of Tendon-Derived Stem Cells—Implications in Tissue Engineering. *Stem Cells Dev* **21**, 790–800 (2012).

317. Stowe, E. J., Keller, M. R. & Connizzo, B. K. Cellular senescence impairs tendon extracellular matrix remodeling in response to mechanical unloading. *Aging Cell* **23**, e14278 (2024).

318. Yan, Z. *et al.* Aged Tendon Stem/Progenitor Cells Are Less Competent to Form 3D Tendon Organoids Due to Cell Autonomous and Matrix Production Deficits. *Front. Bioeng. Biotechnol.* **8**, (2020).

319. Keller, T. C. *et al.* Growth/differentiation factor-5 modulates the synthesis and expression of extracellular matrix and cell-adhesion-related molecules of rat Achilles tendon fibroblasts. *Connective Tissue Research* **52**, 353–364 (2011).

320. Cortella, G. *et al.* ColMA-based bioprinted 3D scaffold allowed to study tenogenic events in human tendon stem cells. *Bioengineering & Translational Medicine* **n/a**, e10723.

321. de Almeida Fuzeta, M. *et al.* Scalable Production of Human Mesenchymal Stromal Cell-Derived Extracellular Vesicles Under Serum-/Xeno-Free Conditions in a Microcarrier-Based Bioreactor Culture System. *Front. Cell Dev. Biol.* **8**, (2020).

322. Wang, Y. *et al.* Exosomes from tendon stem cells promote injury tendon healing through balancing synthesis and degradation of the tendon extracellular matrix. *J Cell Mol Med* **23**, 5475–5485 (2019).

323. Mullen, M. *et al.* Mechanical strain drives exosome production, function, and miRNA cargo in C2C12 muscle progenitor cells. *Journal of Orthopaedic Research* **41**, 1186–1197 (2023).

324. Wu, D. *et al.* Physical modulation of mesenchymal stem cell exosomes: A new perspective for regenerative medicine. *Cell Prolif* **57**, e13630 (2024).

325. Eustes, A. S. & Dayal, S. The Role of Platelet-Derived Extracellular Vesicles in Immune-Mediated Thrombosis. *Int J Mol Sci* **23**, 7837 (2022).

326. Lan, X.-Y. *et al.* NCAM mimetic peptide P2 synergizes with bone marrow mesenchymal stem cells in promoting functional recovery after stroke. *J Cereb Blood Flow Metab* **44**, 1128–1144 (2024).

327. Andrade, A. C. *et al.* Piezo1 activation increases the release of therapeutic extracellular vesicles after mechanical stimulation in bioreactors. 2025.01.09.632205 Preprint at https://doi.org/10.1101/2025.01.09.632205 (2025).

328. Dabrowska, S., Andrzejewska, A., Janowski, M. & Lukomska, B. Immunomodulatory and Regenerative Effects of Mesenchymal Stem Cells and Extracellular Vesicles: Therapeutic Outlook for Inflammatory and Degenerative Diseases. *Front Immunol* **11**, 591065 (2021).

329. Phelps, J., Hart, D. A., Mitha, A. P., Duncan, N. A. & Sen, A. Physiological oxygen conditions enhance the angiogenic properties of extracellular vesicles from human mesenchymal stem cells. *Stem Cell Research & Therapy* **14**, 218 (2023).

330. Baer, M. R. *et al.* Expression of the neural cell adhesion molecule CD56 is associated with short remission duration and survival in acute myeloid leukemia with t(8;21)(q22;q22). *Blood* **90**, 1643–1648 (1997).

331. Soós, A. Á. *et al.* High CD142 Level Marks Tumor-Promoting Fibroblasts with Targeting Potential in Colorectal Cancer. *International Journal of Molecular Sciences* **24**, 11585 (2023).

332. Lee, B.-C. & Kang, K.-S. Functional enhancement strategies for immunomodulation of mesenchymal stem cells and their therapeutic application. *Stem Cell Research & Therapy* **11**, 397 (2020).

333. Castillo-Rodríguez, R. A., Trejo-Solís, C., Cabrera-Cano, A., Gómez-Manzo, S. & Dávila-Borja, V. M. Hypoxia as a Modulator of Inflammation and Immune Response in Cancer. *Cancers (Basel)* **14**, 2291 (2022).

334. Liu, X. *et al.* Immunomodulatory potential of mesenchymal stem cell-derived extracellular vesicles: Targeting immune cells. *Front Immunol* **14**, 1094685 (2023).

335. Al-Azzawi, B. *et al.* The Secretome of Mesenchymal Stem Cells Prevents Islet Beta Cell Apoptosis an IL-10-Dependent Mechanism. *The Open Stem Cell Journal* **6**, (2020).

336. Naldini, A., Pucci, A. & Carraro, F. HYPOXIA INDUCES THE EXPRESSION AND RELEASE OF INTERLEUKIN 1 RECEPTOR ANTAGONIST IN MITOGEN-ACTIVATED MONONUCLEAR CELLS. *Cytokine* **13**, 334–341 (2001).

337. Yu, W. *et al.* Mechanical force-driven TNFα endocytosis governs stem cell homeostasis. *Bone Res* **8**, 1–13 (2021).

338. Bi, Y. *et al.* Identification of tendon stem/progenitor cells and the role of the extracellular matrix in their niche. *Nat Med* **13**, 1219–1227 (2007).

339. Wang, Y. *et al.* Exosomes from tendon stem cells promote injury tendon healing through balancing synthesis and degradation of the tendon extracellular matrix. *J Cell Mol Med* **23**, 5475–5485 (2019).

340. An, Q., Zhou, Z., Xu, C. & Xiao, Q. Exosomes derived from mir-337-3p over-expressing tendon stem cells protect against apoptosis of tenocytes via targeting caspase3. *BMC Musculoskelet Disord* **25**, 561 (2024).

341. Holladay, C., Abbah, S.-A., O'Dowd, C., Pandit, A. & Zeugolis, D. I. Preferential tendon stem cell response to growth factor supplementation. *Journal of Tissue Engineering and Regenerative Medicine* **10**, 783–798 (2016).

342. Zhang, T. *et al.* Small extracellular vesicles derived from tendon stem cells promote the healing of injured Achilles tendons by regulating miR-145-3p. *Acta Biomaterialia* **172**, 280–296 (2023).

343. Chen, Q. *et al.* Tenocyte proliferation and migration promoted by rat bone marrow mesenchymal stem cell-derived conditioned medium. *Biotechnol Lett* **40**, 215–224 (2018).

344. Shi, Z., Wang, Q. & Jiang, D. Extracellular vesicles from bone marrow-derived multipotent mesenchymal stromal cells regulate inflammation and enhance tendon healing. *J Transl Med* **17**, 211 (2019).

345. Haidar-Montes, A. A. *et al.* Mechanobiological Strategies to Enhance Ovine (Ovis aries) Adipose-Derived Stem Cells Tendon Plasticity for Regenerative Medicine and Tissue Engineering Applications. *Animals* **14**, 2233 (2024).

346. Vogler, M. *et al.* Hypoxia Modulates Fibroblastic Architecture, Adhesion and Migration: A Role for HIF-1α in Cofilin Regulation and Cytoplasmic Actin Distribution. *PLOS ONE* **8**, e69128 (2013).

347. Gao, Y., Chu, M., Hong, J., Shang, J. & Xu, D. Hypoxia induces cardiac fibroblast proliferation and phenotypic switch: a role for caveolae and caveolin-1/PTEN mediated pathway. *Journal of Thoracic Disease* **6**, (2014).

348. Chouaib, B., Haack-Sørensen, M., Chaubron, F., Cuisinier, F. & Collart-Dutilleul, P.-Y. Towards the Standardization of Mesenchymal Stem Cell Secretome-Derived Product Manufacturing for Tissue Regeneration. *Int J Mol Sci* **24**, 12594 (2023).

349. Paschalidis, T. *et al.* Dental pulp stem cells' secretome enhances pulp repair processes and compensates TEGDMA-induced cytotoxicity. *Dental Materials* **30**, e405–e418 (2014).

350. Guo, X. *et al.* Adipose-derived mesenchymal stem cells with hypoxic preconditioning improve tenogenic differentiation. *J Orthop Surg Res* **17**, 49 (2022).

351. Giannasi, C. *et al.* Comparison of two ASC-derived therapeutics in an in vitro OA model: secretome versus extracellular vesicles. *Stem Cell Research & Therapy* **11**, 521 (2020).

352. Zaffryar-Eilot, S. & Hasson, P. Lysyl Oxidases: Orchestrators of Cellular Behavior and ECM Remodeling and Homeostasis. *International Journal of Molecular Sciences* **23**, 11378 (2022).

353. Tsuchiya, Y., Yeung, C.-Y. C., Svensson, R. B. & Kjaer, M. Effect of human myoblasts on tenogenic progression in 2D and 3D culture models. *Journal of Anatomy* **n/a**,.

354. Ciardulli, M. C. *et al.* 3D Biomimetic Scaffold for Growth Factor Controlled Delivery: An In-Vitro Study of Tenogenic Events on Wharton's Jelly Mesenchymal Stem Cells. *Pharmaceutics* **13**, 1448 (2021).

355. Zhang, X. *et al.* 3-Dimensional Bioprinting of a Tendon Stem Cell–Derived Exosomes Loaded Scaffold to Bridge the Unrepairable Massive Rotator Cuff Tear. *Am J Sports Med* **52**, 2358–2371 (2024).

356. Zhang, B.-Y., Xu, P., Luo, Q. & Song, G.-B. Proliferation and tenogenic differentiation of bone marrow mesenchymal stem cells in a porous collagen sponge scaffold. *World J Stem Cells* **13**, 115–127 (2021).

357. Costa-Almeida, R., Berdecka, D., Rodrigues, M., Reis, R. L. & Gomes, M. Tendon explant cultures to study the communication between adipose stem cells and native tendon niche. *Journal of Cellular Biochemistry* **119**, 3653–3662 (2017).

358. Schiele, N. R., Marturano, J. E. & Kuo, C. K. Mechanical factors in embryonic tendon development: potential cues for stem cell tenogenesis. *Curr Opin Biotechnol* **24**, 834–840 (2013).

359. Freedman, B. R. *et al.* Dynamic Loading and Tendon Healing Affect Multiscale Tendon Properties and ECM Stress Transmission. *Sci Rep* **8**, 10854 (2018).

360. ZHU, M.-M., MA, Y., TANG, M., PAN, L. & LIU, W.-L. Hypoxia-Induced Upregulation of Matrix Metalloproteinase 9 Increases Basement Membrane Degradation by Downregulating Collagen Type IV Alpha 1 Chain. *Physiol Res* **71**, 825–834 (2022).

361. Gilkes, D. M., Semenza, G. L. & Wirtz, D. Hypoxia and the extracellular matrix: drivers of tumour metastasis. *Nat Rev Cancer* **14**, 430–439 (2014).

362. Rosochowicz, M. A., Lach, M. S., Richter, M., Suchorska, W. M. & Trzeciak, T. Conditioned Medium – Is it an Undervalued Lab Waste with the Potential for Osteoarthritis Management? *Stem Cell Rev Rep* **19**, 1185–1213 (2023).

363. Yamano, S. *et al.* The effect of a bioactive collagen membrane releasing PDGF or GDF-5 on bone regeneration. *Biomaterials* **35**, 2446–2453 (2014).

364. Webb, W. R. *et al.* The application of poly(3-hydroxybutyrate-co-3-hydroxyhexanoate) scaffolds for tendon repair in the rat model. *Biomaterials* **34**, 6683–6694 (2013).

365. Graça, A. L., Domingues, R. M. A., Gomez-Florit, M. & Gomes, M. E. Platelet-Derived Extracellular Vesicles Promote Tenogenic Differentiation of Stem Cells on Bioengineered Living Fibers. *Int J Mol Sci* **24**, 3516 (2023).

366. Gunawardena, T. N. A., Rahman, M. T., Abdullah, B. J. J. & Abu Kasim, N. H. Conditioned media derived from mesenchymal stem cell cultures: The next generation for regenerative medicine. *Journal of Tissue Engineering and Regenerative Medicine* **13**, 569–586 (2019).

367. Gonzalez-Avila, G., Sommer, B., Flores-Soto, E. & Aquino-Galvez, A. Hypoxic Effects on Matrix Metalloproteinases' Expression in the Tumor Microenvironment and Therapeutic Perspectives. *International Journal of Molecular Sciences* **24**, 16887 (2023).

368. Docheva, D., Hunziker, E. B., Fässler, R. & Brandau, O. Tenomodulin Is Necessary for Tenocyte Proliferation and Tendon Maturation. *Mol Cell Biol* **25**, 699–705 (2005).

369. Dex, S. *et al.* Tenomodulin is Required for Tendon Endurance Running and Collagen I Fibril Adaptation to Mechanical Load. *EBioMedicine* **20**, 240–254 (2017).

370. Kadry, Y. A. & Calderwood, D. A. Chapter 22: Structural and signaling functions of integrins. *Biochim Biophys Acta Biomembr* **1862**, 183206 (2020).

371. Citeroni, M. R. *et al.* Amnion-Derived Teno-Inductive Secretomes: A Novel Approach to Foster Tendon Differentiation and Regeneration in an Ovine Model. *Front. Bioeng. Biotechnol.* **9**, (2021).

372. Nirmalanandhan, V. S. *et al.* Combined Effects of Scaffold Stiffening and Mechanical Preconditioning Cycles on Construct Biomechanics, Gene Expression, and Tendon Repair Biomechanics. *Tissue Eng Part A* **15**, 2103–2111 (2009).

373. Liu, H. *et al.* Mohawk promotes the tenogenesis of mesenchymal stem cells through activation of the TGFβ signaling pathway. *Stem Cells* **33**, 443–455 (2015).

374. Chamberlain, C. S. *et al.* Extracellular Vesicle-Educated Macrophages Promote Early Achilles Tendon Healing. *Stem Cells* **37**, 652–662 (2019).

375. Chen, S.-H. *et al.* Extracellular Vesicles of Adipose-Derived Stem Cells Promote the Healing of Traumatized Achilles Tendons. *International Journal of Molecular Sciences* **22**, 12373 (2021).

376. Lui, P. P. Y. Mesenchymal Stem Cell-Derived Extracellular Vesicles for the Promotion of Tendon Repair - an Update of Literature. *Stem Cell Rev Rep* **17**, 379–389 (2021).

377. Losner, J., Courtemanche, K. & Whited, J. L. A cross-species analysis of systemic mediators of repair and complex tissue regeneration. *npj Regen Med* **6**, 21 (2021).

378. Sarmah, H. *et al.* Towards human organ generation using interspecies blastocyst complementation: Challenges and perspectives for therapy. *Front. Cell Dev. Biol.* **11**, (2023).

379. Prestwich, G. D. Simplifying the extracellular matrix for 3-D cell culture and tissue engineering: A pragmatic approach. *Journal of Cellular Biochemistry* **101**, 1370–1383 (2007).

380. Ravi, M., Paramesh, V., Kaviya, S. r., Anuradha, E. & Solomon, F. D. P. 3D Cell Culture Systems: Advantages and Applications. *Journal of Cellular Physiology* **230**, 16–26 (2015).



Appendices

9. APPENDICES

9.1 Appendix A – Publications and presentations

Associated publications

- Work detailed in chapter 1 has been published in:

Citro, Vera, Marta Clerici, Aldo R. Boccaccini, Giovanna Della Porta, Nicola Maffulli, and Nicholas R. Forsyth. "Tendon tissue engineering: An overview of biologics to promote tendon healing and repair." *Journal of tissue engineering* 14 (2023): 20417314231196275[279].

- Work detailed in chapter 3 has been published in:

Clerici, Marta, Vera Citro, Amy L. Byrne, Tina P. Dale, Aldo R. Boccaccini, Giovanna Della Porta, Nicola Maffulli, and Nicholas R. Forsyth. "Endotenon-Derived Type II Tendon Stem Cells Have Enhanced Proliferative and Tenogenic Potential." *International Journal of Molecular Sciences* 24, no. 20 (2023): 15107[9].

- Work detailed in chapter 4 has been published in:

Clerici, Marta, Maria Camilla Ciardulli, Erwin Pavel Lamparelli, Joseph Lovecchio, Emanuele Giordano, Tina P. Dale, Nicholas R. Forsyth, Nicola Maffulli, and Giovanna Della Porta. "Human tendon stem/progenitor cell-derived extracellular vesicle production promoted by dynamic culture." *Artificial Cells, Nanomedicine, and Biotechnology* 53, no. 1 (2025): 1-16[279].

Other publications

1. Citro, Vera, Marta Clerici, Matthew T. Shephard, Tina P. Dale, Aldo R. Boccaccini, and Nicholas R. Forsyth. "Growth Factor-Loaded Mesoporous Silica Particles, Incorporated

in Electrospun PCL Fibres, Provide Topographical and Chemical Cues for Tendon Tissue Engineering." *Advanced Materials Technologies* (2025): 2500246.

2. Citro, Vera, Marta Clerici, Giovanna Della Porta, Nicola Maffulli, Aldo R. Boccaccini, Tina P. Dale, and Nicholas R. Forsyth. "Tenogenic Cues Are Biochemically and Environmentally Distinct for Tendon Stem Cells and Mesenchymal/Stromal Stem Cells." *Stem Cells International* 2025, no. 1 (2025): 9047956.

Oral presentations:

11°I.S.Mu.L.T Congress, Paestum, IT, 2023

Clerici M., Ciardulli MC., Forsyth N.R., Maffulli N., Della Porta G. “Extracellular vesicles (EVs): an intelligent stem cell delivery strategy for tendon therapeutic application”.

31st Annual Meeting of the European Orthopaedic Research Society (EORS), Porto, PT, 2023

M. Clerici, M. C. Ciardulli, N. R. Forsyth, N. Maffulli, and G. Della Porta, “A role for perfusion-delivered shear force in the promotion of TPSC EV production,” in Orthopaedic Proceedings, Bone & Joint, vol. 106, Jan. 2024, pp. 13–13.

Mercia Stem Cell Alliance 11th Annual Scientific Meeting, Nottingham, UK, 2023

Marta Clerici, Maria Camilla Ciardulli, Pasqualina Scala, Erwin P. Lamparelli, Valentina Giudice, Joseph Lovecchio, Emanuele Giordano, Tina P. Dale, Nicholas R. Forsyth, Nicola Maffulli and Giovanna Della Porta. “A role for perfusion delivered shear force in the promotion of hTSPCs EV production”.

TENET-1st General Meeting and Conference of the Cost Actions (CA22170), Salzburg, AU, 2024

Marta Clerici, Maria Camilla Ciardulli, Pasqualina Scala, Erwin P. Lamparelli, Valentina Giudice, Joseph Lovecchio, Emanuele Giordano, Tina P. Dale, Nicholas R. Forsyth, Nicola

Maffulli and Giovanna Della Porta. “Promotion of Extracellular Vesicle Production from Human Tendon Stem/Progenitor Cells via Dynamic Cell Culture”.

TCES/Joint CDT Conference, Glasgow, UK, 2024

Marta Clerici, Maria Camilla Ciardulli, Pasqualina Scala, Erwin P. Lamparelli, Valentina Giudice, Joseph Lovecchio, Emanuele Giordano, Tina P. Dale, Nicholas R. Forsyth, Nicola Maffulli and Giovanna Della Porta. “Promotion of Extracellular Vesicle Production from Human Tendon Stem/Progenitor Cells via Dynamic Cell Culture”.

4th International Biennial Conference BioMaH, Rome, IT, 2024

M. Clerici, M. C. Ciardulli, E. P. Lamparelli, et al., “Extracellular Vesicles from Tendon Stem cells: as a Strategy for Tendon therapeutic delivery,” in 4th Biennial Conference BioMaH, Italian NationalResearch Council, Oct. 2024, isbn: ISBN 978 88 808 672 1.

Poster presentations:

TERMIS 2022, Krakow, PL

M. Clerici, N. R. Forsyth, N. Maffulli, and G. Della Porta, “Identification and characterization of porcine Tendon-Derived Stem Cells (TDSCS),” in Tissue Engineering Part A., vol. 29, Mary Ann Liebert, Inc., 2022.

TERMIS 2023, Manchester, UK

M. Clerici, N. Maffulli, G. Della Porta, and N. R. Forsyth, “Tendon stem cell populations have distinct proliferative and secretome profiles - a key role for physiological oxygen,” in Tissue Engineering Part A., Mary Ann Liebert, Inc., 2023.

11°I.S.Mu.L.T Congress , Paestum, IT, 2023

Clerici M., Ciardulli MC., Forsyth N.R., Maffulli N., Della Porta G. “Extracellular vesicles (EVs): an intelligent stem cell delivery strategy for tendon therapeutic application”.

Mercia Stem Cell Alliance 11th Annual Scientific Meeting, Nottingham, UK, 2023

Marta Clerici, Maria Camilla Ciardulli, Pasqualina Scala, Erwin P. Lamparelli, Valentina Giudice, Joseph Lovecchio, Emanuele Giordano, Tina P. Dale, Nicholas R. Forsyth, Nicola Maffulli and Giovanna Della Porta. “A role for perfusion delivered shear force in the promotion of hTSPCs EV production”.

TERMIS 2024, Seattle, USA

M. Clerici, M. C. Ciardulli, P. Scala, et al., “Dynamic cell culture promotes human Tendon Stem/Progenitor Cell-derived Extracellular Vesicle production,” in Tissue Engineering Part A, Mary Ann Liebert, Inc., Jul. 2024.

9.2 Appendix B – Ethical approval documents, University of Salerno

Azienda Sanitaria Locale Napoli 3 Sud
SERVIZIO COORDINAMENTO COMITATO ETICO
Segreteria T.S.A.
Via Marconi n. 66 – 80059 Torre del Greco
Tel. 081/3174206 **Fax.** 081/3174206
P.E.C. cometicocampaniasud@pec.aslnapoli3sud.it **e-mail** cometicocampaniasud @aslnapoli3sud.it
Dirigente Responsabile: Dott.Celestino Todisco

SERVIZIO COORDINAMENTO COMITATO ETICO DETERMINAZIONE DIRIGENZIALE

N. 151 Del 29/10/2020

§§§

dichiarazione di regolarità tecnica ed amministrativa della stessa resa dal medesimo Dirigente proponente a mezzo di sottoscrizione della presente;

dichiarata altresì espressamente con la sottoscrizione, nella qualità di responsabile del trattamento anche nella fase di pubblicazione, la conformità del presente atto ai principi di cui al D.Lgs. 30 giugno 2003, n. 196 ed al Regolamento Aziendale, in materia di protezione dei dati personali, di cui alla Deliberazione del Direttore Generale n.52 del 17.01.2018, redatto in conformità alle prescrizioni del Regolamento Europeo n.679 del 27.04.2016 relativo alla protezione delle persone fisiche con riguardo al trattamento dei dati personali, nonché alla libera circolazione di tali dati e che abroga la direttiva 95/46/CE, con conseguenziale esclusiva assunzione di responsabilità;

dichiarata, infine, la conformità del presente atto ai principi di cui alla legge 6 novembre 2012, n. 190;

Vista la deliberazione del Commissario straordinario dell'A.S.L. Napoli 3 Sud n. 237 del 12 giugno 2009.

Premesso che:

- con Deliberazione n. 133 del 05/03/2014 la ASL Napoli 3 Sud ha preso atto del protocollo d'intesa per l'istituzione del Comitato Etico Campania Sud (CECS) sottoscritto dal Direttore Generale della ASL Napoli 3 Sud, dal Direttore Generale della ASL Salerno e dal Direttore Generale della A.O.U. San Giovanni di Dio e Ruggi d'Aragona, come indicato nella DGRC n, 16/2014;

- con Deliberazione n. 585 del 04/08/2014 è stato istituito il Servizio di Coordinamento del Comitato Etico Campania Sud;

- con nota prot. della Regione Campania n. 2016.0395772 del 09/06/2016 sono state trasmesse le linee di indirizzo per la stesura delle convenzioni tra l'Istituto e gli Sponsor con l'indicazione del *template* da adottare per il contratto di ricerca;

- con Deliberazione del Direttore Generale Asl Napoli 3 sud n. 251 del 28/11/2016 è stato nominato il dott. Celestino Todisco Dirigente Responsabile del Servizio Coordinamento Comitato Etico Campania Sud;

- con Deliberazione del Direttore Generale ASL Napoli 3 sud n. 325 del 15 maggio 2017 e s.m.i., si è proceduto al rinnovo dei Componenti del Comitato Etico Campania Sud (CECS);

- con nota prot./R.C. n. 2017.0618566 del 20/09/2017 la Direzione Generale per la Tutela della salute e il Coordinamento del S.S.R. ha proceduto alla validazione del nuovo CECS regolarmente costituitosi;

- con nota prot. n. 20553 del 05/02/2020, trasmessa via PEC in pari data dal Servizio Gestione Economica e Finanziaria, acquisita agli Atti di questo Servizio in data 05/02/2020 è stato comunicato il numero di autorizzazione per l'anno 2020, da imputarsi sul conto n. 502011410, autorizzazione n. 189;

- con Deliberazione n.489 del 23/05/2019 immediatamente esecutiva a tutti gli effetti di legge, il Direttore Generale dell'ASL Napoli 3 sud ha preso atto del Regolamento approvato dal CECS;

- gli importi dovuti dai promotori degli studi, per la valutazione degli stessi da parte del Comitato Etico Campania Sud , sono versati sul conto corrente postale dedicato (IBAN IT 02 B 07601 03400 001021004393) intestato a ASL Napoli 3 Sud – Servizio Coordinamento Comitato Etico Campania Sud; e successivamente gli importi andranno ad implementare a cura del G.E.F. il conto n. 502011410;

Considerato che:

- lo studio si svolgerà nel rispetto della normativa vigente e secondo quanto descritto nel protocollo di studio approvato dal Comitato;

- lo Sperimentatore Responsabile e/o lo Sponsor dovrà inviare al CECS una comunicazione di inizio studio e una relazione finale di conclusione dello studio nella quale vanno indicate eventuali pubblicazioni di articoli su riviste scientifiche e tecniche nazionali ed internazionali o di relazioni tecnico-scientifiche in atti di convegni;

Ritenuto di:

dover procedere all'avvio dello studio in oggetto, approvato dal CECS nella seduta del 20/10/2020 con **Parere Unico** N. 30 _r.p.s.o. alle condizioni innanzi richiamate e avente come *Principal Investigator* il prof.F.Oliva e svolto presso il Dipartimento di Ortopedia e Traumatologia Universitaria della AOU Ruggi di Salerno;

D E T E R M I N A

per quanto esposto in narrativa, che qui si intende integralmente riportato:

di procedere all'avvio dello studio in oggetto, approvato dal CECS nella seduta del 20/10/2020 con **Parere Unico** N. 30 _r.p.s.o. alle condizioni innanzi richiamate e avente come *Principal*

Investigator il prof.F.Oliva e svolto presso il Dipartimento di Ortopedia e Traumatologia Universitaria della AOU Ruggi di Salerno; di trasmettere il presente atto al Collegio Sindacale.

Il sottoscritto Dirigente Responsabile provvederà a curare ogni adempimento relativo alla esecuzione della presente determinazione, che viene resa immediatamente esecutiva, nonché alla pubblicazione della stessa sull'Albo Pretorio.

Sottoscritta dal Direttore del Servizio (TODISCO CELESTINO) con firma digitale